UNIVERSITÉ DE LORRAINE | BIBLIOTHÈQUES UNIVERSITAIRES

AVERTISSEMENT
DROIT D'AUTEUR

Ce document est le fruit d'un long travail approuvé par le jury de soutenance et mis à disposition de l'ensemble de la communauté universitaire élargie.

Il est soumis à la propriété intellectuelle de l'auteur. Ceci implique une obligation de citation et de référencement lors de l'utilisation de ce document. Toute contrefaçon, plagiat ou reproduction illicite encourt une poursuite pénale.

Contact bibliothèque : ddoc-theses-contact@univ-lorraine.fr
(Cette adresse ne permet pas de contacter les auteurs)

Code de la Propriété Intellectuelle. articles L 122. 4
Code de la Propriété Intellectuelle. articles L 335.2- L 335.10

UNIVERSITÉ DE LORRAINE
34 COURS LÉOPOLD — CS 25233
54052 NANCY CEDEX
TÉL : 03 54 50 54 00
CONTACT@UNIV-LORRAINE.FR
WWW.UNIV-LORRAINE.FR

École Doctorale :
Sciences et Ingénieries des Molécules, des Produits, des Procédés et de l'Énergie (SIMPPÉ)

Laboratoire Réactions et Génie des Procédés (LRGP-CNRS)

Thèse

Pour l'obtention du titre de

Docteur de l'Université de Lorraine

Mention : Génie des Procédés, des Produits et des Molécules

Conception et fonctionnalisation d'élastomères biosourcés à base d'itaconate carboxylé : de l'ingénierie moléculaire aux nanocomposites verts renforcés par la silice

---

par

Liwei LI

Présentée et soutenue publiquement le 25 septembre 2025

Membres du Jury :

Rapporteurs :

Mme. Anne-Sophie SCHULLER, Maître de Conférences, HDR, Université de Haute-Alsace(France)

M. Shaojian HE, Professeur, Université de l'Électricité de Chine du Nord (Chine)

Présidente du jury :

Mme. Isabelle ROYAUD (Président de jury), Professeure, Université de Lorraine (France)

Examinatrice :

Mme. Mengjiao CHENG, Professeure, Université de Technologie Chimique de Pékin (Chine)

Direction de thèse :

M. Guo-Hua HU (Directeur de thèse), Professeur, Université de Lorraine (France)

M. Liqun ZHANG (Co-directeur de thèse), Professeur, Université Jiaotong de Xi'an (Chine)

Acknowledgments

The journey of my doctoral study is about to come to an end. Looking back on these years of research, my heart is filled with gratitude and emotion. Although the academic path has been long and arduous, it is precisely because of the encouragement, guidance, and companionship of many people that I have been able to persevere and successfully complete this doctoral dissertation. Here, I would like to express my sincerest thanks to all the teachers, colleagues, family, and friends who have cared for and helped me.

First of all, I would like to sincerely thank my supervisors, Professor Guo-Hua HU and Professor Liqun ZHANG. Throughout the entire doctoral period, you have always given me careful guidance and valuable advice. Professor HU is rigorous in scholarship and meticulous in attitude, setting an example of academic standards for me and giving me great help in the expansion of research ideas and the optimization of experimental schemes. Professor ZHANG is sharp-minded and insightful, providing me with firm guidance and support in the selection of research direction and the progress of the project. Thank you both for your thoughtful care in my academic studies, research, and life, which enabled me to move forward steadily and grow continuously during my Ph.D.

I would especially like to thank Professor Runguo WANG. As the guide on my research path, Professor WANG has always led me forward with profound academic insight and broad-mindedness. Throughout the entire doctoral stage, Professor WANG not only gave me full freedom and trust in research but also patiently guided me and helped me find direction when I encountered confusion and bottlenecks. At the same time, Professor WANG also gave me great care and support in life, allowing me to focus on research with peace of mind. His dedication to academics and care for students deeply influenced and inspired me to keep moving forward.

I am also deeply grateful to the members of my Ph.D. defense jury for their time, expertise, and valuable feedback on my dissertation: Mme. Anne-Sophie SCHULLER, M. Shaojian HE,

Mme. Isabelle ROYAUD, and Mme. Mengjiao CHENG. Thank you for your thoughtful review and constructive suggestions, which have helped me further improve my research work.

I would also like to sincerely thank the Laboratoire Réactions et Génie des Procédés of University of Lorraine in France and the Center of Advanced Elastomer Materaials of Beijing University of Chemical Technology in China for providing me with an excellent research platform and good learning environment. The cooperation between the two institutions not only allowed me to deeply experience the value and charm of scientific research, but also greatly broadened my academic horizons. Special thanks to Haijun JI, Hui YANG, Xin ZHANG, Chaoying SUN, Xiaonan WANG, Yiping CHEN, Xiaopeng AN, Minjian QUAN, and Liangyan FU for their help in my research and life. Thanks also to Pan WANG, Fulan HAO, Shuo ZENG, and Hengkui ZHANG—we studied together in France, and that period will always be one of the most treasured memories of my life.

Finally, I thank my family for their constant understanding and support. It is your tolerance and dedication that allowed me to fully devote myself to research without worry. I especially want to thank my girlfriend Li WANG—thank you for always being by my side during my most confused and anxious moments, giving me endless warmth and encouragement. Your understanding and steadfastness are the greatest driving force for me to keep going.

Liwei LI

Nancy, France

June 2025

Abstract

This thesis focuses on the development of sustainable, high-performance rubber materials by synthesizing and functionalizing bio-based itaconate elastomers derived from renewable biomass. To address the limitations of petroleum-based rubbers and natural rubber, a series of carboxylated bio-based elastomers (PDBIBAs) were synthesized via emulsion polymerization using dibutyl itaconate, butadiene, and methacrylic acid. The effects of methacrylic acid content on molecular structure, thermal behavior, and mechanical performance were systematically investigated, and silica-filled nanocomposites were developed to explore interfacial interactions and filler dispersion. Furthermore, dynamic ionic networks were introduced through ZnO-induced cross-linking to construct thermoreversible PDBIBA elastomers with enhanced strength, thermal responsiveness, and recyclability. To broaden material applicability, bio-based itaconate elastomers with different side chain lengths (PDXIBA) were synthesized using dimethyl, diethyl, and dibutyl itaconate as monomers, together with butadiene and methacrylic acid. Their structure, mechanical properties, and biocompatibility were systematically evaluated. Comparative studies with commercial NR, XNBR gloves and the fabrication of silica-reinforced composites highlighted the potential of these materials for disposable glove applications and green nanocomposites. This work not only demonstrates the feasibility of using biomass-derived monomers to create elastomers with tunable properties, but also provides new insights into structure–property relationships, offering a viable path toward sustainable rubber alternative.

Keywords: Bio-based itaconate elastomers; Ionic elastomers; Varied side chains; Nanocomposites; Properties; Applications.

Résumé

Cette thèse porte sur le développement de matériaux en caoutchouc durables et haute performance par la synthèse et la fonctionnalisation d'élastomères à base d'itaconate biosourcé dérivé de la biomasse renouvelable. Afin de pallier les limitations des caoutchoucs d'origine pétrochimique et du caoutchouc naturel, une série d'élastomères carboxylés biosourcés (PDBIBAs) ont été synthétisés par polymérisation en émulsion en utilisant le dibutyl itaconate, le butadiène et l'acide méthacrylique. Les effets de la teneur en acide méthacrylique sur la structure moléculaire, le comportement thermique et les performances mécaniques ont été systématiquement étudiés, et des nanocomposites chargés en silice ont été développés pour explorer les interactions interfaciales et la dispersion des charges. En outre, des réseaux ioniques dynamiques ont été introduits par réticulation induite par ZnO afin de construire des élastomères PDBIBA thermoréversibles présentant une résistance améliorée, une réactivité thermique et une recyclabilité. Pour élargir l'applicabilité des matériaux, des élastomères à base d'itaconate biosourcé avec différentes longueurs de chaînes latérales (PDXIBA) ont été synthétisés en utilisant le diméthyl, le diéthyl et le dibutyl itaconate comme monomères, avec le butadiène et l'acide méthacrylique. Leur structure, leurs propriétés mécaniques et leur biocompatibilité ont été systématiquement évaluées. Des études comparatives avec des gants commerciaux en NR et XNBR ainsi que la fabrication de composites renforcés de silice ont mis en évidence le potentiel de ces matériaux pour des applications de gants jetables et de nanocomposites écologiques. Ce travail démontre non seulement la faisabilité d'utiliser des monomères dérivés de la biomasse pour créer des élastomères aux propriétés modulables, mais fournit également de nouvelles perspectives sur les relations structure–propriétés, offrant une voie viable vers des alternatives durables au caoutchouc.

Mots-clés: Élastomères à base d'itaconate biosourcé; Élastomères ioniques; Chaînes latérales variées; Nanocomposites; Propriétés; Applications.

Table of contents

Acknowledgments ..... **i**

Abstract ..... **iii**

Résumé ..... **iv**

Résumé étendu ..... **ix**

I Introduction ix

II Objectifs de recherche de la thèse ix

III Contenu de la recherche et résultats clés de la thèse x

IV Conclusions générales et perspectives xiv

Chapter 1 General Introduction **1**

1.1 Overview 1

1.2 Research objectives of this thesis 2

1.3 Innovations 3

1.4 Thesis organization 4

Chapter 2 Literature Review and State of the Art **5**

2.1 Biomass resources 5

2.2 Bio-based chemicals 8

2.2.1 Bio-based ethanol 8

2.2.2 Bio-based n-butanol 10

2.2.3 Bio-based ethylene 11

2.2.4 Bio-based butadiene 13

2.2.5 Bio-based isoprene 16

2.2.6 Bio-based itaconic acid 19

2.3 Bio-based synthetic elastomers 22

2.3.1 Bio-based itaconate elastomers 22

2.3.2 Bio-based polyester elastomers 24

2.3.3 Bio-based thermoplastic polyurethane elastomers 27

2.4 Functional elastomers 27

2.5 References 31

Chapter 3 Role of Carboxyl Groups in the Performance Optimization of Bio-based Itaconate Elastomers and Nanocomposites 46

3.1 Introduction 46

3.2 Experimental section 48

3.2.1 Materials 48

3.2.2 Synthesis of PDBIBAs 48

3.2.3 Cross-linking behavior of PDBIBAs and silica/PDBIBA nanocomposites 50

3.2.4 Preparation of cross-linked PDBIBAs and silica/PDBIBA nanocomposites 52

3.3 Characterization methods 52

3.4 Results and discussion 56

3.4.1 Synthesis and characterization of neat PDBIBAs 56

3.4.2 FTIR and ^{1}H NMR characterizations of neat PDBIBAs 57

3.4.3 Thermal properties of neat PDBIBAs 59

3.4.4 Mechanical and dynamic properties of cross-linked PDBIBAs without fillers 61

3.4.5 Interfacial interaction between PDBIBAs and silica 63

3.4.6 Mechanical and dynamic properties of silica/PDBIBA nanocomposites 67

3.4.7 DIN abrasion loss of silica/PDBIBA nanocomposites 69

3.4.8 Thermo-oxidative aging properties of silica/PDBIBA nanocomposites 70

3.4.9 Oil resistance evaluation of silica/PDBIBA nanocomposites 71

3.5 Conclusions 72

3.6 References 73

Chapter 4 Dynamic Evolution of Ionic Bonds and Performance Characteristics in Bio-based Dibutyl Itaconate Elastomers 78

4.1 Introduction 78

4.2 Experimental section 80

4.2.1 Materials 80

4.2.2 Ionic cross-linking behavior of PDBIBA elastomers with ZnO 81

4.2.3 Preparation of cross-linked PDBIBA/ZnO sheets 81
4.3 Characterization methods 82
4.4 Results and discussion 84
4.4.1 FTIR characterization of ZnO-crosslinked PDBIBA: ionic bond formation and structural analysis 84
4.4.2 Morphological and structural analysis of ZnO-crosslinked PDBIBA: TEM and XRD insights 87
4.4.3 Dynamic mechanical analysis of cross-linked PDBIBA/ZnO 90
4.4.4 Stress-strain behavior of cross-linked PDBIBA/ZnO 91
4.4.5 Swelling ratio and cross-linking density of ZnO cross-linked PDBIBA 92
4.4.6 Temperature dependence of the reversibility of ionic bonds between ZnO and carboxyl groups of PDBIBA 93
4.4.7 Temperature-dependent viscoelastic behavior of cross-linked PDBIBA/ZnO 96
4.5 Conclusions 97
4.6 References 98
Chapter 5 Synthesis and Performance Investigation of Bio-based Carboxylated Itaconate Elastomers with Varied Side Chains 102
5.1 Introduction 102
5.2 Experimental section 105
5.2.1 Materials 105
5.2.2 Synthesis of PDXIBA latex with different side chains 105
5.2.3 Preparation of PDXIBA films with different side chains and XNBR films 107
5.2.4 Preparation of silica/PDXIBA, silica/XNBR and silica/ESBR nanocomposites 108
5.3 Characterization methods 110
5.4 Results and discussion 113
5.4.1 Synthesis and characterization of PDXIBA (PDBIBA, PDEIBA, PDMIBA) latex with different side chains 113
5.4.2 Mechanical properties of cross-linked PDXIBA films 119

5.4.3 Abrasion loss of cross-linked PDXIBA films 120
5.4.4 Solvent and oil resistance evaluation of cross-linked PDXIBA elastomer films .. 121
5.4.5 Cytotoxicity and skin sensitization evaluation of PDEIBA, natural and nitrile rubber gloves 123
5.4.6 Interfacial interaction between PDXIBA, XNBR, ESBR and silica. 125
5.4.7 Mechanical properties of silica/PDXIBA, silica/XNBR and silica/ESBR nanocomposites 128
5.4.8 Durability performance: DIN abrasion, aging behavior and oil resistance of silica/PDXIBA, silica/XNBR, and silica/ESBR nanocomposites 129
5.5 Conclusions 133
5.6 References 134
Chapter 6 General Conclusions and Perspectives 137
6.1 General conclusions 137
6.2 Perspectives 139
Appendix 141
Additional materials for Chapter 3 141
Additional materials for Chapter 4 143
Additional materials for Chapter 5 144
Nomenclature 149
Scientific Production 151

Résumé étendu

I Introduction

Avec le développement accéléré de la société moderne, les défis liés aux ressources et à l'environnement prennent une ampleur croissante. Les ressources fossiles non renouvelables, après des siècles d'exploitation intensive, se raréfient, alors que la demande énergétique mondiale ne cesse d'augmenter. Parallèlement, l'essor de l'industrie pétrochimique a entraîné une dégradation sévère de l'environnement, notamment à travers les émissions de gaz à effet de serre responsables du réchauffement climatique.

Dans le domaine des matériaux, la quasi-totalité des matières premières utilisées pour la production de caoutchouc synthétique provient actuellement du pétrole. Cette dépendance renforce non seulement l'épuisement des ressources fossiles, mais accentue également les pressions environnementales. Par conséquent, la recherche de solutions alternatives, durables et à faible émission de carbone, est devenue un objectif mondial prioritaire.

Dans ce contexte, le développement d'élastomères biosourcés issus de ressources renouvelables constitue une voie prometteuse. Cette étude s'inscrit dans cette dynamique en explorant la synthèse d'élastomères à base d'itaconate biosourcé copolymérisé avec du butadiène et de l'acide méthacrylique (MAA). Ces monomères d'itaconate sont dérivés de l'acide itaconique, un composé biosourcé produit par fermentation de glucides issus de cultures à haut rendement telles que le maïs, le blé, le riz ou la canne à sucre. Cette origine confère aux matériaux une réelle durabilité et les distingue nettement des polymères d'origine fossile.

II Objectifs de recherche de la thèse

Cette recherche vise à développer des élastomères biosourcés à base d'itaconate alliant

durabilité, performance et polyvalence d'usage, selon trois axes stratégiques :

(1) Fonctionnalisation à l'acide méthacrylique (MAA) afin d'optimiser les propriétés mécaniques de la matrice et d'améliorer l'interaction interfaciale avec la silice.

(2) Réticulation ionique dynamique induite par ZnO, visant à conférer aux matériaux des propriétés thermoréversibles, une meilleure résistance mécanique et une recyclabilité accrue.

(3) Modulation de la structure des chaînes latérales des monomères d'itaconate afin d'adapter les propriétés des élastomères pour des applications spécifiques telles que les gants de haute performance ou les nanocomposites à base de silice.

Ces approches intégrées permettent d'accéder à une nouvelle génération d'élastomères biosourcés aux propriétés ajustables, capables de répondre aux exigences croissantes en matière de durabilité et de performance, tout en apportant une meilleure compréhension des relations structure–propriétés dans les matériaux polymères verts.

III Contenu de la recherche et résultats clés de la thèse

Rôle des groupes carboxyles dans l'optimisation des performances des élastomères biosourcés à base d'itaconate et des nanocomposites

Dans une optique de développement durable pour l'industrie du caoutchouc, la substitution des caoutchoucs synthétiques fossiles par des élastomères biosourcés devient un objectif stratégique. Afin d'optimiser leurs performances mécaniques et fonctionnelles, la fonctionnalisation chimique s'avère essentielle.

Dans ce travail, des élastomères carboxylés poly(dibutyl itaconate-*co*-butadiene-*co*-methacrylic acid) (PDBIBA) ont été synthétisés par polymérisation en émulsion à partir de dibutyl itaconate, de butadiène et d'acide méthacrylique (MAA), comme illustré à la **Figure 1**. Les structures ont été caractérisées par FTIR, ^{1}H NMR et GPC. La variation de la teneur en MAA a permis d'obtenir des masses molaires comprises entre 173 et 310 kg/mol et des températures de transition vitreuse (T_g) allant de -57 °C à -32 °C.

Parmi les formulations, le PDBIBA-15 (fortement carboxylé) a présenté une résistance à

la traction remarquable de 14.1 MPa, soit une amélioration de 355 % par rapport au PDBIBA-0 sans MAA. Cette performance est attribuée à la formation de liaisons entre les groupes carboxyles et l'oxyde de zinc (ZnO).

L'incorporation de nanoparticules de silice a renforcé davantage les propriétés des nanocomposites PDBIBA, grâce à une meilleure interaction charge–matrice via les groupes carboxyles. Les nanocomposites ont atteint des résistances à la traction de 15.5 à 24.4 MPa, avec des allongements à la rupture allant de 200 % à 393 %. En outre, une teneur élevée en MAA a amélioré la résistance à l'abrasion, à l'huile et au vieillissement, démontrant une durabilité renforcée sous conditions sévères.

Ces résultats confirment que la fonctionnalisation par MAA est une stratégie efficace pour étendre les applications des élastomères biosourcés dans des domaines industriels exigeants.

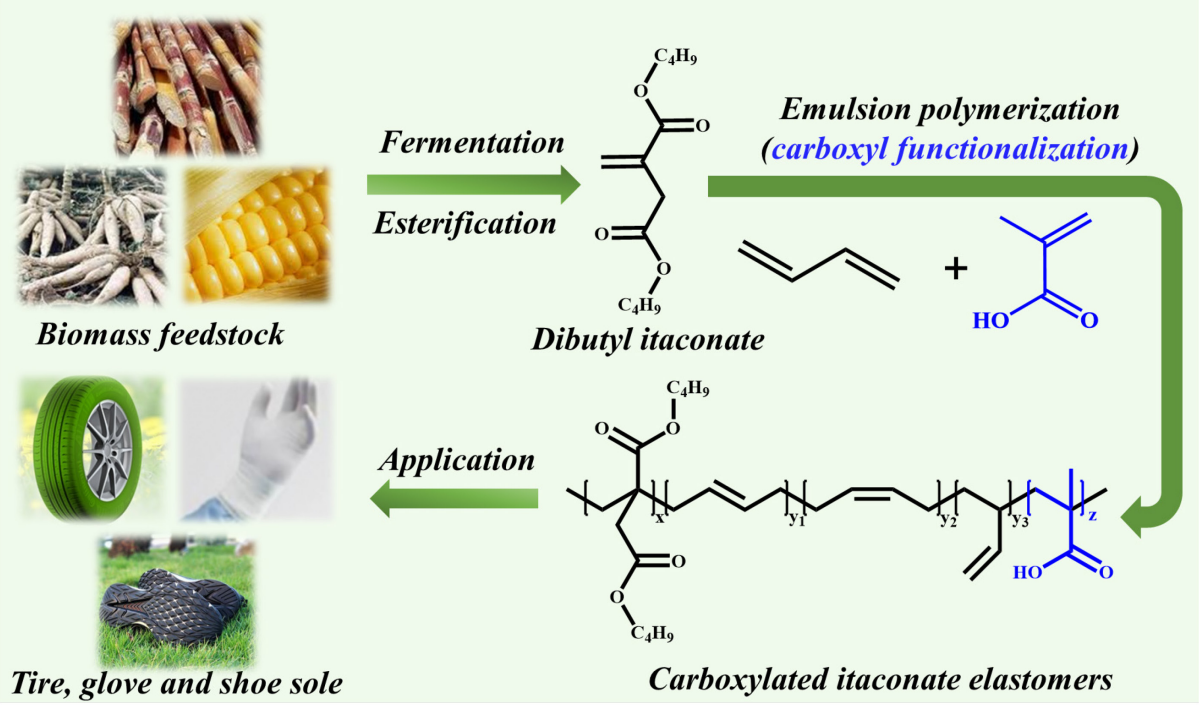

Figure 1. Schéma illustrant la voie de synthèse et d'application des élastomères à base d'itaconate carboxylé dérivés de ressources de biomasse.

Évolution dynamique des liaisons ioniques et caractéristiques de performance des élastomères biosourcés à base d'itaconate de dibutyle

Une stratégie complémentaire a été mise en œuvre pour introduire des propriétés thermoréversibles aux élastomères biosourcés via la réticulation ionique. Les copolymères

PDBIBA porteurs de groupes carboxyles ont été réticulés dynamiquement avec du ZnO, formant des liaisons de carboxylate de zinc (voir **Figure 2**).

Contrairement aux réseaux covalents irréversibles, cette réticulation ionique offre une réponse thermique, une malléabilité accrue et une recyclabilité potentielle. La spectroscopie FTIR a confirmé la formation de liaisons Zn^{2+}–carboxylate. La densité de réticulation ionique a permis une amélioration mécanique significative, avec une augmentation de la résistance à la traction atteignant 467 % par rapport aux échantillons non réticulés.

Toutefois, une concentration excessive en ZnO (>5 %) induit une agrégation et une séparation de phase, comme l'ont révélé les analyses DMA, TEM et XRD. Les mesures par NMR à bas champ et RPA ont montré que ces réseaux sont capables de se désassembler à haute température et de se reformer lors du refroidissement, conférant une bonne résilience structurale au cours de cycles thermiques successifs.

Ces résultats mettent en lumière le potentiel des réticulations ioniques dynamiques dans la conception d'élastomères biosourcés aux propriétés modulables et recyclables.

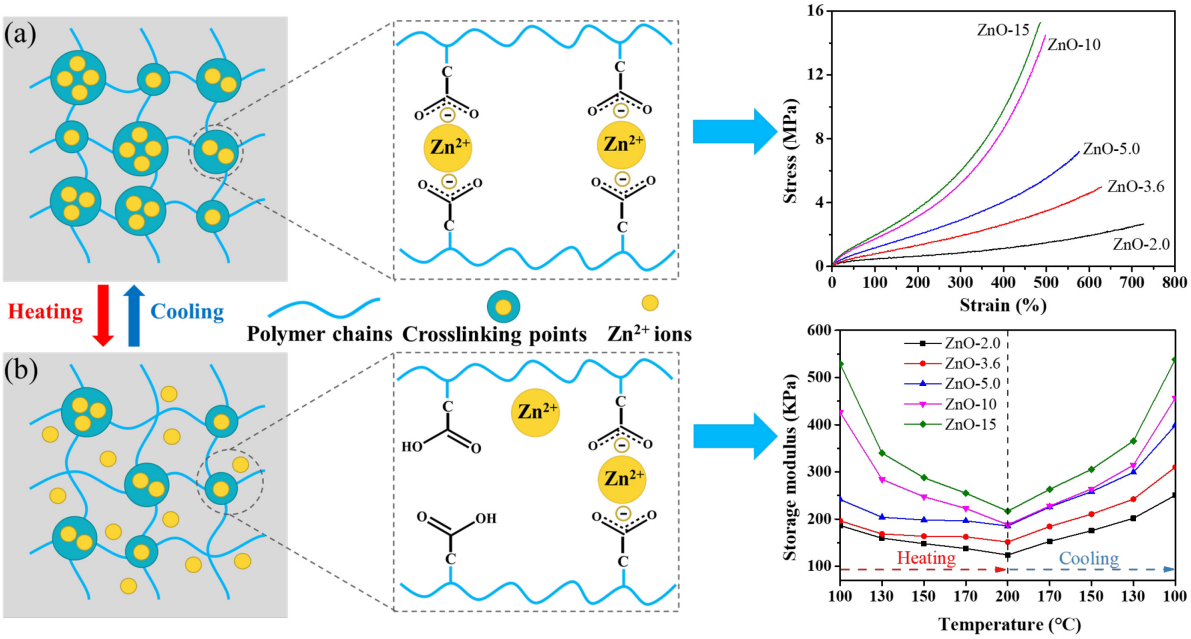

Figure 2. Schéma illustrant le mécanisme de réticulation ionique thermoréversible et les performances mécaniques correspondantes des élastomères PDBIBA réticulés par ZnO.

Synthèse et étude des performances des élastomères biosourcés carboxylés à base d'itaconate avec chaînes latérales variées

Pour répondre à des besoins industriels variés, l'influence de la structure des chaînes latérales des monomères d'itaconate sur les propriétés des élastomères a été explorée. Trois monomères biosourcés – itaconate de dibutyle (DBI), de diéthyle (DEI) et de diméthyle (DMI) – ont été copolymérisés avec du butadiène et du MAA pour produire respectivement les copolymères PDBIBA, PDEIBA et PDMIBA (voir **Figure 3**).

L'étude a montré qu'un raccourcissement des chaînes latérales diminue la masse molaire (de 256 à 99 kg/mol), augmente la T_g (de -46 °C à -16 °C), améliore la résistance à la traction (de 25.5 à 28.0 MPa) et réduit l'allongement à la rupture (de 553 % à 311 %), répondant ainsi aux critères des matériaux de gants haute performance.

Le PDMIBA s'est révélé supérieur en termes de résistance à l'huile et à l'abrasion, tandis que le PDEIBA a présenté une meilleure biocompatibilité, supérieure à celle des gants en latex naturel ou en caoutchouc nitrile.

Des nanocomposites chargés de silice ont également été formulés. À mesure que la chaîne latérale raccourcissait (butyle → méthyle), la polarité de la matrice augmentait, améliorant la dispersion de la charge et la compatibilité interfaciale. La résistance à la traction variait de 24.9 à 29.5 MPa selon les systèmes. Les composites à base de PDMIBA ont affiché les meilleures performances en résistance à l'huile, liées à la densité élevée de groupes esters polaires.

Ces résultats démontrent que l'ingénierie des chaînes latérales constitue un levier efficace pour adapter les performances des élastomères biosourcés à des applications ciblées telles que les gants médicaux et les joints techniques.

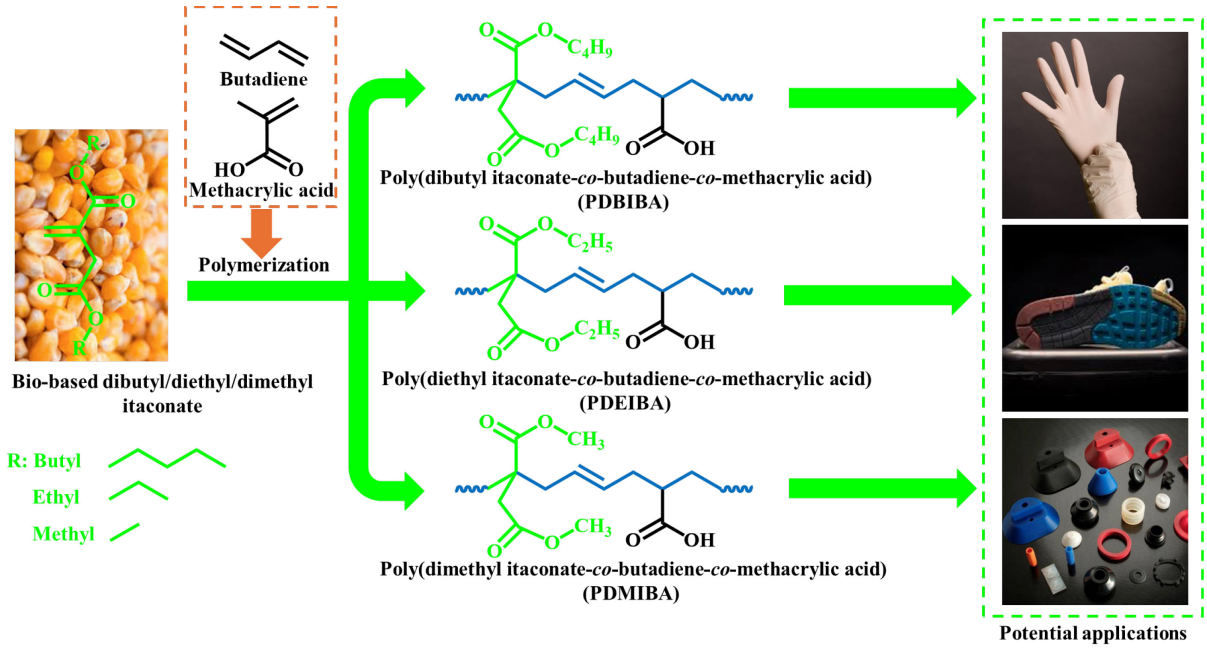

Figure 3. Schéma de la voie de synthèse et des applications potentielles des élastomères biosourcés à base d'itaconate avec des chaînes latérales variées.

IV Conclusions générales et perspectives

Cette thèse a permis de concevoir un système polyvalent d'élastomères biosourcés à base d'itaconate, intégrant trois stratégies complémentaires : la fonctionnalisation carboxylique par MAA, la réticulation ionique dynamique via ZnO, et la modulation de la structure des chaînes latérales.

L'introduction de groupes carboxyles a renforcé à la fois les propriétés mécaniques intrinsèques (résistance à la traction) et les interactions interfaciales avec les charges de silice dans les nanocomposites. La réticulation ionique par carboxylate de zinc a conféré une réponse thermique et une aptitude au reconditionnement. La variation structurale des chaînes latérales a permis d'ajuster finement les propriétés visées : résistance à l'huile, à l'abrasion ou biocompatibilité.

Le PDMIBA s'est démarqué par ses propriétés mécaniques et sa résistance chimique, tandis que le PDEIBA a montré une excellente compatibilité biologique, confirmant leur potentiel pour des applications telles que les gants médicaux jetables ou les pièces techniques résistantes.

Ce travail ouvre de nouvelles perspectives en matière de conception de polymères durables. À l'avenir, des stratégies de fonctionnalisation plus variées (hydroxyle, amine, sulfonate) ainsi que des réseaux réticulés basés sur des ions métalliques mixtes pourraient être explorés. L'intégration de monomères et de charges 100 % biosourcés (terpènes, lignine, cellulose) permettra de concevoir une nouvelle génération d'élastomères écoresponsables répondant aux exigences de l'économie circulaire.

Chapter 1 General Introduction

1.1 Overview

As one of the three pillars of modern polymer material systems, synthetic rubber is widely used in advanced manufacturing, transportation, and daily life due to its excellent reversible deformation ability and viscoelastic properties. Up to now, the synthetic rubber system has evolved into more than a hundred products, including styrene-butadiene rubber, nitrile rubber, neoprene, fluororubber, and silicone rubber. However, the main monomers of most commercial rubber products, such as styrene, butadiene, and isoprene, are mainly derived from petroleum cracking and heavily depend on fossil resources, which not only accelerates energy consumption but also leads to massive carbon emissions. Therefore, developing elastomer systems based on biomass and other renewable resources has become key to achieving sustainable development in the rubber industry. Biomass resources are widely sourced, including animals, plants, and microbial excretions and metabolites, such as branches, sawdust, straw, stalks, seaweed, sugar crops, and municipal waste. With the deepening understanding of microbial functions, microorganisms have been widely applied in medicine, food, fermentation, and chemical industries. In recent years, significant progress has been made in the microbial fermentation of industrial monomers, such as succinic acid, itaconic acid, sebacic acid, glycerol, methanol, and ethanol, which have been widely used in the synthetic industry and provide a new path for constructing green rubber material systems. In this study, bio-based itaconate (dimethyl itaconate, diethyl itaconate and dibutyl itaconate) was used as the main monomer and copolymerized with butadiene and methacrylic acid (MAA) to synthesize a series of bio-based itaconate elastomers (BIE).

1.2 Research objectives of this thesis

This research aims to develop sustainable, high-performance bio-based itaconate elastomers through three strategic approaches: methacrylic acid (MAA) functionalization, ZnO-induced ionic cross-linking, and side chain structure modulation.

(1) Chapter 3 aims to develop high-performance bio-based elastomers by introducing methacrylic acid (MAA) into bio-based poly(dibutyl itaconate-*co*-butadiene-*co*-methacrylic acid) (PDBIBA) via emulsion polymerization to achieve carboxyl functionalization. The goal is to enhance the polarity and mechanical strength of the elastomer matrix itself, while also improving interfacial interactions with silica fillers. As a result, the nanocomposites exhibit better silica dispersion, as well as improved abrasion resistance, aging stability, and oil resistance. This work offers a strategy to advance both intrinsic and composite properties of sustainable elastomeric materials.

(2) Chapter 4 aims to explore the dynamic ionic cross-linking behavior of bio-based poly(dibutyl itaconate-*co*-butadiene-*co*-methacrylic acid) (PDBIBA) induced by zinc oxide (ZnO). By investigating the effects of ZnO content and temperature, the research focuses on understanding the formation, evolution, and reversibility of zinc carboxylate networks, and how these dynamic ionic bonds influence the mechanical strength, thermal responsiveness, and crosslinking density of the material. The goal is to provide a basis for designing recyclable elastomers with tunable properties through controllable ionic interactions.

(3) Chapter 5 aims to develop and evaluate a series of bio-based carboxylated itaconate elastomers (PDXIBA) with different side chains, synthesized via emulsion polymerization using itaconate monomers with varying side chain structures (dimethyl, diethyl, and dibutyl itaconate), along with butadiene and methacrylic acid, for application in disposable gloves and silica-reinforced nanocomposites. By systematically investigating the influence of side chain structure on molecular characteristics, mechanical strength, oil and abrasion resistance, and filler–matrix interactions, the study seeks to clarify the structure–property relationships of PDXIBA materials. Furthermore, by comparing these bio-based elastomers with commercial

carboxylated nitrile rubber (XNBR), the work provides important insights into the advantages, challenges, and industrial feasibility of PDXIBA as a sustainable alternative for high-performance glove materials and multifunctional composites.

1.3 Innovations

Innovation 1: Functionalization design of bio-based itaconate elastomers with tunable properties via carboxyl group introduction

This study systematically utilized methacrylic acid (MAA) as a functional monomer to design and synthesize a series of novel carboxylated bio-based itaconate elastomers (PDBIBA), clarifying the effects of carboxyl groups on the properties of both neat PDBIBA and its silica-based nanocomposites. This functionalization strategy offers a new pathway for developing sustainable rubber materials with excellent comprehensive performance.

Innovation 2: Construction of thermoreversible ionic cross-linked networks for recyclability and property modulation of carboxylated bio-based itaconate elastomers

This study proposed and validated a thermoreversible ionic cross-linking strategy for carboxylated itaconate elastomers induced by ZnO. Through coordination between carboxyl groups on the PDBIBA chains and Zn^{2+} ions, a temperature-responsive and thermoreversible dynamic network structure was achieved. This enables reversible cross-linking upon thermal stimulation, offering new perspectives on utilizing bio-based carboxylated itaconate elastomers as recyclable materials.

Innovation 3: Side chain structure regulation for multi-performance optimization of carboxylated bio-based itaconate elastomers and application expansion

This study designed and synthesized three types of PDXIBA elastomers with varied side chains (using dimethyl itaconate, diethyl itaconate and dibutyl itaconate as monomers), elucidating the impact of itaconate monomer structure on the performance of elastomer films and nanocomposites. The work also explored their potential in bio-based products such as gloves and oil-resistant materials, facilitating the adoption of sustainable elastomers.

1.4 Thesis organization

This thesis is organized into six chapters:

Chapter 1 introduces the background, objectives, innovations, and structure of the thesis.

Chapter 2 reviews biomass resources, bio-based chemicals, bio-based synthetic elastomers and functional elastomers.

Chapter 3 focuses on the synthesis and functionalization of bio-based carboxylated itaconate elastomers (PDBIBA) via emulsion polymerization. It systematically investigates the influence of methacrylic acid content on molecular structure, thermal properties, and mechanical performance. Furthermore, the chapter explores the development of silica/PDBIBA nanocomposites, emphasizing the effect of methacrylic acid content in enhancing filler dispersion and comprehensive properties, providing a foundation for sustainable elastomer applications.

Chapter 4 presents the development of bio-based ionic elastomers through ZnO-induced dynamic cross-linking of PDBIBA. It systematically investigates the effects of ZnO content and temperature on ionic network evolution, mechanical reinforcement, thermoreversible behavior, providing insights for the design of recyclable and sustainable elastomer materials.

Chapter 5 focuses on the synthesis of bio-based carboxylated itaconate elastomers (PDXIBA) with varying side chains through emulsion polymerization. The effects of side chain length on molecular structure, mechanical properties, thermal behavior, oil resistance, and abrasion resistance were systematically evaluated. Comparative studies with commercial XNBR latexes were conducted to assess the application potential of PDXIBA films in disposable glove materials. Furthermore, silica-reinforced nanocomposites were prepared to explore how matrix polarity modulation optimizes filler dispersion and overall composite performance, offering new possibilities for green material development.

Chapter 6 summarizes the key conclusions and outlines future research directions for bio-based elastomer development.

Chapter 2 Literature Review and State of the Art

The sustainable development of the rubber industry is facing severe challenges of fossil resource dependence. Traditional synthetic rubber production is centered on petroleum-based raw materials. With the rapid depletion of non-renewable resources, the industry not only faces economic pressures such as rising raw material costs and supply chain fluctuations, but also bears dual constraints from ecological environment and carbon emission reduction. Under this background, developing novel rubber materials based on biomass resources has become an important breakthrough to solve this predicament. Through green technological routes such as innovative utilization of biomass raw materials, biological fermentation technology and catalytic conversion technology, constructing bio-based rubber systems with adjustable molecular structures and engineering applicability can alleviate excessive dependence on fossil resources, promote the transformation of the industry towards a low-carbon circular model, and maintain the sustainable development of the rubber industry. This section describes a series of high value-added basic chemicals developed from biomass resources, with a focus on bio-based chemicals and bio-based elastomers relevant to this work.

2.1 Biomass resources

Biomass resources refer to organic matter obtained directly or indirectly from the photosynthesis of green plants or microorganisms[1]. According to the European Commission's definition of biomass, biomass resources include all animals, plants, microorganisms, metabolic products, agricultural and forestry wastes, household waste, etc. Biomass resources can be classified into two main categories according to their utilization and origin, as shown in **Figure 2.1**, productive biomass and unused biomass[2-5]. These biomass resources can yield numerous chemicals through methods such as extraction and fermentation. Especially in the current

context of depleting fossil resources and escalating environmental issues, biomass resources have emerged as a highly promising and important source for sustainable development. It is estimated that by 2050, under favorable market conditions, bulk chemicals derived from renewable biomass could reach approximately 113 million tons, accounting for 38% of all organic chemicals [6].

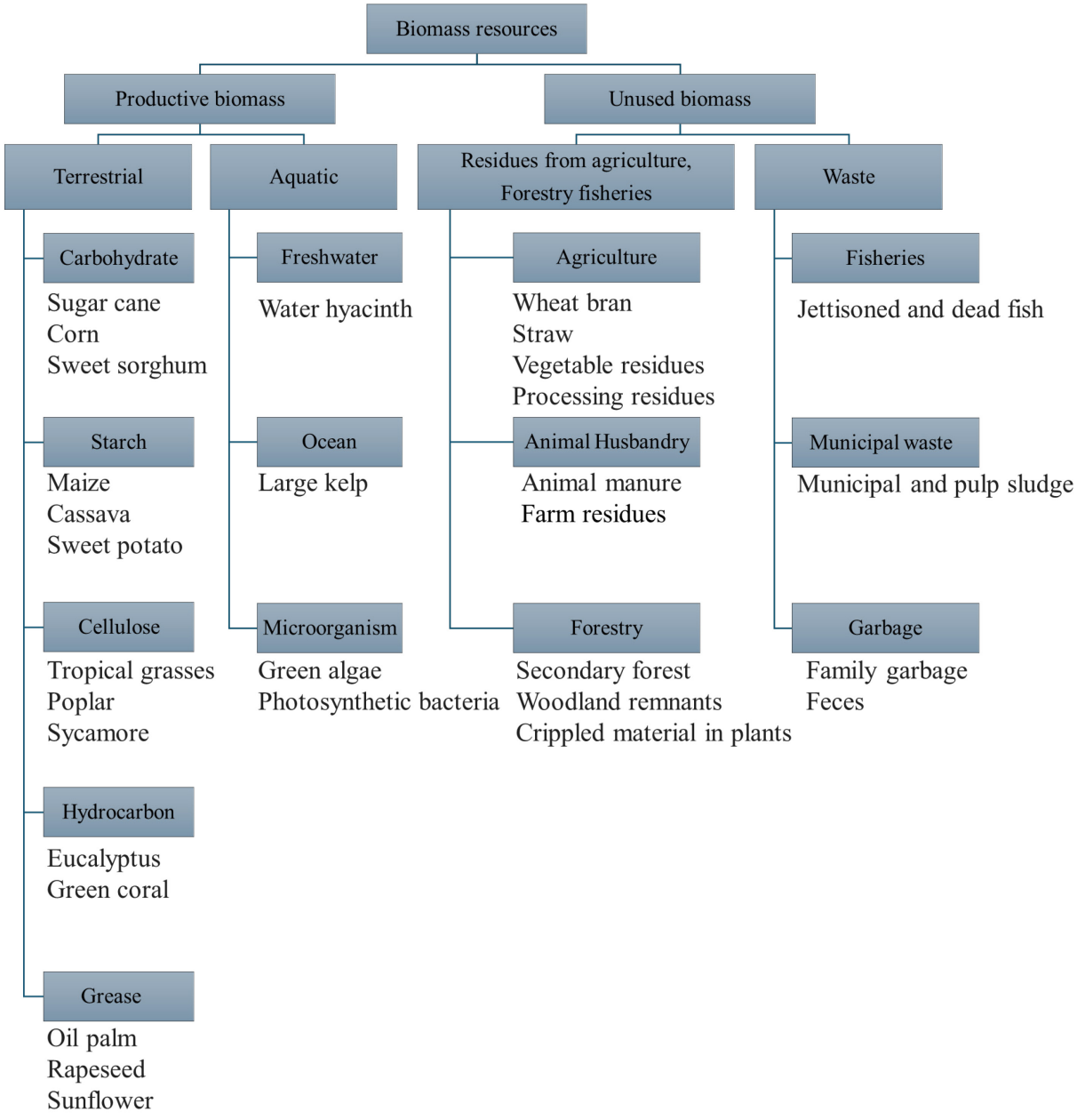

Figure 2.1 Classification of biomass resources[5].

Globally, high-yield crops such as corn, rice, wheat, potatoes, and sugarcane are rich in starch and soluble sugars, making them widely used as fermentation carbon sources in industrial applications to synthesize various bio-based chemicals [7, 8]. As shown in **Figure 2.2,** a

selection of representative bio-based chemicals derived from C1 to C6 carbon sources is presented[6], covering a range of monohydric alcohols, diols, and dicarboxylic acids. At present, high-value-added bio-based products such as ethanol [9-11], butanol [12], ethylene glycol [13], propylene glycol[14], succinic acid [15], ethylene[16, 17], butadiene[18], isoprene[19], itaconic acid [20], fumaric acid [21], lactic acid[22], and glycerol [23] have already been produced on an industrial scale. These developments have played a significant role in facilitating the transition of the chemical industry from dependence on fossil resources to the utilization of renewable biomass resources. The following section introduces several common chemicals, as well as those involved in this study, that can be derived from biomass.

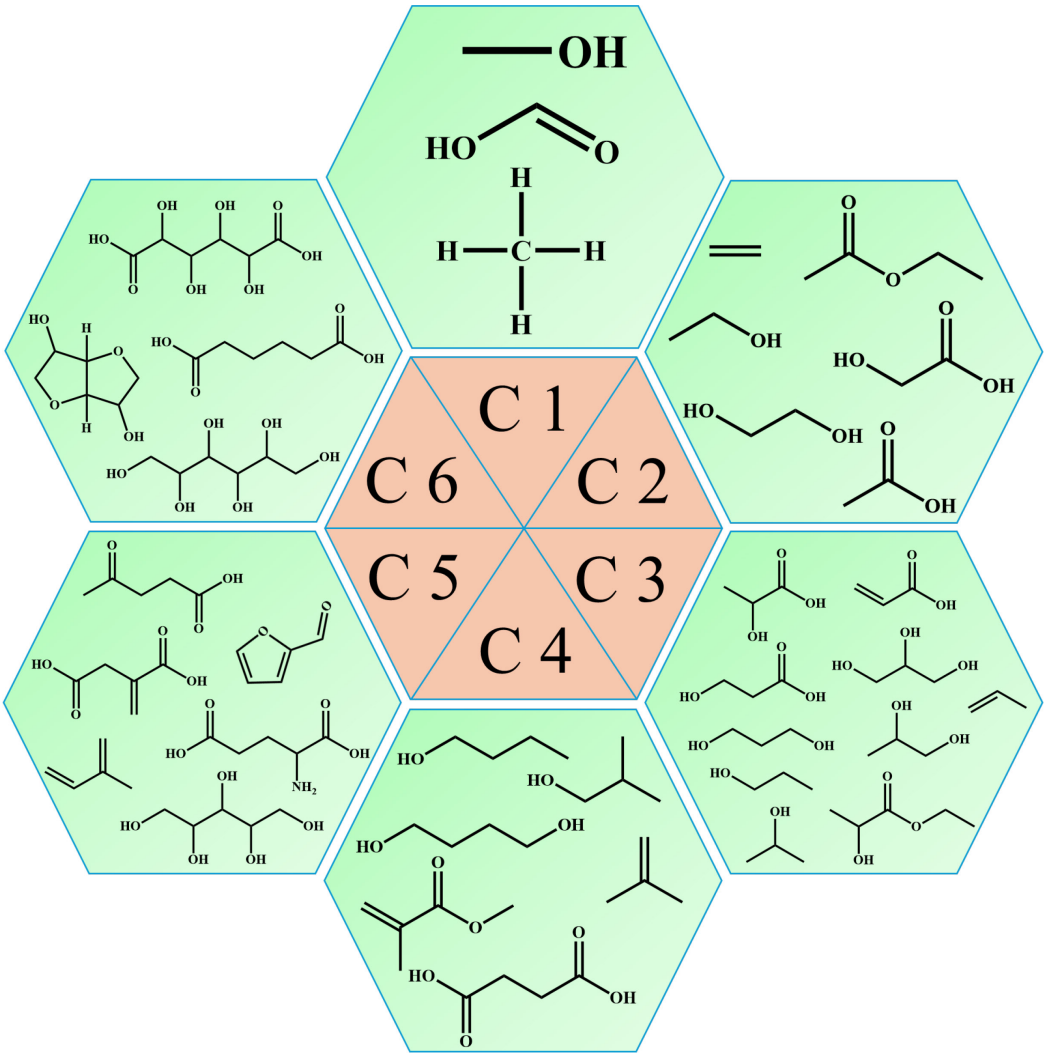

Figure 2.2 New, high value-added and bio-based chemicals derived from biomass[6].

2.2 Bio-based chemicals

2.2.1 Bio-based ethanol

Ethanol, commonly known as alcohol, is an organic compound with a wide range of applications. In recent years, in response to increasingly severe resource and environmental challenges, bioethanol has attracted significant attention as a clean and renewable energy source. Owing to its high oxygen content, ethanol can enhance the combustion of olefins in gasoline, thereby effectively reducing emissions of carbon monoxide and aromatic compounds. Additionally, ethanol has a high octane number, making it a valuable additive for improving the anti-knock performance of fuels [24]. Beyond its use as a fuel, ethanol also serves as a key platform chemical, enabling the production of a variety of high-value chemicals through catalytic transformations (**Figure 2.3**).

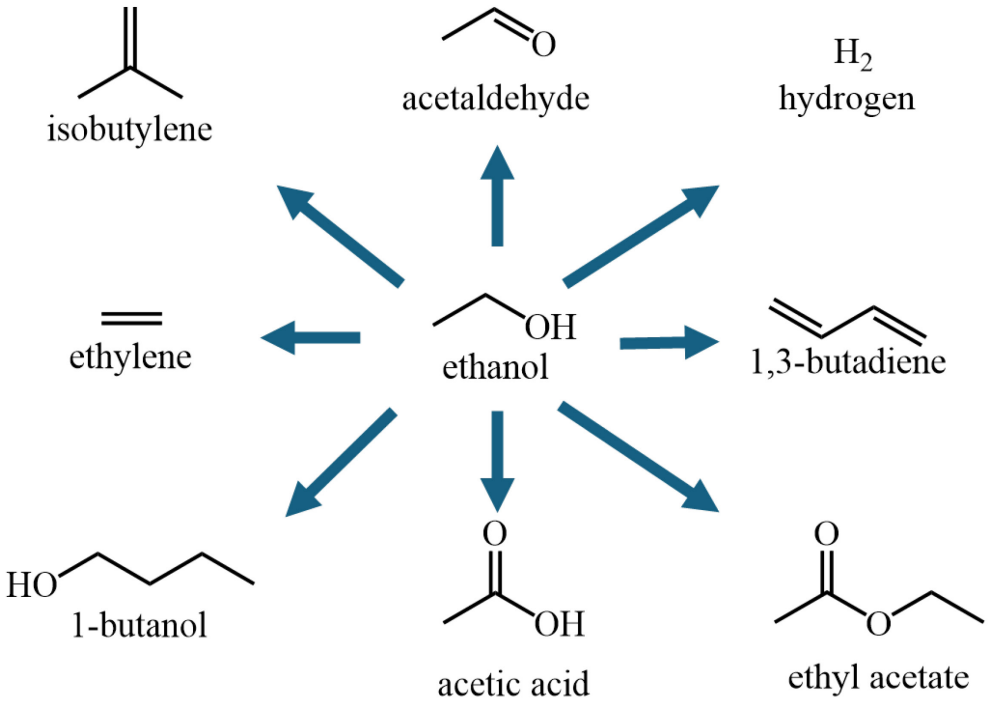

Figure 2.3 Conversion pathways of ethanol to various value-added chemicals[25].

Currently, bio-based ethanol is produced from a variety of agricultural feedstocks, such as corn, sugarcane, wheat, sugar beet, molasses, cassava, and cellulosic biomass[26].

First-generation bioethanol technology uses sucrose-rich crops (such as sugar cane and sugar beet) or starch-based crops (such as corn and wheat) as raw materials and has been

commercially produced on a large scale worldwide[26]. The United States (primarily using corn) and Brazil (primarily using sugar cane) are the two largest producers, accounting for approximately 80% of global production. Sugar cane processing consumes significantly less fossil energy compared to corn. Moreover, there is still potential to optimize bioethanol production processes from sugarcane, which could further reduce energy consumption[27]. However, first-generation bioethanol has raised concerns due to its impact on food prices and the competition between food and fuel, sparking widespread debate and criticism[28].

Second-generation bioethanol technology utilizes agricultural residues and lignocellulosic materials as feedstocks. With advancements in biotechnology, particularly synthetic biology, this technology is approaching maturity. Around the world, demonstration projects for cellulosic bioethanol production have been established[29, 30]. In China, the company China Venture Advanced Biofuel (Hailun) Co., Ltd. completed the country's first commercial-scale cellulosic bioethanol plant in Heilongjiang in April 2022, with an annual production capacity of 30,000 tons.

Third-generation bioethanol technology utilizes microalgae as feedstocks, particularly defatted microalgal biomass (DMB), have emerged as a promising renewable resource for bioethanol production. Rich in carbohydrates, microalgae can be pretreated through chemical, thermal, or enzymatic methods to break down complex carbohydrates into fermentable sugars, which can then be used in microbial fermentation to produce ethanol[31]. Numerous studies have demonstrated that various types of microalgae (such as pseudochoricystis ellipsoidea[32], dunaliella tertiolecta[33], and scenedesmus dimorphus[34]) can yield high sugar and ethanol conversion rates through chemical or enzymatic saccharification. In some cases, ethanol has been successfully produced even without any pretreatment. Overall, DMB is considered a highly promising feedstock for sustainable bioethanol production and is expected to play a significant role in future renewable energy development. Currently, several energy companies are accelerating their research and development efforts. For example, French energy giant TotalEnergies has partnered with Veolia to advance the development of microalgae cultivation technologies.

2.2.2 Bio-based n-butanol

As an important solvent-type bio-based chemical, n-butanol has a long history of research and development. As early as 1852, Wirtz discovered that n-butanol is a common component of fusel oil. Later, in 1862, Pasteur demonstrated through experiments that under anaerobic conditions, lactic acid or calcium lactate could be converted into butanol, revealing the potential for its biological synthesis. Since the late 19th century, the fermentation production of butanol and related solvents (such as acetone) has gradually become a research focus[35]. Between 1912 and 1916, the industrialization of acetone–butanol–ethanol (ABE) fermentation technology was achieved[36]. It became one of the earliest large-scale industrial fermentation processes.

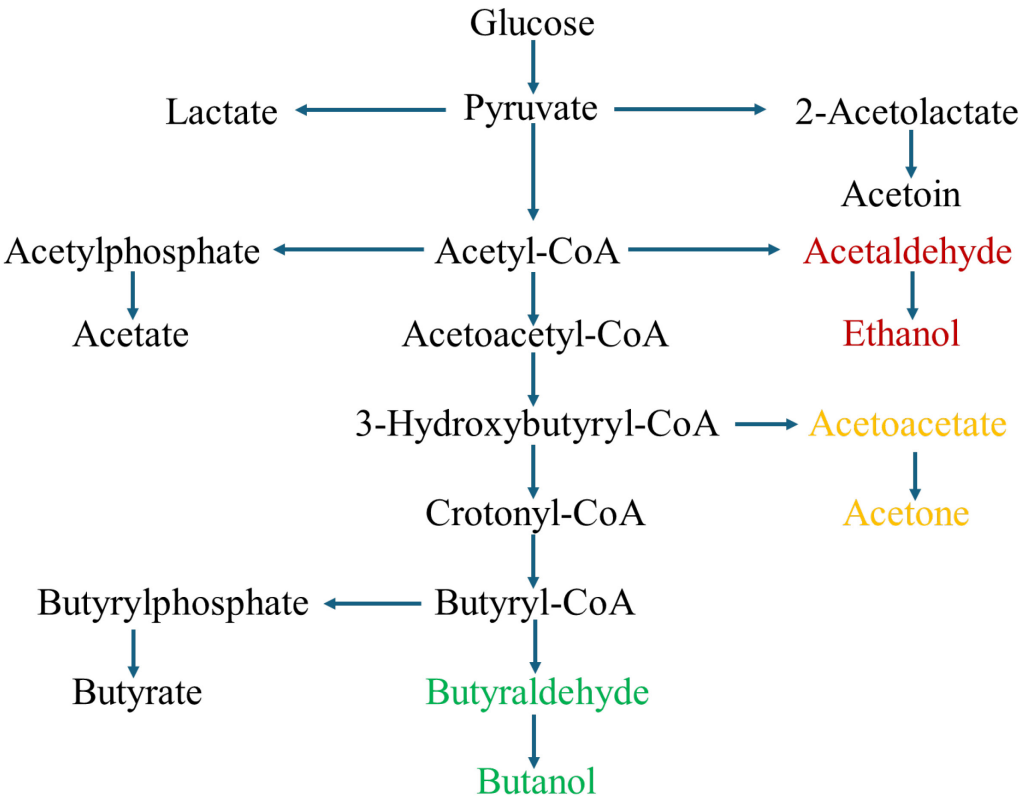

Figure 2.4 Schematic diagram of the metabolic pathway of clostridium acetobutylicum during the ABE fermentation process[37].

Figure 2.4 illustrates the metabolic pathway of clostridium acetobutylicum during the ABE fermentation process. Glucose undergoes glycolysis to form pyruvate, which is further converted into acetyl-CoA, serving as the starting point for the synthesis of multiple products.

Butanol is synthesized through a series of intermediates including acetoacetyl-CoA and butyryl-CoA; acetone is produced via the decarboxylation of acetoacetate; and ethanol is formed by the reduction of acetaldehyde. In addition to the main solvents, organic acids such as lactic acid, acetic acid, and butyric acid are also generated during the metabolic process[37].

Despite the efficiency of this natural metabolic route, the industrial utilization of ABE fermentation has undergone significant historical changes. In the 1950s, with the rapid rise of the petrochemical industry, the biological production of butanol was gradually replaced by petroleum-based chemical synthesis methods, resulting in a sharp decline in fermentation-based production. However, in recent years, driven by concerns over resource depletion, environmental sustainability, and the pursuit of renewable energy alternatives, microbial fermentation for butanol production has regained global attention and is experiencing a resurgence[38].

Given its dual significance in both industrial chemistry and renewable energy, n-butanol has attracted growing interest as a promising next-generation biofuel due to its excellent fuel properties. With an energy density close to that of gasoline, low volatility, low hygroscopicity, and good compatibility with both gasoline and diesel, it can be directly used in existing engine systems without the need for significant infrastructure modifications. Compared to ethanol and biodiesel, n-butanol produces less soot and carbon emissions during combustion, contributing to improved environmental performance[39-41]. Furthermore, with ongoing improvements in production and fermentation technologies, the sustainable production of n-butanol continues to advance, supporting its wider adoption as a fossil fuel alternative.

2.2.3 Bio-based ethylene

As one of the most widely produced basic chemicals in the world, ethylene is a key raw material in the petrochemical industry and is used in the synthesis of a variety of essential chemicals and polymer materials, such as polyethylene, polyvinyl chloride, glycolic acid, and ethylene oxide[42, 43]. Currently, about 99% of global ethylene is derived from petroleum or natural gas through high-temperature cracking of hydrocarbons[17]. However, with the gradual

depletion of petroleum resources and growing concerns over environmental sustainability, the search for alternative production routes has become increasingly urgent.

Among the various alternatives, the production of ethylene from renewable biomass is gaining increasing attention. In particular, the process of producing ethylene through catalytic dehydration of bioethanol has emerged as one of the most promising bio-based approaches. This method involves first fermenting starch, lignocellulose, or other biomass feedstocks to produce ethanol, which is then dehydrated at high temperatures in the presence of suitable catalysts (such as alumina or phosphoric acid) to generate ethylene. The process offers advantages such as high selectivity and relatively mild reaction conditions, and it has already been gradually industrialized and widely recognized[16, 44, 45].

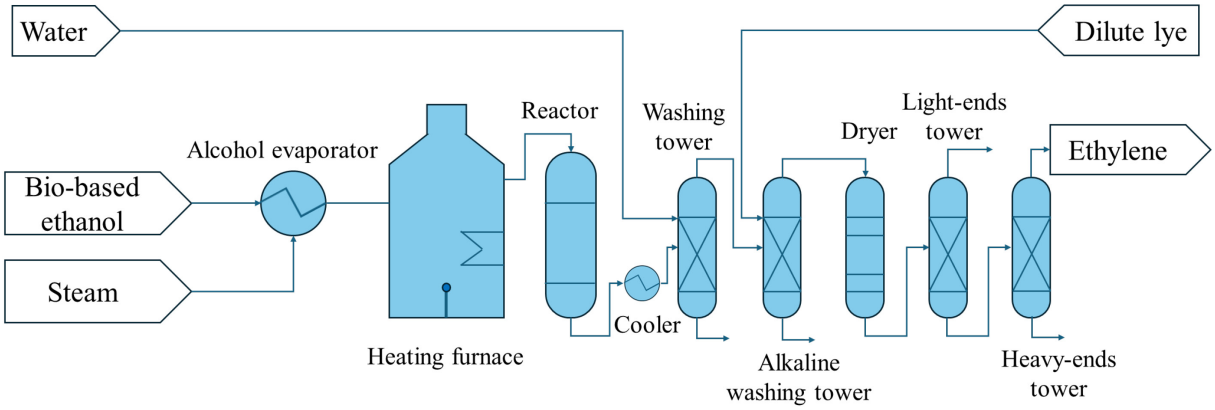

Figure 2.5 Typical process flow diagram for ethylene production via bioethanol dehydration[17].

The process of ethanol dehydration to ethylene mainly involves three steps[17]: preheating, reaction, and purification, as shown in **Figure 2.5**. First, the ethanol feedstock is heated and vaporized through a heat exchanger, then enters the reactor where it undergoes a dehydration reaction at high temperature in the presence of a catalyst to produce crude ethylene gas. The gas then passes through a water scrubber and a caustic scrubber to remove moisture and acidic impurities. Next, it enters a dryer to further eliminate residual water. After drying, the gas flows into a light-ends column and a heavy-ends column, where light gases and high-boiling-point byproducts are separated, respectively. Finally, purified ethylene is obtained from the top of the heavy-ends column.

Compared to other bio-based pathways, such as the dehydration of propanol or butanol to produce olefins[46], the ethanol dehydration route stands out due to its maturity, wide

availability of feedstocks, and strong economic viability. As a result, ethanol dehydration to ethylene is currently the only commercially implemented technology for producing bio-based ethylene.

2.2.4 Bio-based butadiene

From the historical development of synthetic rubber, butadiene monomer has played a central role, forming one of the foundational pillars of the industry. Globally, the annual demand for butadiene exceeds 16 million tons, primarily used in the production of various synthetic rubbers through homopolymerization or copolymerization with other olefinic monomers. These include styrene-butadiene rubber (SBR), polybutadiene rubber (BR), nitrile rubber (NBR), as well as acrylonitrile-butadiene-styrene (ABS) resins.

In the petrochemical sector, butadiene is mainly produced through two primary routes: the first and dominant method is as a byproduct from steam cracking of naphtha for ethylene production—accounting for over 95% of global butadiene supply[47]; the second method involves catalytic dehydrogenation of butane or oxidative dehydrogenation of butene[48]. Since 2008, the economic advantages of shale gas in North America have shifted steam cracking feedstocks from naphtha to lighter alkanes such as ethane and propane, significantly reducing the output of byproduct butadiene and creating tighter supply. Countries such as China, Europe, Poland, and Australia are now actively developing ethylene production strategies based on shale gas, further impacting global butadiene availability.

At the same time, the environmental impact of petroleum-based butadiene production is a growing concern. Current processes emit around 200 million tons of CO_2 annually, contributing substantially to global climate change. Against the backdrop of stricter environmental regulations and shifting feedstock structures, developing sustainable and low-carbon pathways for butadiene production has become an urgent and critical area of research and industrial focus.

Against the backdrop of increasing pressure for sustainable raw material supply and environmental protection, the process of producing butadiene from bio-based ethanol has regained attention. Bioethanol, as a renewable carbon source, can be obtained via fermentation

of first-generation biomass such as sugars and corn, while second-generation bioethanol is derived from lignocellulosic materials like wood and agricultural residues. According to Patel's evaluation, compared to the conventional naphtha-based route, producing 1 kg of butadiene from bioethanol can reduce CO_2 emissions by approximately 1.5 kg, offering a clear environmental advantage[49].

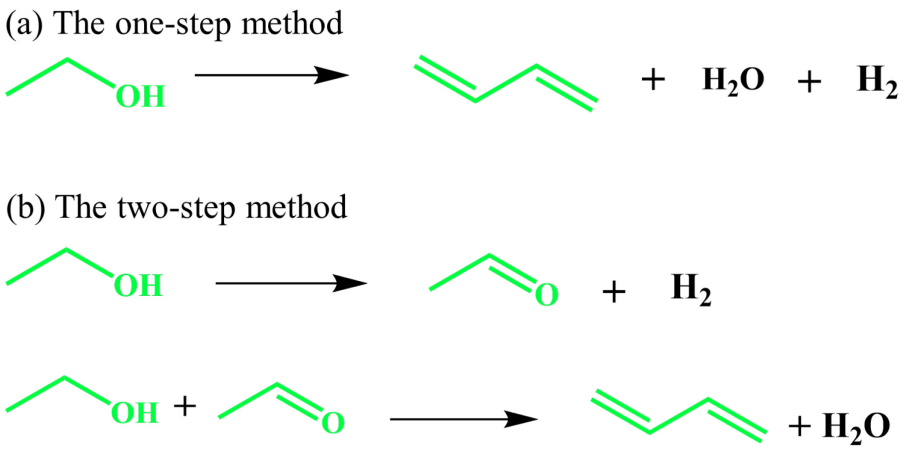

Figure 2.6 Preparation of butadiene by bio-based ethanol[50, 51].

The ethanol-based synthesis of butadiene mainly follows two technical routes, as shown in **Figure 2.6**: the one-step method and the two-step method. The one-step method involves the direct conversion of ethanol into butadiene through a single reaction process that includes dehydrogenation, condensation, dehydration, and other steps[50]. This method was first proposed by Ipatiev in 1903. Although the initial yield was only 1.5%, it laid the foundation for subsequent research. Later, researchers such as Ostromyslensky and Lebedev further optimized the reaction conditions and catalyst systems. Notably, Lebedev developed a $ZnO–Al_2O_3$ catalyst that achieved a selectivity of 18% at 400 °C, which was later improved to up to 70%. German company I.G. Farbenindustrie and American researchers also investigated MgO-based catalysts, reaching yields of up to 60%. However, the industrial application of this method has been limited. The two-step method was developed based on the theoretical proposal by Ostromyslensky[51]. In this route, ethanol is first partially dehydrogenated to acetaldehyde, which then reacts with unconverted ethanol in the presence of a catalyst to form butadiene. This pathway has a clearer reaction mechanism and is easier to control. Union Carbide and Carbon Chemicals Corporation in the United States successfully implemented this method on an

industrial scale using a tantalum oxide catalyst supported on silica (Ta_2O_5/SiO_2), achieving 30% ethanol conversion and 18% butadiene yield per pass[52].

With the advancement of bio-fermentation technology, the variety of bio-based monomers has significantly increased, prompting researchers to explore more routes for the production of bio-based butadiene, as illustrated in **Figure 2.7**. The diagram illustrates three methods for producing 1,3-butadiene[52]. (1) The bio-based butanol dehydration–dehydrogenation method starts with butanol (n-butanol and its isomers) obtained from biological fermentation. Under acid catalysis, butanol is first dehydrated to produce butenes, which are then converted into butadiene through an industrial dehydrogenation process[53, 54]. Butanol is typically produced via ABE fermentation, which yields acetone, butanol, and ethanol as the main products[55, 56]. Although the dehydrogenation of butenes requires high temperatures and thus consumes significant energy, this route is compatible with existing industrial infrastructure and has strong potential for scale-up. (2) The bio-based butanediol (BDO) dehydration method uses bio-derived diols such as 1,4-butanediol[57], 2,3-butanediol[52, 58, 59], or 1,3-butanediol[60, 61] as feedstocks. These compounds undergo catalytic double dehydration to form butadiene. 1,4-BDO can be synthesized from acetylene and formaldehyde followed by hydrogenation, or it can be biologically produced via engineered microbial fermentation of sugars. 2,3-BDO is accessible through sugar or syngas fermentation. 1,3-BDO can be obtained from non-food biomass through fermentation processes. In March 2025, Wanhua Chemical Group in China completed and commissioned the world's first 10,000-ton-per-year bio-based 1,3-BDO production facility. The plant uses proprietary patented technology with innovative catalysts and process design, significantly improving raw material utilization. (3) The tetritol deoxydehydration (DODH) method utilizes four-carbon sugar alcohols (tetritols) obtained from the fermentation of biomass[62-64]. These are converted into butadiene through a one-pot liquid-phase deoxydehydration reaction catalyzed by homogeneous rhenium complexes. However, the industrial availability of tetritols is currently limited, and their high production costs have kept this method at the laboratory stage. Despite this, it offers a novel and sustainable approach for green butadiene synthesis. With the continuous advancement of bio-based

butadiene production technologies, large-scale manufacturing is expected in the near future, gradually replacing petroleum-based butadiene as a monomer for the synthesis of bio-based polybutadiene or bio-based styrene-butadiene rubber.

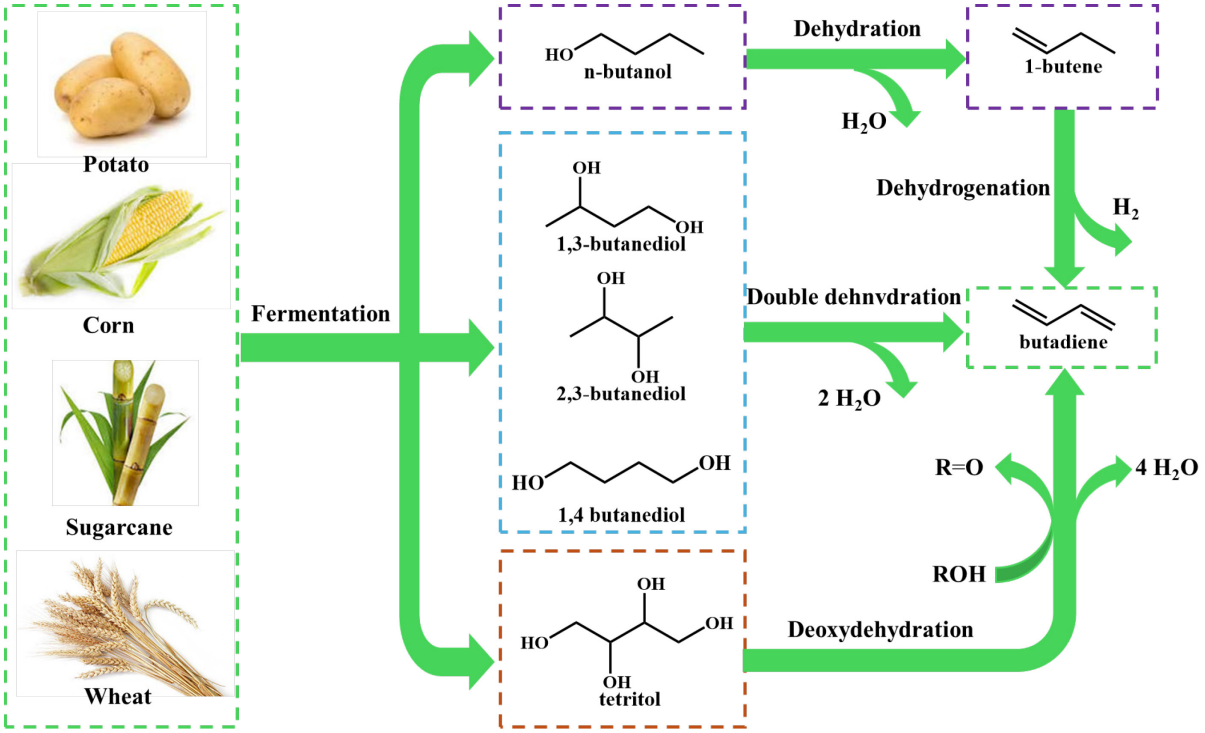

Figure 2.7 Production routes of bio-based 1,3-butadiene[52].

2.2.5 Bio-based isoprene

Isoprene is widely used in the industrial sector, with approximately 95% utilized in the production of rubber, particularly polyisoprene, which is further processed into products such as tires, medical gloves, footwear, golf balls, rubber bands, and condoms. The remaining 5% finds applications in the manufacture of pharmaceuticals, flavorings, perfumes, aviation fuels, and epoxy resin curing agents[19]. As early as 1860, C.G. Williams first isolated isoprene by pyrolyzing natural rubber, named the compound, and correctly deduced its chemical structure. Today, isoprene is almost entirely sourced from fossil fuels, typically obtained through the cracking of C5 fractions or the dehydrogenation of C5 isoparaffins and isoolefins[65]. However, petroleum-based production methods are associated with high energy consumption, elevated costs, low yields, and significant environmental pollution[66]. Therefore, developing greener and more sustainable technologies for isoprene production has become an urgent priority.

At present, a relatively mature method is to combine microbial fermentation and chemical catalysis to synthesize bio-based isobutene[19], and then obtain isoprene through the aldol reaction; Sumitomo Chemical has proposed replacing formaldehyde with methanol and oxygen to simplify the process. However, this route relies on the economic viability of bio-based isobutene, which is usually prepared by dehydration of isobutanol. The overall process is complex, involves multiple transformation steps, and produces many by-products, making large-scale application difficult in the short term.

It is worth noting that in 2017, Abdelrahman et al[67]. proposed a new route using industrially produced bio-based itaconic acid, which is first hydrogenated catalytically to form 3-methyl-tetrahydrofuran, and then undergoes dehydrogenation and ring-opening to obtain bio-based isoprene. In 2020, Heracleous et al[68]. also proposed synthesizing isoprene from bio-based mevalonolactone acid through decarboxylation, but this method releases CO_2 during the process, posing environmental concerns. In general, routes developed from mature bio-based platform compounds have greater industrialization potential, but still require optimization in conversion efficiency and cost control.

Another promising approach for the production of bio-based isoprene is biosynthesis. In fact, isoprene is widely present in the natural environment and is emitted by plants, animals, bacteria, and humans, with plants being the largest contributors—releasing approximately 600 million tons annually[69]. This naturally produced isoprene through the carbon cycle is theoretically sufficient to manufacture 60 billion automobile and truck tires, which is 50 times the current global annual tire production of about 1.2 billion units[70]. However, due to fluctuations in the release cycle and the difficulty of collection, it is economically unfeasible to directly harvest isoprene from plants or animals.

Inspired by the release mechanisms in plants, researchers have turned to microorganisms with fast reproduction, short cultivation cycles, and suitability for large-scale production to achieve controlled isoprene production through aerobic fermentation using sugar-based biomass. Unlike other bio-based monomers, isoprene has a low boiling point (34 °C) and low water solubility, which allows it to be collected in gas form during fermentation. This offers

several potential advantages: reduced feedback inhibition, high-purity recovery, and lower substrate purity requirements[71].

Currently, the biosynthesis of isoprene precursors—IPP (isopentenyl pyrophosphate) and DMAPP (dimethylallyl pyrophosphate)—from carbon sources can be achieved through two primary metabolic pathways[72], as shown in **Figure 2.8**: the mevalonic acid (MVA) pathway[73-75], which starts from acetyl-CoA, and the methylerythritol-4-phosphate (MEP) pathway[76], which uses pyruvate and glyceraldehyde-3-phosphate (G3P) as substrates. The MVA pathway is widely found in eukaryotes and some archaea. It begins with the condensation of two molecules of acetyl-CoA to form acetoacetyl-CoA, followed by a series of enzymatic reactions leading to the production of mevalonate. Mevalonate is then phosphorylated and decarboxylated to generate IPP. In contrast, the MEP pathway is mainly present in many bacteria and the chloroplasts of plants. It starts with pyruvate and G3P, which are converted into 1-deoxy-D-xylulose-5-phosphate (DXP). This compound (DXP) undergoes several enzymatic transformations, including the formation of 2-C-methyl-D-erythritol-4-phosphate (MEP) as a key intermediate, eventually leading to the synthesis of isopentenyl pyrophosphate (IPP) and dimethylallyl pyrophosphate (DMAPP), which serve as precursors for isoprene synthesis. Both pathways can be optimized through synthetic biology approaches to enhance the efficiency and yield of isoprene production, offering a sustainable solution for the bio-based chemical industry.

In recent years, extensive research has been conducted on carbon source selection, strain optimization, and the modification or development of new variants of the key enzyme—isoprene synthase (ISPS). Low-cost carbon sources that have been developed include biomass (glucose, sucrose)[77], methanol[78], syngas[79] and wastewater[80]. Commonly used engineered strains include escherichia coli[81], bacillus subtilis[82], saccharomyces cerevisiae[83], cyanobacteria[84], ralstonia eutropha[85], and clostridium species[86]. These studies continue to advance isoprene biosynthesis systems toward higher efficiency, lower costs, and greater environmental compatibility.

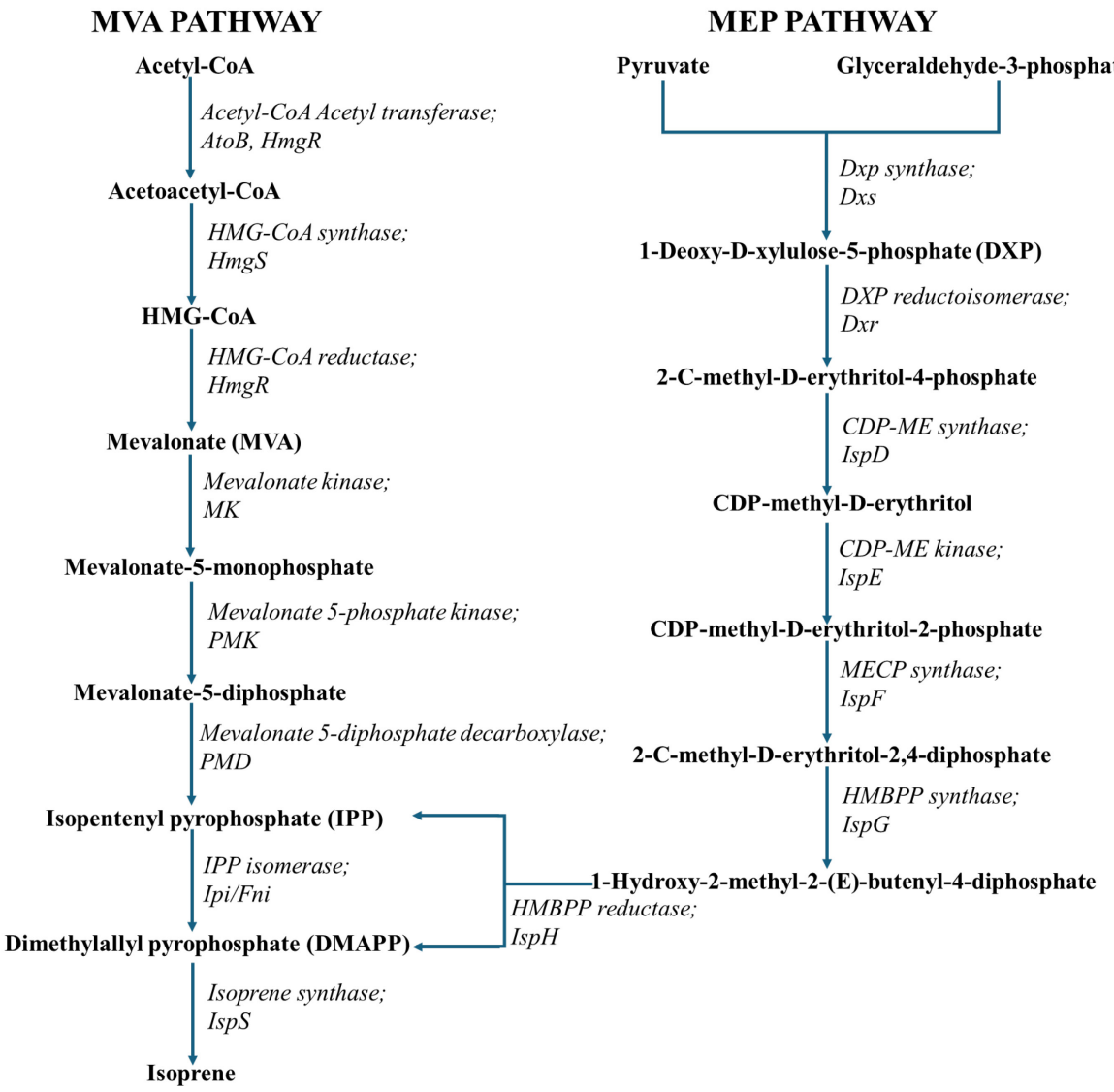

Figure 2.8 Metabolic pathways for the biosynthesis of IPP and DMAPP via the MVA and MEP routes[72].

2.2.6 Bio-based itaconic acid

Itaconic acid was first identified in 1931 when it was discovered to be produced by the fungus Aspergillus itaconicus in biological systems[87]. However, it was not until the 1960s that the biotechnological production of itaconic acid began to take off, primarily through fermentation processes involving Aspergillus terreus, which became the predominant microorganism used in industrial production[88]. Over time, other microorganisms have been identified as potential producers of itaconic acid, expanding the range of biotechnological options. These include fungi like Ustilago maydis[89, 90], Candida rugosa[91], Aspergillus terreus[92]. Each of these strains has unique metabolic pathways and environmental

requirements that make them interesting for different production scenarios. For instance, Ustilago maydis is a plant pathogen known for its ability to produce a range of secondary metabolites, including itaconic acid[93], while Candida rugosa is known for its versatility in producing other valuable compounds in addition to itaconic acid[94]. The raw materials for producing itaconic acid via fermentation are widely available, and the resulting bio-based products have minimal environmental impact and high safety, making this method the primary approach for itaconic acid production. Various strains can ferment raw materials like discarded straw, beets, wastewater, sucrose, xylose, molasses, and glycerol to produce itaconic acid.

The structure of itaconic acid is shown in **Figure 2.9**, and from a structural perspective, it is a C5 dicarboxylic organic acid with α,β-unsaturated functionality. The various functional groups in its molecule make it an effective intermediate for the preparation of numerous organic compounds, serving as a fundamental unit in chemical synthesis. This figure illustrates the conversion pathways of itaconic acid into various high-value compounds through different chemical reactions[95]. Itaconic acid can undergo hydrogenation to form products such as 2-methyltetrahydrofuran, 3-methyltetrahydrofuran-2-one, methylitaconic acid, and 2,3-butanediol. Through decarboxylation, it can be converted into methacrylic acid[96]. Reaction with ammonia results in the formation of itaconic diamide. Under reductive amination conditions, itaconic acid can be transformed into nitrogen-containing compounds such as 5-methyl-2-pyrrolidone, N-methylpyrrolidine, 3,5-dimethyl-2-pyrrolidone, and 2-methyl-1,5-pentanediamine. The design of these derivatives and their potential contribution to a more sustainable polymer industry make itaconic acid a platform chemical well worth further development[97-100].

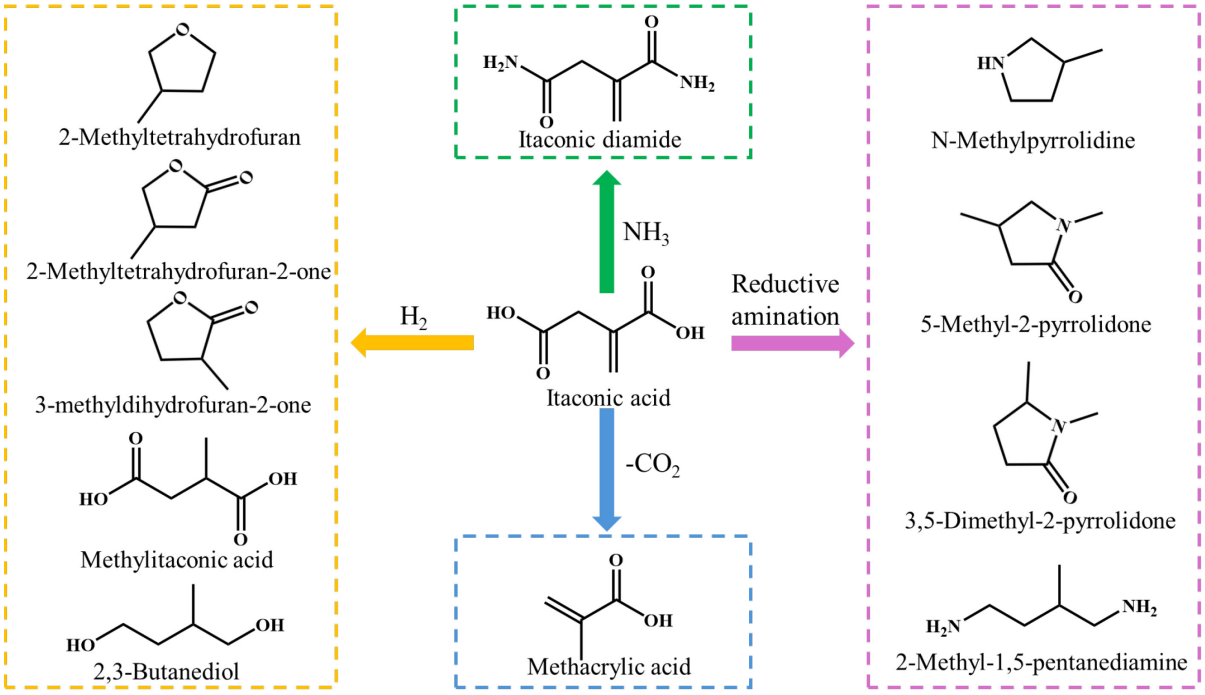

Figure 2.9 Itaconic acid and its typical derivatives[95].

The biotechnological pathway for itaconic acid production yields high output and is currently the primary method used in industrial production. China, the United States, and India are the world's leading producers of itaconic acid[101]. Itaconic acid can also be synthesized through chemical methods; however, due to the need for multiple steps and the low efficiency of these methods, chemical synthesis has not been commercialized. The commercial production of itaconic acid began with Pfizer in the mid-20th century [102]. Following World War II, several other companies entered the market, including Iwata Chemical in Japan, Rhodia in France, Cargill in the United States, Alpha Chemik in India, and Qingdao Langyatai Group Co., Ltd. in China[103, 104]. In 2004, the U.S. Department of Energy recognized itaconic acid for its potential in large-scale, sustainable production, as well as its non-toxic properties, naming it one of the "Top 12 Value-Added Chemicals from Biomass"[105]. In 2022, the global itaconic acid market was valued at 101.5 million USD. It is estimated that the market will grow at a rate of 4.20% from 2022 to 2027, reaching an estimated value of 127.04 million USD by 2027. The industrialization and improved economic viability of itaconic acid bring promising prospects for bio-based materials, with high demand for these materials further driving the itaconic acid market[106, 107].

2.3 Bio-based synthetic elastomers

2.3.1 Bio-based itaconate elastomers

Bio-based itaconate elastomers (BIE) are a type of rubber developed originally in China and are obtained by polymerizing itaconate with conjugated dienes. The bio-based itaconate monomers are produced via esterification reactions between itaconic acid and monohydric alcohols, while the introduction of dienes not only increases the flexibility of the molecular chain but also provides double bonds for subsequent cross-linking of the elastomers. Bio-based itaconate elastomer was first reported by Wang et al.[108], who synthesized a new cross-linkable, high molecular weight poly(diisoamyl itaconate-*co*-isoprene) (PDII) elastomer via emulsion polymerization. **Figure 2.10** shows the schematic illustration of the synthesis of di-isoamyl itaconate and its copolymerization with isoprene. When the mass ratio of diisoamyl itaconate to isoprene was 80/20, the molecular weight reached as high as 352,000 g/mol. Compared to traditional petroleum-based rubbers, the most significant distinction lies in the presence of numerous polar ester groups in BIE, which can form strong hydrogen bonds with "green fillers" such as silica, thereby improving filler dispersion. Subsequently, with a focus on tire tread applications, Lei, Zhou, and Ji successively developed poly(itaconate-*co*-isoprene) (PDBII) [109] with varying side chain lengths, fully bio-based poly(diethyl itaconate-*co*-myrcene) (PDEIMy) [110], poly(dibutyl itaconate-*co*-butadiene) (PDBIB) [111] with different copolymer ratios, significantly advancing the structural design and optimization of BIE.

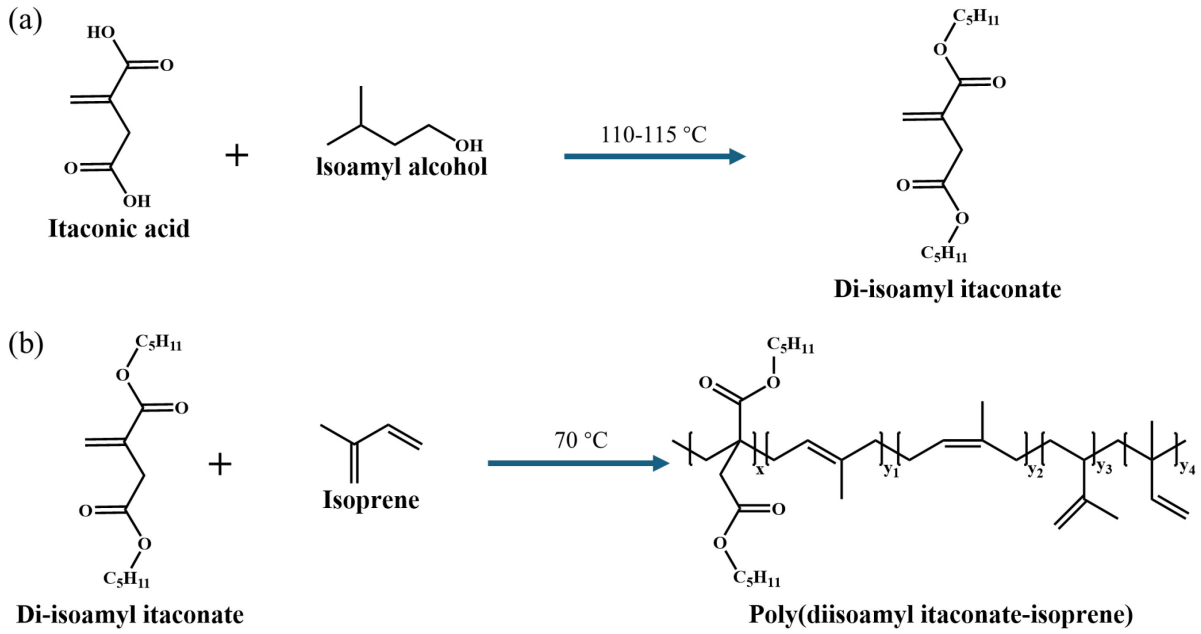

Figure 2.10 Schematic illustration of the synthesis of di-isoamyl itaconate and its copolymerization with isoprene[108].

Meanwhile, based on itaconate rubber, Beijing University of Chemical Technology and Shandong Linglong Tire Co., Ltd. jointly developed a compatible processing route and, for the first time, successfully completed the pilot production of bio-based green tires on an industrial production line[112]. The trial process is shown in **Figure 2.11** (a–e). The resulting tires performed well in terms of dynamic balance and uniformity, and their rolling resistance was evaluated using the MTS rolling resistance testing system (**Figure 2.11** (f)), yielding a rolling resistance coefficient of 7.22 N/kN. To further assess safety performance under complex road conditions, wet braking tests were conducted at a dedicated proving ground (**Figure 2.11** (g)), with a measured wet grip index of 140.7. Both performance indicators meet the B-grade criteria of the European Tire Labeling Regulation 1222/2009. The tires can be produced on existing industrial equipment without the need for modification, showing strong potential for large-scale application in passenger vehicles. At present, the product is moving rapidly into performance evaluation and market promotion phases.

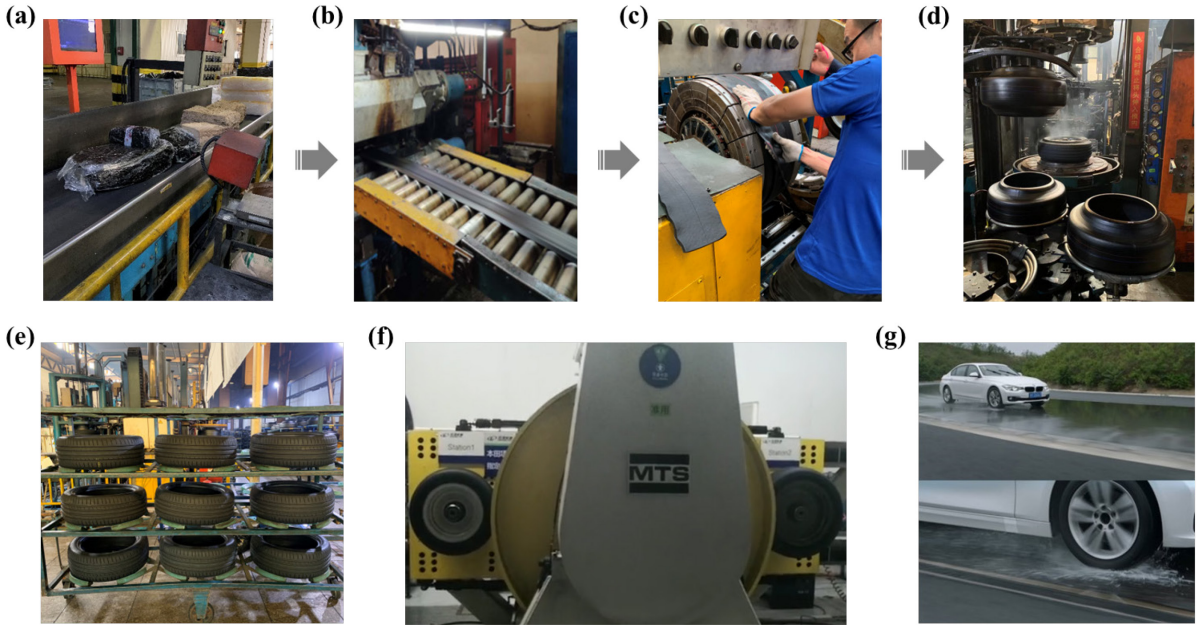

Figure 2.11 Bio-based green tire trial production: (a) Mixer mixing; (b) Tread extrusion; (c) Tread bonding; (d) Vulcanization; (e) Green tire finished product; (f) MTS rolling resistance test; (g) Tire loading test.

2.3.2 Bio-based polyester elastomers

Bio-based polyester elastomers are typically synthesized through the polymerization of renewable diacids and diols. Depending on their cross-linking mechanisms, they can be classified into in-situ cross-linking polyester elastomers and chemically cross-linkable polyester elastomers. Zeimaran [113] synthesized a biodegradable elastomer, poly(1,8-octanediol citrate) (POC), via a polycondensation reaction between citric acid and 1,8-octanediol， as shown in **Figure 2.12**. While POC exhibits excellent biocompatibility and degradability, its inherently poor mechanical strength limits its broader application. To address this, the research team blended POC with the natural polymer chitosan (CS), fabricating POC/CS blend films with varying compositions. The study demonstrated that the incorporation of chitosan significantly enhanced the tensile strength and elastic modulus of the films, while also improving surface roughness and pH stability. More importantly, in vitro experiments showed that the blend films provided excellent adhesion and proliferation of human dermal fibroblasts (HDFs). Besides citric acid, monomers such as glycerol, xylitol, sorbitol, and mannitol can also be used for the synthesis of bio-based polyesters[114-120].

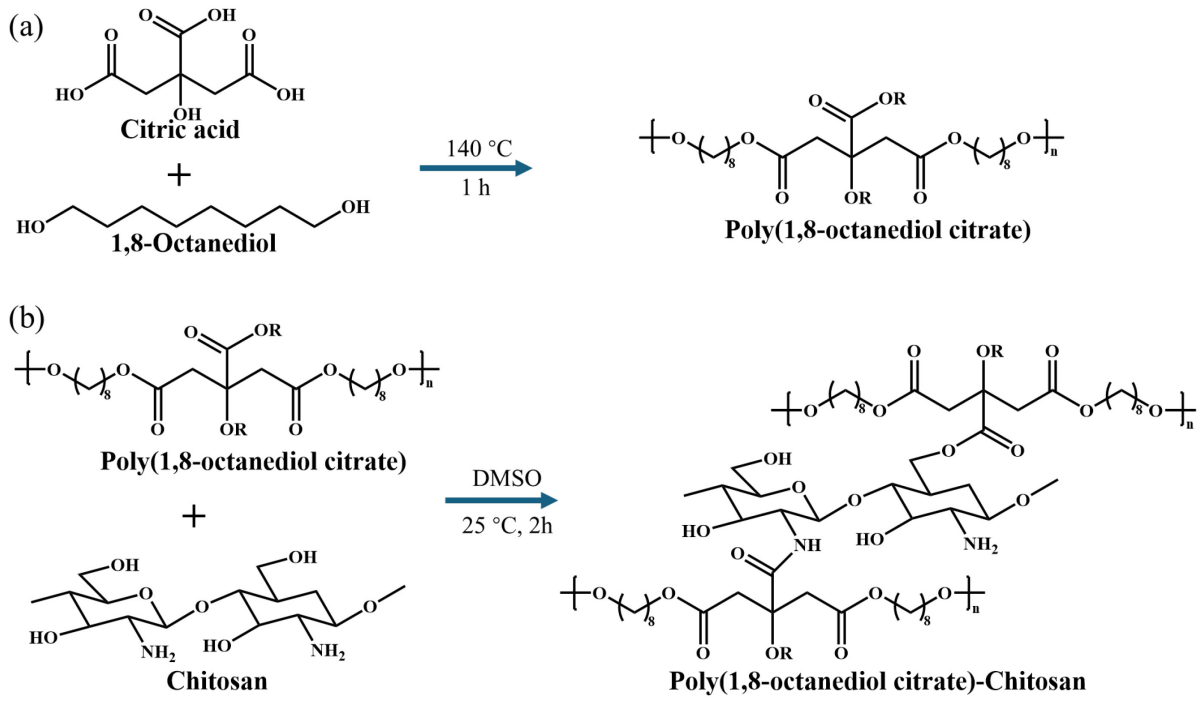

Figure 2.12 Schematic illustration of the synthesis of poly(1,8-octanediol citrate) and its modification with chitosan[113].

Wei et al. [121] were the first to synthesize a primary generation of poly(1,4-butanediol/1,3-propanediol/sebacate/itaconate/succinate) using 1,3-propanediol, 1,4-butanediol, succinic acid, sebacic acid, and itaconic acid as monomers. The synthesis route is schematically illustrated in **Figure 2.13**. The resulting polymer had a number-average molecular weight of approximately 33,000 g/mol. After reinforcement with silica and cross-linking via peroxides, the composite exhibited excellent mechanical performance, with a tensile strength exceeding 20 MPa. Hu et al. [122] introduced lactate units into the polyester backbone to develop a novel lactate-based polyester elastomer, which was used as a toughening agent for polylactic acid (PLA). The study showed that the incorporation of lactate improved the compatibility with PLA and significantly enhanced its toughness. Tang et al. [123]incorporated diethylene glycol into the polymer structure, which improved both cold resistance and oil resistance, contributing to the development of low-temperature, oil-resistant rubber materials.

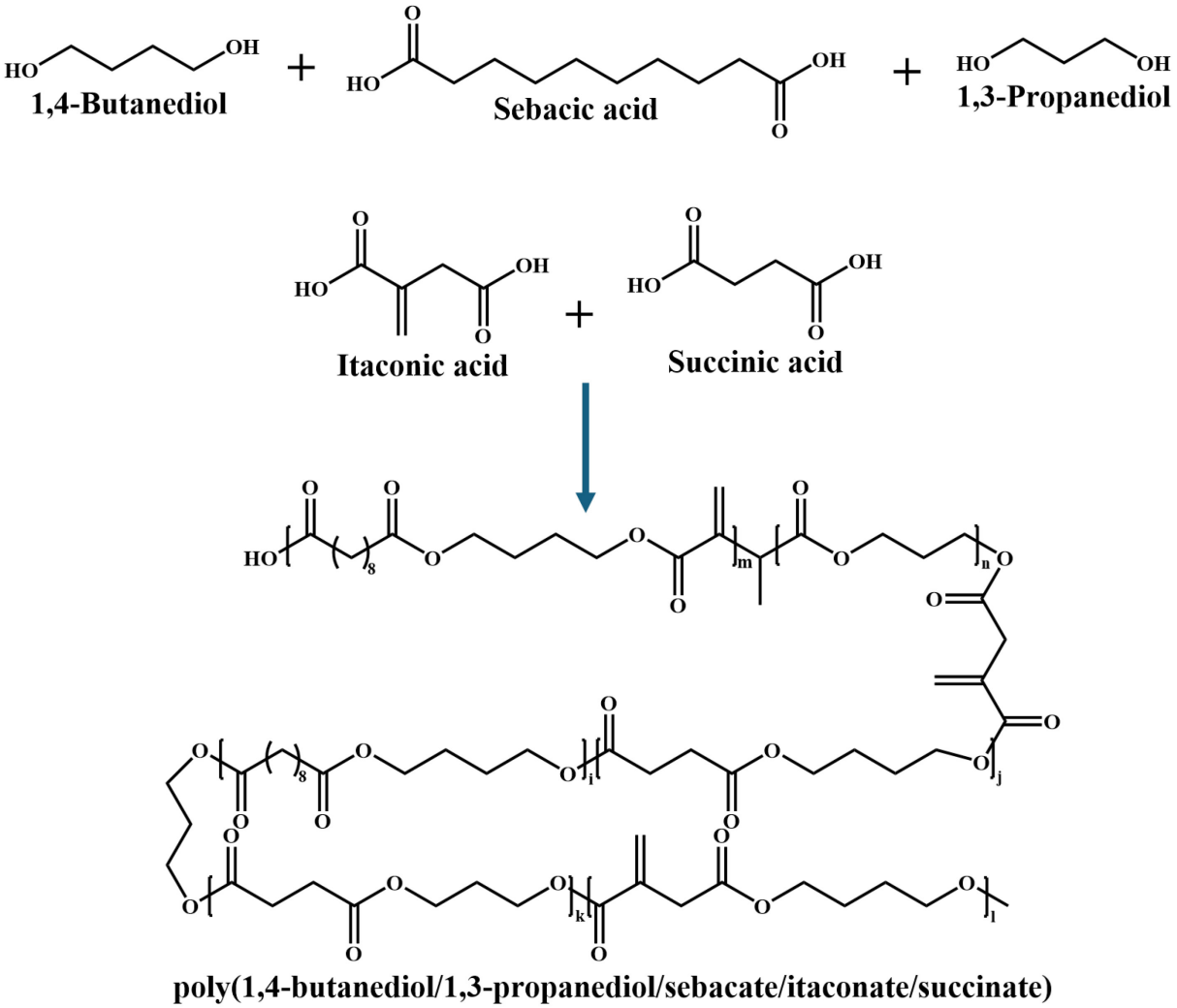

Figure 2.13 Schematic illustration of the synthesis route for poly(1,4-butanediol/1,3-propanediol/sebacate/itaconate/succinate) [121].

This research team has since optimized the stability of double bonds within the polymer chains and successfully constructed a processable molecular structure suitable for large-scale production. They achieved continuous production at the kiloton scale, with the polymer's molecular weight exceeding 80,000 g/mol. Based on this progress, they also developed the world's first biodegradable bio-based tire prototype. Under controlled composting conditions (ISO 14855), tire wear particles demonstrated a degradation rate of over 70%, offering a promising solution to the issue of microplastic pollution from tires. Some of these biodegradable products—such as bio-based cold-resistant oil-resistant rubber, PLA toughening agents, and eco-friendly casual shoes—are currently undergoing market validation. In 2023, Jiangsu Henghui Safety Co., Ltd. began constructing a 10,000-ton production line for bio-based

polyester engineering elastomers, signaling that large-scale commercialization of domestically produced, environmentally friendly high-performance elastomers are on the horizon.

2.3.3 Bio-based thermoplastic polyurethane elastomers

Polyurethanes are typically synthesized through addition reactions involving polyisocyanates, oligomeric polyols, and chain extenders. The hard segments in polyurethane elastomers are commonly derived from traditional petrochemical-based polyisocyanates such as p-phenylene diisocyanate (PPDI), 4,4'-methylenediphenyl diisocyanate (MDI), and isophorone diisocyanate (IPDI), which are currently difficult to obtain from biomass resources. In recent years, several bio-based polyisocyanates have been commercialized. For instance, Mitsui Chemicals developed the world's first bio-based isocyanate—1,5-pentamethylene diisocyanate (PDI)—with a biocarbon content of 70%; Covestro introduced the aliphatic trimeric isocyanate Desmodur® CQ N 7300, which contains 68% biocarbon; and Anhui Fengyuan Group established a 300-ton-per-year production line for lysine-based diisocyanates, with a biocarbon content of 80%[124, 125].

Additionally, some bio-based cyclic carbonates, such as bis(cyclic carbonate) derivatives from vanillin or limonene, have been proposed as alternative hard segment monomers to replace isocyanates[126, 127]. In comparison, bio-based soft segments are more readily available and better developed. For example, Parcheta et al.[128] prepared linear fully bio-based polyester polyols (M_n 2000–2500 g/mol) from succinic acid and propanediol; and Yuan et al. [129] produced hydroxyl-terminated poly(γ-butyrolactone) diols through ring-opening polymerization of γ-butyrolactone. The development of these bio-based monomers contributes significantly to the advancement of sustainable polyurethane elastomers.

2.4 Functional elastomers

Most nanofillers face problems such as aggregation and poor compatibility when directly incorporated into rubber matrices. To solve these issues and to prepare high-performance

composites, in addition to modifying the nanofillers, functional modification of elastomers is also an effective method. Depending on different needs, introducing corresponding functional groups into elastomers to change their polarity, or even endow them with certain reactivity, can enhance the interaction between the matrix and the fillers. Meanwhile, functional modification can also broaden the application range of elastomers and, to some extent, improve the comprehensive properties of the elastomers.

There are many methods for functional modification of elastomers. Common modification methods such as epoxidation and grafting are directly performed on the elastomers. First, the commonly used epoxidized natural rubber (ENR) is introduced, as shown in **Figure 2.14**. David R. Burfield et al. systematically studied various epoxidation methods for natural latex, confirmed that the use of preformed peracetic acid enables efficient and uniform epoxidation, and thoroughly evaluated the structural and property changes of the resulting epoxidized rubber[130]. Varaporn Tanrattanakul et al. used hydrogen peroxide and formic acid to perform in situ epoxidation of natural latex at 50 °C, successfully synthesizing epoxidized natural rubber (ENR) with an epoxide content of 22–39 mol%. The study showed that this method does not require pH adjustment and has high reaction efficiency. The resulting ENR has good thermal stability and uniform epoxidation structure. Compared with natural rubber and commercial ENR, the prepared ENR shows excellent tensile properties, abrasion resistance, and oil resistance, especially with significantly improved oil resistance in various automotive lubricants[131]. ENR can form strong hydrogen bonds and covalent bonds with silica, and is widely used as a matrix or interfacial compatibilizer in silica-based nanocomposites[132, 133]. Karnda Sengloyluan et al. investigated the use of epoxidized natural rubber (ENR) as a compatibilizer in silica-filled natural rubber (NR) tire tread compounds. By introducing ENR with different epoxide contents (ENR-10, ENR-38, ENR-51), they systematically examined its effects on Mooney viscosity, Payne effect, filler flocculation, and mechanical properties of the compounds. The results showed that ENR, especially ENR-38 and ENR-51, could interact with silanol groups on the silica surface through their epoxide groups, effectively improving silica dispersion and filler–rubber compatibility, thus enhancing the mechanical and processing

properties of the material. Although its performance is slightly lower than that of traditional silane coupling agent TESPT (bis[3-(triethoxysilyl)propyl] tetrasulfide), ENR shows promising potential as a "green" compatibilizer[134].

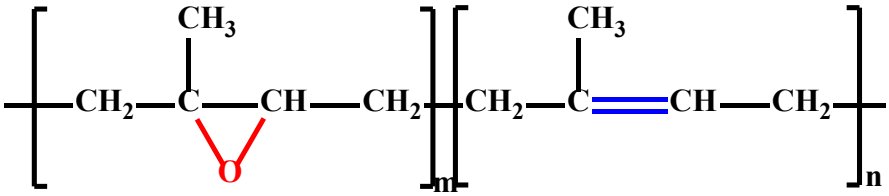

Figure 2.14 Chemical structures of epoxidized natural rubber (ENR).

There are two main synthetic strategies for surface-grafting polymers, as illustrated in **Figure 2.15**: "grafting to" and "grafting from"[135]. The "grafting to" method forms polymer brushes by the reaction between preformed polymers and functional groups on the substrate surface. This method is simple, but limited by steric hindrance, making it difficult to achieve high-density structures. In contrast, the "grafting from" method involves anchoring initiators onto the surface followed by in situ polymerization, allowing polymer chains to grow directly from the surface, which is suitable for preparing high-density polymer brushes. Common "grafting from" methods include surface-initiated atom transfer radical polymerization (SI-ATRP), surface-initiated ring opening metathesis polymerization (SI-ROMP), and surface-initiated reversible-addition fragmentation chain transfer (SI-RAFT), which can precisely control the thickness and structure of the brush layer, and are used in constructing functional layers such as electrodes, dielectrics, and conductive layers in organic electronic devices. This strategy also has advantages in patterning and large-area device fabrication.

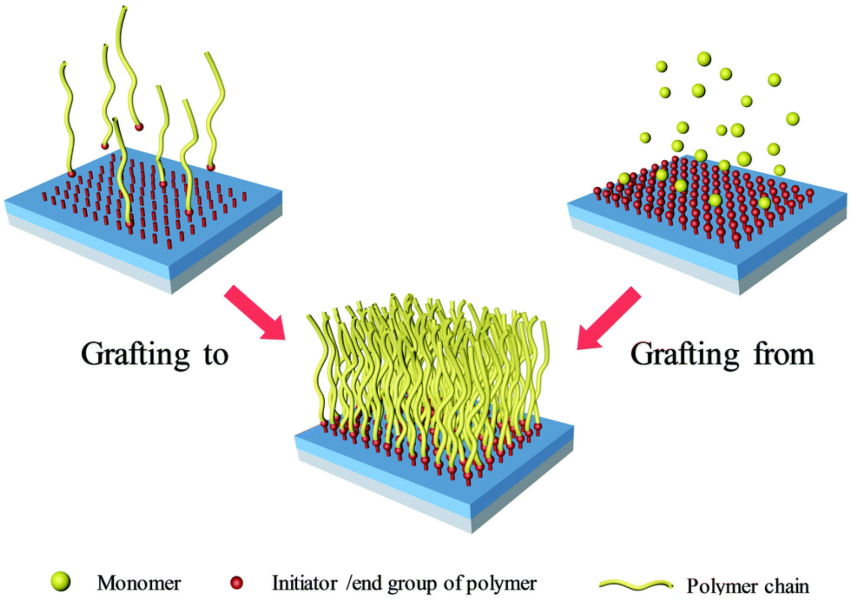

Figure 2.15 The synthetic approaches for creating surface-grafted polymers: "grafting to" and "grafting from"[135].

In addition to direct modification of elastomers, functionalization can also be achieved by incorporating a functional monomer during polymerization, offering a simple and controllable approach. Representative chemical structures of various functionalized elastomers prepared via copolymerization are shown in **Figure 2.16**. Carboxylated nitrile rubber (XNBR), for instance, is synthesized via emulsion polymerization by introducing carboxyl monomers such as acrylic acid or methacrylic acid, which enhance interactions between XNBR and polar fillers [136, 137]. Similarly, carboxylated styrene-butadiene rubber (XSBR) [138] and butadiene-styrene-vinyl pyridine rubber (SBR-VP) [139-141], synthesized through emulsion copolymerization with functional monomers, exhibit improved adhesion and compatibility with fillers like clay. Additionally, various epoxy group-functionalized rubbers, such as poly(dibutyl itaconate-isoprene-glycidyl methacrylate) (PDBIIG) [142] and poly(butadiene-styrene-glycidyl methacrylate) (SBR-GMA) [143], have been synthesized using radical emulsion polymerization. By leveraging these functionalization strategies, elastomers can achieve improved filler dispersion, enhanced mechanical properties, and expanded applicability in advanced engineering materials, further driving the development of high-performance bio-based rubber composites.

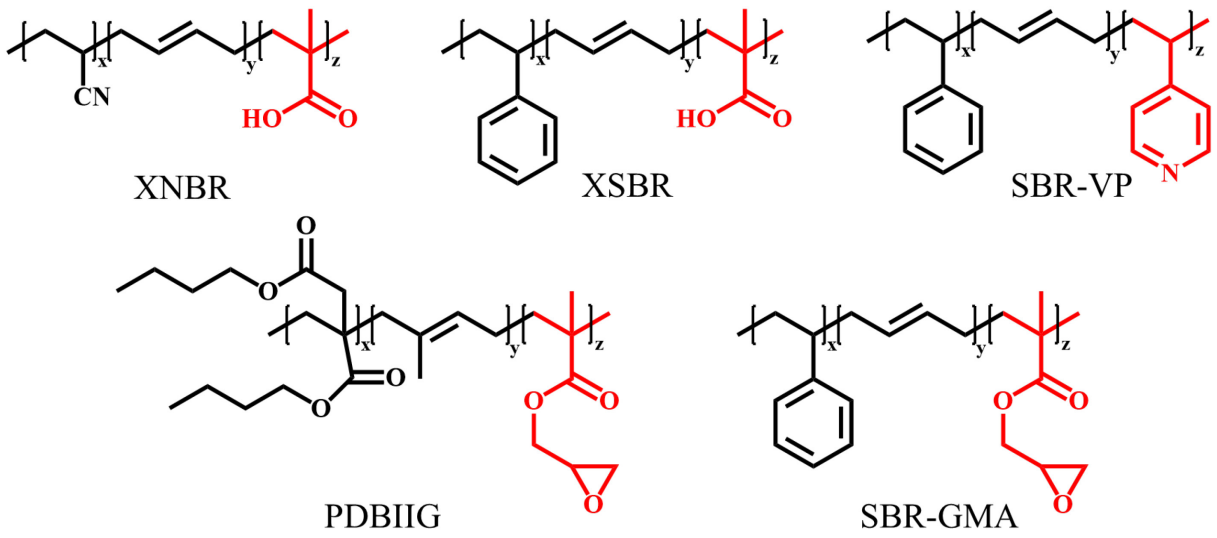

Figure 2.16 Chemical structures of XNBR, XSBR, SBR-VP, PDBIIG, and SBR-GMA.

2.5 References

[1] VASSILEV S V, BAXTER D, ANDERSEN L K, et al. An Overview of the Chemical Composition of Biomass [J]. Fuel, 2010, 89(5): 913-933.

[2] KONUR O. The Scientometric Evaluation of the Research on the Production of Bioenergy from Biomass [J]. Biomass and Bioenergy, 2012, 47: 504-515.

[3] SáNCHEZ J, CURT M D, ROBERT N, et al. Chapter Two - Biomass Resources [M]//LAGO C, CALDéS N, LECHóN Y. The Role of Bioenergy in the Bioeconomy. Academic Press. 2019: 25-111.

[4] JEGUIRIM M, KHIARI B, LIMOUSY L. 1 - Biomass Feedstocks [M]//JEGUIRIM M, LIMOUSY L. Char and Carbon Materials Derived from Biomass. Elsevier. 2019: 1-38.

[5] LONG H, LI X, WANG H, et al. Biomass Resources and Their Bioenergy Potential Estimation: A Review [J]. Renewable and Sustainable Energy Reviews, 2013, 26: 344-352.

[6] DE JONG E, HIGSON A, WALSH P, et al. Product Developments in the Bio-based Chemicals Arena [J]. Biofuels, Bioproducts and Biorefining, 2012, 6(6): 606-624.

[7] CHINTHAPALLI R, SKOCZINSKI P, CARUS M, et al. Biobased Building Blocks and Polymers—Global Capacities, Production and Trends, 2018–2023 [J]. Industrial

Biotechnology, 2019, 15(4): 237-241.

[8] SINGH P. Sugar Industry: A Hub of Useful Bio-Based Chemicals [M]//MOHAN N, SINGH P. Sugar and Sugar Derivatives: Changing Consumer Preferences. Singapore; Springer Singapore. 2020: 171-194.

[9] BINOD P, SINDHU R, SINGHANIA R R, et al. Bioethanol Production from Rice Straw: An Overview [J]. Bioresource Technology, 2010, 101(13): 4767-4774.

[10] KIM S, DALE B E. Global Potential Bioethanol Production from Wasted Crops and Crop Residues [J]. Biomass and Bioenergy, 2004, 26(4): 361-375.

[11] BALAT M, BALAT H, ÖZ C. Progress in Bioethanol Processing [J]. Progress in Energy and Combustion Science, 2008, 34(5): 551-573.

[12] NGUYEN N P, RAYNAUD C, MEYNIAL-SALLES I, et al. Reviving the Weizmann Process for Commercial n-Butanol Production [J]. Nature communications, 2018, 9(1): 3682.

[13] SUN J, LIU H. Selective Hydrogenolysis of Biomass-derived Xylitol to Ethylene Glycol and Propylene Glycol on Supported Ru Catalysts [J]. Green Chemistry, 2011, 13(1): 135-142.

[14] PFLüGL S, MARX H, MATTANOVICH D, et al. 1,3-Propanediol Production from Glycerol with Lactobacillus Diolivorans [J]. Bioresour Technol, 2012, 119: 133-140.

[15] AHN J H, SEO H, PARK W, et al. Enhanced Succinic Acid Production by Mannheimia Employing Optimal Malate Dehydrogenase [J]. Nature Communications, 2020, 11(1): 1970.

[16] HULEA V. Toward Platform Chemicals from Bio-Based Ethylene: Heterogeneous Catalysts and Processes [J]. ACS Catalysis, 2018, 8(4): 3263-3279.

[17] ZHANG M, YU Y. Dehydration of Ethanol to Ethylene [J]. Industrial & Engineering Chemistry Research, 2013, 52(28): 9505-9514.

[18] CESPI D, PASSARINI F, VASSURA I, et al. Butadiene from Biomass, A Life Cycle Perspective to Address Sustainability in the Chemical Industry [J]. Green Chemistry, 2016, 18(6): 1625-1638.

[19] MORAIS A R C, DWORAKOWSKA S, REIS A, et al. Chemical and Biological-based Isoprene Production: Green Metrics [J]. Catalysis Today, 2015, 239: 38-43.

[20] OKABE M, LIES D, KANAMASA S, et al. Biotechnological Production of Itaconic Acid and its Biosynthesis in Aspergillus Terreus [J]. Appl Microbiol Biotechnol, 2009, 84(4): 597-606.

[21] SEBASTIAN J, DOMINGUEZ K V, BRAR S K, et al. Fumaric Acid Production Using Alternate Fermentation Mode by Immobilized Rhizopus Oryzae-a Greener Production Strategy [J]. Chemosphere, 2021, 281: 130858.

[22] ABDEL-RAHMAN M A, TASHIRO Y, SONOMOTO K. Recent Advances in Lactic Acid Production by Microbial Fermentation Processes [J]. Biotechnol Advances, 2013, 31(6): 877-902.

[23] TAHERZADEH M J, ADLER L, LIDéN G. Strategies for Enhancing Fermentative Production of Glycerol—A Review [J]. Enzyme and Microbial Technology, 2002, 31(1): 53-66.

[24] SáNCHEZ Ó J, CARDONA C A. Trends in Biotechnological Production of Fuel Ethanol from Different Feedstocks [J]. Bioresource Technology, 2008, 99(13): 5270-5295.

[25] ANGELICI C, WECKHUYSEN B M, BRUIJNINCX P C A. Chemocatalytic Conversion of Ethanol into Butadiene and Other Bulk Chemicals [J]. ChemSusChem, 2013, 6(9): 1595-1614.

[26] MUñOZ I, FLURY K, JUNGBLUTH N, et al. Life Cycle Assessment of Bio-based Ethanol Produced from Different Agricultural Feedstocks [J]. The International Journal of Life Cycle Assessment, 2014, 19(1): 109-119.

[27] DIAS M O S, ENSINAS A V, NEBRA S A, et al. Production of Bioethanol and other Bio-based Materials from Sugarcane Bagasse: Integration to Conventional Bioethanol Production Process [J]. Chemical Engineering Research and Design, 2009, 87(9): 1206-1216.

[28] GOHAIN M, HASIN M, ELDIEHY K S H, et al. Bio-ethanol Production: A Route to Sustainability of Fuels Using Bio-based Heterogeneous Catalyst Derived from Waste [J].

Process Safety and Environmental Protection, 2021, 146: 190-200.

[29] BHALLA A, BANSAL N, KUMAR S, et al. Improved Lignocellulose Conversion to Biofuels with Thermophilic Bacteria and Thermostable Enzymes [J]. Bioresource Technology, 2013, 128: 751-759.

[30] PHITSUWAN P, SAKKA K, RATANAKHANOKCHAI K. Improvement of Lignocellulosic Biomass in Planta: A Review of Feedstocks, Biomass Recalcitrance, and Strategic Manipulation of Ideal Plants Designed for Ethanol Production and Processability [J]. Biomass and Bioenergy, 2013, 58: 390-405.

[31] MAURYA R, PALIWAL C, GHOSH T, et al. Applications of De-oiled Microalgal Biomass towards Development of Sustainable Biorefinery [J]. Bioresource Technology, 2016, 214: 787-796.

[32] GAO M-T, SHIMAMURA T, ISHIDA N, et al. Investigation of Utilization of the Algal Biomass Residue after Oil Extraction to Lower the Total Production Cost of Biodiesel [J]. Journal of Bioscience and Bioengineering, 2012, 114(3): 330-333.

[33] LEE O K, KIM A L, SEONG D H, et al. Chemo-enzymatic Saccharification and Bioethanol Fermentation of Lipid-extracted Residual Biomass of the Microalga, Dunaliella Tertiolecta [J]. Bioresource Technology, 2013, 132: 197-201.

[34] CHNG L M, CHAN D J C, LEE K T. Sustainable Production of Bioethanol Using Lipid-Extracted Biomass from Scenedesmus Dimorphus [J]. Journal of Cleaner Production, 2016, 130: 68-73.

[35] VOLESKY B, SZCZESNY T. Bacterial Conversion of Pentose Sugars to Acetone and Butanol; Proceedings of the Pentoses and Lignin, Berlin, Heidelberg, F 1983//, 1983 [C]. Springer Berlin Heidelberg.

[36] JIN C, YAO M, LIU H, et al. Progress in the Production and Application of n-Butanol as A Biofuel [J]. Renewable and Sustainable Energy Reviews, 2011, 15(8): 4080-4106.

[37] DüRRE P. Fermentative Butanol Production [J]. Annals of the New York Academy of Sciences, 2008, 1125(1): 353-362.

[38] LIU F, LIU L, FENG X. Separation of Acetone–butanol–ethanol (ABE) from Dilute

Aqueous Solutions by Pervaporation [J]. Separation and Purification Technology, 2005, 42(3): 273-282.

[39] RAKOPOULOS D C, RAKOPOULOS C D, GIAKOUMIS E G, et al. Effects of Butanol–diesel Fuel Blends on the Performance and Emissions of a High-speed DI Diesel Engine [J]. Energy Conversion and Management, 2010, 51(10): 1989-1997.

[40] HANSEN A C, KYRITSIS D C, LEE C F F. Characteristics of Biofuels and Renewable Fuel Standards [M]. Biomass to Biofuels. 2010: 1-26.

[41] CHOTWICHIEN A, LUENGNARUEMITCHAI A, JAI-IN S. Utilization of Palm Oil Alkyl Esters as An Additive In Ethanol–diesel and Butanol–diesel Blends [J]. Fuel, 2009, 88(9): 1618-1624.

[42] WU C-Y, WU H-S. Ethylene Formation from Ethanol Dehydration Using ZSM-5 Catalyst [J]. ACS Omega, 2017, 2(8): 4287-4296.

[43] MORSCHBACKER A. Bio-Ethanol Based Ethylene [J]. Polymer Reviews, 2009, 49(2): 79-84.

[44] SUN J, WANG Y. Recent Advances in Catalytic Conversion of Ethanol to Chemicals [J]. ACS Catalysis, 2014, 4(4): 1078-1090.

[45] TRIPODI A, BELOTTI M, ROSSETTI I. Bioethylene Production: from Reaction Kinetics to Plant Design [J]. ACS Sustainable Chemistry & Engineering, 2019, 7(15): 13333-13350.

[46] DE REVIERE A, GUNST D, SABBE M, et al. Sustainable Short-chain Olefin Production through Simultaneous Dehydration of Mixtures of 1-Butanol and Ethanol over HZSM-5 and γ-Al_2O_3 [J]. Journal of Industrial and Engineering Chemistry, 2020, 89: 257-272.

[47] RODGERS S, MENG F, POULSTON S, et al. Renewable Butadiene: A Case for Hybrid Processing via Bio- and Chemo-catalysis [J]. Journal of Cleaner Production, 2022, 364: 132614.

[48] BRUIJNINCX P C, WECKHUYSEN B M. Shale Gas Revolution: an Opportunity for the Production of Biobased Chemicals? [J]. Angewandte Chemie (International ed in

English), 2013, 52(46): 11980-11987.

[49] PATEL A D, MEESTERS K, DEN UIL H, et al. Sustainability Assessment of Novel Chemical Processes at Early Stage: Application to Biobased Processes [J]. Energy & Environmental Science, 2012, 5(9): 8430-8444.

[50] LEBEDEV S V. Preparation of Bivinyl Directly from Alcohol. I [J]. Zh Obshch Khim, 1933, 3: 698-717.

[51] TOUSSAINT W J, DUNN J T, JACHSON D R. Production of Butadiene from Alcohol [J]. Industrial & Engineering Chemistry, 1947, 39(2): 120-125.

[52] MAKSHINA E V, DUSSELIER M, JANSSENS W, et al. Review of Old Chemistry and New Catalytic Advances in the On-purpose Synthesis of Butadiene [J]. Chemical Society Reviews, 2014, 43(22): 7917-7953.

[53] MASCAL M. Chemicals from Biobutanol: Technologies and Markets [J]. Biofuels, Bioproducts and Biorefining, 2012, 6(4): 483-493.

[54] XUE C, CHENG C. Chapter Two - Butanol Production by Clostridium [M]//LI Y, GE X. Advances in Bioenergy. Elsevier. 2019: 35-77.

[55] MAYANK R, AMRITA R, AND MOHOLKAR V S. Mathematical Models of ABE Fermentation: Review and Analysis [J]. Critical Reviews in Biotechnology, 2013, 33(4): 419-447.

[56] VEZA I, MUHAMAD SAID M F, LATIFF Z A. Recent Advances in Butanol Production by Acetone-butanol-ethanol (ABE) Fermentation [J]. Biomass and Bioenergy, 2021, 144: 105919.

[57] YIM H, HASELBECK R, NIU W, et al. Metabolic Engineering of Escherichia Coli for Direct Production of 1,4-Butanediol [J]. Nature Chemical Biology, 2011, 7(7): 445-452.

[58] MAINA S, PRABHU A A, VIVEK N, et al. Prospects on Bio-based 2,3-Butanediol and Acetoin Production: Recent Progress and Advances [J]. Biotechnology Advances, 2022, 54: 107783.

[59] TINôCO D, SELDIN L, LUIZ DE ANDRADE COUTINHO P, et al. Optimization of Fermentation Conditions as A Metabolic Strategy for the High-Yield and High-

Selectivity Bio-based 2,3-Butanediol Production [J]. Journal of Industrial and Engineering Chemistry, 2023, 125: 345-359.

[60] KATAOKA N, VANGNAI A S, TAJIMA T, et al. Improvement of (R)-1,3-butanediol Production by Engineered Escherichia Coli [J]. Journal of Bioscience and Bioengineering, 2013, 115(5): 475-480.

[61] LIU Y, CEN X, LIU D, et al. Metabolic Engineering of Escherichia Coli for High-Yield Production of (R)-1,3-butanediol [J]. ACS Synthetic Biology, 2021, 10(8): 1946-1955.

[62] TSHIBALONZA N N, MONBALIU J-C M. The Deoxydehydration (DODH) Reaction: a Versatile Technology for Accessing Olefins from Bio-based Polyols [J]. Green Chemistry, 2020, 22(15): 4801-4848.

[63] ONODERA K, NAKAJI Y, YABUSHITA M, et al. Selective Synthesis of 1,3-Butadiene by Vapor-phase Dehydration of 1,4-butanediol over Cerium Oxide Catalyst [J]. Applied Catalysis A: General, 2023, 663: 119321.

[64] RAJU S, MORET M-E, KLEIN GEBBINK R J M. Rhenium-Catalyzed Dehydration and Deoxydehydration of Alcohols and Polyols: Opportunities for the Formation of Olefins from Biomass [J]. ACS Catalysis, 2015, 5(1): 281-300.

[65] YE L, LV X, YU H. Engineering Microbes for Isoprene Production [J]. Metab Eng, 2016, 38: 125-138.

[66] LV X, XIE W, LU W, et al. Enhanced Isoprene Biosynthesis in Saccharomyces Cerevisiae by Engineering of the Native Acetyl-CoA And Mevalonic Acid Pathways with A Push-pull-restrain Strategy [J]. J Biotechnol, 2014, 186: 128-136.

[67] ABDELRAHMAN O A, PARK D S, VINTER K P, et al. Renewable Isoprene by Sequential Hydrogenation of Itaconic Acid and Dehydra-Decyclization of 3-Methyl-Tetrahydrofuran [J]. ACS Catalysis, 2017, 7(2): 1428-1431.

[68] HERACLEOUS E, PACHATOURIDOU E, LOUIE L, et al. Efficient Route for the Production of Isoprene via Decarboxylation of Bioderived Mevalonolactone [J]. ACS Catalysis, 2020, 10(16): 9649-9661.

[69] GUENTHER A, KARL T, HARLEY P, et al. Estimates of Global Terrestrial Isoprene

Emissions Using MEGAN (Model of Emissions of Gases and Aerosols from Nature) [J]. Atmos Chem Phys, 2006, 6(11): 3181-3210.

[70] WHITED G M, FEHER F J, BENKO D A, et al. TECHNOLOGY UPDATE: Development of a Gas-phase Bioprocess for Isoprene-monomer Production Using Metabolic Pathway Engineering [J]. Industrial Biotechnology, 2010, 6(3): 152-163.

[71] YANG J, XIAN M, SU S, et al. Enhancing Production of Bio-isoprene Using Hybrid MVA Pathway and Isoprene Synthase in E. coli [J]. PLOS ONE, 2012, 7(4): e33509.

[72] ISAR J, JAIN D, JOSHI H, et al. MICROBIAL Isoprene Production: An Overview [J]. World J Microbiol Biotechnol, 2022, 38(7): 122.

[73] MILLER B, OSCHINSKI C, ZIMMER W. First Isolation of An Isoprene Synthase Gene from Poplar and Successful Expression of the Gene in Escherichia Coli [J]. Planta, 2001, 213(3): 483-487.

[74] SILVER G M, FALL R. Enzymatic Synthesis of Isoprene from Dimethylallyl Diphosphate in Aspen Leaf Extracts 1 [J]. Plant Physiology, 1991, 97(4): 1588-1591.

[75] MARTIN V J J, PITERA D J, WITHERS S T, et al. Engineering a Mevalonate Pathway in Escherichia Coli for Production of Terpenoids [J]. Nat Biotechnol, 2003, 21(7): 796-802.

[76] ROHMER M. The Discovery of A Mevalonate-independent Pathway for Isoprenoid Biosynthesis in Bacteria, Algae and Higher Plants [J]. Nat Prod Rep, 1999, 16(5): 565-574.

[77] WANG S, LI R, YI X, et al. Isoprene Production on Enzymatic Hydrolysate of Peanut Hull Using Different Pretreatment Methods [J]. BioMed Research International, 2016, 2016(1): 4342892.

[78] ALDRIDGE J, CARR S, WEBER KARRIE A, et al. Anaerobic Production of Isoprene by Engineered Methanosarcina Species Archaea [J]. Applied and Environmental Microbiology, 2021, 87(6): e02417-02420.

[79] MARCELLIN E, BEHRENDORFF J B, NAGARAJU S, et al. Low Carbon Fuels and Commodity Chemicals from Waste Gases – Systematic Approach to Understand Energy

Metabolism in a Model Acetogen [J]. Green Chemistry, 2016, 18(10): 3020-3028.

[80] CARR S, ALDRIDGE J, BUAN N R. Isoprene Production from Municipal Wastewater Biosolids by Engineered Archaeon Methanosarcina acetivorans [J/OL] 2021, 11(8):10.3390/app11083342

[81] LEE H-W, PARK J-H, KIM W-K, et al. Engineered Escherichia Coli Strains as Platforms for Biological Production of Isoprene [J]. FEBS Open Bio, 2020, 10(5): 780-788.

[82] GOMAA L, LOSCAR M E, ZEIN H S, et al. Boosting Isoprene Production via Heterologous Expression of the Kudzu Isoprene Synthase Gene (kIspS) into Bacillus Spp. Cell Factory [J]. AMB Express, 2017, 7(1): 161.

[83] LV X, XIE W, LU W, et al. Enhanced Isoprene Biosynthesis in Saccharomyces Cerevisiae by Engineering of the Native Acetyl-CoA And Mevalonic Acid Pathways with A Push-pull-restrain Strategy [J]. J Biotechnol, 2014, 186: 128-136.

[84] LIU H, CAO Y, GUO J, et al. Study on the Isoprene-producing Co-culture System of Synechococcus Elongates–Escherichia Coli through Omics Analysis [J]. Microbial Cell Factories, 2021, 20(1): 6.

[85] HYEOK-WON L, LT, SUP, et al. Production of Bio-Based Isoprene by the Mevalonate Pathway Cassette in Ralstonia eutropha [J]. J Microbiol Biotechnol, 2019, 29(10): 1656-1664.

[86] JANKE C, GAIDA S, JENNEWEIN S. The Production of Isoprene from Cellulose Using Recombinant Clostridium Cellulolyticum Strains Expressing Isoprene Synthase [J]. MicrobiologyOpen, 2020, 9(4): e1008.

[87] WILLKE T, WELTER K, VORLOP K D. Biotechnological Production of Itaconic Acid from Sugar [J]. ZUCKERINDUSTRIE, 2001, 126(6): 444-447.

[88] KUENZ A, KRULL S. Biotechnological Production of Itaconic Acid—Things You Have to Know [J]. Applied Microbiology and Biotechnology, 2018, 102(9): 3901-3914.

[89] MAASSEN N, PANAKOVA M, WIERCKX N, et al. Influence of Carbon and Nitrogen Concentration on Itaconic Acid Production by the Smut Fungus Ustilago Maydis [J]. Engineering in Life Sciences, 2014, 14(2): 129-134.

[90] HOLLIDAY R. Ustilago Maydis [M]//KING R C. Bacteria, Bacteriophages, and Fungi: Volume 1. Boston, MA; Springer US. 1974: 575-595.

[91] MILASINOVIC N, KRUSIC M K, KNEZEVIC-JUGOVIC Z, et al. Hydrogels of N-isopropylacrylamide Copolymers with Controlled Release of A Model Protein [J]. International Journal of Pharmaceutics, 2010, 383(1-2): 53-61.

[92] KLEMENT T, BüCHS J. Itaconic Acid – A Biotechnological Process in Change [J]. Bioresource Technology, 2013, 135: 422-431.

[93] GEISER E, PRZYBILLA S K, FRIEDRICH A, et al. Ustilago Maydis Produces Itaconic Acid via the Unusual Intermediate Trans-aconitate [J]. Microbial Biotechnology, 2016, 9(1): 116-126.

[94] DOMíNGUEZ DE MARíA P, SáNCHEZ-MONTERO J M, SINISTERRA J V, et al. Understanding Candida Rugosa Lipases: An Overview [J]. Biotechnology Advances, 2006, 24(2): 180-196.

[95] TELEKY B-E, VODNAR D C. Recent Advances in Biotechnological Itaconic Acid Production, and Application for a Sustainable Approach [J/OL] 2021, 13(20):10.3390/polym13203574

[96] BOHRE A, NOVAK U, GRILC M, et al. Synthesis of Bio-based Methacrylic Acid from Biomass-derived Itaconic Acid over Barium Hexa-aluminate Catalyst by Selective Decarboxylation Reaction [J]. Molecular Catalysis, 2019, 476: 110520.

[97] SAHA B C. Emerging biotechnologies for Production of Itaconic Acid and its Applications as A Platform Chemical [J]. J Ind Microbiol Biotechnol, 2017, 44(2): 303-315.

[98] TELEKY B-E, VODNAR D C. Biomass-Derived Production of Itaconic Acid as a Building Block in Specialty Polymers [J/OL] 2019, 11(6):10.3390/polym11061035

[99] LIU X, WANG X, LIU Q, et al. A Sustainable Process for the Production of 2-methyl-1,4-butanediol by Hydrogenation of Biomass-derived Itaconic Acid [J]. Catalysis Today, 2016, 274: 88-93.

[100] GEILEN F M, ENGENDAHL B, HARWARDT A, et al. Selective and Flexible

Transformation of Biomass-derived Platform Chemicals by A Multifunctional Catalytic System [J]. Angewandte Chemie (International ed in English), 2010, 49(32): 5510-5514.

[101] SRIARIYANUN M, HEITZ J H, YASURIN P, et al. Itaconic Acid: A Promising and Sustainable Platform Chemical? [J]. Applied Science and Engineering Progress, 2019, 12(2): 75-82.

[102] BAFANA R, PANDEY R A. New Approaches for Itaconic Acid Production: Bottlenecks and Possible Remedies [J]. Critical Reviews in Biotechnology, 2018, 38(1): 68-82.

[103] DA CRUZ J C, CAMPORESE SéRVULO E F, DE CASTRO A M. Chapter 10 - Microbial Production of Itaconic Acid [M]//HOLBAN A M, GRUMEZESCU A M. Microbial Production of Food Ingredients and Additives. Academic Press. 2017: 291-316.

[104] CUNHA DA CRUZ J, MACHADO DE CASTRO A, CAMPORESE SéRVULO E F. World Market and Biotechnological Production of Itaconic Acid [J]. 3 Biotech, 2018, 8(3): 138.

[105] WERPY T A, HOLLADAY J E, WHITE J F. Top Value Added Chemicals From Biomass: I. Results of Screening for Potential Candidates from Sugars and Synthesis Gas [R]. United States, 2004.

[106] ZHANG R, LIU H, NING Y, et al. Recent Advances on the Production of Itaconic Acid via the Fermentation and Metabolic Engineering [J/OL] 2023, 9(1):71[

[107] TELEKY B-E, VODNAR D C. Recent Advances in Biotechnological Itaconic Acid Production, and Application for a Sustainable Approach [J/OL] 2021, 13(20):3574[

[108] WANG R, MA J, ZHOU X, et al. Design and Preparation of a Novel Cross-Linkable, High Molecular Weight, and Bio-Based Elastomer by Emulsion Polymerization [J]. Macromolecules, 2012, 45(17): 6830-6839.

[109] LEI W, RUSSELL T P, HU L, et al. Pendant Chain Effect on the Synthesis, Characterization, and Structure–Property Relations of Poly(di-n-alkyl itaconate-co-isoprene) Biobased Elastomers [J]. ACS Sustainable Chemistry & Engineering, 2017, 5(6): 5214-5223.

[110] LEI W, YANG X, QIAO H, et al. Renewable Resource-based Elastomer Nanocomposite

Derived from Myrcene, Ethanol, Itaconic Acid and Nanosilica: Design, Preparation and Properties [J]. European Polymer Journal, 2018, 106: 1-8.

[111] ZHOU X, JI H, HU G-H, et al. A Solvent-less Green Synthetic Route toward A Sustainable Bio-based Elastomer: Design, Synthesis, and Characterization of Poly(dibutyl itaconate-co-butadiene) [J]. Polymer Chemistry, 2019, 10(45): 6131-6144.

[112] TANG S, LI J, WANG R, et al. Current Trends in Bio-based Elastomer Materials [J]. SusMat, 2022, 2(1): 2-33.

[113] ZEIMARAN E, POURSHAHRESTANI S, PINGGUAN-MURPHY B, et al. Development of Poly (1, 8-octanediol citrate)/chitosan Blend Films for Tissue Engineering Applications [J]. Carbohydrate Polymers, 2017, 175: 618-627.

[114] BRUGGEMAN J P, DE BRUIN B-J, BETTINGER C J, et al. Biodegradable poly(polyol sebacate) polymers [J]. Biomaterials, 2008, 29(36): 4726-4735.

[115] FLAIG F, RAGOT H, SIMON A, et al. Design of Functional Electrospun Scaffolds Based on Poly(glycerol sebacate) Elastomer and Poly(lactic acid) for Cardiac Tissue Engineering [J]. ACS Biomaterials Science & Engineering, 2020, 6(4): 2388-2400.

[116] BRUGGEMAN J P, BETTINGER C J, NIJST C L E, et al. Biodegradable Xylitol-based Polymers [J]. Advanced Materials, 2008, 20(10): 1922-1927.

[117] GEETI D K, NIRANJAN K. Environmentally Benign Bio-based Waterborne Polyesters: Synthesis, Thermal- and Bio-degradation Studies [J]. Prog Org Coat, 2019, 127: 419-428.

[118] PIĄTEK-HNAT M, BOMBA K, PĘKSIŃSKI J. Synthesis and Selected Properties of Ester Elastomer Containing Sorbitol [J/OL] 2020, 10(5):10.3390/app10051628

[119] SONSECA Á, CAMARERO-ESPINOSA S, PEPONI L, et al. Mechanical and Shape-Memory Properties of Poly(mannitol sebacate)/cellulose Nanocrystal Nanocomposites [J]. Journal of Polymer Science Part A: Polymer Chemistry, 2014, 52(21): 3123-3133.

[120] STEBBINS N D, YU W, UHRICH K E. Linear, Mannitol-based Poly(anhydride-esters) with High Ibuprofen Loading and Anti-inflammatory Activity [J]. Biomacromolecules, 2015, 16(11): 3632-3639.

[121] WEI T, LEI L, KANG H, et al. Tough Bio-Based Elastomer Nanocomposites with High

Performance for Engineering Applications [J]. Advanced Engineering Materials, 2012, 14(1-2): 112-118.

[122] HU X, KANG H, LI Y, et al. Direct Copolycondensation of Biobased Elastomers Based on Lactic Acid with Tunable and Versatile Properties [J]. Polymer Chemistry, 2015, 6(47): 8112-8123.

[123] TANG S, LI J, WANG Z, et al. Design and Synthesis of Novel Bio-Based Polyester Elastomer with Tunable Oil Resistance [J]. Macromolecular Rapid Communications, 2023, 44(17): 2300166.

[124] MORALES-CERRADA R, TAVERNIER R, CAILLOL S. Fully Bio-Based Thermosetting Polyurethanes from Bio-Based Polyols and Isocyanates [J/OL] 2021, 13(8):10.3390/polym13081255

[125] TACHIBANA K, ABE H. Studies on Thermo-mechanical and Thermal Degradation Properties of Bio-based Polyurethanes Synthesized from Vanillin-derived Diol and Lysine Diisocyanate [J]. Polymer Degradation and Stability, 2019, 167: 283-291.

[126] GHASEMLOU M, DAVER F, IVANOVA E P, et al. Bio-based Routes to Synthesize Cyclic Carbonates and Polyamines Precursors of Non-isocyanate Polyurethanes: A Review [J]. European Polymer Journal, 2019, 118: 668-684.

[127] SCHMIDT S, GATTI F J, LUITZ M, et al. Erythritol Dicarbonate as Intermediate for Solvent- and Isocyanate-free Tailoring of Bio-Based Polyhydroxyurethane Thermoplastics and Thermoplastic Elastomers [J]. Macromolecules, 2017, 50(6): 2296-2303.

[128] PARCHETA P, GŁOWIŃSKA E, DATTA J. Effect of Bio-based Components on the Chemical Structure, Thermal Stability and Mechanical Properties of Green Thermoplastic Polyurethane Elastomers [J]. European Polymer Journal, 2020, 123: 109422.

[129] YUAN L, ZHOU W, SHEN Y, et al. Chemically Recyclable Polyurethanes Based on Bio-renewable γ-butyrolactone: from Thermoplastics to Elastomers [J]. Polymer Degradation and Stability, 2022, 204: 110116.

[130] BURFIELD D R, LIM K-L, LAW K-S. Epoxidation of Natural Rubber Latices: Methods of Preparation and Properties of Modified rubbers [J]. Journal of Applied Polymer Science, 1984, 29(5): 1661-1673.

[131] TANRATTANAKUL V, WATTANATHAI B, TIANGJUNYA A, et al. In Situ Epoxidized Natural Rubber: Improved Oil Resistance of Natural Rubber [J]. Journal of Applied Polymer Science, 2003, 90(1): 261-269.

[132] ADIBI A, JUBINVILLE D, CHEN G, et al. In-situ Surface Grafting of Lignin onto An Epoxidized Natural Rubber Matrix: A Masterbatch Filler for Reinforcing Rubber Composites [J]. Reactive and Functional Polymers, 2024, 197: 105856.

[133] XU T, JIA Z, LUO Y, et al. Interfacial Interaction between the Epoxidized Natural Rubber and Silica in Natural Rubber/Silica Composites [J]. Applied Surface Science, 2015, 328: 306-313.

[134] SENGLOYLUAN K, SAHAKARO K, DIERKES W K, et al. Silica-reinforced Tire Tread Compounds Compatibilized by Using Epoxidized Natural Rubber [J]. European Polymer Journal, 2014, 51: 69-79.

[135] WANG S, WANG Z, LI J, et al. Surface-grafting Polymers: from Chemistry to Organic Electronics [J]. Materials Chemistry Frontiers, 2020, 4(3): 692-714.

[136] KANG H, ZUO K, WANG Z, et al. Using A Green Method to Develop Graphene Oxide/elastomers Nanocomposites with Combination of High Barrier and Mechanical Performance [J]. Composites Science and Technology, 2014, 92: 1-8.

[137] MAHMOOD N, KHAN A U, STöCKELHUBER K W, et al. Carbon Nanotubes-filled Thermoplastic Polyurethane–urea and Carboxylated Acrylonitrile Butadiene Rubber Blend Nanocomposites [J]. Journal of Applied Polymer Science, 2014, 131(11).

[138] CAO X, XU C, LIU Y, et al. Preparation and Properties of Carboxylated Styrene-butadiene Rubber/cellulose Nanocrystals Composites [J]. Carbohydrate Polymers, 2013, 92(1): 69-76.

[139] HE S-J, WANG Y-Q, FENG Y-P, et al. The Preparation of An Elastomer/silicate Layer Nanocompound with An Exfoliated Structure and A Strong Ionic Interfacial Interaction

by Utilizing an Elastomer Latex Containing Pyridine Groups [J]. Nanotechnology, 2010, 21(11): 115601.

[140] TANG Z, WU X, GUO B, et al. Preparation of Butadiene–styrene–vinyl Pyridine Rubber–Graphene Oxide Hybrids through Co-coagulation Process and in Situ Interface Tailoring [J]. Journal of Materials Chemistry, 2012, 22(15): 7492-7501.

[141] MAO Y, WEN S, CHEN Y, et al. High Performance Graphene Oxide Based Rubber Composites [J]. Sci Rep, 2013, 3: 2508.

[142] QIAO H, XU W, CHAO M, et al. Preparation and Performance of Silica/Epoxy Group-Functionalized Biobased Elastomer Nanocomposite [J]. Industrial & Engineering Chemistry Research, 2017, 56(4): 881-889.

[143] KIM K, LEE J-Y, CHOI B-J, et al. Styrene-butadiene-glycidyl Methacrylate Terpolymer/silica Composites: Dispersion of Silica Particles and Dynamic Mechanical Properties [J]. Composite Interfaces, 2014, 21(8): 685-702.

Chapter 3 Role of Carboxyl Groups in the Performance Optimization of Bio-based Itaconate Elastomers and Nanocomposites

This chapter explores the functionalization of bio-based itaconate elastomers by introducing carboxyl groups through methacrylic acid (MAA) to enhance both the intrinsic properties of the elastomer matrix and its compatibility with silica fillers. As a result, in the absence of filler, the introduced carboxyl groups formed ionic cross-links with zinc oxide, which significantly improved the mechanical properties of the elastomer itself. In nanocomposites, the presence of carboxyl groups promoted better filler dispersion and stronger polymer–filler interactions, leading to enhanced mechanical strength, abrasion resistance, aging stability, and oil resistance. This work presents an effective strategy for developing sustainable, high-performance elastomer nanocomposites through carboxyl groups functionalization.

3.1 Introduction

Rubber is widely used in national defense, industry and daily life due to its unique elasticity [1, 2]. Traditional synthetic rubbers, such as styrene-butadiene rubber[3], polybutadiene rubber[4], and nitrile rubber[5], are primarily derived from fossil resources. However, as fossil resources gradually deplete, energy demands continue to rise, and environmental issues become increasingly severe, finding sustainable alternatives has become critically important.

Bio-based itaconate elastomers have attracted growing interest due to their renewable origin. Since Wang et al. first reported cross-linkable poly(diisoamyl itaconate-*co*-isoprene) (PDII)[6], researchers have developed a variety of itaconate-based elastomers, such as poly(itaconate-*co*-isoprene) (PDBII)[7], fully bio-based poly(diethyl itaconate-*co*-myrcene) (PDEIMy)[8], poly(dibutyl itaconate-*co*-butadiene) (PDBIB)[9], by adjusting backbone structure and side chain length, especially for green tire applications.

However, challenges such as filler aggregation and poor interfacial compatibility remain in nanocomposite systems. Functionalization of elastomers has proven to be an effective solution. Methods such as epoxidation[10-12], grafting[13, 14], or copolymerizing with functional monomers improve matrix polarity and filler dispersion[15-22]. Therefore, introducing polar functional groups particularly carboxyl groups, into bio-based itaconate elastomers presents a promising strategy for tailoring material properties and boosting nanocomposite performance, which is the focus of this chapter.

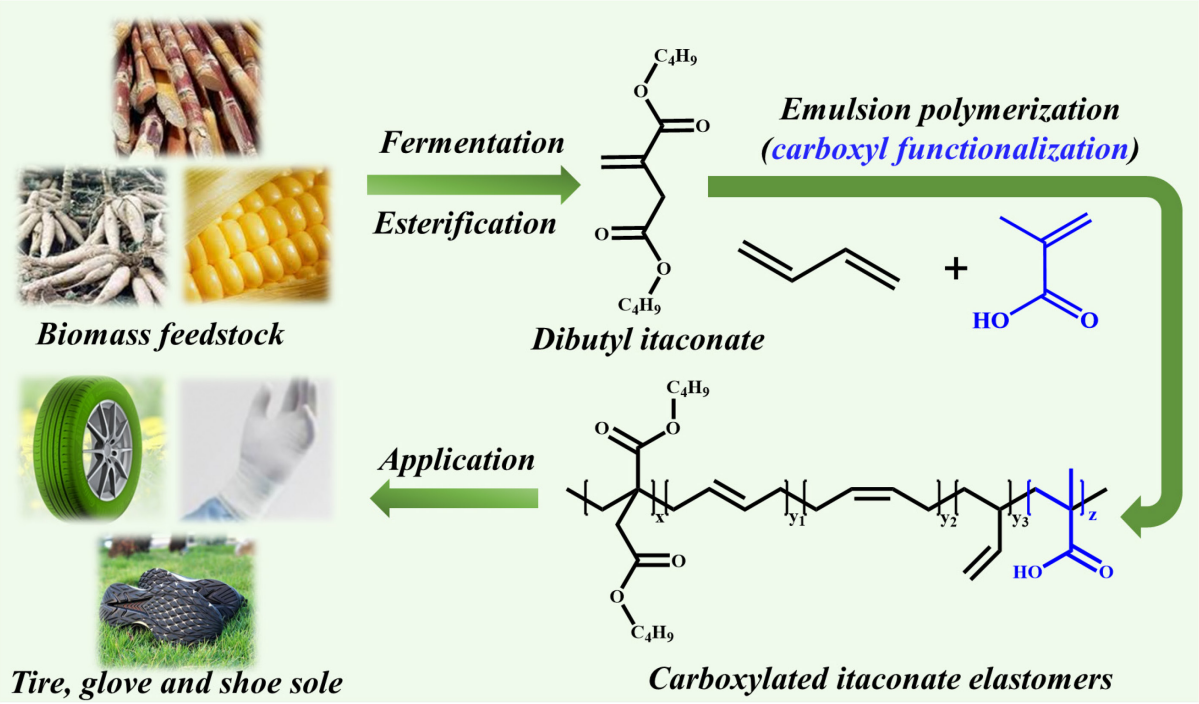

Figure 3.1 Schematic illustration of the synthesis and application pathway of carboxylated itaconate elastomers derived from biomass feedstocks.

In this work, we adopted a functionalization strategy using methacrylic acid to modify the molecular chains of poly(dibutyl itaconate) elastomers, as shown in **Figure 3.1**. By introducing corresponding carboxyl groups into the elastomer, we aimed to alter the polarity of the itaconate elastomer and even impart some reactivity to enhance the interaction between the matrix and the filler. Carboxylating the elastomer not only broadens its application scope but also improves its overall performance to some extent. Using dibutyl itaconate as a bio-based monomer, we conducted emulsion polymerization with butadiene and methacrylic acid to synthesize carboxylated poly(dibutyl itaconate-*co*-butadiene-*co*-methacrylic acid) elastomers (PDBIBAs). Furthermore, the silica/PDBIBA nanocomposites were prepared using a Haake mixer. Due to

the hydrogen bonding interactions between silica and PDBIBAs, silica aggregation was suppressed. We investigated the effects of introducing carboxyl groups on the interfacial interactions between silica and the elastomer, the dispersion of silica, as well as the dynamic and static mechanical properties, oil resistance, and aging resistance of the nanocomposites. This work on the functionalization of elastomers through polymerization to improve the interfacial interactions between the filler and the matrix provides a new approach for developing nanocomposites with desired properties.

3.2 Experimental section

3.2.1 Materials

Dibutyl itaconate (DBI) was obtained from Guangdong Suzhong Chemical Technology Co., Ltd., China. Butadiene (BD) was obtained from Sinopec Qilu Petrochemical Co., Ltd, China. Methacrylic acid (MAA), sodium dodecyl benzene sulfonate (SDBS), Sodium salt of polynaphthalene sulphonic acid (dispersing agent NNO), ethylene diamine tetraacetic acid (EDTA), ferrous sulfate ($FeSO_4$), potassium persulfate ($K_2S_2O_8$), ethanol absolute were obtained from Shanghai Macklin Biochemical Co., Ltd, China. Deionized water was provided by Shandong Chambroad Petrochemicals Co., Ltd., China.

3.2.2 Synthesis of PDBIBAs

The emulsion polymerization reaction takes place in a sealed 2L reactor. **Figure 3.2** shows the complete reactor system used in the experiment, while **Figure 3.3** illustrates the reactor schematic and the polymerization route for PDBIBAs. The recipe for the polymerization is shown in **Table 3.1**. The monomers involved in the reaction include dibutyl itaconate (DBI), butadiene (BD), and methacrylic acid (MAA). Initially, deionized water, sodium dodecyl benzene sulfonate (SDBS), polynaphthalene sulfonic acid sodium salt (dispersing agent NNO), ferrous sulfate ($FeSO_4$), and ethylene diamine tetraacetic acid (EDTA) were added to the reactor. Subsequently, dibutyl itaconate (DBI) and methacrylic acid (MAA) were introduced in

sequence at room temperature. The stirring speed was set at 280 rpm. After purging the reactor with nitrogen, butadiene was introduced into the system. Once all valves were confirmed to be closed, heating was started, and the pre-emulsification process was initiated. The temperature was set to 50 °C. After 15 min, the set temperature was reached, and the pre-emulsification continued for 1 h. After pre-emulsification, potassium persulfate ($K_2S_2O_8$) was added as an initiator. The reaction proceeded for 8 h, leading to the formation of latex.



Figure 3.2 The complete polymerization reactor system used in the experiment.

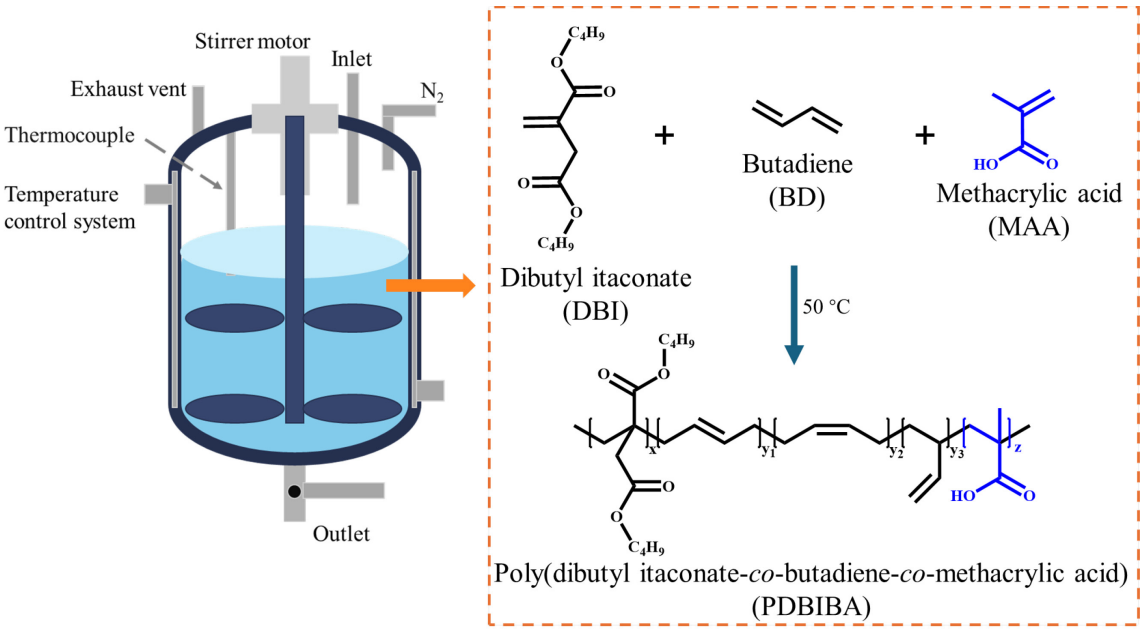

Figure 3.3 The polymerization reaction reactor and route.

Table 3.1 Recipe for emulsion polymerization.

Ingredients	Dosage/g
Dibutyl itaconate (DBI)	240
Butadiene (BD)	160
Methacrylic acid (MAA)	0, 4, 12, 28, 40, 60
Sodium dodecyl benzene sulfonate (SDBS)	12
Sodium salt of polynaphthalene sulphonic acid (Dispersing Agent NNO)	2
$K_2S_2O_8$	1.2
$FeSO_4$	0.4
Ethylene diamine tetraacetic acid (EDTA)	0.8
Deionized water	800

The latex was then poured into anhydrous ethanol, leading to the precipitation of solid PDBIBA gum. The gum was thoroughly washed with deionized water three times and then dried in a vacuum oven at 60 °C until a constant weight was achieved. PDBIBA gums with varying MAA content were synthesized under identical conditions. The notation PDBIBA-n refers to the neat polymer prepared with varying feed ratios of MAA, where " n " denotes the weight percentage of MAA relative to the combined mass of DBI and Bd used in the polymerization.

3.2.3 Cross-linking behavior of PDBIBAs and silica/PDBIBA nanocomposites

Table 3.2 lists the compositions of the PDBIBAs and silica/PDBIBA mixtures used to study cross-linking behavior. PDBIBA gums and zinc oxide, stearic acid, an accelerator, sulfur at room temperature were mixed on a two-roll mill with 15 cm diameter and 30 cm length rolls, operating at a speed ratio of 1:1.27. Cold water circulated through the rolls to maintain near-room temperature during mixing. The cross-linking behavior of the resulting PDBIBA mixtures was evaluated using a MD2000AN Rotorless Rheometer (GOTECH Testing Machines Inc.) via isothermal time sweep at 150 °C for 60 min.

Table 3.2 Compounding formulation for cross-linked PDBIBAs and silica/PDBIBA nanocomposites.

Ingredients	Dosage (phr) [a]	
	PDBIBAs	silica/PDBIBAs
PDBIBA-n	100	100
Silica 1165	-	50
Si69 [b]	-	5
Antioxidant RD [c]	-	2
Antioxidant 4020 [d]	-	0.75
ZnO	5	5
Stearic acid (SA)	0.5	0.5
Accelerator CZ [e]	1	1
Accelerator M [f]	0.7	0.7
Sulfur (S)	1	1

a Parts per 100 parts of rubber (by mass)

b Bis [3-(triethoxysilyl) propyl] tetrasulfide

c Poly (1,2-dihydro-2,2,4-trimethyl-quinoline)

d N-1,3-dimethylbutyl-N'-phenyl-p-phenylenediamine

e 2-mercapt-obenzothiazole

f N-cyclohexylbenzothiazole-2-sulphenamide

For silica/PDBIBA nanocomposites, the process involved the use of a Haake mixer (Rheomix 600OS) and a two-roll mill. The PDBIBA gums, silica, and Si69 were first added into a Haake mixer at room temperature and pre-mixed at a rotation speed of 45 rpm. The mixture was then removed, and the mixer temperature was raised to 150 °C. The pre-mixed materials were reintroduced and mixed for 5 min at this elevated temperature, maintaining a rotation speed of 45 rpm. Subsequently, after cooling to room temperature, the compound was transferred to a two-roll mill, where zinc oxide, stearic acid, antioxidant, sulfur, and accelerator were incorporated at room temperature. Similarly, the cross-linking behavior of the silica/PDBIBA mixtures was also tested under the same conditions. The optimal vulcanization times (T_{90}) are listed in **Table 3.3**.

Table 3.3 Optimal vulcanization times (T_{90}) of PDBIBAs and silica/PDBIBA mixtures with different MAA contents.

PDBIBAs and silica/PDBIBA	T_{90}/min
PDBIBA-0	3.4
PDBIBA-1	6.0
PDBIBA-3	12.6
PDBIBA-7	21.1
PDBIBA-10	43.1
PDBIBA-15	46.9
Silica/PDBIBA-0	43.2
Silica/PDBIBA-1	42.3
Silica/PDBIBA-3	39.9
Silica/PDBIBA-7	36.2
Silica/PDBIBA-10	35.4
Silica/PDBIBA-15	35.6

3.2.4 Preparation of cross-linked PDBIBAs and silica/PDBIBA nanocomposites

Following this, the PDBIBAs and silica/PDBIBA compound was vulcanized through compression molding at 150 °C under a pressure of 15 MPa into 1 mm-thick sheets, resulting in the cross-linked PDBIBAs and silica/PDBIBA nanocomposites.

3.3 Characterization methods

Fourier transform infrared spectroscopy (FTIR)

To analyze the characteristic functional groups, the FTIR spectra of neat PDBIBAs were recorded by a Bruker Tensor 27 spectrometer (Bruker, Germany) using a universal attenuated total reflectance (UATR) mode within the spectral range of 400−4000 cm^{-1} and resolution of 4.0 cm^{-1}, with a germanium crystal as the ATR element.

^{1}H Nuclear magnetic resonance (^{1}H NMR)

To characterize the molecular structure of the neat PDBIBAs, their ^{1}H NMR spectra were recorded on a Bruker AV400 spectrometer (Bruker, Germany) operating at 400 MHz. Neat PDBIBA elastomers were dissolved in deuterated chloroform ($CDCl_3$).

Gel permeation chromatography (GPC)

The molecular weight of neat PDBIBAs were measured using Waters 515-717-2410 GPC system with an RI detector (Waters 2410) and threecolumn Waters Styragel (HT6E-HT5-HT3). Tetrahydrofuran (THF) was pumped at 1.0 mL/min as an eluent and polystyrene standard was used for calibration.

Differential scanning calorimetry (DSC)

To obtain the glass transition temperature of the neat PDBIBAs, differential scanning calorimetry (DSC) analyses of neat PDBIBAs were conducted using a DSC1 STARe system (Mettler-Toledo, Switzerland) under an N_2 atmosphere. The specific steps are as follows: the samples (5−6 mg) were first heated to 100 °C and maintained at 100 °C for 5 min, then cooled down to -80 °C, and finally heated again to 100 °C with a heating rate of 10 °C/min.

Thermogravimetric analysis (TGA)

To evaluate the thermal stability of the neat PDBIBAs, Mettler-Toledo thermal gravimetric analyzer was used to perform the thermogravimetric analysis (TGA) of the neat PDBIBA elastomers. The experiment was carried out under nitrogen flow in the temperature range of 30−800 °C at a heating rate of 10 °C/min.

Transmission electron microscopy (TEM)

To examine the dispersion state of silica, the detailed microscopic structures were observed using a transmission electron microscope (Tecnai G2 20 S-TWIN) operated at an accelerating voltage of 100 kV. Prior to observation, the silica/PDBIBA nanocomposites were cryo-microtomed into approximately 100 nm-thick sections using a Leica EM UC7/FC7.

Mechanical properties

To assess the macroscopic tensile strength and deformation behavior of cross-linked PDBIBAs and silica/PDBIBA nanocomposites, the tensile properties of the samples were tested using a CMT 4104 tensile instrument (SANS Test Machine Co., Ltd., Shenzhen, China) at a stretch rate of 500 mm/min according to GB/T528-2009 at ambient temperature. Each tensile curve represents the average of five independent specimens to ensure reproducibility. Cyclic tensile tests were conducted with a rate of 200 mm/min for both loading and unloading.

Rubber processing analysis (RPA)

To investigate the interfacial interaction between PDBIBAs and silica, storage modulus−strain curves of PDBIBA/silica compounds were obtained by a rheometer (RPA2000, Alpha Technologies Co., Ltd.). Specific conditions are as follows: strain range, 0.28−200%; test temperature, 60 °C; test frequency, 1.0 Hz.

Dynamic mechanical thermal analysis (DMTA)

To evaluate the temperature-dependent viscoelastic behavior, the dynamic mechanical analyses (DMTA) analyses of samples were conducted using a DMA1 with STARe System (Mettler Toledo, Switzerland) under a tension mode. Specific conditions are as follows: temperature range, -80 to 100 °C; heating rate, 3.0 °C/min; test deformation, 0.3%; test frequency, 10.0 Hz, a commonly used setting in elastomer testing to simulate high-frequency service conditions such as vibration or repeated impact.

Measurement of cross-linking density by low-field NMR

The cross-linking density tester used in this study was manufactured by Niumag Analytical Instrument Co., Ltd., Jiangsu, China. Vulcanized rubber samples were prepared for testing by cutting them into dimensions of 3 cm in length and 0.2 cm in width. The testing temperature was set at 90 °C, and each sample was measured five times to ensure accuracy, with the median value recorded as the final result.

DIN abrasion loss of silica/PDBIBA nanocomposites

The DIN abrasion test is conducted according to GB 9867-2008. The silica/PDBIBA compound was compression-molded using a custom mold at 150 °C under a pressure of 15 MPa into cylindrical specimens with a diameter of 16 mm and a height of 10 mm, for the optimal vulcanization time. The testing conditions for the DIN abrasion test are as follows: a travel distance of 40 m, a load of 10 N, and a drum rotation speed of 40±1 r/min. Experimental Steps:

(1) Measure the mass of the sample using an electronic balance and denote it as m_1.

(2) Secure the sample in the testing apparatus so that its surface is flush with the fixed edge line. Adjust the knob to ensure that the sample surface protrudes by 2±0.2 mm. During the actual testing process, if the abrasion performance of the sample is expected to be poor and the abrasion thickness exceeds 2 mm, the instrument should be stopped, and the clamp should be

adjusted to return the sample to the initial exposed thickness before restarting the test.

(3) The sample is abraded from the start to the endpoint on the sandpaper, covering a total distance of 40 m. During the operation of the instrument, continuously use a brush to clean debris from the sandpaper. After the test, remove the sample from the fixed column and use a brush to remove any fragments and dust.

(4) Reweigh the sample to obtain its weight, denoted as m_2. The abrasion mass loss (Δm) is calculated using the following formula: $\Delta m = m_1 - m_2$. Measure the sample density using the electronic balance drainage method to calculate the abrasion volume.

Thermo-oxidative aging experiments of silica/PDBIBA nanocomposites

Silica/PDBIBA nanocomposites were placed in a GT-7017-E aging oven for thermo-oxidative aging at a temperature of 100 °C for 72 h. The mechanical properties of silica/PDBIBA nanocomposites were evaluated before and after aging to assess the material's resistance to thermal-oxidative degradation. This resistance was quantified using the "mechanical property retention ratio," denoted as R, a dimensionless parameter representing the fraction of the original mechanical property retained after aging, as given below:

$$R_\sigma = \frac{\sigma}{\sigma_0} \times 100\%$$

$$R_\varepsilon = \frac{\varepsilon}{\varepsilon_0} \times 100\%$$

where R_σ and R_ε represent the retention ratios of tensile strength and elongation at break, respectively; σ and ε are the tensile strength and elongation at break after aging, while σ_0 and ε_0 are the corresponding values before aging.

Oil resistance evaluation of silica/PDBIBA nanocomposites

According to the GB/T 1690-2010 testing standard, the oil resistance of silica/PDBIBA nanocomposites is evaluated by measuring the mechanical property retention ratio (R) and the percentage of mass gain and that of volume gain after immersion in IRM-903# oil at 100 °C for 72 h.

$$Percentage\ of\ mass\ \ gain\ (\Delta m) = \frac{m_2 - m_1}{m_1} \times 100\%$$

where:

m_1: mass of the sample before oil immersion (g)

m_2: mass of the sample after oil immersion (g)

$$Percentage\ of\ volume\ \ gain\ (\Delta V) = \frac{V_2 - V_1}{V_1} \times 100\%$$

V_1: volume of the sample before oil immersion (mm^3)

V_2: volume of the sample after oil immersion (mm^3)

3.4 Results and discussion

3.4.1 Synthesis and characterization of neat PDBIBAs

The emulsion copolymerization of dibutyl itaconate (DBI), butadiene (BD), and methacrylic acid (MAA) was initiated using potassium persulfate ($K_2S_2O_8$) at a constant temperature of 50 °C, and the reaction was maintained for 8 h. As a result, a series of copolymers with varying contents of MAA units were synthesized. **Table 3.4** presents key data on the molecular characteristics of these copolymers, including number-average molecular weight (M_n), molecular weight distribution ($Đ$), yield, viscosity, and particle size of the latex. PDBIBA-n denotes a neat polymer synthesized with MAA feed content of n wt%, calculated based on the total mass of DBI and Bd in the polymerization

For the copolymer without MAA, denoted as PDBIBA-0, the M_n is around 310 kg/mol. However, as MAA is introduced, M_n ranges from 173 kg/mol to 254 kg/mol. This reduction in molecular weight can be attributed to the carboxyl groups in MAA, which participated in chain transfer reactions and limit polymer chain growth during the emulsion polymerization process. It also leads to an increase in the molecular weight distribution ($Đ$). The copolymerization process is efficient, as evidenced by the high polymer yields, ranging from 73% to 97%. The yield tends to decrease at higher MAA content, likely due to chain transfer or chain termination involving MAA, which may interfere with the polymerization process [23-25].The viscosity of the latex is low, between 8 and 9 mPa·s. The average particle size, measured as the Z-average diameter, ranges from 83 to 93 nm.

Table 3.4. The number-average molecular weight (M_n), molecular weight distribution ($Đ$), yield, viscosity, and latex particle size of PDBIBAs with different MAA contents.

Neat PDBIBAs	M_n (kg/mol)	$Đ$	Yield (%)	Viscosity (mPa·s)	Z-average (nm)
PDBIBA-0	310	1.5	95	8	88
PDBIBA-1	249	1.9	95	8	92
PDBIBA-3	254	1.9	97	9	90
PDBIBA-7	250	3.7	96	9	93
PDBIBA-10	236	2.7	77	8	83
PDBIBA-15	173	1.9	73	8	84

3.4.2 FTIR and ^{1}H NMR characterizations of neat PDBIBAs

The chemical structure of neat PDBIBAs was analyzed and confirmed through FTIR spectra. **Figure 3.4** (a) shows the FTIR spectra of the synthesized neat PDBIBAs, with key peaks corresponding to various chemical groups clearly identified. **Table 3.5** provides the assignments of the main FTIR absorption peaks. An important feature in the spectra is the peak at 1698 cm^{-1}, which can be clearly seen in the **Figure 3.4** (b) and grows in intensity with increasing MAA content. This peak is attributed to the stretching vibration of carboxylic acid dimer structures[26-28]. The increase in peak intensity correlates with higher MAA content, confirming that MAA is successfully incorporated into the polymer backbone.

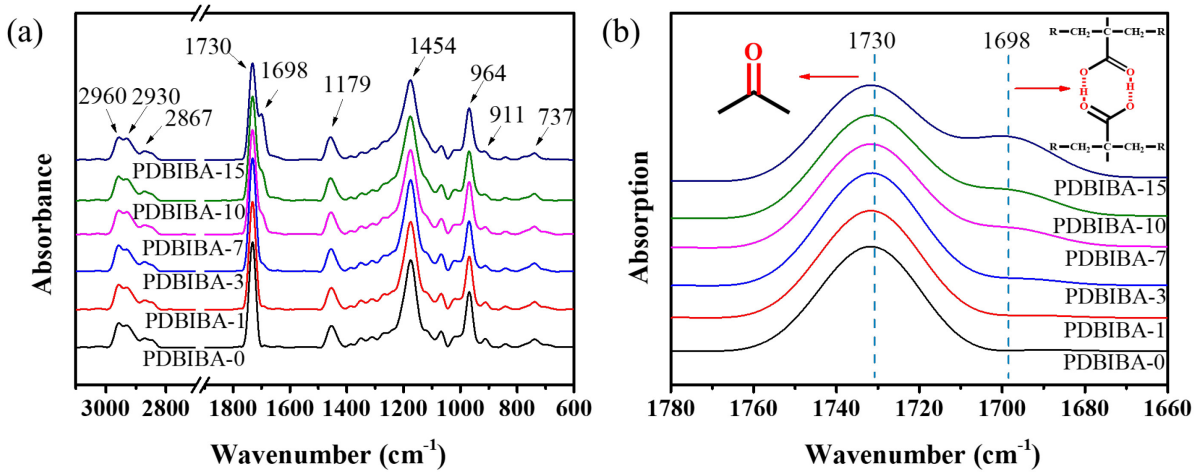

Figure 3.4 (a) FTIR spectra of the neat PDBIBAs with different amounts of MAA; (b) Magnified spectra from 1780 to 1660 cm^{-1}.

Table 3.5 Assignments of the main FTIR absorption peaks for neat PDBIBAs

Wavenumber (cm^{-1})	Vibration	Source
2960	ν ($-CH_3$)	DBI, MAA
2930	ν ($-CH_2$)	DBI, BD, MAA
2867	ν (-CH)	DBI, MAA
1730	ν (-C=O)	DBI, MAA
1698	Hydrogen-bonded carboxylic acid dimers	MAA
1454	δ ($-CH_3$), δ ($-CH_2$)	DBI, BD, MAA
1179	ν (C-O-C)	DBI
964	δ (-C-H)	Trans-BD
911	δ (-C-H)	Vinyl-BD
737	δ (-C-H)	Cis-BD

^{1}H NMR spectra was employed to investigate the microstructure of neat PDBIBAs copolymers in more detail, with **Figure 3.5** and **Figure S3.1** displaying the ^{1}H NMR spectra of neat PDBIBAs. Several characteristic peaks corresponding to different structural units in the copolymer were observed, showing the specific arrangements of butadiene and dibutyl itaconate monomers, as well as the incorporation of methacrylic acid. A distinctive peak at 1.13 ppm is assigned to the $-CH_3$ protons of the MAA units, indicating the successful incorporation of MAA into the copolymer chain. The calculated compositions of each structural unit in the polymers, based on ^{1}H NMR spectra, are presented in the **Table 3.6.** Importantly, the structural composition of MAA in the copolymer gradually increases, suggesting a direct correlation between the MAA feed ratio and the final copolymer composition. This suggests that higher MAA content in the monomer mixture results in more carboxylated units being integrated into the polymer.

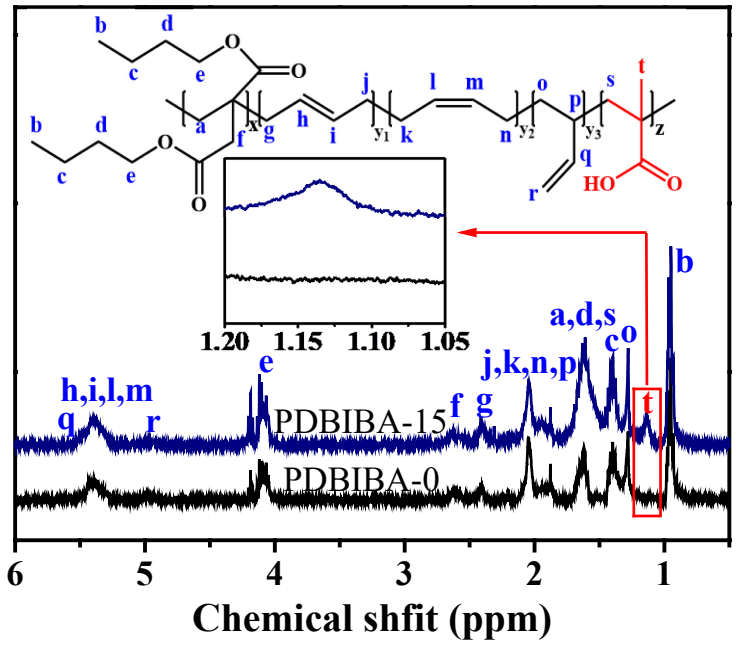

Figure 3.5 ^{1}H NMR spectra of neat PDBIBAs.

Table 3.6 Compositions of neat PDBIBAs with different MAA contents.

Neat PDBIBAs	Polymer composition (wt%)			
	DBI	Vinyl-BD	Cis-BD and trans-BD	MAA
PDBIBA-0	61.9	3.8	34.3	0
PDBIBA-1	63.1	3.8	31.4	1.7
PDBIBA-3	61.7	3.1	30.1	5.1
PDBIBA-7	60.7	2.6	29.0	7.7
PDBIBA-10	61.0	2.1	25.9	11.0
PDBIBA-15	54.3	2.3	28.4	15.0

3.4.3 Thermal properties of neat PDBIBAs

The glass transition temperature (T_g) directly influences the mechanical properties of elastomers. For optimal performance, elastomers should exhibit T_g values below room temperature to ensure flexibility under operating conditions. Ideally, elastomers should have T_g values below -30 °C, enabling them to maintain their rubber-like elasticity in a wide range of environments. In the case of neat PDBIBAs, differential scanning calorimetry (DSC) was used to study their thermal behavior, specifically analyzing the impact of MAA content on T_g. As depicted in the **Figure 3.6**, which measured the thermal properties of the copolymers from -70 °C to 50 °C, no crystalline peaks were observed, indicating that the neat PDBIBAs are completely amorphous. The introduction of MAA into the copolymer significantly increases

the T_g. The T_g values of PDBIBAs increase progressively from -57 °C (PDBIBA-0) to -32°C (PDBIBA-15) with increasing MAA content. The increase in T_g can be attributed to the introduction of MAA, which enhances the polarity of the polymer and restricts the movement of macromolecular chains to some extent. Despite this increase, the T_g values remain sufficiently low to ensure that the copolymers exhibit rubber-like elasticity at room temperature, making them suitable for elastomeric applications.

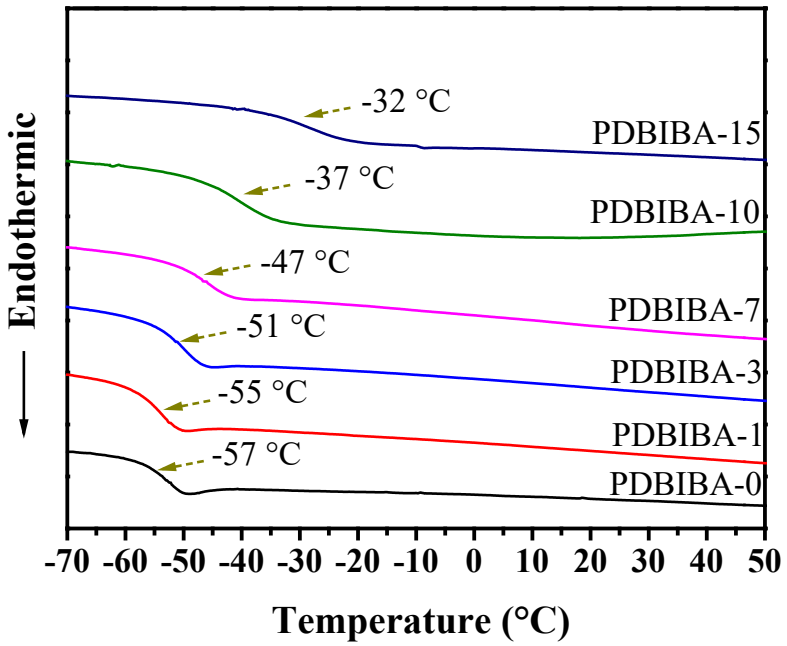

Figure 3.6 DSC curves of neat PDBIBAs with different MAA contents.

To evaluate the thermal stability of neat PDBIBAs with varying MAA content, thermogravimetric analysis (TGA) was conducted, as depicted in the provided **Figure 3.7** (a) The key thermal degradation parameters, including the temperature at 5% weight loss ($T_{5\%}$) and the temperature at the maximum degradation rate (T_{max}), are summarized in the **Table 3.7**. $T_{5\%}$ (the temperature corresponding to 5% weight loss) was chosen as a representative indicator of the onset of thermal degradation, as it reflects the initial decomposition temperature of the polymer and provides a convenient measure of its thermal stability. The results clearly show a decline in thermal stability, $T_{5\%}$ decreases significantly as the MAA content increases, particularly for PDBIBA-15, which has a $T_{5\%}$ value of 279 °C. All copolymers, except for PDBIBA-15, exhibit $T_{5\%}$ values above 300 °C, indicating their suitability for use in elastomer engineering materials. **Figure 3.7** (b) shows that the degradation process of the PDBIBAs occurs in three distinct stages, influenced by the three types of structural units: dibutyl itaconate

(DBI), butadiene (BD), and methacrylic acid (MAA).

Stage one, 99 °C to 260 °C: Degradation in this range is primarily attributed to the moisture absorption of the hydrophilic carboxyl groups introduced by the MAA units[29]. The absorbed moisture promotes early weight loss, which explains the observed decrease in $T_{5\%}$ with higher MAA content.

Stage two, 260 °C to 430 °C: The second phase of degradation is associated with the breakdown of the ester groups in the side chains of the DBI units [30]. This stage represents the major weight loss observed in the TGA curves, and the T_{max} values, ranging from 389 °C to 401 °C.

Stage three, 430 °C to 520 °C: The final degradation stage corresponds to the random breakdown of the polymer backbone, leading to complete mass loss[31].

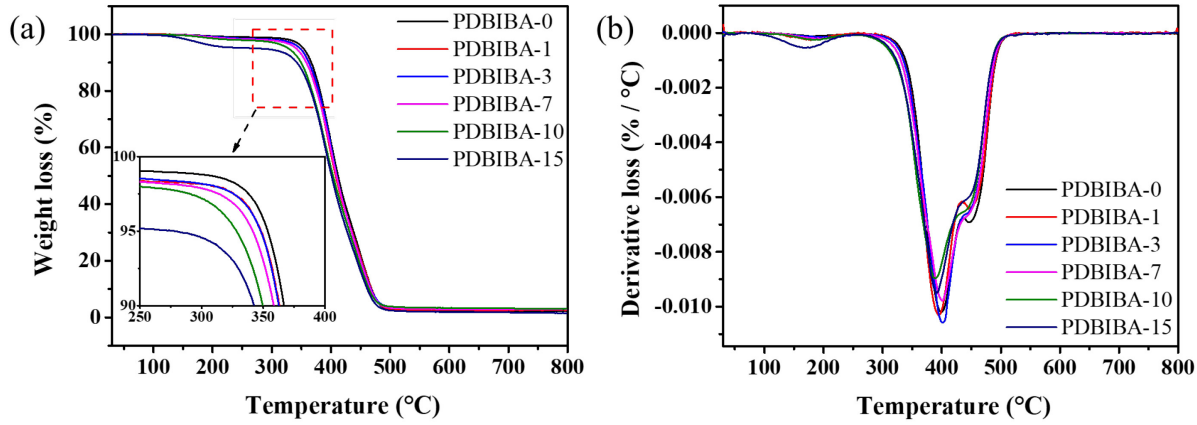

Figure 3.7 (a) TGA thermograms and (b) DTG (derivative thermograms) of neat PDBIBAs.

Table 3.7 Characteristic parameters of neat PDBIBAs determined by TGA

Neat PDBIBAs	$T_{5\%}$ [a] (°C)	T_{max} [b] (°C)
PDBIBA-0	354	400
PDBIBA-1	348	395
PDBIBA-3	348	401
PDBIBA-7	342	401
PDBIBA-10	328	392
PDBIBA-15	279	389

a $T_{5\%}$ is set as the initial degradation temperature at 5% weight loss.

b T_{max} is the temperature at the maximum degradation rate.

3.4.4 Mechanical and dynamic properties of cross-linked PDBIBAs without fillers

Figure 3.8 (a) illustrates the mechanical properties of unfilled cross-linked PDBIBAs with

varying MAA contents, and the corresponding data are presented in **Table S3.1**. As MAA content increases, there is a notable rise in the tensile strength of the PDBIBAs, while the elongation at break reaches its peak with PDBIBA-3 and then gradually declines. For instance, PDBIBA-0, which does not contain MAA, shows a tensile strength of only 3.1 MPa, with an elongation at break of 283%. However, with the introduction of carboxyl groups from MAA, the tensile strength significantly increases. For example, PDBIBA-15 achieves a tensile strength of 14.1 MPa, reflecting an increase of 355%, and its elongation at break improves to 317%. The improvement in mechanical properties is attributed to the carboxyl groups' ability to engage in cross-linking reactions with zinc oxide. This reaction forms ionic clusters and ionic cross-linked networks, which enhance the mechanical performance of the PDBIBAs[32, 33]. The cross-linking not only strengthens the material but also contributes to its toughness properties, as observed in the in **Figure 3.8** (b). The toughness of PDBIBAs also increases with higher MAA content. Toughness is the material's ability to absorb energy and undergo plastic deformation without fracturing. PDBIBA-0 exhibits the lowest toughness, while PDBIBA-15 shows the highest toughness, indicating that the material's resistance to impact and deformation improves as the MAA content increases. Additionally, as a bio-based elastomer, PDBIBAs exhibit excellent potential for sustainable applications. Its enhanced mechanical properties, combined with its bio-derived origin, make it an ideal candidate for the development of bio-based gloves and other latex products, offering a greener alternative for personal protective equipment and various latex-based applications while maintaining high performance.

The dynamic mechanical analysis directly demonstrates the formation of ionic cross-links through the emergence of an ionic transition and its associated tan δ peak, as shown in **Figure 3.8** (c) and (d). The α-relaxation associated with the glass transition shifts to higher temperatures with increasing carboxyl content, from -41 °C for PDBIBA-0 to -6 °C for PDBIBA-15, due to the higher measurement frequency (10 Hz) compared to DSC. The ionic transition, corresponding to the relaxation of polymer chains constrained in the vicinity of ionic aggregates, is absent in PDBIBA-0 but becomes evident in the carboxylated samples. This transition originates from the restricted mobility of polymer segments trapped within the ionic clusters,

which behave as an ionically aggregated phase. T_i appears consistently in the range of 53–57 °C. Meanwhile, the tan δ peak associated with T_i gradually broadens with carboxyl content, reflecting the restricted mobility of polymer chains due to ionic clusters[28, 34].

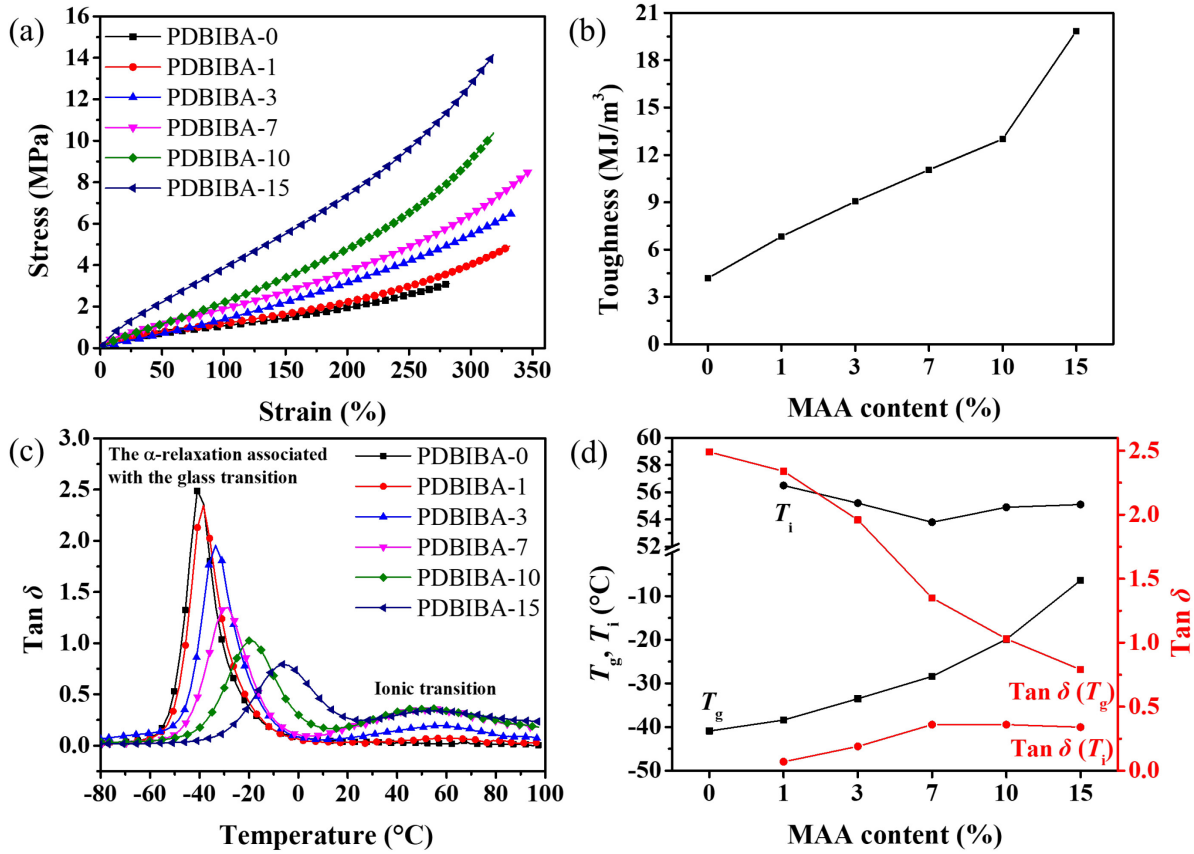

Figure 3.8 (a) Stress-strain curves; (b) Toughness; (c) Tan δ-temperature curves; (d) The α-relaxation associated with the glass transition and ionic transition, along with their corresponding tan δ values of unfilled cross-linked PDBIBAs with different MAA contents(heating rate, 3.0 °C/min; test deformation, 0.3%; test frequency, 10.0 Hz).

3.4.5 Interfacial interaction between PDBIBAs and silica

The addition of reinforcing fillers such as silica plays a crucial role in improving the mechanical properties of elastomers. It enhances their strength, elasticity, and durability, expanding their application scope beyond non-reinforced latex products to meet the demands of various fields. To better understand the influence of these fillers at the microscopic level, rubber processing analysis (RPA) is used to investigate the effect of different interfaces in nanocomposites on the filler network and viscoelasticity. Two types of filler networks are usually present in filler-filled nanocomposites: one is formed by the filler-filler contact with

each other, which is called filler-filler network, and the other is formed by bridging neighboring fillers through macromolecules, which is called filler-rubber network. Both types of filler networks increase the deformation resistance of the rubber material to some extent, thus increasing the storage modulus. At low strains, the presence of the filler-rubber network results in a composite with a high storage modulus. As the strain increases, the filler-filler network structure is destroyed and the storage modulus decreases dramatically, a phenomenon known as the Payne effect[35]. Usually smaller initial storage modulus and lower Payne effect imply relatively better filler dispersion[36-38].

The Rubber Process Analyzer (RPA) and Transmission Electron Microscopy (TEM) were used to study the filler network structure and interfacial interactions of silica/PDBIBA nanocomposites with varying MAA content. In the silica/PDBIBA-0 (50 phr silica) composite without carboxyl groups, the initial storage modulus is the highest, as shown in **Figure 3.9**. This high initial modulus reflects a strong filler-filler network. Although the silane coupling agent and the ester groups in PDBIBA molecular chains can form chemical bonds and hydrogen bonds with silica, respectively, to promote silica dispersion, unavoidable self-aggregation still occurs in the matrix. This phenomenon is confirmed by the TEM images in **Figure 3.10** (a). The TEM clearly shows large silica agglomerates, which result in dominant filler-filler interactions. As strain increases, storage modulus rapidly decreases, indicating the breakdown of this filler-filler network, which is characteristic of a pronounced Payne effect. The strong filler network and poor dispersion cause significant modulus loss under strain. After the introduction of carboxyl groups in the form of MAA (as seen in silica/PDBIBA-1 through silica/PDBIBA-15), the initial modulus gradually decreases in the RPA curves. Particularly for silica/PDBIBA-10 and silica/PDBIBA-15, storage modulus remains almost constant in the strain range from 0.27% to 20%. This behavior is indicative of a well-dispersed filler network and strong polymer-filler bonding. The introduction of MAA improves the dispersion of silica within the PDBIBA matrix, as observed in the TEM images in the **Figure 3.10** (b, c, d, e, f), where the particle agglomerates become smaller and more uniformly distributed. This improved dispersion results from hydrogen bonding between the carboxyl groups in PDBIBA and the hydroxyl groups on silica.

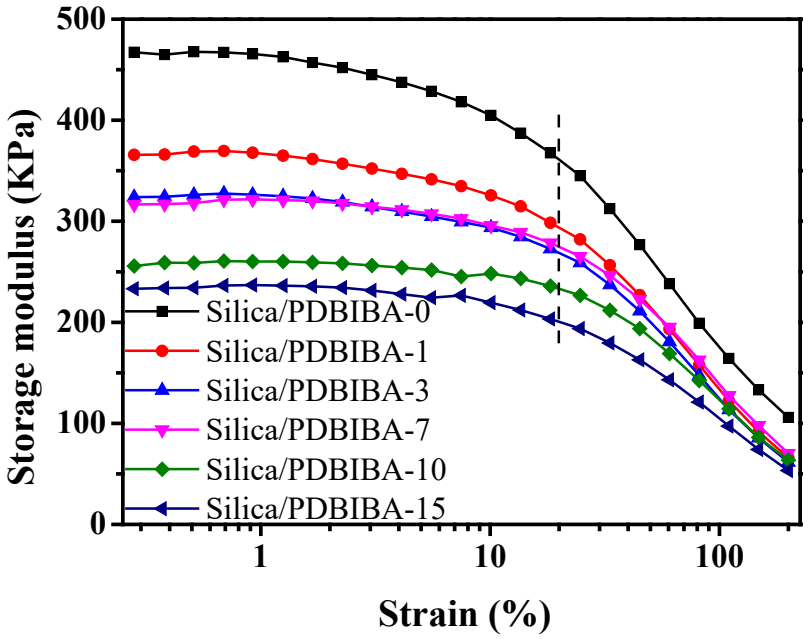

Figure 3.9 Storage modulus strain of uncross-linked silica/PDBIBA (50 phr silica) compounds.

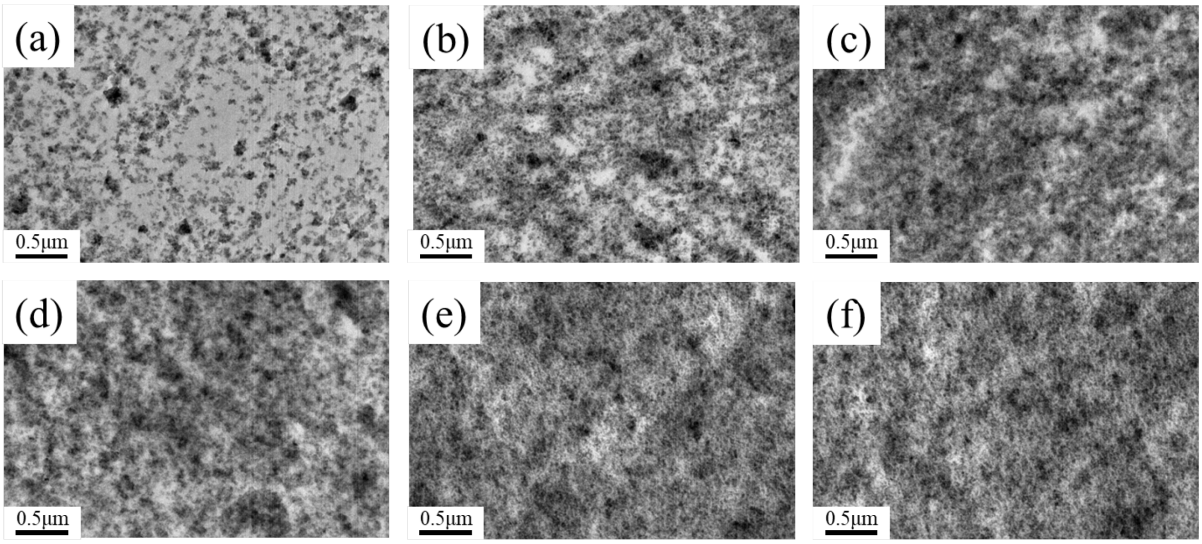

Figure 3.10 TEM images for silica/PDBIBA nanocomposites with different MAA contents: (a) Silica/PDBIBA-0; (b) Silica/PDBIBA-1; (c) Silica/PDBIBA-3; (d) Silica/PDBIBA-7; (e) Silica/PDBIBA-10; (f) Silica/PDBIBA-15.

The formation of hydrogen bonds between the carboxyl groups in PDBIBAs and the hydroxyl groups on the silica surface is further supported by FTIR analysis. As shown in **Figure 3.11** (a), the broad O-H stretching band of silica centered at ~3437 cm^{-1} gradually shifts to lower wavenumbers with increasing MAA content, decreasing to 3385 cm^{-1} for silica/PDBIBA-0 and 3288 cm^{-1} for silica/PDBIBA-7. This red shift indicates stronger hydrogen bonding between the silanol groups on silica and the carboxyl groups in the PDBIBA matrix. Additionally, in

Figure 3.11 (b), the Si-O-Si stretching peak of silica (~1100 cm^{-1}) and the C-O-C stretching region (~1162–1173 cm^{-1}) both shift slightly in the composites, particularly in silica/PDBIBA-7, further suggesting enhanced interfacial interactions through hydrogen bonding[6, 39]. These spectral changes confirm that the introduction of carboxyl groups promotes the formation of hydrogen bonds (**Figure 3.11** (c)), thereby strengthening the polymer–filler interface.

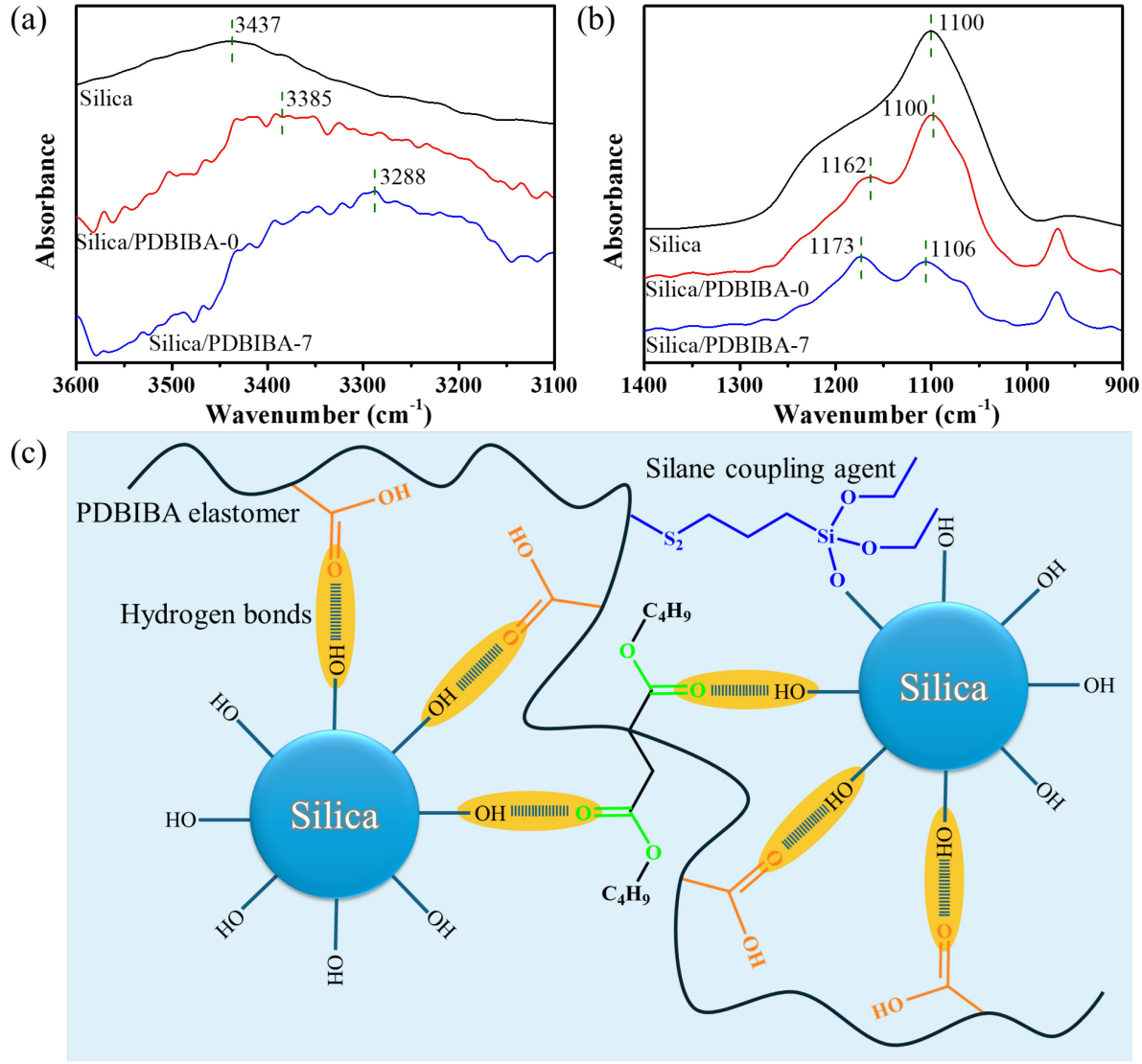

Figure 3.11 (a) FTIR spectra of silica, silica/PDBIBA-0, and silica/PDBIBA-7 in the O-H stretching region. (b) FTIR spectra of the same samples in the Si-O-Si and C-O-C stretching region. (c) Schematic diagram of interfacial interactions in silica/PDBIBA nanocomposites.

3.4.6 Mechanical and dynamic properties of silica/PDBIBA nanocomposites

The **Figure 3.12** provides the mechanical properties and structural characteristics of silica/PDBIBA nanocomposites with varying MAA content. In **Figure 3.12** (a), the tensile strength of the nanocomposites increases significantly from 15.5 MPa for silica/PDBIBA-0 to 24.4 MPa for silica/PDBIBA-15. For instance, in the case of PDBIBA-7, the addition of silica leads to a remarkable improvement, with the tensile strength increasing from 8.5 MPa in the non-reinforced material to 23.5 MPa, reflecting a 176% enhancement. Additionally, the elongation at break improves from 347% to 377%. The corresponding data are presented in **Table S3.2**. This improvement in tensile strength is attributed to enhanced interfacial bonding between the silica filler and the polymer matrix. The elongation at break initially increases, peaking at 393% for silica/PDBIBA-3, before it begins to decline with higher MAA content. As MAA content increases, the cross-linking density rises due to the interaction between the carboxyl groups and silica, limiting polymer chain mobility and reducing the elongation at break for higher MAA nanocomposites, such as silica/PDBIBA-10 and silica/PDBIBA-15. **Figure 3.12** (b) further supports this trend, showing that the Young's modulus of the nanocomposites increases with MAA content. This increase in stiffness results from the higher cross-linking density that restricts chain movement. **Figure 3.12** (c), depicting the cyclic stress-strain behavior, reveals that nanocomposite with higher MAA content exhibits greater resilience under repeated deformation, showing higher stress values at comparable strain levels. This resilience highlights the composite's capability to withstand cyclic loads.

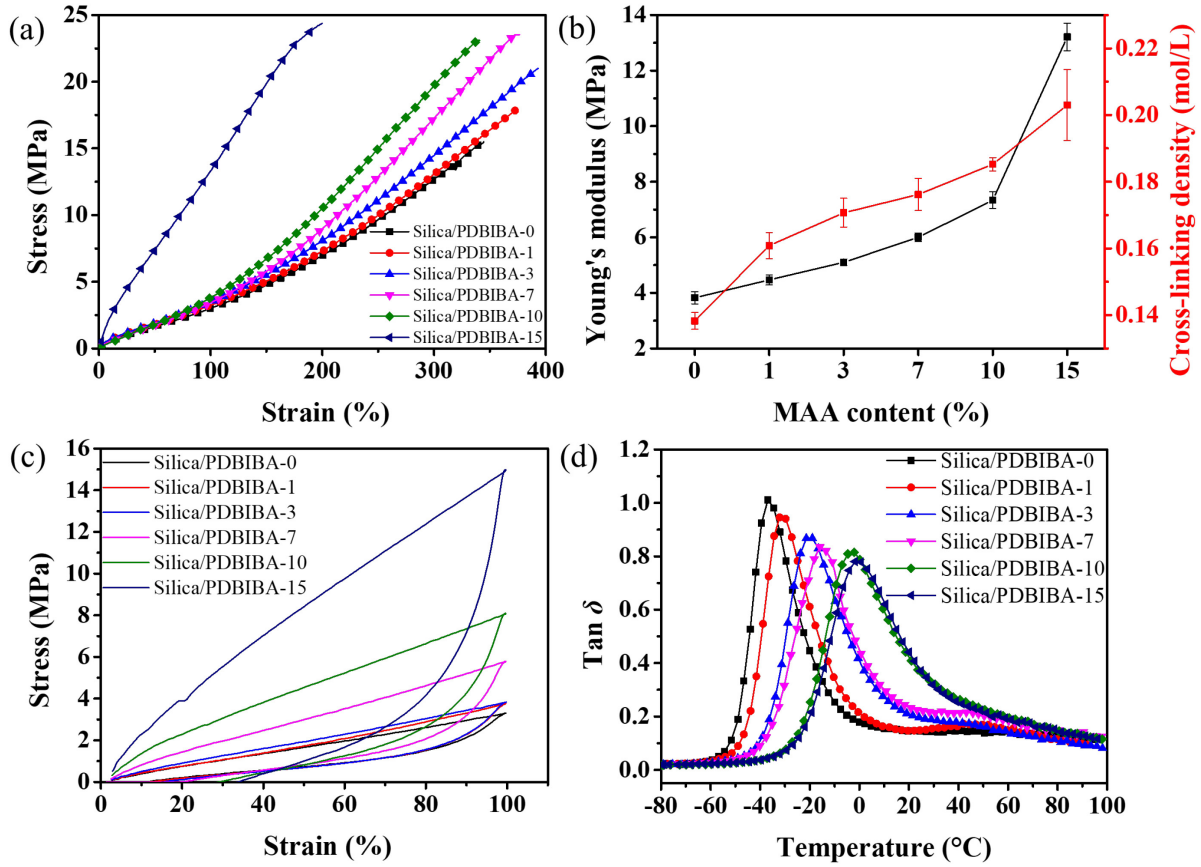

Figure 3.12 Silica/PDBIBA nanocomposites with different MAA contents: (a) Stress-strain curves; (b) Young's modulus and cross-linking density; (c) Cyclic tensile test; (d) Temperature dependence of loss tangent (heating rate, 3.0 °C/min; test deformation, 0.3%; test frequency, 10.0 Hz).

The tan δ versus temperature curves for silica/PDBIBA nanocomposites with varying MAA content are shown in **Figure 3.12** (d), with the corresponding data listed in **Table 3.8**. As MAA content increases, the α-relaxation associated with the glass transition shifts to higher temperatures. For instance, the temperature of the α-relaxation associated with the glass transition for silica/PDBIBA-0 is around -37 °C, while for silica/PDBIBA-15, it rises closer to -2 °C. The variation in the α-relaxation associated with the glass transition is not only related to the intrinsic properties of PDBIBAs but is also influenced by the interfacial interactions in the composite. As the MAA content increases, the interfacial interactions between silica and PDBIBAs become stronger, further restricting the motion of PDBIBAs chain segments, shifting the α-relaxation associated with the glass transition to higher temperatures. Meanwhile, the restricted chain segment motion also contributes to a reduction in the tan δ peak value of the composite to some extent. In the tire industry, it is widely accepted that a higher tan δ value at 0 °C indicates better wet skid performance, while a lower tan δ value at 60 °C corresponds to

reduced rolling resistance[40, 41]. However, the data suggests that higher MAA content in the silica/PDBIBA nanocomposites leads to increased tan δ at 60 °C, indicating higher rolling resistance, which makes these materials less suitable for tire applications requiring low rolling resistance. On the other hand, the widening of the tan $\delta > 0.3$ temperature range with increasing MAA content demonstrates their enhanced energy dissipation capabilities across a broader temperature range, showing potential for applications in damping materials.

Table 3.8 Dynamic mechanical properties of silica/PDBIBA nanocomposites.

Cross-linked silica/PDBIBA	Temperature of the α-relaxation associated with the glass transition / °C	Tan $\delta > 0.3$ / °C	Tan δ		
			0 °C	60 °C	MAX
Silica/PDBIBA-0	-37	-47~-15	0.179	0.145	1.011
Silica/PDBIBA-1	-32	-42~-8	0.155	0.134	0.923
Silica/PDBIBA-3	-21	-31~7	0.419	0.146	0.868
Silica/PDBIBA-7	-16	-30~8	0.436	0.184	0.835
Silica/PDBIBA-10	-2	-17~31	0.788	0.195	0.815
Silica/PDBIBA-15	-2	-17~32	0.778	0.188	0.780

3.4.7 DIN abrasion loss of silica/PDBIBA nanocomposites

Abrasion resistance is a critical performance attribute of materials, directly impacting their service life and operational safety. The DIN abrasion and shore A hardness of silica/PDBIBA nanocomposites is shown in **Figure 3.13**. The introduction of carboxyl groups into silica/PDBIBA nanocomposites significantly enhances their abrasion resistance, as shown by the reduction in abrasion volume from 0.198 cm^3 to 0.114 cm^3. The primary reasons for this improvement are the increased hardness of the nanocomposites and the stronger interfacial interactions between the polymer matrix and the silica filler.

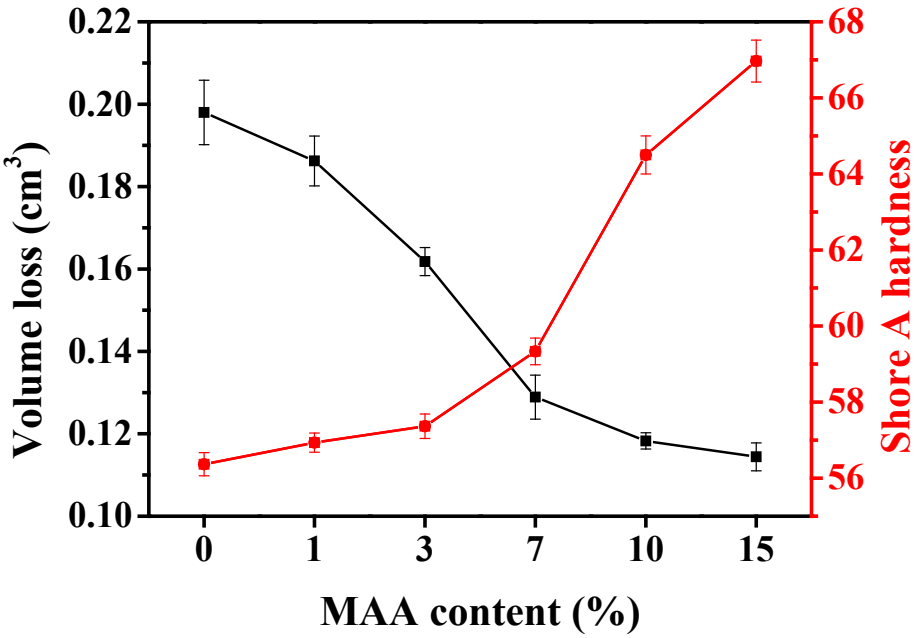

Figure 3.13 DIN abrasion loss and shore A hardness of silica/PDBIBA nanocomposites with different MAA contents.

3.4.8 Thermo-oxidative aging properties of silica/PDBIBA nanocomposites

Aging of elastomer products is an unavoidable challenge in practical applications. The **Figure 3.14** illustrates the mechanical property retention ratio (R) of silica/PDBIBA nanocomposites after aging at 100 °C for 72 h, and the corresponding data are presented in **Table S3.3**. As the MAA content increases, the retention ratios of tensile strength (R_σ) of the silica/PDBIBA nanocomposites shows an upward trend. This is because the MAA units in the PDBIBA molecular chain increase the polarity of the rubber macromolecules, strengthen the interfacial interactions between silica and PDBIBAs, and enhance the cross-linking density. These effects reduce the attack of oxygen on the double bonds[42-45], providing protection for the unsaturated bonds and improving the aging resistance of the material. However, when the carboxyl content becomes excessively high, such as in the silica/PDBIBA-15 composite, the tensile strength retention exceeds 100%, yet the retention ratios of elongation at break (R_ε) decreases. This is due to the excessive cross-linking of the material after aging, which significantly reduces the elongation at break. Consequently, although the strength retention of the material may still improve, its overall flexibility and toughness decrease, which negatively affects its durability under aging conditions.

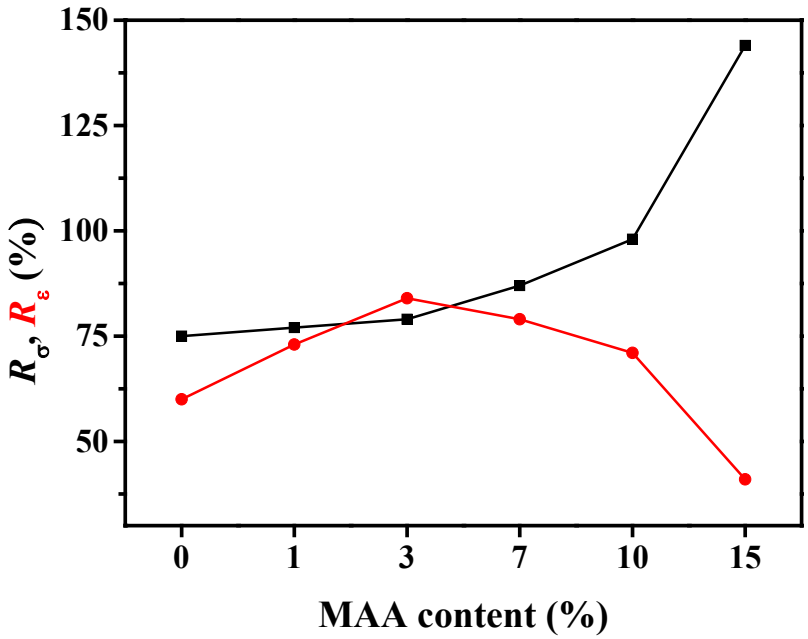

Figure 3.14 Thermo-oxidative aging properties of silica/PDBIBA nanocomposites: retention ratios of tensile strength (R_σ) and elongation at break (R_ε) after aging at 100 °C for 72 h.

3.4.9 Oil resistance evaluation of silica/PDBIBA nanocomposites

Traditional petroleum-based oil-resistant rubbers, such as nitrile rubber (NBR), acrylate rubber (AR), and fluororubber (FKM), play a crucial role in the rubber industry. To assess the oil resistance of silica/PDBIBA nanocomposites, tests were carried out in accordance with the GB/T 1690-2010 standard. The samples were immersed in IRM-903# oil at 100 °C for 72 h. As seen in **Figure 3.15** (a), the retention ratios of tensile strength (R_σ) and elongation at break (R_ε) increase as the MAA content rises. For instance, the tensile strength and elongation at break retention of the silica/PDBIBA-0 nanocomposites are 5% and 29%, respectively, whereas in silica/PDBIBA-15, these values improve significantly to 24% and 60%. The corresponding data are presented in **Table S3.4**. Additionally, **Figure 3.15** (b) demonstrates that higher MAA content leads to lower percentage of mass gain (Δm) and that of volume gain (ΔV). This is because the polar MAA units increases the polarity of the PDBIBA matrix, thereby enhancing its resistance to non-polar oils. In addition, the incorporation of MAA contributes to a higher cross-linking density within the polymer network, forming a denser and more tightly bound matrix that effectively hinders the diffusion of non-polar oil molecules. Furthermore, the higher MAA content strengthens the interfacial interaction between PDBIBA and silica, improving the

dispersion of silica particles throughout the matrix. This enhanced interfacial bonding reduces the voids and pathways for non-polar oils to penetrate the composite. Consequently, the synergistic effects of increased polarity, stronger interfacial interactions, and a more densely cross-linked network significantly improve the oil resistance of the composite material.

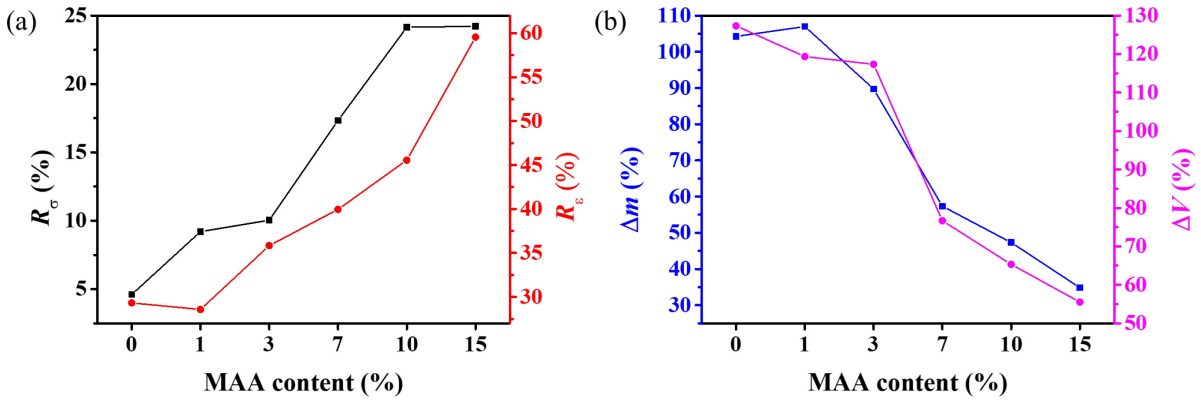

Figure 3.15 (a) Retention ratios of tensile strength (R_σ) and elongation at break (R_ε); (b) Percentage of mass gain (Δm) and that of volume gain (ΔV) of silica/PDBIBA nanocomposites after being soaked in IRM-903# oil at 100 °C for 72 h.

3.5 Conclusions

This study synthesized bio-based poly(dibutyl itaconate-*co*-butadiene-*co*-methacrylic acid) (PDBIBAs) elastomers via emulsion polymerization, with a molecular weight ranging from 173 to 310 kg/mol. Increasing the MAA content led to a rise in T_g from -57 °C to -32 °C, and significantly enhanced the mechanical properties due to cross-linking reactions between carboxyl groups and zinc oxide, improving both strength and toughness, with the tensile strength increasing from 3.1 MPa for PDBIBA-0 to 14.1 MPa for PDBIBA-15. For silica/PDBIBA nanocomposites, the introduction of carboxyl groups facilitated stronger interfacial interactions with silica, resulting in increased tensile strength. RPA analysis and TEM images confirmed well-dispersed silica networks. The carboxyl groups also improved abrasion resistance, reducing the abrasion volume due to increased composite hardness and better dispersion of silica. Thermo-oxidative aging tests demonstrated that samples with higher MAA content retained more tensile strength after aging, although this came with a reduction in elongation at break, reflecting a trade-off between strength and flexibility. Oil resistance tests

indicated that higher MAA content led to reduced mass and volume gain, as well as improved retention ratio of tensile strength and elongation at break, due to enhanced polarity and stronger polymer-silica interactions. In conclusion, the carboxylation of itaconate elastomers significantly enhances mechanical strength, abrasion resistance, aging stability, and oil resistance of silica nanocomposites, making these materials potentially suitable for demanding applications.

3.6 References

[1] HUANG J, ZHANG L, TANG Z, et al. Bioinspired Engineering of Sacrificial Bonds into Rubber Networks towards High-performance and Functional Elastomers [J]. Composites Communications, 2018, 8: 65-73.

[2] HU J, LIU W, YANG L, et al. Research on Classification Methods for Rubber Based on Terahertz Time-domain Spectroscopy with Data Fusion Strategy [J]. Infrared Physics & Technology, 2024, 139: 105324.

[3] DHANORKAR R J, MOHANTY S, GUPTA V K. Synthesis of Functionalized Styrene Butadiene Rubber and Its Applications in SBR–silica Composites for High Performance Tire Applications [J]. Industrial & Engineering Chemistry Research, 2021, 60(12): 4517-4535.

[4] PRABHU C P, MOHANTY S, GUPTA V K. Modification of Polybutadiene Rubber: A Review [J]. Rubber Chemistry and Technology, 2021, 94(3): 410-431.

[5] KOTOVA S, BUHTIYAROVA N, MIKHAILOV S. Improved Properties of Nitrile Butadiene Rubber [J]. Rubber World, 2013, 248(5): 18-20.

[6] WANG R, MA J, ZHOU X, et al. Design and Preparation of A Novel Cross-linkable, High Molecular Weight, and Bio-Based Elastomer by Emulsion Polymerization [J]. Macromolecules, 2012, 45(17): 6830-6839.

[7] LEI W, RUSSELL T P, HU L, et al. Pendant Chain Effect on the Synthesis, Characterization, and Structure–property Relations of Poly(di-n-alkyl itaconate-co-

isoprene) Biobased Elastomers [J]. ACS Sustainable Chemistry & Engineering, 2017, 5(6): 5214-5223.

[8] LEI W, YANG X, QIAO H, et al. Renewable Resource-based Elastomer Nanocomposite Derived from Myrcene, Ethanol, Itaconic Acid and Nanosilica: Design, Preparation and Properties [J]. European Polymer Journal, 2018, 106: 1-8.

[9] ZHOU X, JI H, HU G-H, et al. A Solvent-less Green Synthetic Route toward a Sustainable Bio-based Elastomer: Design, Synthesis, and Characterization of Poly(dibutyl itaconate-co-butadiene) [J]. Polymer Chemistry, 2019, 10(45): 6131-6144.

[10] SENGLOYLUAN K, SAHAKARO K, DIERKES W K, et al. Silica-reinforced Tire Tread Compounds Compatibilized by Using Epoxidized Natural Rubber [J]. European Polymer Journal, 2014, 51: 69-79.

[11] XU T, JIA Z, LUO Y, et al. Interfacial Interaction between the Epoxidized Natural Rubber and Silica in Natural Rubber/silica Composites [J]. Applied Surface Science, 2015, 328: 306-313.

[12] VARUGHESE S, TRIPATHY D K. Chemical Interaction between Epoxidized Natural Rubber and Silica: Studies on Cure Characteristics and Low-temperature Dynamic Mechanical Properties [J]. Journal of Applied Polymer Science, 1992, 44(10): 1847-1852.

[13] WANG S, WANG Z, LI J, et al. Surface-grafting Polymers: from Chemistry to Organic Electronics [J]. Materials Chemistry Frontiers, 2020, 4(3): 692-714.

[14] BHATTACHARYA A, MISRA B N. Grafting: a Versatile Means to Modify Polymers: Techniques, Factors and Applications [J]. Progress in Polymer Science, 2004, 29(8): 767-814.

[15] KIM K, LEE J-Y, CHOI B-J, et al. Styrene-butadiene-glycidyl Methacrylate Terpolymer/silica Composites: Dispersion of Silica Particles and Dynamic Mechanical Properties [J]. Composite Interfaces, 2014, 21(8): 685-702.

[16] QIAO H, XU W, CHAO M, et al. Preparation and Performance of Silica/epoxy Group-functionalized Biobased Elastomer Nanocomposite [J]. Industrial & Engineering Chemistry Research, 2017, 56(4): 881-889.

[17] HE S-J, WANG Y-Q, FENG Y-P, et al. The Preparation of an Elastomer/silicate Layer Nanocompound with an Exfoliated Structure and a Strong Ionic Interfacial Interaction by Utilizing an Elastomer Latex Containing Pyridine Groups [J]. Nanotechnology, 2010, 21(11): 115601.

[18] TANG Z, WU X, GUO B, et al. Preparation of Butadiene–styrene–vinyl Pyridine Rubber–Graphene Oxide Hybrids through Co-coagulation Process and in Situ Interface Tailoring [J]. Journal of Materials Chemistry, 2012, 22(15): 7492-7501.

[19] MAO Y, WEN S, CHEN Y, et al. High Performance Graphene Oxide Based Rubber Composites [J]. Sci Rep, 2013, 3: 2508.

[20] CAO X, XU C, LIU Y, et al. Preparation and Properties of Carboxylated Styrene-butadiene rubber/cellulose Nanocrystals Composites [J]. Carbohydrate Polymers, 2013, 92(1): 69-76.

[21] KANG H, ZUO K, WANG Z, et al. Using a Green Method to Develop Graphene oxide/elastomers Nanocomposites with Combination of High Barrier and Mechanical Performance [J]. Composites Science and Technology, 2014, 92: 1-8.

[22] MAHMOOD N, KHAN A U, STöCKELHUBER K W, et al. Carbon Nanotubes-filled Thermoplastic Polyurethane–urea and Carboxylated Acrylonitrile Butadiene Rubber Blend Nanocomposites [J]. Journal of Applied Polymer Science, 2014, 131(11).

[23] SCHREUR-PIET I, HEUTS J P A. Amphiphilic Statistical Copolymers from Catalytic Chain Transfer as Reactive Surfactants in Emulsion Polymerization [J]. ACS Applied Polymer Materials, 2021, 3(9): 4616-4624.

[24] LEE W H, BOOTH J R, BON S A F. On Particle Size Distributions in Catalytic Chain Transfer Emulsion Polymerization: Chain-extension and the Use of Derived Macromonomers as Reactive Surfactants in Emulsion Polymerization [J]. Biomacromolecules, 2020, 21(11): 4599-4614.

[25] LOVELL P A, SCHORK F J. Fundamentals of Emulsion Polymerization [J]. Biomacromolecules, 2020, 21(11): 4396-4441.

[26] IBARRA L, MARCOS-FERNáNDEZ A, ALZORRIZ M. Mechanistic Approach to the

Curing of Carboxylated Nitrile Rubber (XNBR) by Zinc Peroxide/zinc Oxide [J]. Polymer, 2002, 43(5): 1649-1655.

[27] IBARRA L, ALZORRIZ M. Ionic Elastomers Based on Carboxylated Nitrile Rubber and Calcium Oxide [J]. Journal of Applied Polymer Science, 2003, 87(5): 805-813.

[28] BASU D, DAS A, STöCKELHUBER K W, et al. Evidence for an in Situ Developed Polymer Phase in Ionic Elastomers [J]. Macromolecules, 2014, 47(10): 3436-3450.

[29] HAN S O, DRZAL L T. Water Absorption Effects on Hydrophilic Polymer Matrix of Carboxyl Functionalized Glucose Resin and Epoxy Resin [J]. European Polymer Journal, 2003, 39(9): 1791-1799.

[30] ÖZLEM S, HACALOGLU J. Thermal Degradation of Poly(n-butyl methacrylate), Poly(n-butyl acrylate) and Poly(t-butyl acrylate) [J]. Journal of Analytical and Applied Pyrolysis, 2013, 104: 161-169.

[31] RAY S, COONEY R P. Chapter 9 - Thermal Degradation of Polymer and Polymer Composites [M]//KUTZ M. Handbook of Environmental Degradation of Materials (Third Edition). William Andrew Publishing. 2018: 185-206.

[32] IBARRA L, ALZORRIZ M. Ionic Elastomers Based on Carboxylated Nitrile Rubber and Magnesium Oxide [J]. Journal of Applied Polymer Science, 2007, 103(3): 1894-1899.

[33] IBARRA L, RODRíGUEZ A, MORA-BARRANTES I. Crosslinking of Unfilled Carboxylated Nitrile Rubber with Different Systems: Influence on Properties [J]. Journal of Applied Polymer Science, 2008, 108(4): 2197-2205.

[34] MALMIERCA M A, GONZáLEZ-JIMéNEZ A, MORA-BARRANTES I, et al. Characterization of Network Structure and Chain Dynamics of Elastomeric Ionomers by Means of 1H Low-Field NMR [J]. Macromolecules, 2014, 47(16): 5655-5667.

[35] PAYNE A R. The Dynamic Properties of Carbon Black-loaded Natural Rubber Vulcanizates. Part I [J]. Rubber Chemistry and Technology, 1963, 36(2): 432-443.

[36] YANG R, SONG Y, ZHENG Q. Payne Effect of Silica-filled Styrene-butadiene Rubber [J]. Polymer, 2017, 116: 304-313.

[37] FU W, WANG L. Research on Payne Effect of Natural Rubber Reinforced by Graft-

modified silica [J]. Journal of Applied Polymer Science, 2016, 133(36).

[38] SHEN J, LIU J, GAO Y, et al. Elucidating and Tuning the Strain-induced Non-linear Behavior of Polymer Nanocomposites: A Detailed Molecular Dynamics Simulation Study [J]. Soft Matter, 2014, 10(28): 5099-5113.

[39] WANG R, YAO H, LEI W, et al. Morphology, Interfacial Interaction, and Properties of A Novel Bioelastomer Reinforced by Silica and Carbon Black [J]. Journal of Applied Polymer Science, 2013, 129(3): 1546-1554.

[40] TAKINO H, NAKAYAMA R, YAMADA Y, et al. Viscoelastic Properties of Elastomers and Tire Wet Skid Resistance [J]. Rubber Chemistry and Technology, 1997, 70(4): 584-594.

[41] WANG M-J. Effect of Polymer-Filler and Filler-Filler Interactions on Dynamic Properties of Filled Vulcanizates [J]. Rubber Chemistry and Technology, 1998, 71(3): 520-589.

[42] SHELTON J R. Aging and Oxidation of Elastomers [J]. Rubber Chemistry and Technology, 1957, 30(5): 1251-1290.

[43] TASAKORN P, AMATYAKUL W. Photochemical Reduction of Molecular Weight and Number of Double Bonds in Natural Rubber Film [J]. Korean Journal of Chemical Engineering, 2008, 25(6): 1532-1538.

[44] ZHENG T, ZHENG X, ZHAN S, et al. Study on the Ozone Aging Mechanism of Natural Rubber [J]. Polymer Degradation and Stability, 2021, 186: 109514.

[45] CATALDO F. On the Ozone Protection of Polymers Having Non-conjugated Unsaturation [J]. Polymer Degradation and Stability, 2001, 72(2): 287-296.

Chapter 4 Dynamic Evolution of Ionic Bonds and Performance Characteristics in Bio-based Dibutyl Itaconate Elastomers

This chapter focuses on bio-based ionic elastomers formed by ZnO-induced ionic cross-linking of PDBIBA. The effects of ZnO content and temperature on ionic structure and material performance were investigated. Zinc carboxylate bonds were confirmed, and increasing ZnO content significantly improved mechanical properties, thermal responsiveness, and network reversibility. The dynamic ionic network exhibited clear thermally reversible behavior and phase-separated ionic domains, offering a promising approach for developing reprocessable and high-performance elastomer materials.

4.1 Introduction

Vulcanization converts weak linear rubber polymers into a three-dimensional network structure through covalent cross-linking. This cross-linking imparts excellent stability, enabling the material to resist external stresses and thermal effects, thereby enhancing its mechanical properties and thermal stability. However, the irreversible nature of these covalent bonds limits the recyclability and reprocessability of vulcanized rubber, posing challenges for sustainable applications[1, 2]. To address these limitations, researchers have developed ionic elastomers, which have garnered increasing attention due to their thermoplasticity and broad application potential[3].

Ionic elastomers incorporate a small amount of organic groups, such as carboxyl, sulfonic, or phosphonic groups, into the polymer backbone. These groups interact with metal ions via electrostatic interactions to form dynamic ionic cross-linked networks. Unlike traditional vulcanized rubbers with irreversible cross-links, the ionic bonds in these networks are reversible under appropriate thermal conditions, allowing the network structure to

disassociate and reassemble. This dynamic nature enables reprocessing and recycling while offering opportunities to tailor material properties[4-7].

The structural understanding of ionic polymers remains under debate, but Eisenberg's theoretical model is widely accepted[8, 9]. Eisenberg's model proposes that ionic polymers can be classified into two components, as illustrated in **Figure 4.1**: (1) multiplets, consisting of a small number of ion pairs (6–8 pairs) forming aggregates such as quadrupoles or hexapoles, acting as physical cross-links; and (2) ionic clusters, which contain a large number of ion pairs and non-ionic hydrocarbon groups. These clusters, due to restricted polymer chain mobility and thermodynamic incompatibility with the matrix, exhibit phase-separated characteristics. They function as both physical cross-linking points and reinforcing fillers, significantly improving the mechanical properties of elastomers[10-12]. The formation and distribution of these clusters are primarily influenced by the chemical nature of the polymer backbone and the concentration of ionic groups[9].

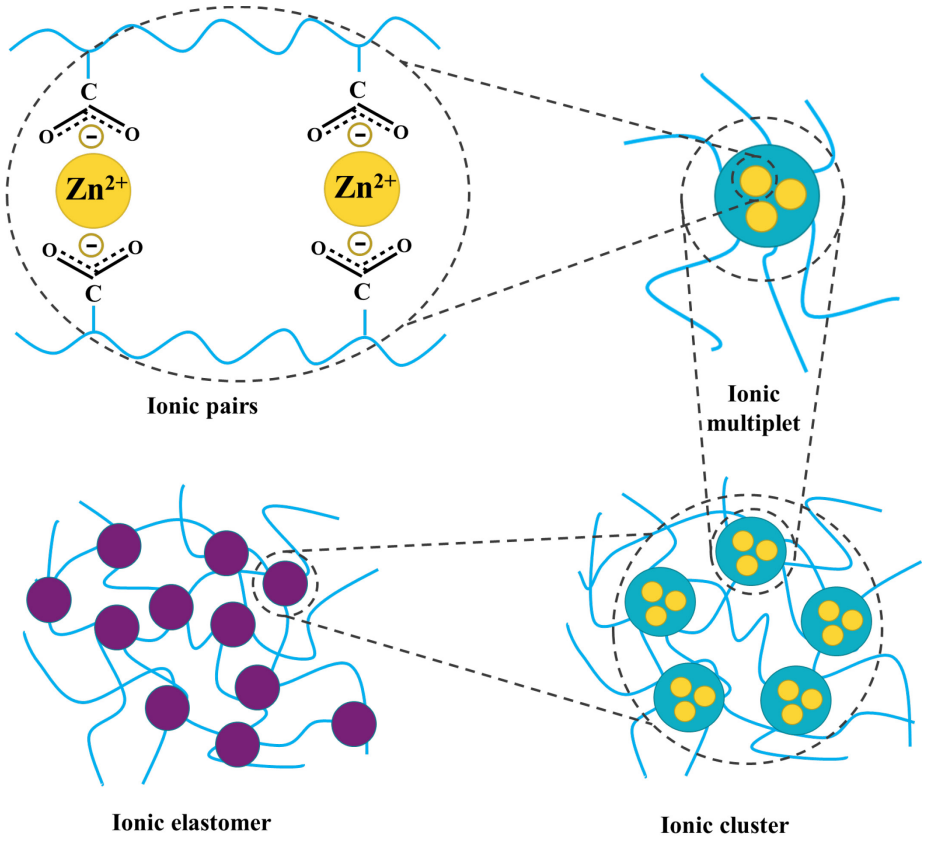

Figure 4.1 Schematic illustration of ionic elastomer, using an ionic polymer composed of carboxyl-functionalized polymer and zinc ion as an example.

Previous studies on ionic elastomers, including carboxylated nitrile rubber (XNBR) [10-16], ethylene-acrylic acid ionomers (EAA) [17-22], sulfonated polystyrene ionomers (SPS) [23-27], polyurethane ionomers (PUIS) [28-31], and polydimethylsiloxane ionomers (PDMS) [32, 33], have demonstrated tunable properties driven by ionic aggregation and phase separation. However, dibutyl itaconate-based elastomers (PDBIBA) remain largely unexplored. This study investigates the effects of ZnO-induced ionic cross-linking on the mechanical and thermal properties of PDBIBA, focusing on how ZnO content and temperature influence the evolution of zinc carboxylate structures and the resulting material characteristics. Using fourier transform infrared spectroscopy (FTIR), low-field nuclear magnetic resonance (NMR), and rubber process analysis (RPA), we demonstrate how dynamic ionic cross-linking points stabilize the network structure and shape its dynamic behavior, providing new insights into the structure-property relationships of PDBIBA ionic elastomers.

4.2 Experimental section

4.2.1 Materials

Carboxylated dibutyl itaconate-based elastomers (PDBIBA) were synthesized via emulsion polymerization of dibutyl itaconate (DBI), butadiene (BD), and methacrylic acid (MAA). The polymerization was carried out in a sealed reactor at 50 °C for 8 h using potassium persulfate as the initiator to yield a latex. The specific PDBIBA used in this section corresponds to the PDBIBA-7 sample described in Chapter 3. The carboxylated dibutyl itaconate elastomer (PDBIBA), shown in **Figure 4.2** for its chemical structure, had a number-average molecular weight of 250,000 g/mol. Its composition included 60.7% DBI units (x), 20.9% trans-BD units (y_1), 8.1% cis-BD units (y_2), 2.6% vinyl-BD units (y_3), and 7.7% methacrylic acid units (z). Zinc oxide (ZnO) was used as a cross-linking agent to form ionic cross-links. ZnO was chosen because it is an important activator widely used in the rubber industry, and it reacts readily with

carboxyl groups to form stable ionic cross-links. It was purchased from Xilong Chemical Company (Guangzhou, China), with a purity of 99.5% and a density of 5.6 g/cm³.

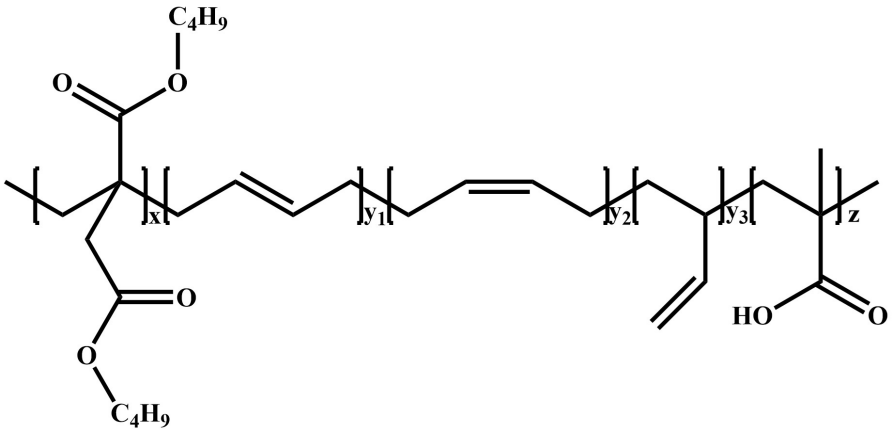

Figure 4.2 Chemical structure of the carboxylated dibutyl itaconate elastomer (PDBIBA) used in this work.

4.2.2 Ionic cross-linking behavior of PDBIBA elastomers with ZnO

PDBIBA and ZnO were mixed on a two-roll mill with 15 cm diameter and 30 cm length rolls, operating at a speed ratio of 1:1.27. Cold water circulated through the rolls to maintain near-room temperature during mixing. The cross-linking behavior of the resulting PDBIBA/ZnO mixtures was evaluated using a MD2000AN Rotorless Rheometer (GOTECH Testing Machines Inc.) via isothermal time sweep at 150 °C for 60 min. **Table 4.1** lists the compositions of the PDBIBA/ZnO mixtures used to study cross-linking behavior.

Table 4.1. Compositions of the PDBIBA and ZnO mixtures used to study the cross-linking behavior. "phr" stands for parts per hundred parts of resin (PDBIBA).

Sample name	PDBIBA (phr)	ZnO (phr)	Molar ratio (ZnO/COOH)
ZnO-2.0	100	2.0	0.28
ZnO-3.6	100	3.6	0.50
ZnO-5.0	100	5.0	0.69
ZnO-10	100	10	1.38
ZnO-15	100	15	2.08

4.2.3 Preparation of cross-linked PDBIBA/ZnO sheets

Neat PDBIBA, being uncross-linked, could not be directly molded into sheets. In contrast, the PDBIBA/ZnO mixtures were successfully processed into sheets by compression molding

using a hot press at 150 °C under 15 MPa pressure for the optimal vulcanization time (T_{90}), as determined by rheometry. The optimal vulcanization times are listed in **Table 4.2**. The resulting 1-mm thick cross-linked PDBIBA/ZnO sheets were then analyzed through various characterization techniques.

Table 4.2 Optimal vulcanization times for PDBIBA and ZnO mixtures with varying ZnO content.

Sample name	ZnO-2.0	ZnO-3.6	ZnO-5.0	ZnO-10	ZnO-15
T_{90} (min)	52.1	51.7	51.0	45.6	33.8

4.3 Characterization methods

The testing methods for FTIR, DMTA, mechanical properties, and TEM of the cross-linked PDBIBA/ZnO are the same as those described in Section 3.3.

Small-angle X-ray scattering (SAXS)

SAXS measurements were performed using a SAXS instrument (Xeuss 2.0, Xenocs, France) equipped with a Cu Kα X-ray source (λ = 0.154189 nm) operating at 30 W. The scattered X-rays were detected using a 2D Pilatus 3R 300K detector (Dectris), which has a pixel size of 172 μm. The sample-to-detector distance (SDD) was set to 539 mm, and the beam center was located at x = 63.94 and z = 573.68. Measurements were carried out in transmission mode on cross-linked PDBIBA/ZnO sheets with a thickness of approximately 1 mm.

Each sample was exposed for 300 s at room temperature. The 2D scattering patterns were corrected for background and instrumental smearing, and then azimuthally averaged to obtain the 1D scattering intensity profiles, $I(q)$. The scattering vector q is defined as $q = \frac{4\pi \sin\theta}{\lambda}$, where θ is the scattering angle. The radius of gyration (R_g) and zero-angle scattering intensity $I(0)$ were extracted from SAXS data using Guinier approximation within the low-q region using the PRIMUS module in the ATSAS software package.

X-ray diffraction (XRD) analysis

XRD analysis was performed using a RINT2000 vertical goniometer equipped with a standard sample holder and a fixed monochromator. The X-ray source operated at 40 kV and 50 mA, emitting Cu-Kα radiation with a wavelength of 1.5406 Å.

Swelling analysis

The cross-linked PDBIBA/ZnO samples were square sheets with a side length of 1 cm and a thickness of 1 mm. After measuring the dry sample mass (m_0), it was immersed in the solvent. The swollen sample was weighed every 12 h, and swelling equilibrium was considered to be reached when the mass stabilized (approximately 72 h). Once equilibrium was attained, the sample was quickly removed, excess solvent was gently wiped off with filter paper, and the sample was weighed again (m_1). The swelling ratio was then calculated using the following equation,

$$Q = \frac{(m_1 - m_0)/\rho_s}{m_0/\rho_r}$$

where ρ_s and ρ_r represent the densities of the solvent and the rubber, respectively.

Measurement of cross-linking density by low-field NMR

The cross-linking density of cross-linked PDBIBA/ZnO was measured using a low-field NMR from Jiangsu Niumag Analytical Instrument Co., Ltd. The tests were conducted at temperatures of 30 °C, 50 °C, 100 °C, 150 °C, and 200 °C, with each sample held at the designated temperature for 30 min before testing. Ten measurements were taken at each temperature, and the median value was used for analysis.

Dynamic behavior and reversibility analysis using rubber process analysis (RPA)

To assess the reversibility and dynamic behavior of the ionic cross-linked network, measurements were conducted using the RPA2000 rubber analyzer. For the storage modulus-strain measurements, the test conditions included a strain range of 0.28–200% and test temperatures of 100 °C, 130 °C, 150 °C, 170 °C, and 200 °C, followed by cooling in steps to 170 °C, 150 °C, 130 °C, and 100 °C. The test frequency was set to 1 Hz. For the loss factor-strain measurements, the strain range was 0.28–42%, with the same test temperatures and a frequency of 10 Hz.

4.4 Results and discussion

4.4.1 FTIR characterization of ZnO-crosslinked PDBIBA: ionic bond formation and structural analysis

FTIR is widely used as a crucial tool for analyzing ionic cross-linked networks. For example, Basu and Vislavath et al. demonstrated the critical role of ZnO in the cross-linking process of XNBR, identifying different microstructures of the carboxylic groups and zinc carboxylate ionic cross-links in XNBR, as shown in **Figure 4.3**[10, 34].

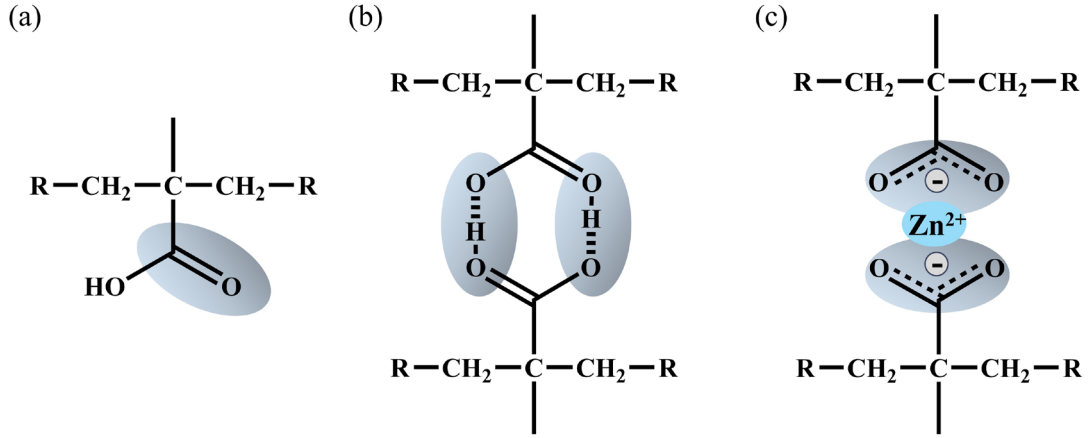

Figure 4.3 Schematic representation of ionic interactions in XNBR ionic elastomers: (a) free carboxylic acid groups (IR peak at 1730 cm^{-1}), (b) hydrogen-bonded carboxylic acid dimers (IR peak at 1698 cm^{-1}), and (c) zinc carboxylate ionic cross-links formed through interaction with ZnO (IR peak at 1586 cm^{-1}).

Figure 4.4 (a) shows the FTIR spectra at room temperature for the neat PDBIBA and PDBIBA cross-linked with varying amounts of ZnO (2 to 15 phr) using hot pressing at 150 °C under 15 MPa for the optimal vulcanization times (T_{90}). These spectra indicate the formation of ionic bonds between the carboxyl groups of PDBIBA and ZnO. **Figure 4.4** (b) illustrates the carbonyl region of the FTIR spectra (1800–1500 cm^{-1}). **Table 4.3** provides the assignments of the main FTIR absorption peaks. Compared to neat PDBIBA, the cross-linked PDBIBA/ZnO show a new peak appears at 1585 cm^{-1}, attributed to the formation of zinc carboxylate bonds through ionic interactions between Zn^{2+} ions and the carboxyl groups in PDBIBA. At the same time, the peak at 1698 cm^{-1}, corresponding to hydrogen-bonded carboxylic acid dimers, decreases in intensity with increasing ZnO content, indicating the consumption of carboxylic acid groups.

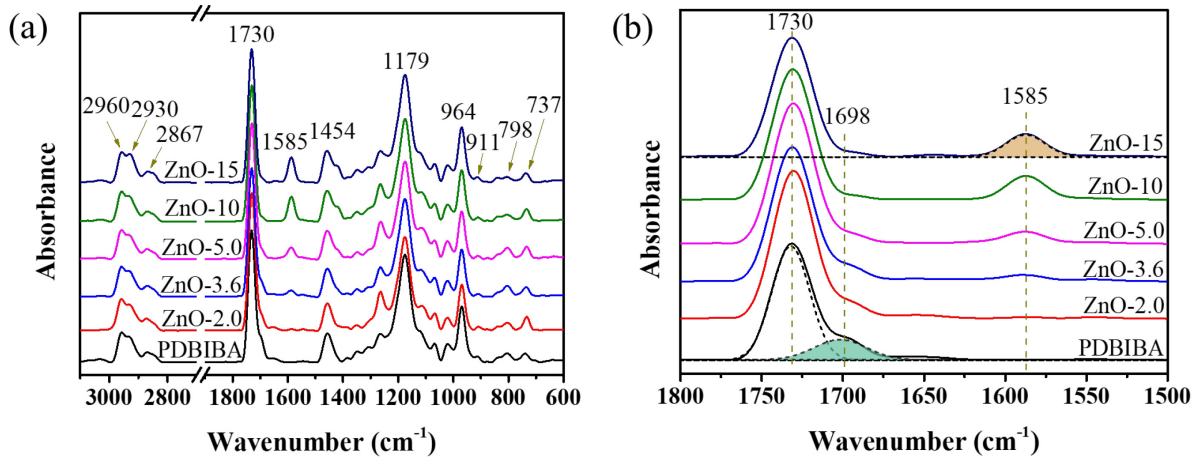

Figure 4.4 (a) FTIR spectra (3100 cm^{-1} to 600 cm^{-1}) at room temperature for 1-mm thick cross-linked PDBIBA/ZnO sheets with varying ZnO content, compressed at 150 °C, 15 MPa, for 52.1–33.8 min (ZnO-2.0 to ZnO-15). (b) Magnified region (1800 cm^{-1} to 1500 cm^{-1}) with peak fitting for ZnO-15. FTIR analysis shows the formation of zinc carboxylate bonds, with increasing ZnO content reducing carboxylic acid groups and enhancing ionic bond formation, as indicated by intensity changes in the 1698 cm^{-1} and 1585 cm^{-1} peaks.

Table 4.3. Assignments of the main FTIR absorption peaks for neat PDBIBA and cross-linked PDBIBA/ZnO with varying ZnO content.

Wavenumber (cm^{-1})	Vibration	Source
2960	ν ($-CH_3$)	DBI, MAA
2930	ν ($-CH_2$)	DBI, BD, MAA
2867	ν (-CH)	DBI, MAA
1730	ν (-C=O)	DBI, MAA
1698	Hydrogen-bonded carboxylic acid dimers	MAA
1585	Zinc carboxylate bonds	MAA
1454	δ ($-CH_3$), δ ($-CH_2$)	DBI, BD, MAA
1179	ν (C-O-C)	DBI
964	δ (-C-H)	Trans-BD
911	δ (-C-H)	Vinyl-BD
798	δ (C-O-C)	DBI
737	δ (-C-H)	Cis-BD

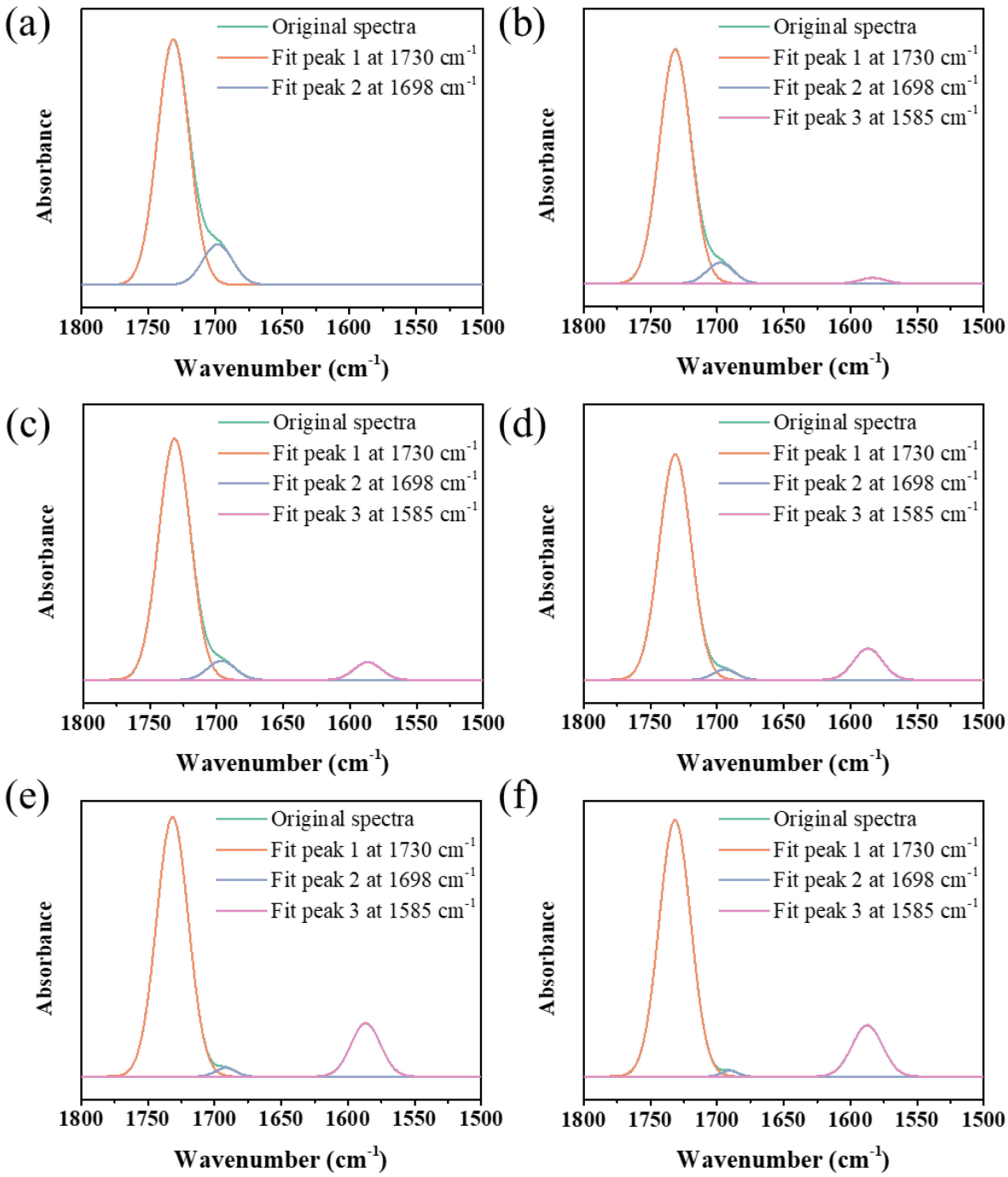

Figure 4.5 Curve fitting of the carbonyl region of the partial FTIR spectra in the wavenumber range 1800–1500 cm^{-1}: (a) Neat PDBIBA; (b) ZnO-2.0; (c) ZnO-3.6; (d) ZnO-5.0; (e) ZnO-10; (f) ZnO-15.

Quantitative analysis through curve fitting, as summarized in **Figure 4.5** and **Figure 4.6**, further highlights the extent of ionic bond formation. As ZnO content increases from 2 to 15 phr, the relative area of the vibrational bands at 1698 cm^{-1} decreases from 0.16 to 0.02, indicating a reduction in carboxyl groups as they are converted into ionic bonds. Meanwhile, the area of vibrational bands at 1585 cm^{-1} increases from 0.05 to 0.34 with rising ZnO content,

then plateaus at higher concentrations. This suggests that the strength of ionic association increases, but after a certain ZnO concentration, the limited availability of carboxyl groups restricts further ionic bond formation.

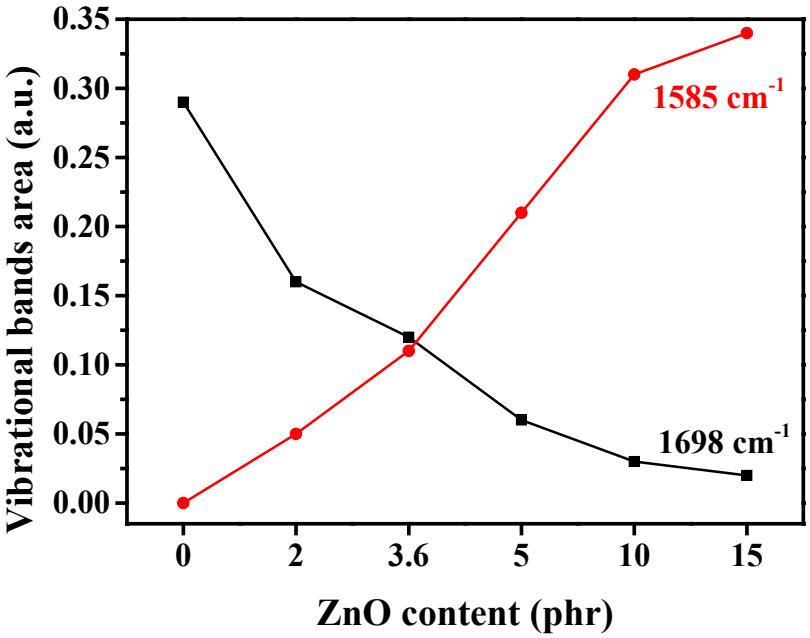

Figure 4.6 Vibrational bands areas at 1698 cm^{-1} and 1585 cm^{-1} with varying ZnO content. When the ZnO content is 0, the sample corresponds to neat PDBIBA. Increasing ZnO (2–15 phr) converts carboxyls to ionic bonds (1698 cm^{-1} ↓, 1585 cm^{-1} ↑), plateauing as carboxyls deplete.

4.4.2 Morphological and structural analysis of ZnO-crosslinked PDBIBA: TEM and XRD insights

A morphological analysis of ZnO particle distribution and aggregation in cross-linked PDBIBA/ZnO was performed using transmission electron microscopy (TEM). The TEM images in **Figure 4.7** show that at 2 phr ZnO (**Figure 4.7** (a) and (b)), spherical particles ranging from 50 nm to 200 nm are evenly distributed within the matrix. These particles are likely residual ZnO. Although most of the ZnO may have fully reacted with the carboxyl groups to form ionic cross-links, a small amount of unreacted ZnO may still be present in the form of fine particles. No significant aggregation is observed at this low concentration. However, at higher concentrations (3.6 phr and above), ZnO particles gradually grow larger (**Figure 4.7** (c), (d), (e), and (f)), as excess ZnO forms separate particles no longer needed for cross-linking.

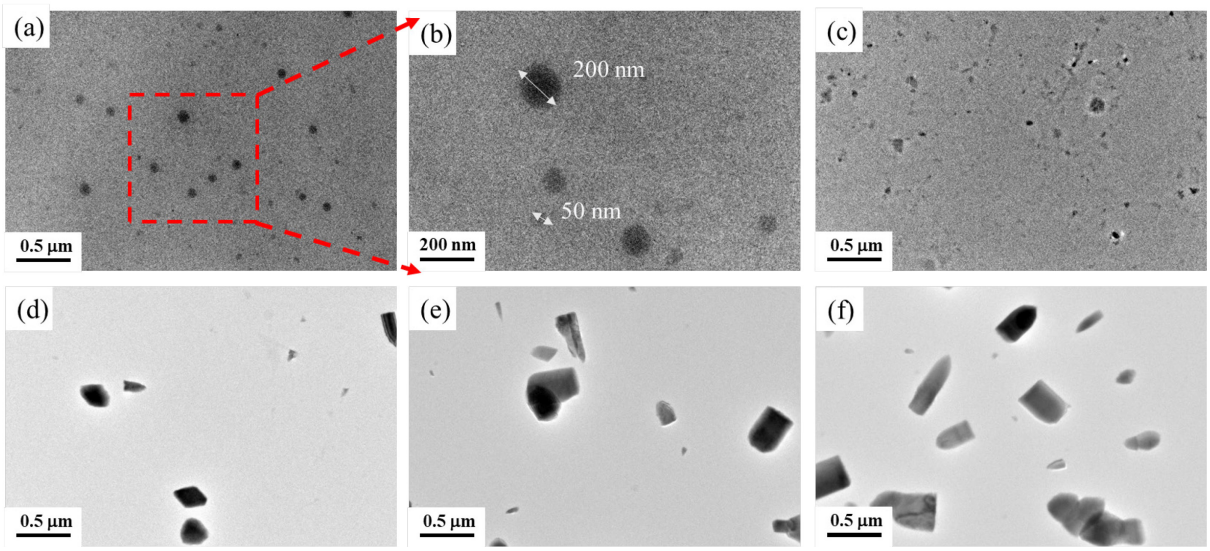

Figure 4.7 TEM images of cross-linked PDBIBA/ZnO sheets with varying ZnO content: (a) ZnO-2.0; (b) magnified ZnO-2.0; (c) ZnO-3.6; (d) ZnO-5.0; (e) ZnO-10; (f) ZnO-15. TEM analysis shows evenly distributed ZnO spherical particles (50–200 nm) at 2 phr ZnO, while higher concentrations (3.6 phr and above) result in ZnO particle aggregation due to excess ZnO.

To investigate the nanostructure of ionic clusters that are undetectable by TEM, small-angle X-ray scattering (SAXS) analysis was performed. Two-dimensional SAXS patterns were collected for samples with varying ZnO content, and Fit2D software was applied to obtain the corresponding one-dimensional scattering intensity curves. The low-q region of each curve (Guinier region) was then linearly fitted using the ATSAS software to extract the radius of gyration (R_g) and the extrapolated zero-angle scattering intensity $I(0)$. The R_g reflects the spatial extent of the scatterers, representing the average distribution of electron density around the center of the object. Therefore, R_g can be used as an indirect measure of the ionic cluster size, providing structural information that is often inaccessible by TEM. $I(0)$ is related to number of ionic cluster. As shown in **Figure 4.8** (a), the scattering intensity profiles evolve with increasing ZnO content. The calculated R_g values, plotted in **Figure 4.8** (b, left axis), increase from approximately 0.88 nm at 2 phr to 2.98 nm at 15 phr, indicating the formation of larger ionic clusters. Meanwhile, the corresponding $I(0)$ values (**Figure 4.8** (b), right axis) also increase, suggesting a rise in the number of the ionic clusters. This simultaneous increase in both cluster size and scattering intensity indicates that higher Zn^{2+} content promotes more extensive ionic cross-linking, leading to the development of larger and more numerous ionic associations.

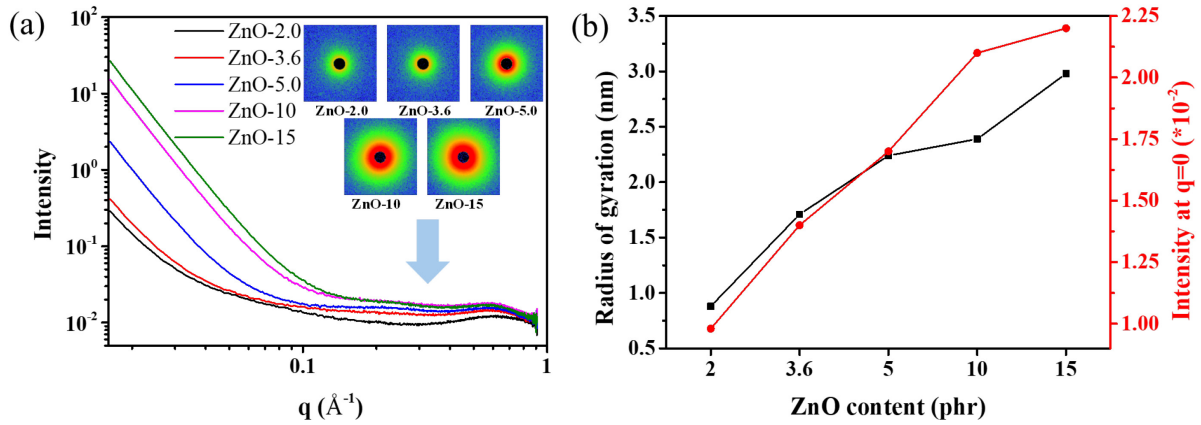

Figure 4.8 (a) SAXS intensity profiles of cross-linked PDBIBA/ZnO sheets with varying ZnO contents (2–15 phr) as a function of scattering vector *q*; (b) R_g and *I*(0) obtained from Guinier fitting plotted against ZnO content. With increasing ZnO content, R_g increases from approximately 0.88 nm to 2.98 nm, and *I*(0) rises from 0.0098 to 0.022, indicating a progressive growth in the size and number of ionic clusters.

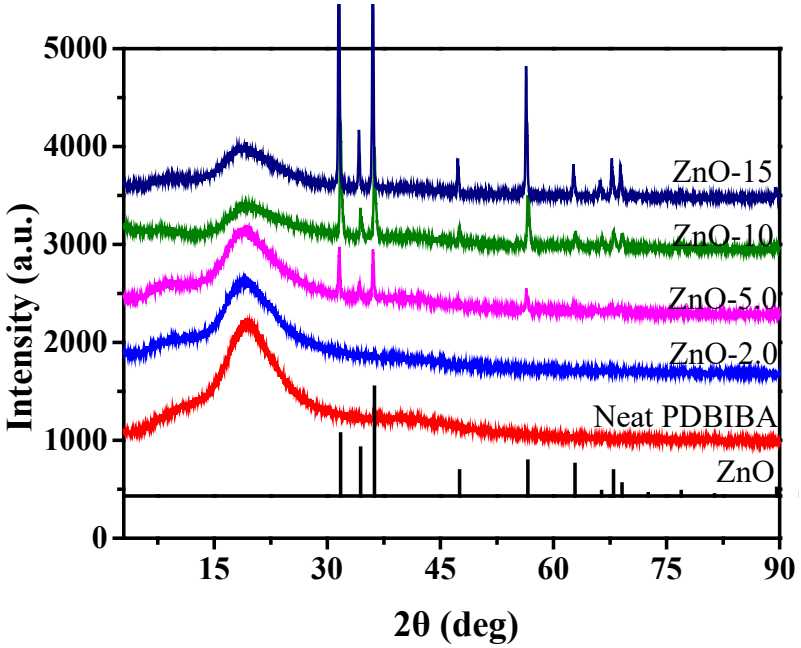

Figure 4.9 XRD patterns of ZnO, neat PDBIBA, and cross-linked PDBIBA/ZnO sheets show no ZnO peaks at 2 phr, indicating complete ionic bond formation, while at 5–15 phr ZnO, characteristic peaks appear, confirming particle aggregation.

To further verify the structural state of ZnO in the system, X-ray diffraction (XRD) analysis was performed. **Figure 4.9** presents XRD curves of ZnO, neat PDBIBA, and cross-linked PDBIBA/ZnO with varying ZnO content. For neat PDBIBA, a broad peak at 2θ = 15° confirms its amorphous nature. At 2 phr ZnO, no ZnO peaks are detected, confirming that most of the ZnO has been converted into ionic bonds. As ZnO content increases to 5, 10, and 15 phr, characteristic ZnO peaks appear at 31.7°, 34.4°, 36.3°, 47.5°, 56.6°, and 62.7°, with intensities increasing at higher concentrations. These results confirm that excess ZnO leads to particle

aggregation, forming distinct ZnO regions within the polymer matrix. These XRD results complement the TEM observations and validate the presence of unreacted ZnO at higher loadings.

4.4.3 Dynamic mechanical analysis of cross-linked PDBIBA/ZnO

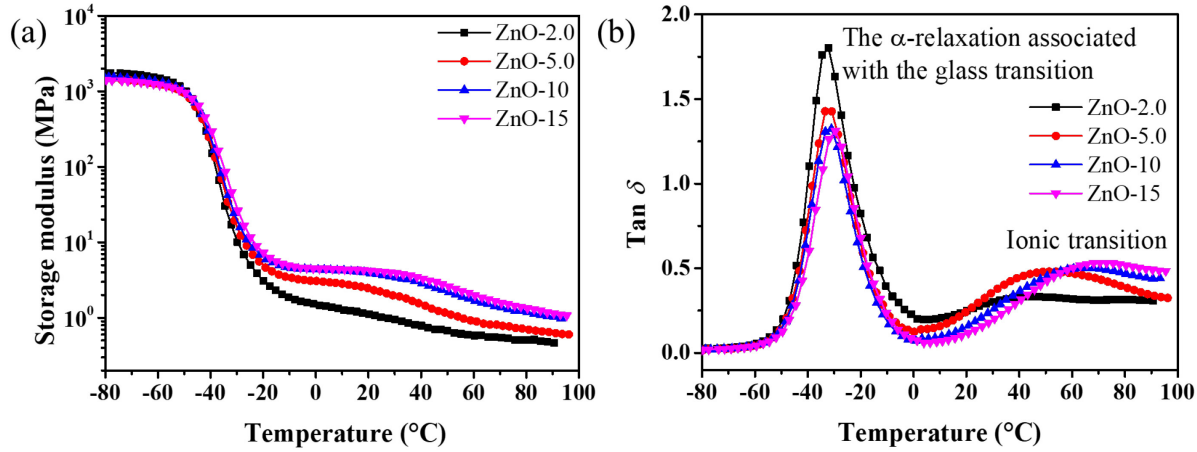

Figure 4.10 (a) Storage modulus and (b) tan δ vs. temperature for cross-linked PDBIBA/ZnO. Higher ZnO content increases initial storage modulus and stability, indicating denser ionic cross-links, while (b) the tan δ curve shows the α-relaxation associated with the glass transition and ionic transition.

In **Figure 4.10** (a), the storage modulus of cross-linked PDBIBA/ZnO decreases with increasing temperature, as expected. Below -50 °C, all samples show high storage modulus, indicating the polymer chains are in the glassy state. As temperature increases, storage modulus drops sharply, reflecting the α-relaxation associated with the glass transition where the polymer chains shift to the rubbery state. The initial storage modulus and the extent of the decrease vary with ZnO content. ZnO-2.0 exhibits the lowest initial storage modulus and the largest decrease, indicating a less cross-linked network with limited ionic interactions. In contrast, ZnO-10 and ZnO-15 show higher initial storage modulus values and more stable decreases, suggesting denser ionic cross-links at higher ZnO concentrations. In **Figure 4.10** (b), the tan δ versus temperature curve shows two distinct transitions. The first transition, between -60 °C and 0 °C, corresponds to the α-relaxation associated with the glass transition, where the polymer chains transition from the glassy to the rubbery state. This is influenced by the flexibility of the polymer chains and cross-linking density. The second peak in the tan δ curve, between 10 and 100 °C, corresponds to the ionic transition temperature (T_i), which originates from the

relaxation of polymer chain segments confined in the vicinity of ionic aggregates. These ionic clusters act as reversible physical cross-links, forming a microphase-separated ionic network that restricts chain mobility. [6, 8, 9, 35].

As ZnO content increases, the α-relaxation associated with the glass transition shifts to higher temperatures, from -35 °C for ZnO-2.0 to -30 °C for ZnO-15 (**Figure 4.11** (a)), while the tan δ peak decreases from 1.76 to 1.31 (**Figure 4.11** (b)), reflecting increased ionic cross-linking that restricts chain segment motion and reduces energy dissipation. Meanwhile, T_i rises from 45 °C for ZnO-2.0 to 71 °C for ZnO-15 (**Figure 4.11** (a)), indicating stronger ionic aggregation and greater restrictions on chain motion. The tan δ peak increases from 0.33 for ZnO-2.0 to 0.53 for ZnO-15 (**Figure 4.11** (b)), showing enhanced energy dissipation during the ionic transition. This is attributed to phase separation driven by ionic aggregation, where increased ZnO content forms larger ionic clusters that restrict polymer chain movement, leading to higher internal friction and energy dissipation during dynamic deformation.

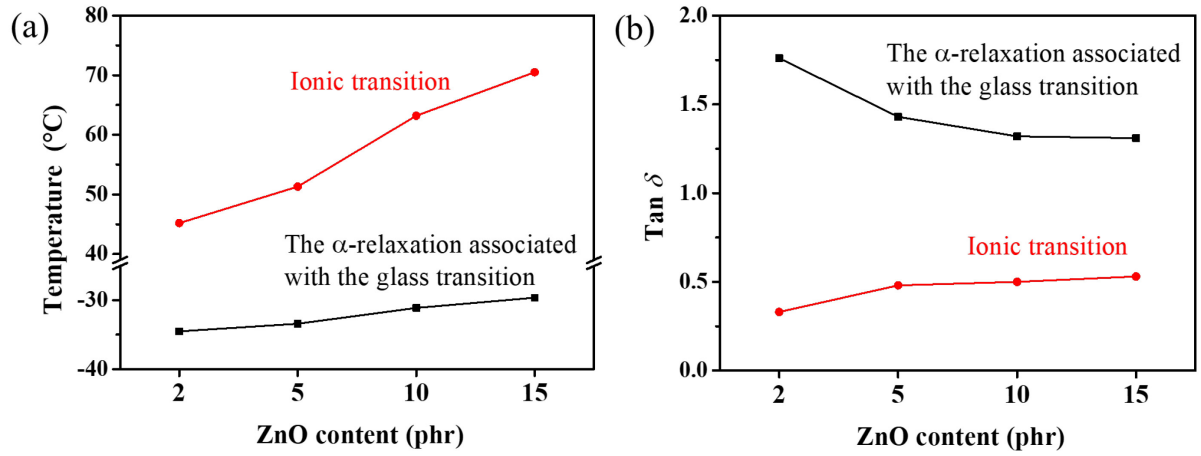

Figure 4.11 (a) The α-relaxation associated with the glass transition and ionic transition, and (b) tan δ for cross-linked PDBIBA/ZnO with varying ZnO content.

4.4.4 Stress-strain behavior of cross-linked PDBIBA/ZnO

Figure 4.12 shows the stress-strain behavior of cross-linked PDBIBA/ZnO with varying ZnO content, and **Table S4.1** presents the derived parameters. Adding ZnO increases tensile strength significantly, from 2.7 MPa at 2 phr to 15.3 MPa at 15 phr (467% increase). This improvement is due to ion-rich regions where ionic bonds act as sacrificial bonds, absorbing

energy and delaying polymer failure. While elongation at break decreases from 727% to 487%, the large tensile strength increase demonstrates good flexibility.

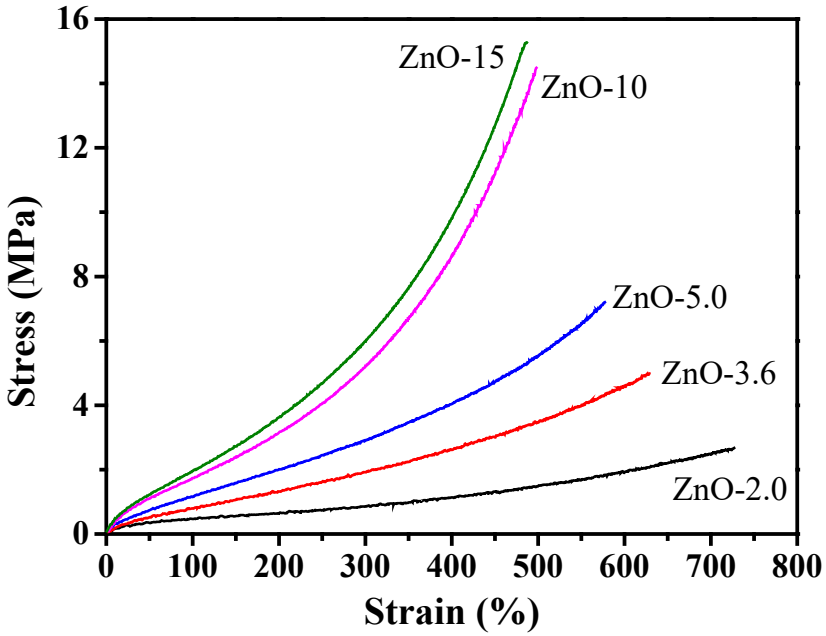

Figure 4.12 Stress-strain curves of 1-mm thick sheets of cross-linked PDBIBA/ZnO with varying amount of ZnO. Neat PDBIBA could not be compression-molded into sheets due to its uncross-linked nature.

4.4.5 Swelling ratio and cross-linking density of ZnO cross-linked PDBIBA

The cross-linked PDBIBA/ZnO samples were immersed in toluene for 72 h at room temperature to determine the swelling ratio. As shown in the left bars of **Figure 4.13**, the swelling ratio decreases significantly with increasing ZnO content (2 phr to 15 phr), indicating that higher ZnO levels result in a more tightly cross-linked polymer network with less room for polymer chain expansion. The ionic cross-links formed by ZnO restrict polymer chain movement, limiting swelling. Cross-linking density, measured via low-field NMR (right bars of **Figure 4.13**), increases with ZnO content, showing the opposite trend to the swelling ratio, as expected. The rise in cross-linking density enhances the material's mechanical properties, as observed in the stress-strain analysis. At 10 phr ZnO and above, cross-linking density reaches its maximum, suggesting efficient ionic bond formation at higher ZnO concentrations.

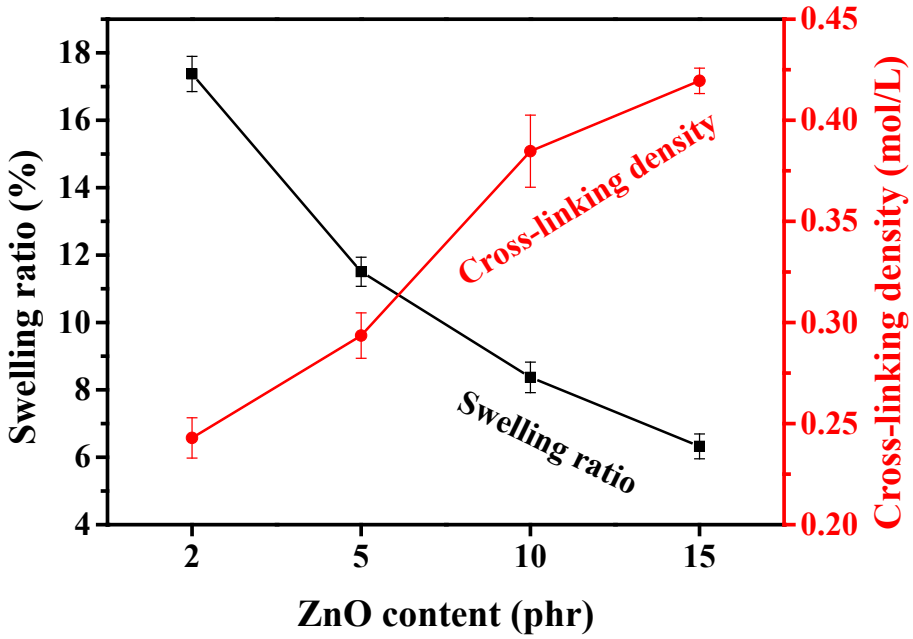

Figure 4.13 Swelling ratio and cross-linking density of 1-mm thick cross-linked PDBIBA/ZnO with varying ZnO content. Increasing ZnO content decreases swelling and increases cross-linking density, peaking at 15 phr ZnO.

4.4.6 Temperature dependence of the reversibility of ionic bonds between ZnO and carboxyl groups of PDBIBA

To quantitatively explore how temperatures affect the overall cross-linking density of cross-linked PDBIBA/ZnO, low-field NMR analysis was employed to directly measure the evolution of cross-linking density at different temperatures, providing a more quantitative perspective on the thermal reversibility of the ionic network. The results are shown in **Figure 4.14**. The cross-linking density curves of cross-linked ZnO-10 at different temperatures (30 °C, 50 °C, 100 °C, 150 °C, and 200 °C) illustrate the cross-linking density of the material under heating and cooling cycles. The heating and cooling processes were automatically controlled by the instrument. The heating process was relatively fast, with each heating stage typically reaching the desired temperature within 5 min. However, due to the sealed state of the instrument, the cooling process was slower. Specifically, cooling from 200 °C to 150 °C and from 150 °C to 100 °C could take up to 10 min, while cooling from 100 °C to 50 °C and from 50 °C to 30 °C could require up to 20 and 30 min. Before measurements began, the sample was

placed at each test temperature for 30 min, and multiple tests were conducted at each stage until the measured values stabilized.

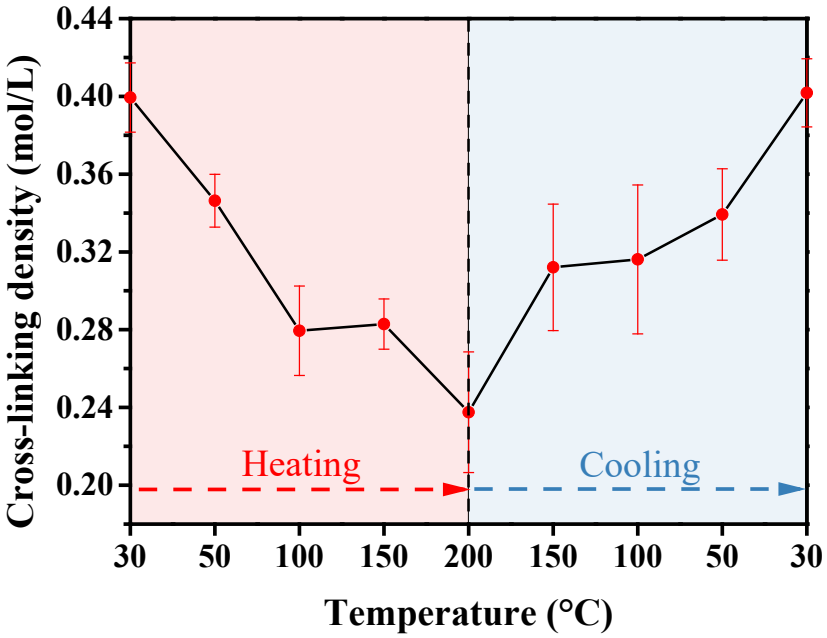

Figure 4.14 Cross-linking density curves of ZnO-10 ionic elastomers at varying temperature. Low-field NMR analysis tracked cross-linking density changes upon heating from 30 °C to 200 °C, following by cooling from 200 °C to 30 °C, highlighting the thermal reversibility of the ionic network.

At 30 °C, the cross-linking density was 0.399 mol/L, indicating a well-formed ionic network at room temperature. As the temperature increased, the cross-linking density gradually declined, reaching a minimum value of 0.238 mol/L at 200 °C, suggesting that some zinc carboxylate bonds were disrupted under thermal activation. Interestingly, as the temperature decreased, the cross-linking density began to recover. At 150 °C, the cross-linking density returned to 0.312 mol/L, and as the temperature further decreased, the cross-linking density continued to increase. At 30 °C, the final cross-linking density recovered fully to the initial measurement level within the experimental error, reaching 0.402 mol/L.

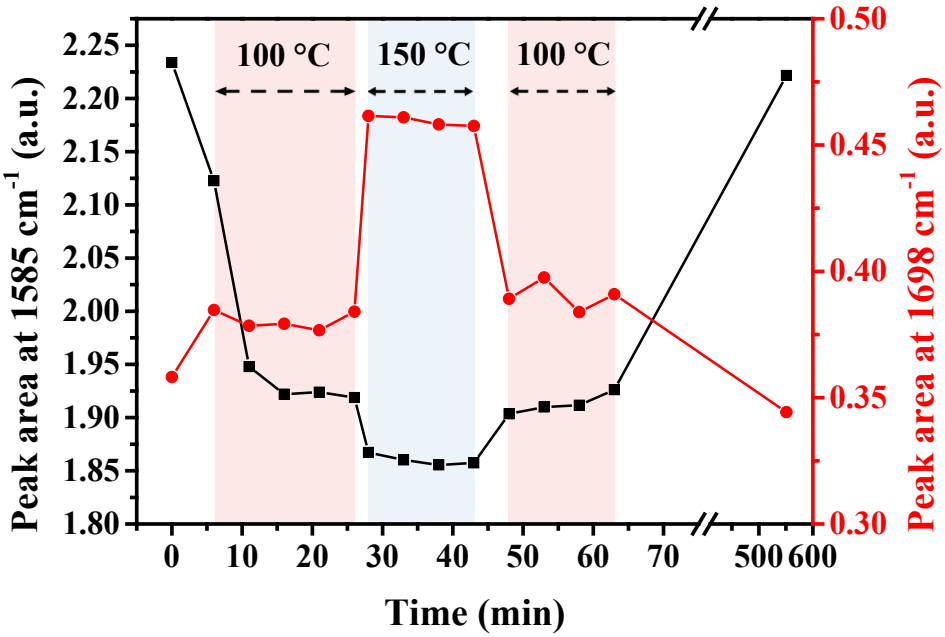

Figure 4.15 Evolution of the fitted peak areas at 1585 cm^{-1} and 1698 cm^{-1} over time during heating and cooling cycles for the cross-linked ZnO-10 sample. Starting from room temperature, FTIR measurements were conducted at 5-min intervals after reaching each target temperature. The temperature reached 100 °C within 6 min, then was kept at this temperature from 6 min to 26 min. The temperature was then raised to 150 °C by 28 min, and kept at this temperature from 28 min to 43 min. It was then cooled down to 100 °C by 48 min, kept at this temperature until 63 min, and finally cooled back to room temperature (26 °C).

To further investigate the thermoreversible behavior of zinc carboxylate associations, a cross-linked ZnO-10 sample was subjected to programmed heating and cooling cycles while monitoring the fitted peak areas of the FTIR bands at 1585 cm^{-1} and 1698 cm^{-1} over time, as shown in **Figure 4.15**. During heating, the decrease in the 1585 cm^{-1} peak area and the increase in the 1698 cm^{-1} peak area indicate partial dissociation of zinc carboxylate associations and the formation of carboxylic acid groups. Upon cooling, the opposite trend is observed, suggesting the reformation of ionic bonds. These reversible spectral changes demonstrate the dynamic dissociation and reconstruction behavior of zinc carboxylate structures under thermal stimuli.

Figure 4.16 illustrates the thermoreversible behavior of Zn^{2+}-carboxylate ionic cross-links in the PDBIBA elastomer system. At room temperature (**Figure 4.16** (a)), Zn^{2+} ions coordinate with carboxylate groups on polymer chains to form stable ionic cross-links. The enlarged view shows the formation of zinc carboxylate structures. Upon heating (**Figure 4.16** (b)), these ionic bonds partially dissociate, leading to the reduction or disappearance of cross-linking points, the

release of free Zn^{2+} ions, and the appearance of unbound carboxylic acid groups. This corresponds to the decrease in cross-linking density (**Figure 4.14)** and the reduction in the FTIR peak area of zinc carboxylate structures (**Figure 4.15**). When the system is cooled, the Zn^{2+} ions re-coordinate with carboxylate groups, restoring the ionic cross-linking network. This is consistent with the increase in cross-linking density (**Figure 4.14**) and the recovery of the FTIR peak area of zinc carboxylate structures (**Figure 4.15**) upon cooling.

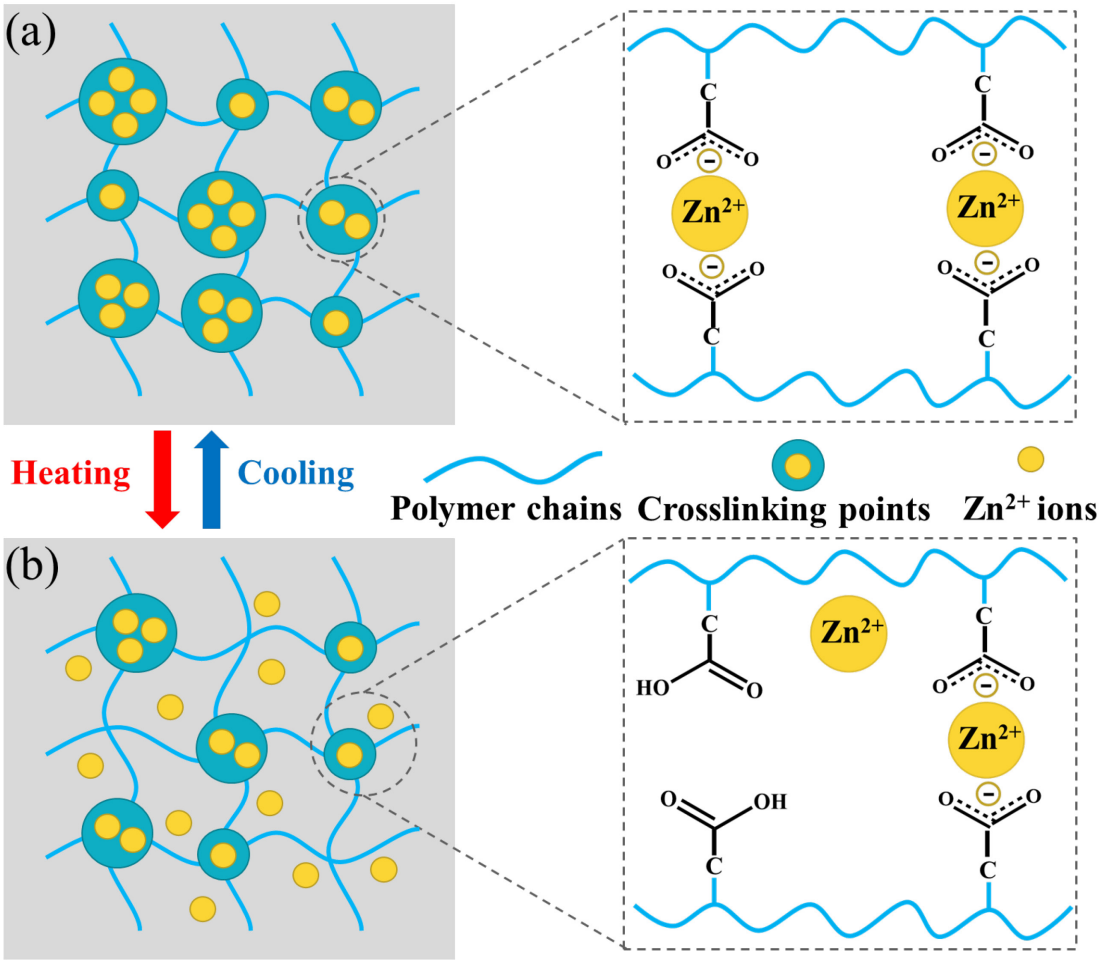

Figure 4.16 Schematic diagram of ionic bond dissociation and recombination. Zinc carboxylate structures dissociate at high temperatures and reform upon cooling, demonstrating the full thermal reversibility of the ionic cross-linking process.

4.4.7 Temperature-dependent viscoelastic behavior of cross-linked PDBIBA/ZnO

The temperature-sensitive reversibility of ionic bonds in cross-linked PDBIBA/ZnO is further demonstrated by its viscoelastic behavior, analyzed through rubber process analysis (RPA). This analysis reveals how temperature affects the storage modulus and loss factor (tan

δ), reinforcing the dynamic and reversible nature of the ionic network. As shown in **Figure 4.17**, storage modulus decreases with rising temperature due to thermal dissociation of ionic bonds and network relaxation. Samples with higher ZnO content (ZnO-10 and ZnO-15) experience a greater decrease in storage modulus but recover it more effectively during cooling, as denser ionic networks facilitate bond reformation. In contrast, ZnO-2.0, with lower cross-linking, shows a smaller decrease in storage modulus.

Tan *δ* behaves differently across samples. For ZnO-2.0, tan *δ* increases with temperature, indicating higher energy dissipation from enhanced chain mobility in the sparse network. For ZnO-3.6 to ZnO-15, tan *δ* decreases as higher ZnO content promotes rapid ionic bond reformation, restricting chain mobility and reducing energy loss. Upon cooling, tan *δ* increases for ZnO-3.6 to ZnO-15, reflecting efficient bond reformation and increased energy dissipation. This dynamic and reversible behavior highlights the material's adaptability and potential for thermal healing applications.

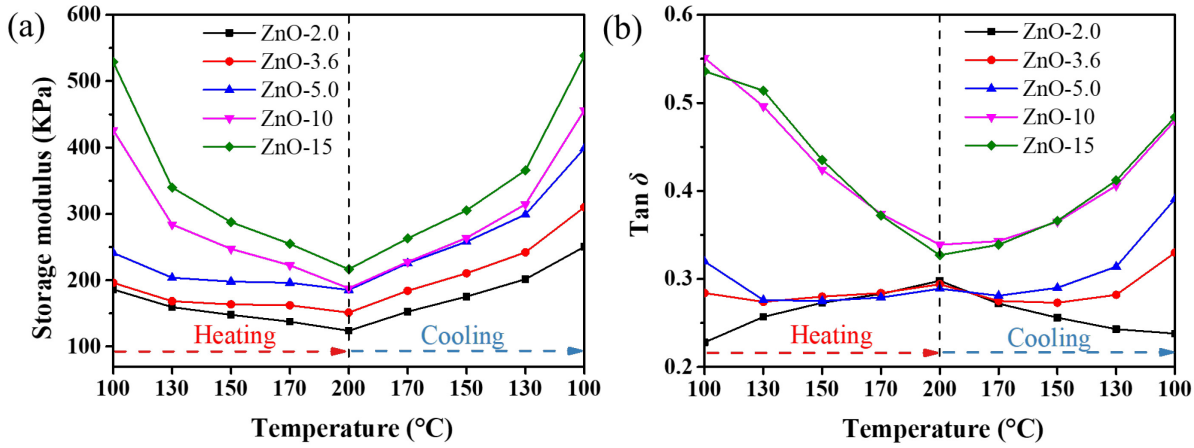

Figure 4.17 Temperature-dependent changes in (a) storage modulus and (b) tan *δ* for cross-linked PDBIBA/ZnO with varying content during heating from 100 °C to 200 °C, followed by cooling from 200 °C to 100 °C. PDBIBA/ZnO's ionic bonds weaken with heat and recover upon cooling, enabling thermal adaptability.

4.5 Conclusions

This study investigates the dynamic evolution of ionic bonds and performance in bio-based dibutyl itaconate (PDBIBA) ionic elastomers cross-linked with zinc oxide (ZnO). FTIR

confirmed the formation of zinc carboxylate bonds, which increased with ZnO content up to saturation, while excessive ZnO (>5 phr) caused ZnO aggregation and phase separation, as shown by TEM and XRD. Additionally, SAXS measurements showed that the radius of gyration of the ionic clusters ranged from 0.88 to 2.98 nm. The tensile strength increased by 467% (from 2.7 MPa at 2 phr ZnO to 15.3 MPa at 15 phr ZnO), attributed to the sacrificial nature of ionic bonds. Dynamic mechanical analysis revealed an increase in glass transition temperature from -35 °C to -30 °C and ionic transition temperature from 45 °C to 71 °C as ZnO content increased. Low-field NMR and rubber process analysis demonstrated the thermal reversibility of the ionic network, with cross-linking density decreasing from 0.399 mol/L at 30 °C to 0.238 mol/L at 200 °C and fully recovering upon cooling. Swelling ratio decreased from 17.4% at 2 phr ZnO to 6.3% at 15 phr ZnO, while cross-linking density increased from 0.243 mol/L at 2 phr to 0.42 mol/L at 15 phr. The study highlights ZnO-crosslinked PDBIBA elastomers as sustainable, materials with reversible cross-linking and tunable properties, potentially applicable in recyclable materials.

4.6 References

[1] CORAN A Y. 7 - Vulcanization [M]//MARK J E, ERMAN B, EIRICH F R. Science and Technology of Rubber (Second Edition). San Diego; Academic Press. 1994: 339-385.

[2] FISHER H L. Vulcanization of Rubber [J]. Industrial & Engineering Chemistry, 1939, 31(11): 1381-1389.

[3] ANTONY P, DE S K. Ionic Thermoplastic Elastomers: A Review [J]. Journal of Macromolecular Science, Part C, 2001, 41(1-2): 41-77.

[4] MACKNIGHT W J, LUNDBERG R D. Elastomeric Ionomers [J]. Rubber Chemistry and Technology, 1984, 57(3): 652-663.

[5] KIM H. Modifications in Electronic Properties of Polystyrene Methacrylic Acid by Neutralization and Fast Electrons [J]. The Journal of Physical Chemistry B, 2009, 113(28): 9359-9363.

[6] HIRD B, EISENBERG A. Sizes and Stabilities of Multiplets and Clusters in Carboxylated and Sulfonated Styrene Ionomers [J]. Macromolecules, 1992, 25(24): 6466-6474.

[7] BASU D, DAS A, STöCKELHUBER K W, et al. Nanostructured Ionomeric Elastomers [M]//STöCKELHUBER K W, DAS A, KLüPPEL M. Designing of Elastomer Nanocomposites: From Theory to Applications. Cham; Springer International Publishing. 2017: 235-266.

[8] EISENBERG A, HIRD B, MOORE R B. A New Multiplet-cluster Model for the Morphology of Random Ionomers [J]. Macromolecules, 1990, 23(18): 4098-4107.

[9] EISENBERG A. Clustering of Ions in Organic Polymers. A Theoretical Approach [J]. Macromolecules, 1970, 3(2): 147-154.

[10] BASU D, DAS A, STöCKELHUBER K W, et al. Evidence for an in Situ Developed Polymer Phase in Ionic Elastomers [J]. Macromolecules, 2014, 47(10): 3436-3450.

[11] MALMIERCA M A, GONZáLEZ-JIMéNEZ A, MORA-BARRANTES I, et al. Characterization of Network Structure and Chain Dynamics of Elastomeric Ionomers by Means of ^{1}H Low-field NMR [J]. Macromolecules, 2014, 47(16): 5655-5667.

[12] IBARRA L, ALZORRIZ M. Vulcanization of Carboxylated Nitrile Rubber (XNBR) by Zinc Peroxide [J]. Polymer International, 1999, 48(7): 580-586.

[13] XU C, HUANG X, LI C, et al. Design of "Zn^{2+} Salt-Bondings" Cross-linked Carboxylated Styrene Butadiene Rubber with Reprocessing and Recycling Ability via Rearrangements of Ionic Cross-linkings [J]. ACS Sustainable Chemistry & Engineering, 2016, 4(12): 6981-6990.

[14] IBARRA L, ALZORRIZ M. Ionic Elastomers Based on Carboxylated Nitrile Rubber and Magnesium Oxide [J]. Journal of Applied Polymer Science, 2007, 103(3): 1894-1899.

[15] IBARRA L, ALZORRIZ M. Vulcanization of Carboxylated Nitrile Rubber (XNBR) by a Mixed Zinc Peroxide–sulphur System [J]. Polymer International, 2000, 49(1): 115-121.

[16] IBARRA L, MARCOS-FERNáNDEZ A, ALZORRIZ M. Mechanistic Approach to the Curing of Carboxylated Nitrile Rubber (XNBR) by Zinc Peroxide/zinc Oxide [J]. Polymer, 2002, 43(5): 1649-1655.

[17] BUITRAGO C F, JENKINS J E, OPPER K L, et al. Room Temperature Morphologies of Precise Acid- and Ion-Containing Polyethylenes [J]. Macromolecules, 2013, 46(22): 9003-9012.

[18] PAINTER P C, BROZOSKI B A, COLEMAN M M. FTIR Studies of Calcium and Sodium Ionomers Derived from An Ethylene–methacrylic Acid Copolymer [J]. Journal of Polymer Science: Polymer Physics Edition, 1982, 20(6): 1069-1080.

[19] BUITRAGO C F, BOLINTINEANU D S, SEITZ M E, et al. Direct Comparisons of X-ray Scattering and Atomistic Molecular Dynamics Simulations for Precise Acid Copolymers and Ionomers [J]. Macromolecules, 2015, 48(4): 1210-1220.

[20] BUITRAGO C F, ALAM T M, OPPER K L, et al. Morphological Trends in Precise Acid- and Ion-containing Polyethylenes at Elevated Temperature [J]. Macromolecules, 2013, 46(22): 8995-9002.

[21] PREGI E, KUN D, WACHA A, et al. The Role of Ionic Clusters in the Determination of the Properties of Partially Neutralized Ethylene-acrylic Acid Ionomers [J]. European Polymer Journal, 2021, 142: 110110.

[22] SEITZ M E, CHAN C D, OPPER K L, et al. Nanoscale Morphology in Precisely Sequenced Poly(ethylene-co-acrylic acid) Zinc Ionomers [J]. Journal of the American Chemical Society, 2010, 132(23): 8165-8174.

[23] BALDING P, BORRELLI R, VOLKOVINSKY R, et al. Physical Properties of Sodium Poly(styrene sulfonate): Comparison to Incompletely Sulfonated Polystyrene [J]. Macromolecules, 2022, 55(5): 1747-1762.

[24] BRIJMOHAN S B, SWIER S, WEISS R A, et al. Synthesis and Characterization of Cross-linked Sulfonated Polystyrene Nanoparticles [J]. Industrial & Engineering Chemistry Research, 2005, 44(21): 8039-8045.

[25] CASTAGNA A M, WANG W, WINEY K I, et al. Influence of Cation Type on Structure and Dynamics in Sulfonated Polystyrene Ionomers [J]. Macromolecules, 2011, 44(13): 5420-5426.

[26] CASTAGNA A M, WANG W, WINEY K I, et al. Structure and Dynamics of Zinc-

Neutralized Sulfonated Polystyrene Ionomers [J]. Macromolecules, 2011, 44(8): 2791-2798.

[27] CASTAGNA A M, WANG W, WINEY K I, et al. Influence of the Degree of Sulfonation on the Structure and Dynamics of Sulfonated Polystyrene Copolymers [J]. Macromolecules, 2010, 43(24): 10498-10504.

[28] DIETERICH D, KEBERLE W, WITT H. Polyurethane Ionomers, a New Class of Block Polymers [J]. Angewandte Chemie International Edition in English, 1970, 9(1): 40-50.

[29] EGBOH H S, GHAFFAR A, GEORGE M H, et al. Synthesis and Characterization of Some Polyurethane Ionomers [J]. Polymer, 1982, 23(8): 1167-1171.

[30] KRóL P, KRóL B. Structures, Properties and Applications of the Polyurethane Ionomers [J]. Journal of Materials Science, 2020, 55(1): 73-87.

[31] YARUSSO D J, COOPER S L. Microstructure of Ionomers: Interpretation of Small-angle X-ray Scattering Data [J]. Macromolecules, 1983, 16(12): 1871-1880.

[32] BATRA A, COHEN C, KIM H, et al. Counterion Effect on the Rheology and Morphology of Tailored Poly(dimethylsiloxane) Ionomers [J]. Macromolecules, 2006, 39(4): 1630-1638.

[33] DA VIA F, SURIANO R, BOUMEZGANE O, et al. Self-healing Behavior in Blends of PDMS-based Polyurethane Ionomers [J]. Polymers for Advanced Technologies, 2022, 33(2): 556-565.

[34] VISLAVATH P, BILLA S, S P, et al. Heterogeneous Coordination Environment and Unusual Self-Assembly of Ionic Aggregates in a Model Ionomeric Elastomer: Effect of Curative Systems [J]. Macromolecules, 2022, 55(15): 6739-6749.

[35] IBARRA L, RODRíGUEZ A, MORA-BARRANTES I. Crosslinking of Unfilled Carboxylated Nitrile Rubber with Different Systems: Influence on Properties [J]. Journal of Applied Polymer Science, 2008, 108(4): 2197-2205.

Chapter 5 Synthesis and Performance Investigation of Bio-based Carboxylated Itaconate Elastomers with Varied Side Chains

This chapter focuses on the development and evaluation of carboxylated bio-based itaconate elastomers with varied side chain structures (PDXIBA), synthesized using itaconate monomers with different ester side chains, including dimethyl itaconate (DMI), diethyl itaconate (DEI), and dibutyl itaconate (DBI), as potential materials for disposable gloves. The influence of side chain length on the mechanical properties, abrasion resistance, and oil resistance of the latex films was systematically investigated. Compared with dibutyl itaconate, shorter side chains led to increased polarity and enhanced performance in these aspects. Among them, PDMIBA exhibited good oil resistance, while PDEIBA showed better biocompatibility than both nitrile and natural rubber gloves. Additionally, silica-filled nanocomposites based on PDXIBA, XNBR, and ESBR matrices were studied to explore the effects of matrix polarity and side chain structure on filler dispersion and composite performance. The results demonstrate that carboxylated itaconate elastomers possess tunable properties and strong potential as sustainable alternatives to petroleum-based glove and composite materials.

5.1 Introduction

With increasing concerns over fossil resource depletion and environmental impact, developing bio-based elastomers from renewable biomass has become a key focus in the rubber industry[1-3]. Academician Liqun Zhang's team proposed the concept of bio-based engineering elastomers and developed itaconate rubbers with high molecular weight and cross-linking capability using bio-based itaconic acid. Subsequent studies optimized their structure and functionality, significantly improving mechanical and interfacial properties[4, 5]. These efforts have primarily focused on applications in sustainable green tire tread materials[6-8].

However, in addition to applications in the tire field, the potential of bio-based elastomers in other high-performance protective materials is also worth attention. For example, in the field of personal protection, especially disposable latex gloves, finding materials that combine excellent mechanical properties, chemical resistance, and biosafety has become an important research direction. According to data, the global sales volume of disposable gloves is showing an upward trend. In 2022, the global sales volume of disposable gloves was 622.5 billion pieces, with a compound annual growth rate of 7.14% from 2017 to 2022. It is expected that the global sales volume of disposable gloves will rise to 829.3 billion pieces by 2025. Pune, India – The Brainy Insights predicts that the global medical nitrile glove market, valued at 4 billion USD in 2023, will grow to 11.35 billion USD by 2033. Against the backdrop of the continuously expanding disposable latex glove market, the development of new environmentally friendly and high-performance glove materials is particularly important. Traditional natural rubber (NR) gloves have good elasticity and comfort but may cause protein allergy problems[9]; while nitrile rubber (NBR) gloves, mainly derived from petroleum-based raw materials, overcome allergy risks and possess good oil and chemical resistance, but still have certain shortcomings in flexibility and comfort[10]. In addition, the non-renewability and environmental impact of petroleum-based synthetic rubber also drive the exploration of more sustainable alternative materials. Therefore, the development of bio-based elastomers with excellent mechanical properties, chemical resistance, and biosafety has become a research hotspot.

Against this background, carboxylated itaconate latex has emerged as a potential candidate for disposable glove materials due to its bio-based origin, high polarity, tunable mechanical properties, and excellent film-forming ability. In previous work, we introduced methacrylic acid (MAA) into the dibutyl itaconate elastomers through emulsion polymerization, and demonstrated that the copolymer system possesses excellent mechanical properties, providing a new approach for the development of high-performance bio-based elastomers. However, to further optimize its comprehensive performance, we selected diethyl itaconate (DEI) and dimethyl itaconate (DMI) to replace dibutyl itaconate (DBI). Firstly, compared with n-butanol, ethanol and methanol are more mature and have lower production costs for DEI and DMI,

making them more economical for industrial production. In addition, as the side chain shortens (DBI → DEI → DMI), the polarity of the material increases, which may significantly affect its mechanical properties, oil resistance, and chemical resistance. Therefore, in this work, we used three itaconate monomers with different side chains, namely dimethyl itaconate (DMI), diethyl itaconate (DEI), and dibutyl itaconate (DBI), to synthesize and prepare three types of carboxylated itaconate elastomer (PDXIBA: PDMIBA, PDEIBA, PDBIBA) films, and systematically studied the effect of side chain structure variation on the properties of itaconate latex materials, which provides important guidance for the application of such bio-based materials in the field of disposable protective gloves.

In addition, to more comprehensively evaluate the application potential of carboxylated itaconate latex in disposable glove materials, this study also purchased two types of commercial carboxylated nitrile (XNBR) latex (Nipol LX550L and SH-830), currently used in the industry for the production of nitrile gloves, and conducted comparative studies with the synthesized carboxylated itaconate (PDXIBA) latex. These two XNBR latexes, as representatives of petroleum-based synthetic elastomers, have mature commercial applications, and their mechanical properties, chemical resistance, and processability have been widely verified. Therefore, a horizontal comparison between PDXIBA latex and industrial XNBR latex helps to clarify the advantages and challenges of bio-based itaconate elastomers in the glove field. Meanwhile, in order to expand the multifunctional application of the materials, this work further investigated the performance differences of PDXIBA, XNBR, and ESBR in silica-filled nanocomposites. By introducing high specific surface area silica filler, the effects of different side chain structures on the mechanical properties, dynamic properties, filler dispersion, and oil resistance of the composites were studied, so as to further elucidate the regulatory roles of side chain length, matrix polarity, and filler-matrix interaction on the comprehensive performance of the composites.

5.2 Experimental section

5.2.1 Materials

Dibutyl itaconate (DBI) was obtained from Guangdong Suzhong Chemical Technology Co., Ltd., China. Diethyl itaconate (DEI) and dimethyl itaconate (DMI) were obtained from Guangdong Wengjiang Chemical Reagent Co., Ltd., China. Butadiene (BD) was obtained from Sinopec Qilu Petrochemical Co., Ltd, China. Methacrylic acid (MAA), sodium dodecyl benzene sulfonate (SDBS), Sodium salt of polynaphthalene sulphonic acid (dispersing agent NNO), ethylene diamine tetraacetic acid (EDTA), ferrous sulfate ($FeSO_4$), potassium persulfate ($K_2S_2O_8$), ethanol absolute were obtained from Shanghai Macklin Biochemical Co., Ltd, China. Deionized water was provided by Shandong Chambroad Petrochemicals Co., Ltd., China. Ethanol, calcium chloride, and potassium hydroxide were provided by Beijing Tongguang Fine Chemicals Co., Ltd, China. Nipol LX550L was purchased from Zeon Corporation, Japan. SH-830 was purchased from Hengtai Plastics Raw Materials Trading Department, Zhangmutou, Dongguan, China. Zinc oxide, sulfur, and accelerator BZ (ZDBC) dispersions were purchased from Dongguan Benke Latex Co., Ltd, China.

5.2.2 Synthesis of PDXIBA latex with different side chains

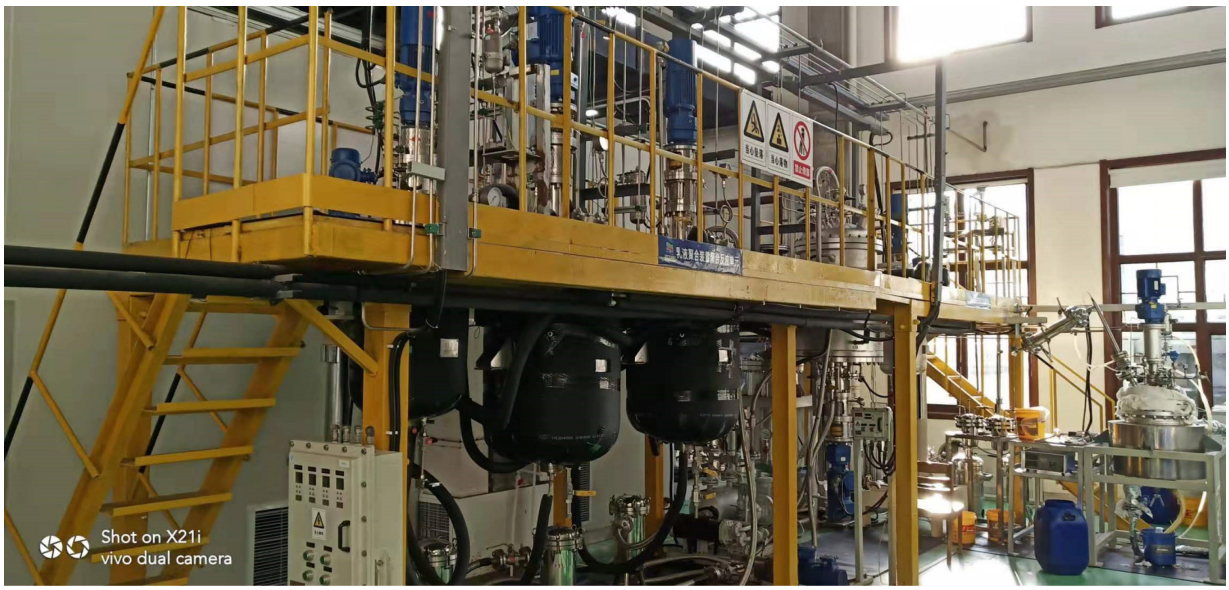

Figure 5.1 The 200 L reactor system used for scale-up synthesis.

This experiment utilized a 200L reactor for scale-up synthesis, as shown in **Figure 5.1**, primarily based on the following considerations: compared to the laboratory-scale 2L reactor, the 200L reactor is more representative of industrial production conditions, facilitating the evaluation of the feasibility and stability of the synthesis process. This ensures better reproducibility of experimental results and provides data support for the future industrial application of glove materials. The polymerization equation is shown in **Figure 5.2**. The three itaconate-based elastomers were synthesized using the same polymerization formulation. Specifically, itaconate monomers (DBI, DEI, or DMI) and butadiene (BD) were used as the main monomers with a mass ratio of 60:40. In addition, the third monomer, methacrylic acid (MAA), was incorporated at 7 wt% relative to the total mass of the main monomers. The polymerization formulation is shown in **Table 5.1**. Initially, 48 kg of deionized water, 0.72 kg of SDBS, 0.12 kg of dispersing agent NNO, 0.072 kg of $FeSO_4$, 0.048 kg of EDTA and 0.01kg of SFS were sequentially added to the reactor. Then, 14.4 kg of DBI/DEI/DMI and 1.68 kg of MAA were added at room temperature. The stirring speed was set to 280 rpm. After purging the reactor with nitrogen, 9.6 kg of BD was introduced into the system. Once all valves were confirmed to be closed, heating was initiated, and the pre-emulsification process began. The temperature was set to 50 °C. After 15 min, the set temperature was reached, and pre-emulsification continued for 1 h. After pre-emulsification, potassium persulfate ($K_2S_2O_8$) was added as an initiator. The reaction proceeded for 8 h, forming a latex. Finally, the latex was coagulated with ethanol, and the gum was dried in an oven at 60 °C until a constant weight was reached, yielding the PDXIBA (PDBIBA, PDEIBA, PDMIBA) copolymers.

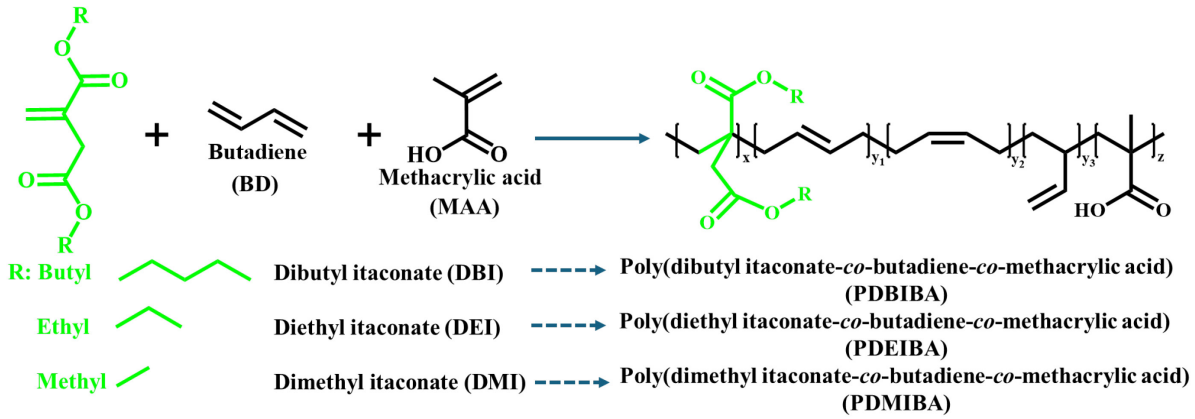

Figure 5.2 The polymerization reaction route of PDBIBA, PDEIBA and PDMIBA.

Table 5.1 Recipe for emulsion polymerization in a 200L sealed reactor.

Ingredients	Dosage/kg
Dibutyl /diethyl/dimethyl itaconate (DBI/DEI/DMI)	14.4
Butadiene (BD)	9.6
Methacrylic acid (MAA)	1.68
Sodium dodecyl benzene sulfonate (SDBS)	0.72
Sodium salt of polynaphthalene sulphonic acid (Dispersing agent NNO)	0.12
$K_2S_2O_8$	0.072
$FeSO_4$	0.024
Ethylene diamine tetraacetic acid (EDTA)	0.048
Sodium hydroxymethanesulfinate (SFS)	0.01
Deionized water	48

5.2.3 Preparation of PDXIBA films with different side chains and XNBR films

The vulcanization formulation of PDXIBA (PDBIBA, PDEIBA, PDMIBA) films is shown in **Table 5.2**. The preparation method of films is as follows: First, water was added to the latex to adjust the solid content to 30%. Then, under continuous stirring, zinc oxide (ZnO), sulfur (S), and accelerator BZ (ZDBC) were sequentially added and stirred continuously for 3 h to ensure thorough mixing. After mixing, the solution was filtered and set aside for further use. For the preparation of films, the calcium chloride ($CaCl_2$) immersion method was adopted. The specific steps were as follows: A ceramic rod with a diameter of 3 cm was immersed in a 30% aqueous solution of calcium chloride ($CaCl_2$) for 5 seconds, then removed and dried. Next, the treated ceramic rod was immersed in the previously prepared latex for 5 min, then removed and air-dried at room temperature. The dried ceramic rod was then placed in an oven at 120 °C for 1 h for vulcanization， as shown in **Figure 5.3**. After vulcanization, the ceramic rod was demolded, and the resulting film was washed in clean water to obtain the film. The film thickness is approximately 0.5 mm. The preparation of XNBR films was consistent with the method

described above.

Table 5.2 Vulcanization formulation of PDXIBA (PDBIBA, PDEIBA, PDMIBA) and XNBR (Nipol LX550L, SH-830) films.

Ingredients	Dosage [a] (phr [b])
Latex	100
Zinc oxide dispersion [c] (ZnO)	5
Accelerator BZ dispersion [d] (ZDBC)	0.5
Sulfur dispersion (S)	1

a The dosage refers to the solid content.

b Parts per 100 parts of rubber (by mass)

c The dispersion refers to a stable suspension of ZnO, S, or ZDBC particles, with a concentration of 50%.

d Zinc di-n-butyldithiocarbamate

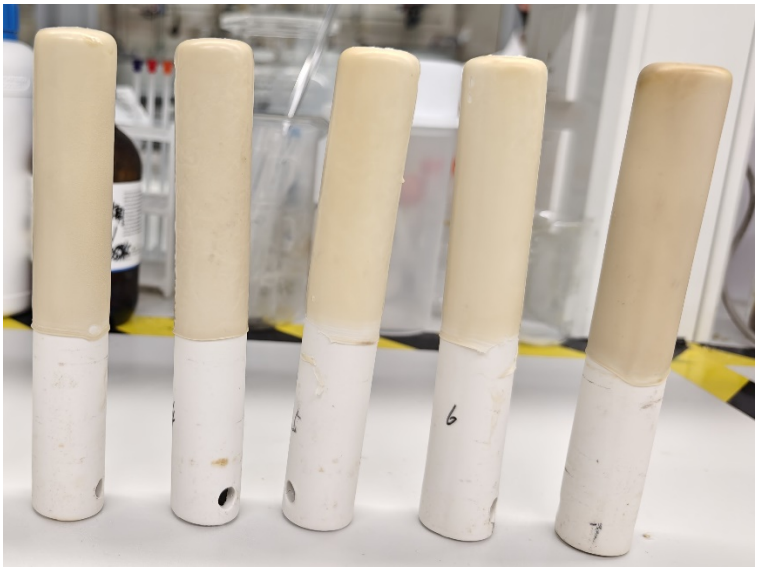

Figure 5.3 Film formation of different types of rubber on ceramic rods. From left to right: PDBIBA, PDEIBA, PDMIBA, Nipol LX550L, and SH-830.

5.2.4 Preparation of silica/PDXIBA, silica/XNBR and silica/ESBR nanocomposites

For the preparation of silica/PDXIBA nanocomposites, the process involved the use of a Haake mixer and a two-roll mill. The compounding formulation is shown in **Table 5.3**. First, the rubber was plasticized for 1 min on a two-roll mill, followed by mixing at room temperature with other components (excluding the accelerator and sulfur). The mixture was then transferred to the Haake mixer and mixed at 150 °C for 5 min. Afterward, the accelerator and sulfur were added using a two-roll mill at room temperature. Following this, the optimal vulcanization time

for the compound was established using a rotorless rheometer at 150 °C for 60 min, and the test results are summarized in **Table 5.4**. The compound was vulcanized into 1 mm-thick sheets through compression molding at 150 °C under a pressure of 15 MPa within the optimum vulcanization time, leading to the production of cross-linked silica/PDXIBA nanocomposites. The preparation methods of silica/XNBR nanocomposites and silica/ESBR nanocomposites are the same as that of silica/PDXIBA nanocomposites.

Table 5.3 Compounding formulation for silica/PDXIBA, silica/XNBR and silica/ESBR nanocomposites.

Ingredients	Dosage (phr) [a]
PDXIBA, XNBR, ESBR	100
Silica 1165	50
Si69 [b]	5
Antioxidant RD [c]	2
Antioxidant 4020 [d]	0.75
Zinc oxide (ZnO)	5
Stearic acid (SA)	0.5
Accelerator CZ [e]	1
Accelerator M [f]	0.7
Sulfur (S)	1

a Parts per 100 parts of rubber (by mass)

b Bis [3-(triethoxysilyl) propyl] tetrasulfide

c Poly (1,2-dihydro-2,2,4-trimethyl-quinoline)

d N-1,3-dimethylbutyl-N'-phenyl-p-phenylenediamine

e 2-mercapt-obenzothiazole

f N-cyclohexylbenzothiazole-2-sulphenamide

Table 5.4 Optimal vulcanization times of silica/PDXIBA, silica/XNBR and silica/ESBR nanocomposites.

Silica/rubber nanocomposites	T_{90}/min
Silica/PDBIBA	42.5
Silica/PDEIBA	37.7
Silica/PDMIBA	42.9
Silica/Nipol LX550L	42.1
Silica/SH-830	43.1
Silica/ESBR	31.6

5.3 Characterization methods

The characterization methods used in this section, including GPC, FTIR, ^{1}H NMR, DSC, TGA, TEM, mechanical testing, RPA, DMTA, DIN abrasion loss, thermo-oxidative aging properties, and oil resistance evaluation, are identical to those described in Section 3.3 and are not repeated here.

Abrasion loss of cross-linked PDXIBA and XNBR films by Taber abrasion tester

Films with dimensions of 10×10 cm and a thickness of 0.5 mm were mounted on a horizontal rotating platform. The films were subjected to abrasion using an abrasive wheel under controlled conditions. The rotational speed was set to 60 rpm, and the test was conducted for a total of 3000 revolutions. The mass of each films was measured before and after the test. The mass loss was calculated to evaluate the abrasion resistance of the materials.

Solvent resistance test of cross-linked PDXIBA and XNBR films

The solvent resistance of the elastomer films was assessed by monitoring their mass and volume changes after immersion in toluene. Square specimens with a side length of 10 mm and a thickness of 0.5 mm were cut from the vulcanized films. Each sample was weighed (m_1), and its initial volume (V_1) was calculated based on the measured dimensions. The specimens were then immersed in toluene at room temperature (approximately 25 °C) for 24 h. After immersion, the samples were removed, gently wiped with filter paper to eliminate surface solvent, and immediately reweighed (m_2). Final volume (V_2) was determined in the same way.

The percentage of mass gain (Δm) and volume gain (ΔV) were calculated using the following formulas:

$$Percentage\ of\ mass\ \ gain\ (\Delta m) = \frac{m_2 - m_1}{m_1} \times 100\%$$

where:

m_1: mass of the sample before solvent immersion (g)

m_2: mass of the sample after solvent immersion (g)

$$Percentage\ of\ volume\ \ gain\ (\Delta V) = \frac{V_2 - V_1}{V_1} \times 100\%$$

V_1: volume of the sample before solvent immersion (mm^3)

V_2: volume of the sample after solvent immersion (mm^3)

Cytotoxicity of PDEIBA, natural rubber (NR) and nitrile (XNBR) gloves

A 4 cm × 6 cm piece was cut from the palm area of each glove sample. The samples were sterilized by ultraviolet (UV) irradiation for 30 min, followed by three washes with phosphate-buffered saline (PBS), each for 5 min. According to an extraction ratio of 6 cm^2/mL, 8 mL of complete culture medium was added to each sample and incubated for 24 h. The extract was sterilized using a 0.22 μm filter. Working concentrations of the extract were prepared as follows: 1%, 12.5%, 25%, 50%, 75%, and 100%. The samples were divided into four groups: Control, NR, XNBR, and PDEIBA. The Control group received 100 μL/well of complete culture medium. For the experimental groups of NR, XNBR, and PDEIBA, 100 μL/well of the corresponding extract at each working concentration was added. Each treatment was performed in triplicate (n = 3). L929 fibroblasts in the logarithmic growth phase were harvested and counted. The cell concentration was adjusted and seeded into 96-well plates at a density of 8 × 10^3 cells/well. Cells were incubated overnight at 37 °C in a humidified incubator with 5% CO_2 to allow adherence.

After 24 h of treatment according to the groupings above, the culture medium was removed, and each well was washed three times with PBS. Then, 100 μL of culture medium containing 0.5 mg/mL MTT was added to each well, and the cells were incubated for 4 h under the same conditions. After incubation, the supernatant was discarded, and 100 μL of DMSO was added to each well. The plate was gently shaken for 10 min to dissolve the formazan crystals.

Absorbance was measured at 570 nm using a microplate reader. Relative cell viability (%) was calculated using the following formula:

$$Relative\ cell\ viability\ (\%) = \frac{OD_{experimental}}{OD_{control}} \times 100\%$$

Where:

$OD_{experimental}$: absorbance value of the experimental group

$OD_{control}$: absorbance value of the control group

Skin sensitization evaluation of PDEIBA, natural rubber (NR), and nitrile (XNBR) gloves

Hair on the dorsal skin of guinea pigs was removed 24 h prior to the experiment. Two areas measuring 2 cm × 2 cm on both sides of the spine were marked with a marker pen. Hair within the marked regions was trimmed and then completely removed using a depilatory cream. The skin was then rinsed with sterile water.

On Day 0, Day 7, and Day 14, the test samples were applied to the dorsal skin (2 cm × 2 cm area). The application site was covered with two layers of gauze and one layer of polyethylene film, then sealed and fixed with non-irritating adhesive tape. After 6 h, the patches were removed, and the residual sample was washed off.

Photographs were taken before administration and on Days 7 and 14 (prior to re-administration) for documentation (not for scoring). At 24 and 48 h after the final administration, skin reactions (erythema and edema) were observed, photographed, and scored.

Based on the severity of skin irritation reactions, including erythema (redness) and edema (swelling), responses are classified into five grades, each assigned a score of 0, 1, 2, 3, or 4. For erythema: 0 indicates no erythema, 1 indicates barely perceptible erythema, 2 indicates moderate erythema, 3 indicates severe erythema, and 4 indicates dark red erythema accompanied by scab formation. For edema: 0 indicates no edema, 1 indicates barely perceptible swelling, 2 indicates slight edema with elevated edges, 3 indicates clearly defined swelling of approximately 1 mm, and 4 indicates swelling greater than 1 mm with a large affected area.

$$Irritation\ Score = \frac{Total\ Erythema\ Score + Total\ Edema\ Score}{Number\ of\ Test\ Animals}$$

Based on the average irritation score, skin irritation is categorized as follows: no irritation

(0–0.49), slight irritation (0.50–2.99), moderate irritation (3.00–5.99), and severe irritation (6.00–8.00).

Scanning electron microscopy (SEM) of cross-linked PDXIBA and XNBR films after abrasion testing

The test was conducted using a field emission scanning electron microscope (FE-SEM, S-4800, Hitachi, Japan) at an accelerating voltage of 5 kV. Prior to observation, the samples were coated with a thin layer of gold.

5.4 Results and discussion

5.4.1 Synthesis and characterization of PDXIBA (PDBIBA, PDEIBA, PDMIBA) latex with different side chains

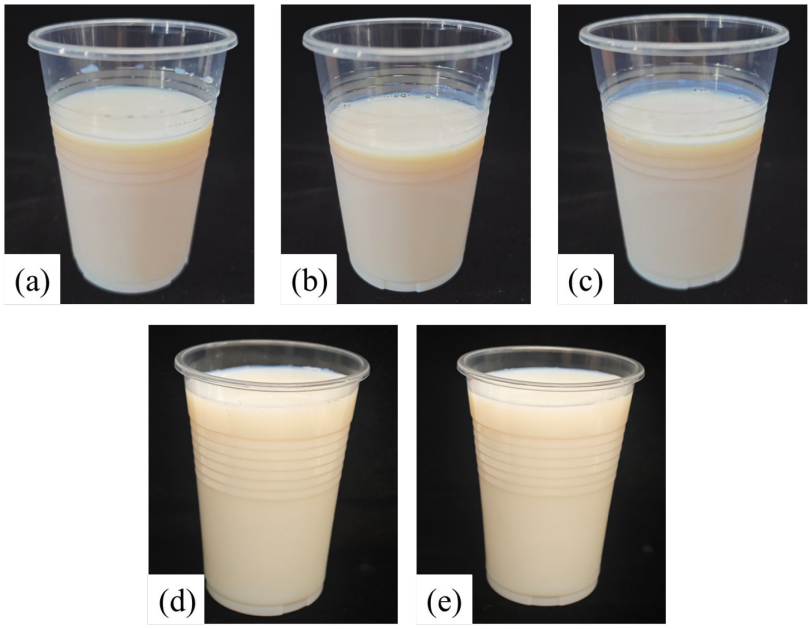

Figure 5.4 Visual appearance of latex samples after polymerization. (a) PDBIBA latex, (b) PDEIBA latex, (c) PDMIBA latex, (d) Nipol LX550L latex, and (e) SH-830 latex.

Figure 5.4 shows the visual appearance of the latex samples after polymerization. All five latex samples appear as milky white liquids with uniform appearance, no visible phase separation, and overall exhibit good dispersion state. **Table 5.5** summarizes the number-average molecular weight (M_n), molecular weight distribution ($Đ$), yield, solid content, viscosity, and particle size (Z-Average) of different PDXIBA (PDBIBA, PDEIBA, PDMIBA) latexes and

commercial XNBR (Nipol LX550L, SH-830) latexes to investigate the effect of different monomer structures on polymer properties. In terms of molecular weight (M_n), the M_n of the synthesized PDXIBA latexes is significantly higher than that of the XNBR latexes. Among them, PDBIBA has the highest M_n (256 kg/mol), followed by PDEIBA (179 kg/mol), and PDMIBA with the lowest M_n (99 kg/mol). This trend is primarily influenced by the steric hindrance effect and side chain size of the monomers. dibutyl itaconate (DBI) has a larger steric hindrance due to its longer butyl side chain, which restricts free radical chain transfer, resulting in a higher molecular weight polymer. In contrast, dimethyl itaconate (DMI) has a smaller methyl side chain with weaker steric hindrance, making chain transfer more likely, thereby reducing M_n[11, 12]. Additionally, PDEIBA and PDMIBA exhibit broader molecular weight distributions $Đ$ (3.25 and 3.27, respectively), indicating stronger chain transfer or branching reactions during polymerization, whereas PDBIBA has the narrowest $Đ$ (1.94), suggesting a more uniform molecular structure. In comparison, the M_n of XNBR latexes is significantly lower than that of the synthesized PDXIBA latexes. Regarding solid content, viscosity, and particle size, the XNBR latexes show significantly higher values than the synthesized latexes, which is likely due to differences in polymerization processes. Future research can further optimize polymerization formulations and processing techniques to enhance the suitability of PDXIBA latexes for latex-based product manufacturing.

Table 5.5. The number-average molecular weight, molecular weight distribution, yield, solid, viscosity, and latex particle size of PDXIBA latexes and XNBR latexes.

Sample names	M_n (kg/mol)	$Đ$	Yield (%)	Solid (%)	Viscosity (mPa·s)	Z-Average (nm)
PDBIBA	256	1.94	93	32.3	11	80
PDEIBA	179	3.25	92	32.0	8	84
PDMIBA	99	3.27	95	33.1	10	86
Nipol LX550L	62	2.58	-	47.5	46	133
SH-830	86	2.74	-	46.7	34	122

As shown in **Figure 5.5**, the primary structural difference between PDXIBA and XNBR lies in the presence of itaconate units versus acrylonitrile units. The detailed assignment of each

absorption peak to its corresponding functional group has already been described in the **Table 5.6**. The most significant structural difference in XNBR latex is the presence of acrylonitrile units. The XNBR latex exhibits a distinct absorption peak at 2237 cm^{-1}, corresponding to the stretching vibration of the -CN group from acrylonitrile units, which is a key factor contributing to its superior oil resistance, solvent resistance, and mechanical properties. Additionally, because the carbonyl (C=O) groups in XNBR latex originate exclusively from the carboxyl groups in methacrylic acid, its C=O absorption peak intensity is relatively weak. In contrast, the carbonyl absorption in PDXIBA elastomers arises not only from the carboxyl groups of methacrylic acid but also from the ester groups of itaconate units, leading to a significantly stronger absorption peak.

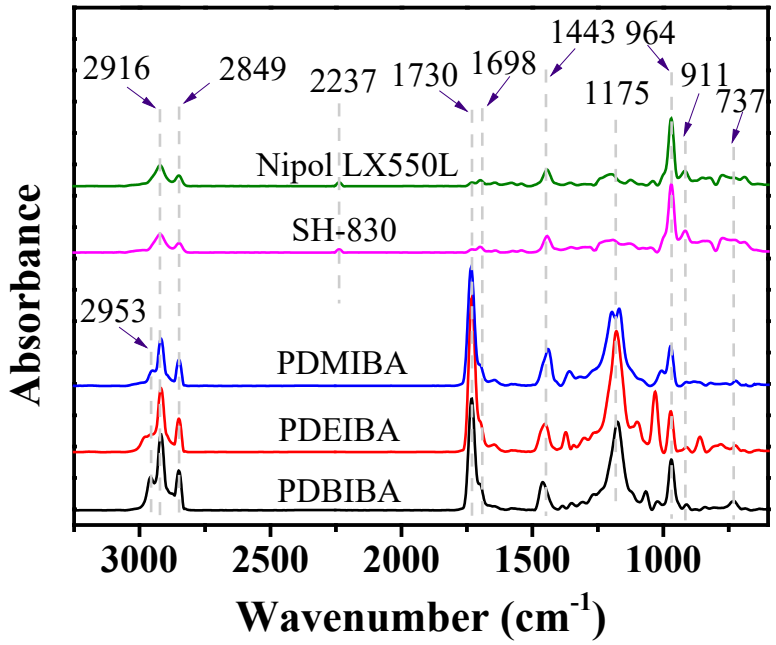

Figure 5.5 FTIR spectra of neat PDXIBA and XNBR.

Table 5.6 Assignments of the main FTIR absorption peaks for neat PDXIBA and XNBR

Wavenumber (cm^{-1})	Vibration	Source
2953	ν ($-CH_3$)	DBI, DEI, DMI, MAA
2916	ν ($-CH_2$)	DBI, DEI, DMI, AN, BD, MAA
2849	ν (-CH)	DBI, DEI, DMI, AN, BD, MAA
2237	ν (-CN)	AN
1730	ν (-C=O)	DBI, DEI, DMI, MAA
1698	Hydrogen-bonded carboxylic acid dimers	MAA
1443	δ ($-CH_3$), δ ($-CH_2$)	DBI, DEI, DMI, AN, BD, MAA
1175	ν (C-O-C)	DBI, DEI, DMI
964	δ (-C-H)	Trans-BD
911	δ (-C-H)	Vinyl-BD
737	δ (-C-H)	Cis-BD

As shown in **Figure 5.6**, the molecular structures of the neat PDXIBA and XNBR were characterized by ^{1}H NMR spectra. The spectra reveal distinct chemical shifts corresponding to protons in different chemical environments, thereby confirming the compositions and structural features of the materials. Additionally, by integrating the peak areas of the corresponding hydrogen shifts in the ^{1}H NMR spectra, we determined the actual composition ratios of the PDXIBA and XNBR, which are summarized in **Table 5.7**. PDXIBA elastomers primarily consist of itaconate units (DBI/DEI/DMI), accounting for 65.4%–67.4%, whereas XNBR primarily rely on acrylonitrile (AN) units to provide polarity, with AN units accounting for only 30.6% and 35.2%. Additionally, the butadiene (BD) content in XNBR is significantly higher (56.8% and 62.2%) compared to PDXIBA elastomers (26.0%–27.5%). Moreover, the proportion of vinyl-BD structures in XNBR (9.5% and 10.3%) is much higher than that in PDXIBA elastomers (1.8%–2.2%). The MAA content in PDXIBA elastomers is 6.6%–7.1%, while in XNBR, the MAA content is 7.2% and 8.0%. Although the acrylonitrile unit content in XNBR is lower, its high polarity significantly enhances oil resistance, chemical resistance, and

mechanical performance, giving XNBR distinct advantages in demanding applications.

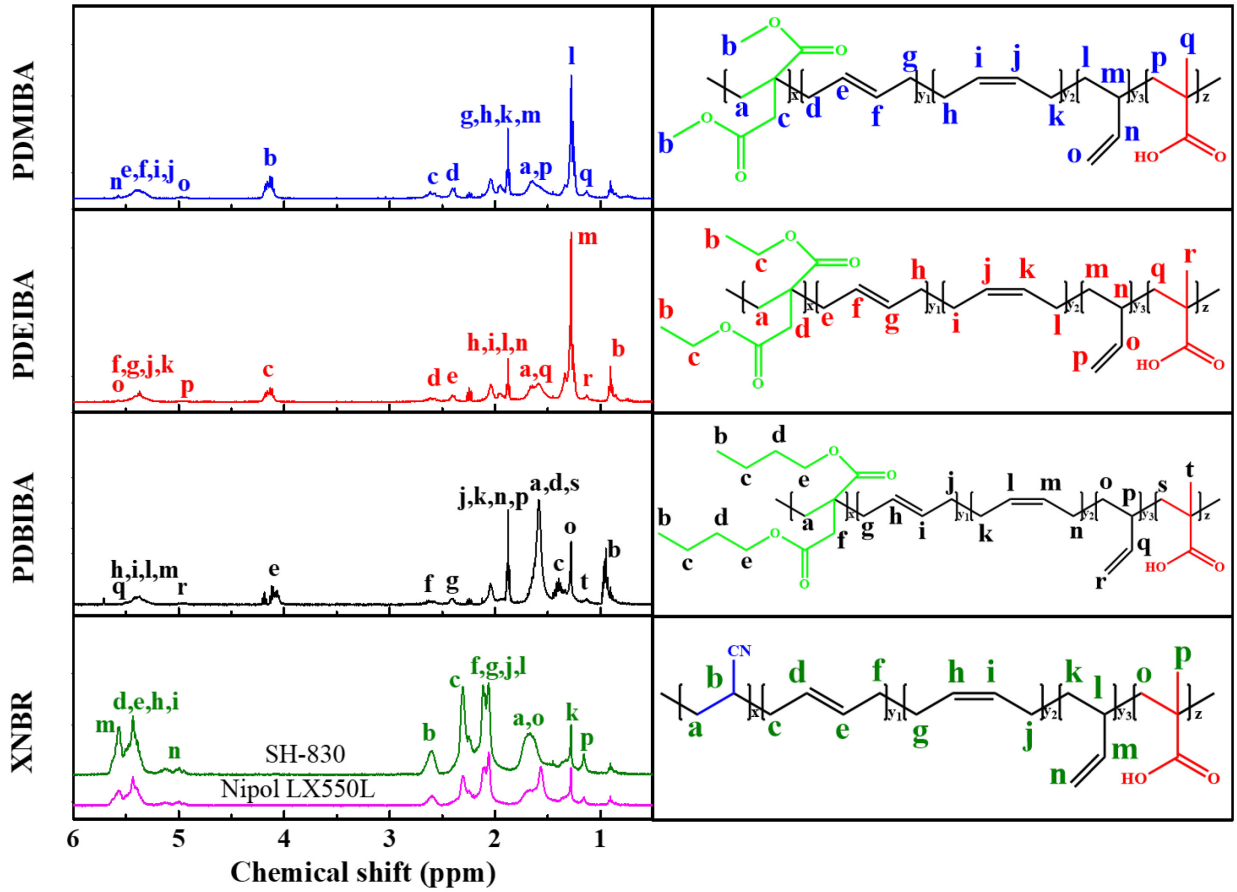

Figure 5.6 ^{1}H NMR spectra of neat PDXIBA and XNBR.

Table 5.7 Compositions of neat PDXIBA and XNBR.

Neat PDXIBA and XNBR	Polymer composition (wt%)			
	DBI/DEI/DMI/AN	Vinyl-BD	Cis-BD and trans-BD	MAA
PDBIBA	67.4	2.1	23.9	6.6
PDEIBA	65.4	1.8	25.7	7.1
PDMIBA	67.0	2.2	24.1	6.7
Nipol LX550L	30.6	10.3	51.9	7.2
SH-830	35.2	9.5	47.3	8.0

The glass transition temperature (T_g) is a crucial parameter for polymer materials, representing the transition temperature at which the amorphous regions of polymer chains shift from a frozen state to a mobile state. This parameter determines whether a polymer behaves as

an elastomer at its operating temperature[13]. The DSC in **Figure 5.7** results indicate that as the size of the side group decreases, T_g increases accordingly. PDBIBA (-46 ℃) has the lowest T_g due to its long butyl side chain. In contrast, PDEIBA (-17 ℃) and PDMIBA (-16 ℃), with shorter ethyl and methyl side chains, exhibit higher T_g values as their molecular packing is tighter, restricting chain movement. Comparatively, XNBR (Nipol LX550L -40 ℃, SH-830 -32 ℃) has a higher T_g than PDXIBA elastomers due to the strong polarity of the acrylonitrile (AN) unit, which increases intermolecular interactions. Overall, PDBIBA exhibits the best low-temperature flexibility, whereas XNBR, due to its stronger polarity, is likely to demonstrate superior heat resistance and mechanical strength.

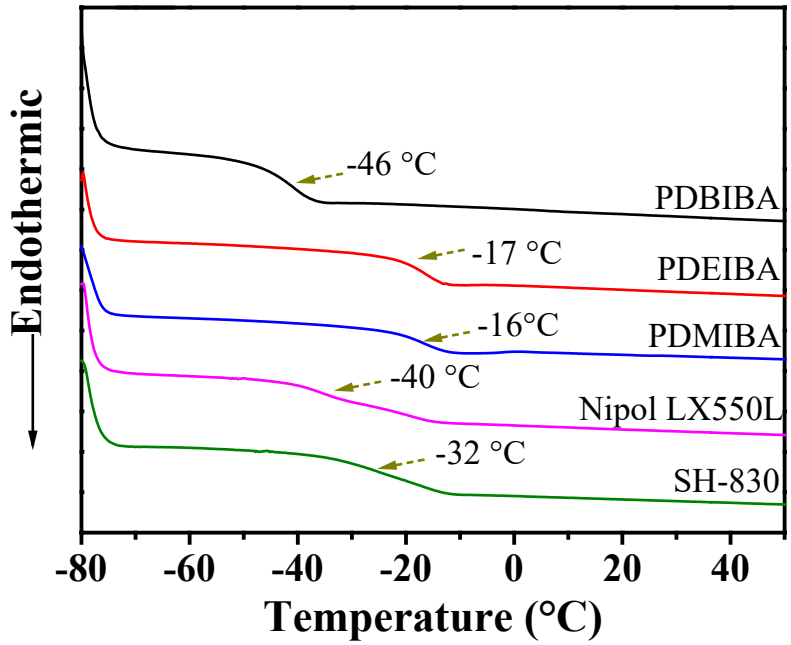

Figure 5.7 DSC curves of neat PDXIBA and XNBR.

According to the TGA and DTG curve analysis in **Figure 5.8**, 5% weight loss ($T_{5\%}$) of XNBR (368 °C and 369 °C) is significantly higher than that of PDXIBA elastomers (350–352 °C), indicating that XNBR exhibits greater stability during the early thermal degradation stage. However, this series of PDXIBA elastomers all exhibit good thermal stability ($T_{5\%}$ > 300 °C), which can essentially meet the thermal stability requirements for elastomers in most engineering applications. Meanwhile, the thermal degradation process of itaconate rubbers occurs in two distinct stages. Stage 1 (270–400 °C) is mainly associated with the decomposition of side chain ester groups and carboxyl groups[14, 15]. Compared to PDBIBA and PDEIBA, PDMIBA exhibits noticeable weight loss at around 200 °C, which is attributed to the lower

thermal stability of its methyl ester side groups, making it more prone to alcohol elimination reactions at high temperatures. In contrast, XNBR contains only carboxyl groups without ester groups, making this stage less pronounced. Stage 2 (400–500 °C) corresponds to the random degradation and carbonization of the polymer backbone. Overall, XNBR demonstrates superior thermal stability.

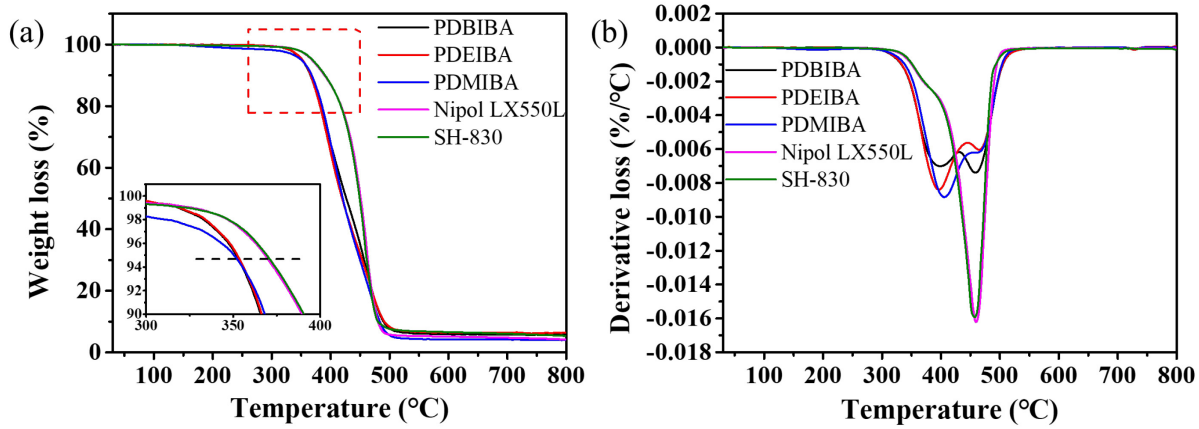

Figure 5.8 (a) TGA thermograms and (b) DTG (derivative thermograms) of neat PDXIBA and XNBR.

5.4.2 Mechanical properties of cross-linked PDXIBA films

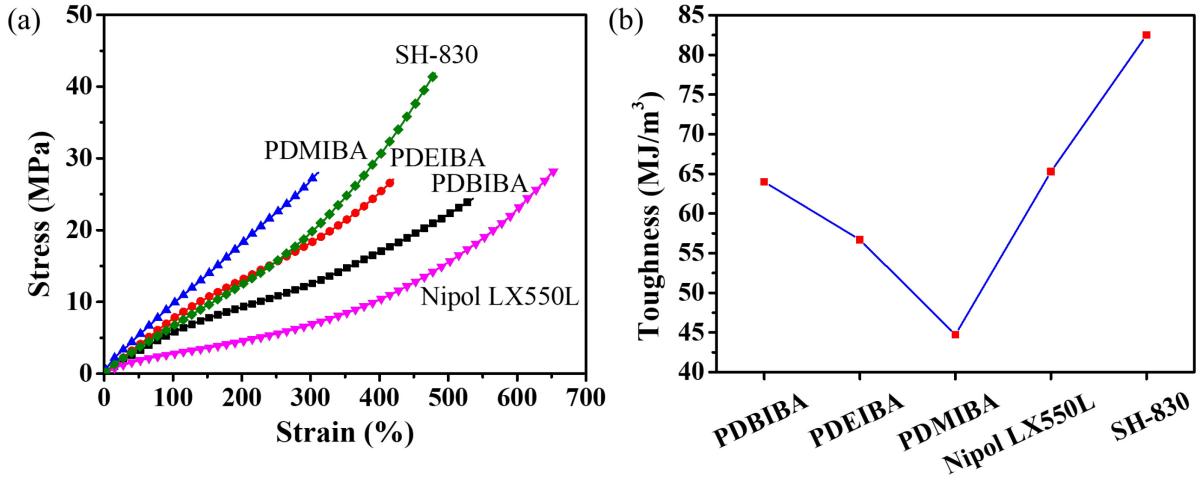

Figure 5.9 (a) Stress–strain curves of cross-linked PDXIBA and XNBR films including PDBIBA, PDEIBA, PDMIBA, Nipol LX550L, and SH-830. (b) Toughness (area under the stress–strain curves) for the corresponding materials.

Mechanical properties are crucial for latex products such as gloves, directly affecting product safety and practical performance. The stress-strain curves of PDXIBA elastomers (PDBIBA, PDEIBA, PDMIBA) and XNBR (Nipol LX550L, SH-830) are shown in the **Figure 5.9** (a), with the corresponding data listed in **Table S5.1**. The results indicate that the tensile

strength of PDXIBA elastomers increases progressively as the side group becomes shorter. This trend can be attributed to two main factors: (1) The shortening of the side group leads to a higher T_g, which is considered to be in the "leathery state" [16], where both high elasticity and rigidity coexist. In this state, the cross-linked elastomer products experience greater energy dissipation, enhancing tensile strength; (2) The shorter ethyl and methyl groups in PDEIBA and PDMIBA contribute to a higher cohesive energy density, strengthening intermolecular interactions and further improving mechanical performance. However, as shown in **Figure 5.9** (b), the toughness of PDEIBA and PDMIBA decreases with the shortening of the side chains. In comparison, the tensile strength of PDMIBA is already close to that of Nipol LX550L, indicating its favorable mechanical properties. Meanwhile, SH-830 exhibits even higher tensile strength due to its higher acrylonitrile content. Overall, the PDXIBA elastomer films exhibit high strength (>25.5 MPa) and toughness (>44.7 MJ/m^3), meeting the fundamental tensile performance requirements for glove materials. This suggests their potential application in disposable and industrial protective gloves.

5.4.3 Abrasion loss of cross-linked PDXIBA films

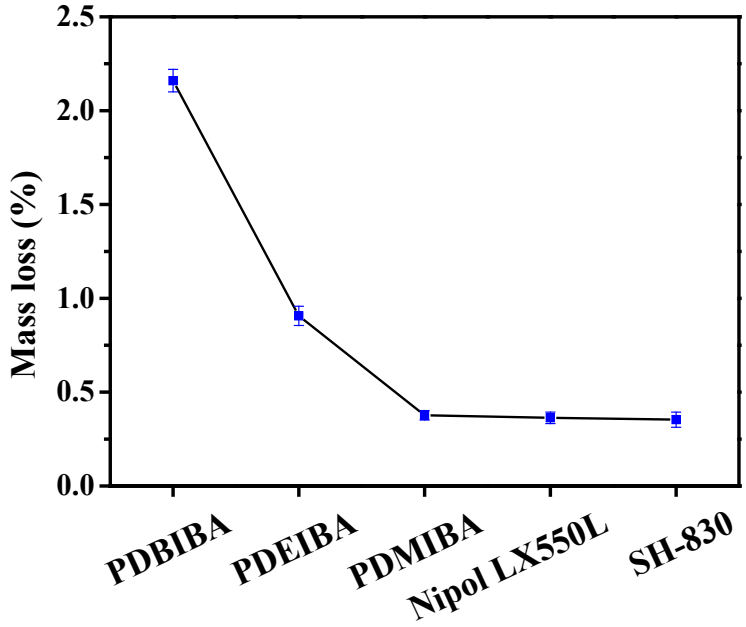

Figure 5.10 Abrasion loss of cross-linked PDXIBA and XNBR films.

Abrasion resistance is an important performance indicator for rubber products such as gloves, determining their durability and resistance to damage during long-term use. A Taber

abrasion tester was used to evaluate the abrasion resistance of PDXIBA and XNBR films under specific abrasion conditions, with the mass loss measured as shown in the **Figure 5.10**. The results indicate that as the side groups shorten to ethyl (PDEIBA) and methyl (PDMIBA), the introduction of rigid structural units enhances the material's abrasion resistance. Among them, PDMIBA exhibits abrasion resistance comparable to that of XNBR latex, demonstrating excellent abrasion performance.

The corresponding SEM images of the abrasion surfaces are shown in **Figure 5.11**. PDBIBA and PDEIBA exhibit rougher surfaces with more wear debris and grooves, indicating greater material loss. In contrast, PDMIBA shows a smoother and more intact surface, similar to Nipol LX550L and SH-830. These surface morphologies are consistent with the abrasion resistance results, further confirming that shorter side chains improve abrasion resistance.

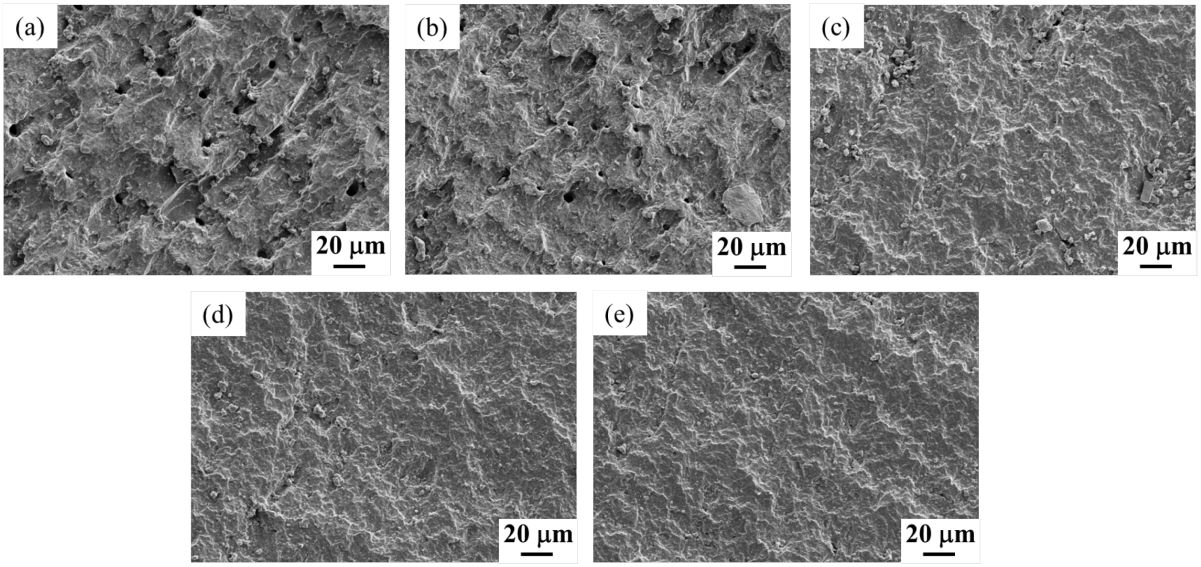

Figure 5.11 SEM images of the abrasion surfaces of cross-linked PDXIBA and XNBR films after abrasion testing:(a) PDBIBA, (b) PDEIBA, (c) PDMIBA, (d) Nipol LX550L, and (e) SH-830.

5.4.4 Solvent and oil resistance evaluation of cross-linked PDXIBA elastomer films

The **Figure 5.12** (a) illustrates the percentage of mass gain (Δm) and volume gain (ΔV) of PDXIBA and XNBR films after being immersed in toluene for 24 h to evaluate their solvent resistance. The results show that the swelling of PDXIBA elastomers in toluene decreases as the side chains become shorter. This is mainly because toluene is a non-polar solvent that exhibits strong swelling effects on non-polar or low-polarity rubbers. In comparison, XNBR

exhibits superior solvent resistance in both solvents compared to PDXIBA elastomers, and its swelling degree decreases with increasing acrylonitrile (AN) content. SH-830, classified as a high-AN nitrile rubber, demonstrates the best solvent resistance. However, the solvent resistance of PDMIBA is already close to that of the medium-AN grade Nipol LX550L, indicating its potential for good stability in certain non-polar solvents.

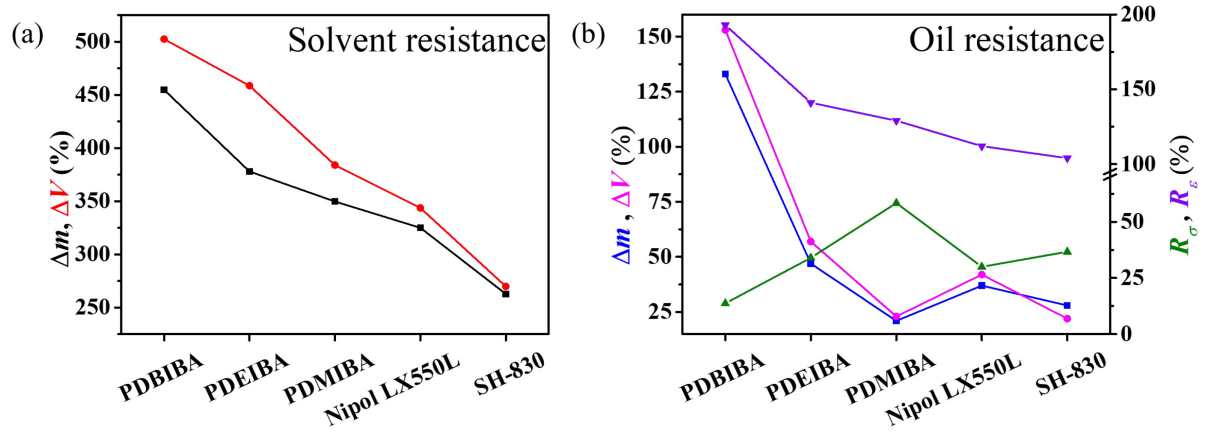

Figure 5.12 (a) Percentage of mass gain (Δm) and volume gain (ΔV) of cross-linked PDXIBA and XNBR films after 24 h immersion in toluene at room temperature, reflecting their solvent resistance. (b) Percentage of mass gain (Δm) and volume gain (ΔV), along with the retention ratios of tensile strength (R_σ) and elongation at break (R_ε) of the same films after 24 h immersion in IRM-903# oil at 100 °C, illustrating their oil resistance and mechanical stability.

The oil resistance of PDXIBA and XNBR films after immersion in IRM-903# oil at 100 °C for 24 h is shown in the **Figure 5.12** (b), with data summarized in **Table S5.2**, including percentage of mass gain (Δm) and volume gain (ΔV), along with the retention ratios of tensile strength (R_σ) and elongation at break (R_ε). Overall, the oil resistance of PDXIBA elastomers improves progressively with increasing side-group polarity. Among them, PDBIBA, due to its large butyl ester side group, exhibits the most severe oil swelling effect, leading to significant degradation of mechanical properties. In contrast, PDEIBA, with its more polar ethyl ester side group, demonstrates improved oil resistance stability. PDMIBA, benefiting from the stronger polarity of the methyl ester side group, further enhances its resistance to oil penetration, while the shorter side group reduces swelling space, resulting in the best oil resistance performance among the PDXIBA.

In comparison, the oil resistance of XNBR is significantly influenced by the acrylonitrile (AN) content, with a clear gradient of oil resistance observed across different AN levels. Based

on AN content, nitrile rubber can be classified into three categories: low-AN (< 25%), medium-AN (25-33%), and high-AN (33-45%). The higher the AN content, the better the oil resistance. Among the tested samples, Nipol LX550L falls into the medium-AN category, while SH-830 belongs to the high-AN category. The test results indicate that PDMIBA has surpassed the oil resistance of medium-AN Nipol LX550L. At the same time, in terms of mechanical property retention, it has already surpassed high AN nitrile rubber (SH-830), and in terms of swelling resistance, it is comparable to SH-830, indicating its potential to compete with high AN nitrile rubber under certain conditions.

5.4.5 Cytotoxicity and skin sensitization evaluation of PDEIBA, natural and nitrile rubber gloves

Based on the preceding results, PDXIBA films exhibit excellent comprehensive properties, making them promising candidates for glove applications. By tailoring the side chain structure of the itaconate-based monomers, latexes with different mechanical and functional characteristics can be obtained to meet diverse application requirements. As shown in **Figure 5.13**, PDEIBA latex has been successfully used to fabricate both disposable gloves (**Figure 5.13** (a) and (b)) and industrial protective gloves (**Figure 5.13** (c) and (d)). To further assess the biosafety of disposable PDEIBA gloves and validate their suitability for skin-contact applications, a series of comparative studies were conducted. These include in cytotoxicity tests using L929 fibroblasts and in skin sensitization tests, with commercial natural rubber (NR) and nitrile (XNBR) gloves serving as references.

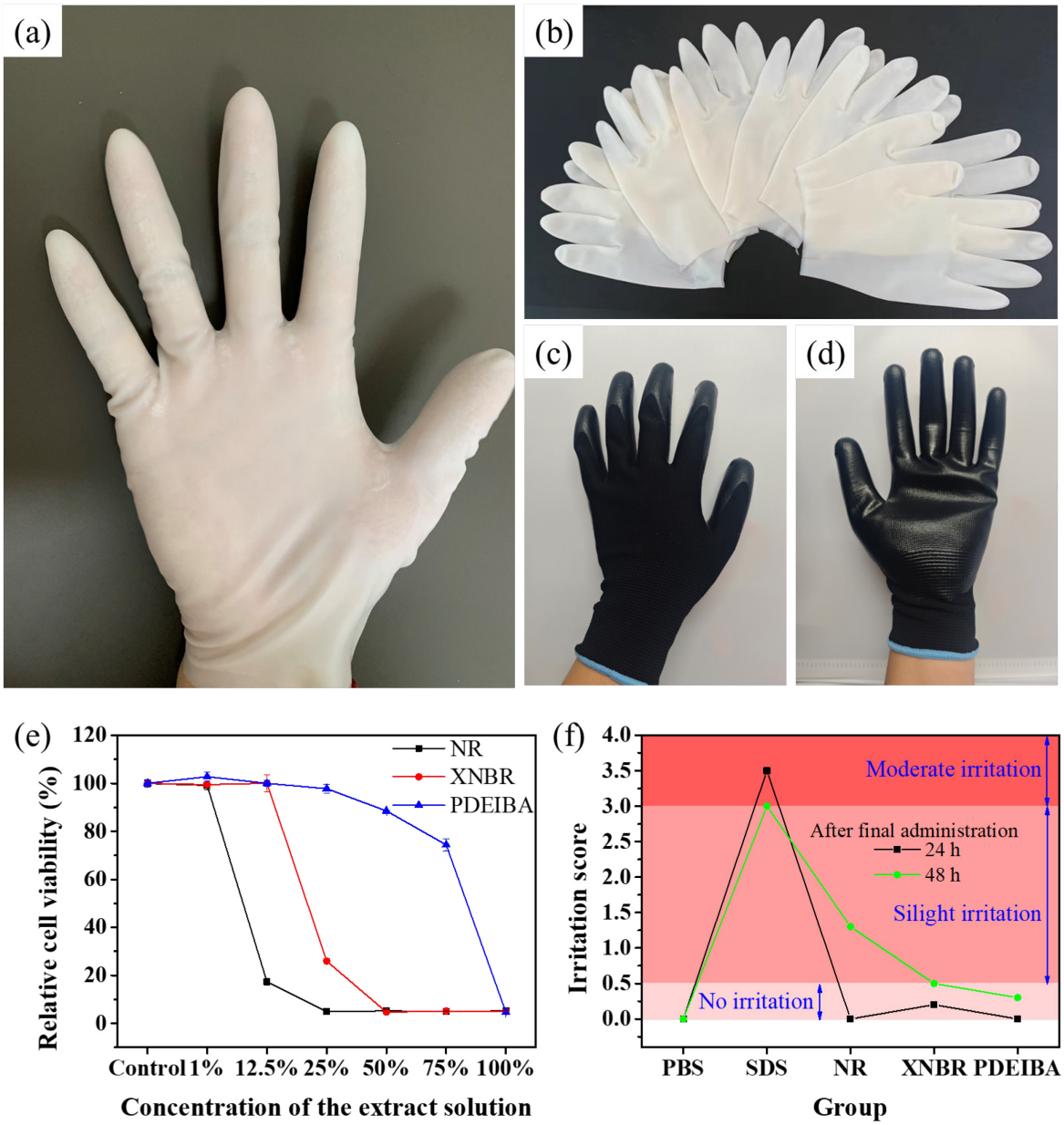

Figure 5.13 PDEIBA gloves prepared from PDEIBA latex: (a) and (b) show disposable gloves; (c) and (d) show protective gloves. (e) Changes in the viability of L929 cells after 24 h of co-culture with NR, XNBR, and PDEIBIA glove samples. (f) Skin irritation scores of PBS, SDS, and glove materials (NR, XNBR, and PDEIBA) at 24 h and 48 h after the final administration. PBS (phosphate-buffered saline) was used as the negative control to represent a non-irritating baseline, while SDS (sodium dodecyl sulfate) served as the positive control due to its known irritant properties. The irritation scores reflect the degree of erythema and edema observed on intact skin, allowing evaluation of the biocompatibility of the tested glove materials.

Figure 5.13 (e) illustrates the cytotoxic effects of NR, XNBR, and PDEIBA glove extracts on L929 cells after 24 h of exposure at various extract concentrations. NR exhibited the highest cytotoxicity, with cell viability dropping below 20% at 12.5% concentration and approaching 5% at ≥25%. XNBR showed similar trends but with slightly better tolerance, maintaining higher

viability at 12.5% and showing significant reduction from 25% upward. In contrast, PDEIBA demonstrated the lowest cytotoxicity. Cell viability remained above 70% at 75% concentration, only showing marked toxicity at 100%. These results indicate that PDEIBA has superior biocompatibility compared to NR and XNBR. Furthermore, based on the observed skin reactions at the administration sites shown in **Figure S5.1** and their evaluation using the assessment criteria described in the characterization methods section, the erythema and edema scores at 24 h and 48 h after the final administration were obtained, as summarized in **Table S5.3**. The resulting skin irritation scores of PBS, SDS, and glove materials (NR, XNBR, and PDEIBA) are presented in **Figure 5.13** (f). PBS (negative control) caused no irritation, while SDS (positive control) showed moderate irritation at both time points. NR exhibited a delayed slight irritation at 48 h (1.3), likely due to trace proteins present in natural rubber latex, which are known to trigger allergic skin reactions. XNBR caused no irritation at 24 h (0.2) and slight irritation at 48 h (0.5). PDEIBA induced the lowest irritation, with scores of 0 and 0.3, remaining within the “no irritation” range. Combined with the cytotoxicity results, these findings confirm that PDEIBA exhibits superior biocompatibility compared to both NR and XNBR, with lower cytotoxicity and reduced skin irritation.

5.4.6 Interfacial interaction between PDXIBA, XNBR, ESBR and silica.

Building on the previous research, in order to further enhance the overall performance of PDXIBA elastomers, particularly in terms of abrasion resistance, oil resistance, and mechanical properties, we have prepared silica-reinforced nanocomposites to investigate the reinforcing effects of inorganic fillers on material performance. Additionally, to comprehensively evaluate the application potential of PDXIBA elastomers, this study introduces styrene-butadiene rubber (ESBR) as an additional reference material, alongside comparisons with XNBR. Therefore, subsequent work will focus on a systematic investigation of the microstructure, mechanical properties, abrasion resistance, and oil resistance of silica-filled systems to clarify the impact of fillers on material performance and assess the feasibility of PDXIBA elastomers in various application scenarios.

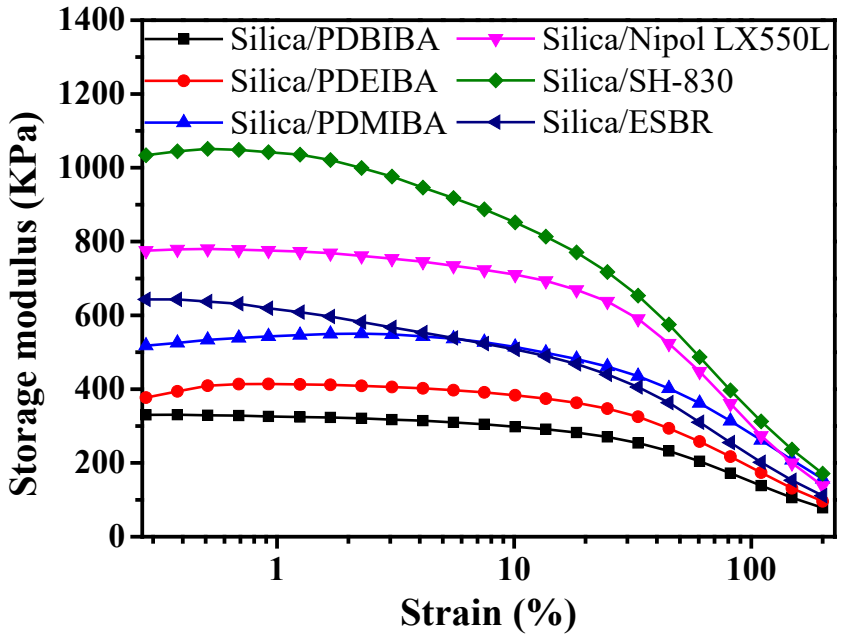

Figure 5.14 Storage modulus-strain of silica/PDXIBA, silica/XNBR and silica/ESBR nanocomposites.

The filler network structure of silica-filled nanocomposites with different matrices was analyzed by RPA, as shown in the **Figure 5.14**. For silica/PDXIBA nanocomposites, as the side chains become shorter, the initial storage modulus of the compound increases. This is due to the increase in polarity, where the enhanced hydrogen bonding interaction between the PDXIBA and silica improves the interfacial interaction. Generally, hydrogen bonding improves the dispersion of fillers. We judged the dispersion of silica based on the length of the plateau region in the storage modulus-strain relationship. Silica/PDMIBA, silica/PDBIBA and silica/PDEIBA have longer plateau regions compared to silica/XNBR, and the storage modulus decreases less within 20% strain, showing a weaker Payne effect, indicating better filler dispersion. SH-830 has higher polarity than Nipol LX550L. Although it demonstrates a higher affinity with silica, the plateau region is shorter and the Payne effect is more pronounced, indicating poor filler dispersion. Among all the samples, ESBR is a non-polar rubber with the weakest interfacial interaction with silica. Silica/ESBR shows the most pronounced Payne effect, indicating the worst silica dispersion. TEM tests were conducted on different silica-filled nanocomposites, as shown in the **Figure 5.15.** The dark regions represent silica, while the bright regions represent the elastomer matrix. From images (a), (b) and (c), it can be seen that silica is uniformly dispersed in PDXIBA, with no significant voids or silica aggregates observed. In contrast, images (d), (e), and (f) show that due to poor compatibility, silica dispersion in XNBR

and ESBR is highly non-uniform, with many voids and silica aggregates visible, further corroborating the explanation of the Payne effect observed in RPA.

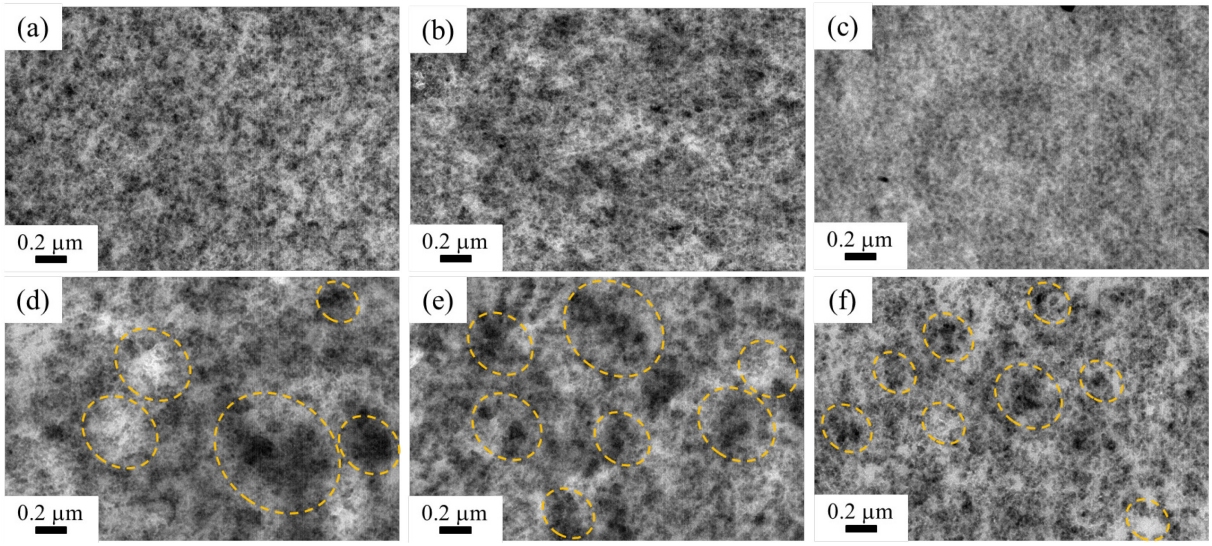

Figure 5.15 TEM images of silica/PDXIBA, silica/XNBR and silica/ESBR nanocomposites. (a) Silica/PDBIBA; (b) Silica/PDEIBA; (c) Silica/PDMIBA; (d) Silica/Nipol LX550L; (e) Silica/SH-830; (f) Silica/ESBR.

Next, we further analyze the dispersion mechanism of silica in these matrices. Silica surfaces contain a large number of hydroxyl groups and have high surface energy, making them prone to agglomeration, which leads to poor dispersion in rubber and poor compatibility with the rubber matrix [17, 18]. In the rubber industry, the most commonly used method to address this issue is the use of silane coupling agents. For example, Si69, contains ethoxy groups that can react with hydroxyl groups on the silica surface, as well as sulfur groups that can cross-link with rubber, thereby effectively coupling silica with rubber to improve dispersion and interfacial adhesion.

For silica/PDXIBA nanocomposites, PDBIBA, PDEIBA, and PDMIBA can not only form chemical bonding interactions with silica via Si69, but also rely on the ester and carboxyl groups in their molecular chains to form hydrogen bonding interactions with the silanol groups on the silica surface, further promoting silica dispersion. As the side chains become shorter, the polarity of the PDXIBA matrix increases, enhancing the hydrogen bonding interactions between the ester groups and the silanol groups on the silica surface, which contributes to improved filler dispersion within the elastomer network. For silica/XNBR nanocomposites, SH-830 has higher polarity than Nipol LX550L, but the dispersion of silica still primarily relies

on the presence of carboxyl groups and the silane coupling agent Si69. Although the increased polarity enhances the affinity between the elastomer and silica, excessive polar adsorption—especially involving cyano groups—may actually promote localized filler aggregation. This is reflected by the shorter plateau region and more pronounced Payne effect in RPA, indicating poorer filler dispersion. For silica/ESBR, ESBR can only rely on Si69 for coupling with silica to enhance the interfacial adhesion between the matrix and silica, but the effect is limited in improving silica dispersion, as evidenced by the short plateau region in RPA.

5.4.7 Mechanical properties of silica/PDXIBA, silica/XNBR and silica/ESBR nanocomposites

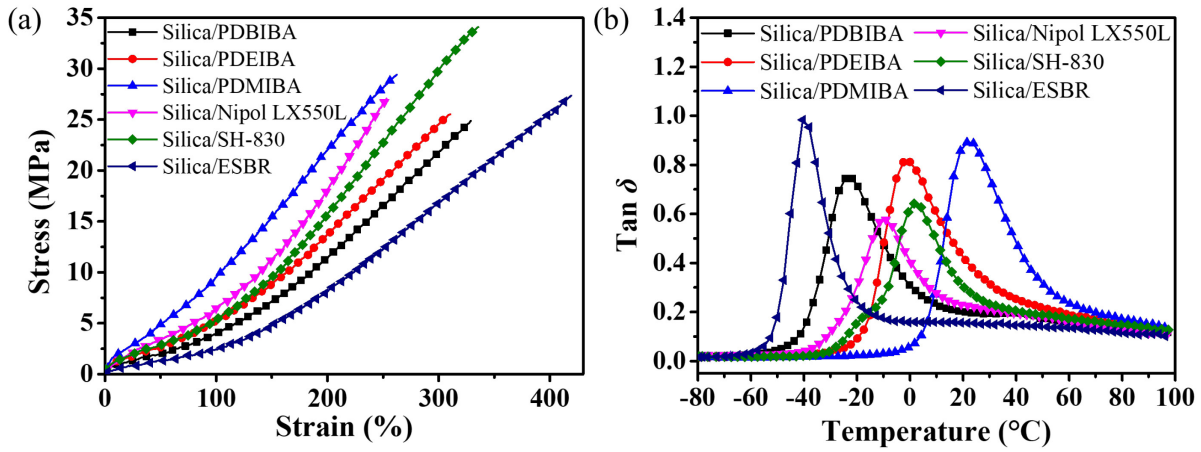

Figure 5.16 (a) Stress-strain curves; (b) Tan δ-temperature curves of silica/PDXIBA, silica/XNBR and silica/ESBR nanocomposites.

The **Figure 5.16** (a) presents the mechanical properties of silica-filled nanocomposites based on different PDXIBA (PDBIBA, PDEIBA, PDMIBA), XNBR (Nipol LX550L, SH-830), and ESBR, with the corresponding data summarized in the **Table S5.4**. As the side group size decreases (DBI → DEI → DMI), both tensile strength and stress at different strains exhibit an increasing trend, with PDMIBA demonstrating the highest tensile strength and stress levels. This trend is primarily attributed to the increased polarity of the side groups, where the higher polarity of PDMIBA enhances interactions with hydroxyl groups on the silica surface, improving filler dispersion and interfacial adhesion, thus leading to enhanced mechanical properties. Compared to XNBR, the tensile strength of the PDMIBA composite (29.5 MPa) is already close to that of the medium-acrylonitrile Nipol LX550L (27.1 MPa) but remains lower than that of the high-acrylonitrile SH-830 (34.1 MPa). Since ESBR is a non-polar rubber with

higher molecular chain flexibility, its elongation at break (424%) is significantly higher than that of the itaconate-based and XNBR-based nanocomposites.

As shown in the **Figure 5.16** (b), the relationship between tan δ and temperature for various matrix-based nanocomposites was obtained through dynamic mechanical thermal analysis (DMTA) testing, with the corresponding temperature of the α-relaxation associated with the glass transition and tan δ values summarized in the **Table S5.5**. As the side chains of the itaconate elastomer shorten, the temperature of the α-relaxation associated with the glass transition for the silica/PDXIBA nanocomposites gradually increases, along with the corresponding tan δ. This is because the shortening of the side chains enhances the polarity of the matrix, leading to stronger hydrogen bonding interactions between the matrix and the silica filler. Consequently, the molecular chains are more constrained during motion, simultaneously driving the movement of surrounding silica particles, thereby increasing energy dissipation. Similarly, compared to Nipol LX550L, SH-830 contains more acrylonitrile units, resulting in stronger polar adsorption between the matrix and the silica filler, which leads to a similar trend of an increase in the temperature of the α-relaxation associated with the glass transition and in tan δ. On the other hand, ESBR, due to its lower temperature of the α-relaxation associated with the glass transition (-40 °C), exhibits better low-temperature flexibility and a lower loss factor (0.137) at 60 °C, indicating reduced rolling resistance. This characteristic makes ESBR one of the widely used rubber matrix materials in the tire industry.

5.4.8 Durability performance: DIN abrasion, aging behavior and oil resistance of silica/PDXIBA, silica/XNBR, and silica/ESBR nanocomposites

Figure 5.17 (a) shows the DIN abrasion volume loss of silica-filled nanocomposites with different matrices. For the itaconate system, as the side chains of the itaconate monomer become shorter, the abrasion loss exhibits a significant decreasing trend. This is mainly because, as the side chains shorten, the polarity of the matrix gradually increases, enhancing the interaction between the matrix and silica, thereby improving the bonding strength of the filler within the matrix and consequently enhancing abrasion resistance. Among them, silica/PDMIBA shows

abrasion resistance close to that of silica/Nipol LX550L but has a certain gap compared to silica/SH-830 and silica/ESBR.

Elastomer materials undergo performance degradation over time due to environmental factors such as temperature, oxygen, humidity, light exposure, and chemical media, a process known as aging. Aging is unavoidable in practical applications, especially in automotive tires, seals, industrial damping materials, and conveyor belts, where elastomer products are particularly susceptible. Therefore, we investigated the mechanical property changes of silica-filled nanocomposite samples with different matrices before and after thermal-oxidative aging. **Figure 5.17** (b) presents the retention ratios of tensile strength (R_σ) and elongation at break (R_ε) of the samples after 168 h of aging at 100 °C, with the corresponding data shown in **Table S5.6**. As the side chains of the itaconate monomer gradually shorten, the retention ratios of mechanical properties of the composites gradually increase. This is due to the increase in molecular chain polarity, which enhances the cohesive energy density and intermolecular interactions, thereby providing a certain level of protection for unsaturated double bonds [19, 20]. Additionally, the silica/PDMIBA nanocomposites exhibit higher R_σ and R_ε compared to silica/SH-830 and silica/Nipol LX550L, while silica/ESBR shows the lowest property retention. This indicates that silica/PDMIBA possesses superior aging resistance, offering significant advantages for elastomer products used in harsh environments by ensuring greater reliability and extended service life.

According to the GB/T 1690-2010 standard, the oil resistance of silica-filled nanocomposites with different matrices was studied after immersion in IRM-903# oil at 100 °C for 72 h. The evaluation focused on the retention ratios of tensile strength (R_σ) and elongation at break (R_ε), as well as percentage of mass gain (Δm) and volume gain (ΔV), as illustrated in **Figure 5.17** (c) and (d), with the corresponding data summarized in the **Table S5.7**. Materials with better oil resistance should exhibit higher mechanical property retention and lower mass and volume expansion after oil immersion.

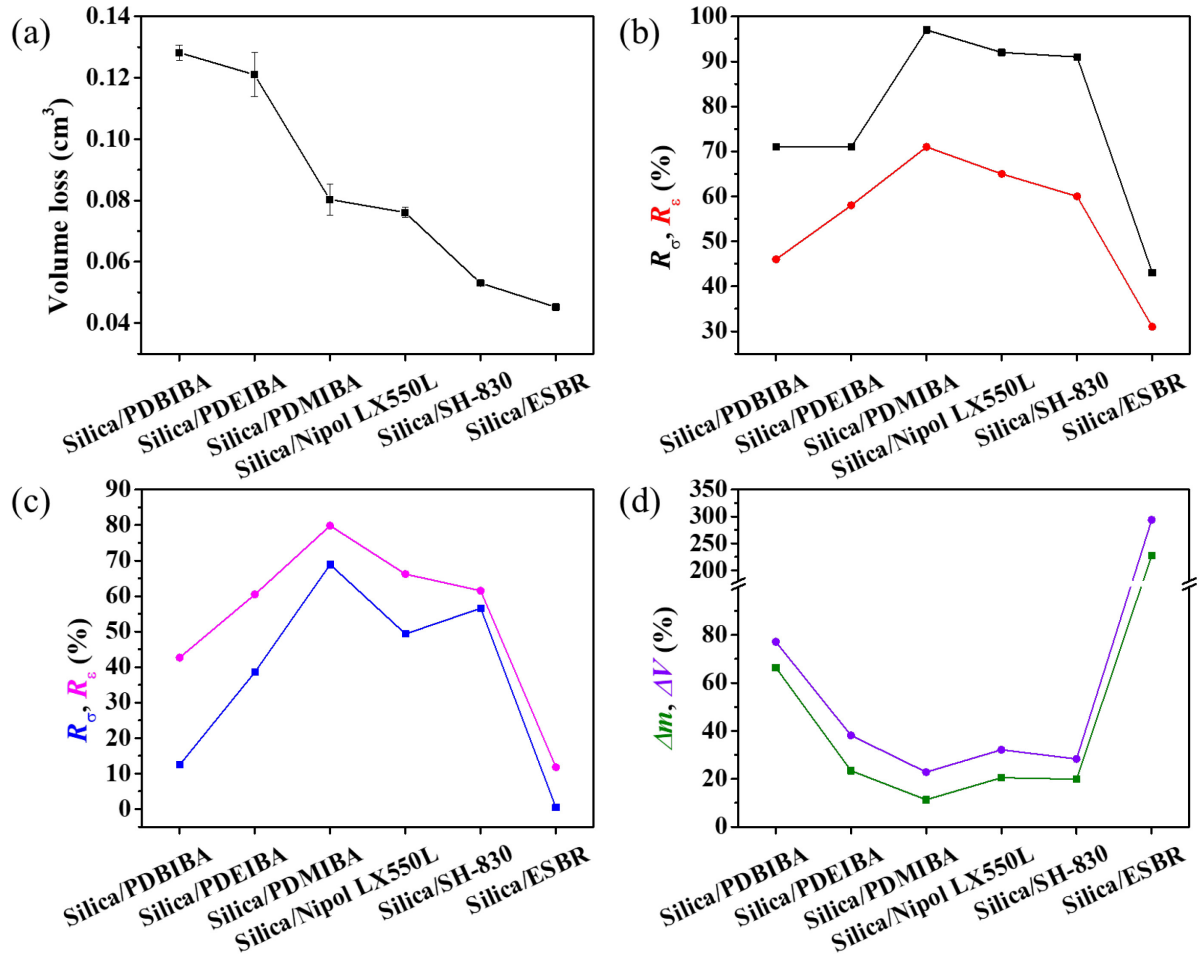

Figure 5.17 Durability evaluation of silica/PDXIBA, silica/XNBR, and silica/ESBR nanocomposites: (a) Volume loss after DIN abrasion test; (b) Retention ratios of tensile strength (R_σ) and elongation at break (R_ε) after thermo-oxidative aging at 100 °C for 168 h; (c) Retention ratios of tensile strength (R_σ) and elongation at break (R_ε); (d) Percentage of mass gain (Δm) and volume gain (ΔV) after immersion in IRM-903# oil at 100 °C for 72 h.

First, from **Figure 5.17** (c), it can be seen that as the side chains of the itaconate monomer gradually shorten, R_σ and R_ε increases. Using silica/XNBR with varying acrylonitrile content and non-polar ESBR as references, silica/PDMIBA shows significantly better mechanical property retention. In addition, the percentage of mass gain (Δm) and volume gain (ΔV) are also crucial indicators for evaluating oil resistance. As shown in **Figure 5.17** (d), with the gradual shortening of the itaconate side chains, the Δm and ΔV of the composites decrease, indicating that the ability of the composites to block non-polar oil penetration into the molecular chains is enhanced. Among all the samples, silica/PDMIBA exhibits the highest oil resistance, while non-polar silica/ESBR exhibits the worst oil resistance.

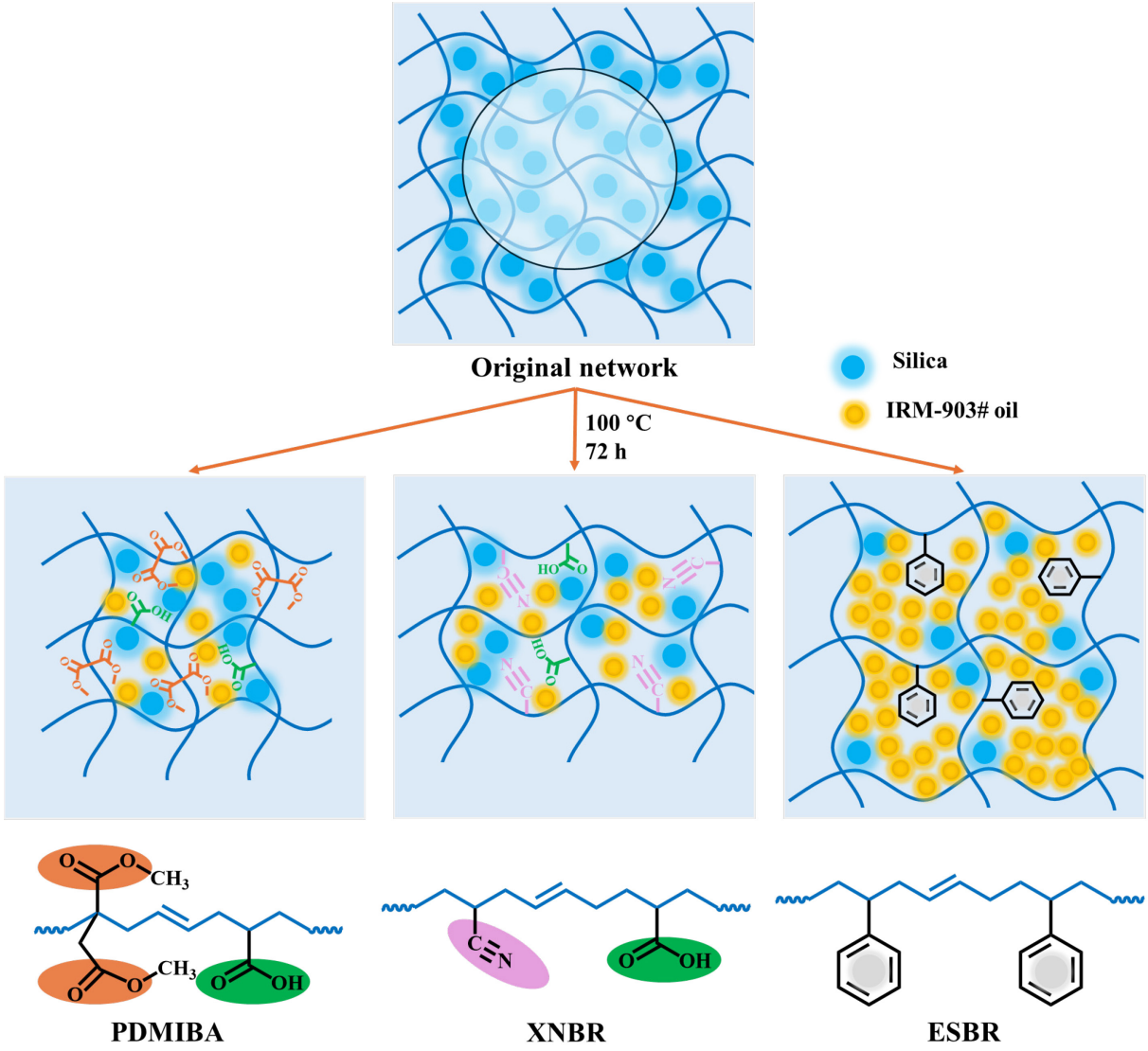

Figure 5.18 Schematic illustration of oil resistance performance for different silica-reinforced elastomers (PDMIBA, XNBR, and ESBR) after immersion in IRM-903# oil at 100 °C for 72 h.

To gain a deeper understanding of the oil resistance of nanocomposites with different polymer matrices, PDMIBA, SH-830, and ESBR were selected for further analysis based on the contributions of methyl ester groups, cyano groups, and benzene rings in the molecular chains to oil resistance. Based on the volume expansion, a rough schematic diagram of their oil resistance was drawn, as shown in **Figure 5.18**. Among these groups, methyl ester has high polarity and is symmetrically distributed on dimethyl itaconate (high contribution to oil resistance), cyano groups have the highest polarity (high contribution to oil resistance), while benzene rings have almost no polarity (low contribution to oil resistance). When PDMIBA and SH-830 are used as matrix materials, their molecular chain networks exhibit strong resistance

to non-polar oils and can maintain material properties in oil media. However, PDMIBA shows better oil resistance. The dimethyl itaconate units in PDMIBA introduce a high density of polar ester groups along the molecular chains, forming a continuous polar barrier that effectively hinders the intrusion of non-polar oil molecules[21]. In contrast, although SH-830 contains highly polar cyano groups, their distribution is less dense, resulting in a weaker blocking effect. ESBR, on the other hand, is a non-polar polymer whose benzene rings contribute little to overall polarity, making it highly susceptible to oil penetration. Therefore, PDMIBA demonstrates the best oil resistance, followed by SH-830, with ESBR performing the worst.

5.5 Conclusions

In this study, a series of bio-based carboxylated itaconate elastomers (PDXIBA), including PDBIBA, PDEIBA, and PDMIBA, were synthesized by emulsion polymerization using three monomers with different side chain structures, namely dibutyl itaconate (DBI), diethyl itaconate (DEI), and dimethyl itaconate (DMI), together with butadiene and methacrylic acid. The molecular structure, thermal behavior, mechanical properties, and oil/solvent resistance of these elastomers were systematically studied and compared with commercial petroleum-based carboxylated nitrile rubber (XNBR). The results showed that the synthesized PDXIBA latexes had higher number-average molecular weights (M_n 99–256 kg/mol), which were higher than those of XNBR (62 and 86 kg/mol). As the side chain shortened, the glass transition temperature (T_g) increased from -46 °C to -16 °C, the tensile strength of the PDXIBA elastomers increased from 25.5 MPa to 28 MPa, and the elongation at break decreased from 553% to 311%, meeting the basic tensile performance requirements for glove materials. At the same time, PDMIBA films exhibited abrasion and oil resistance comparable to nitrile rubber. In addition, PDEIBA gloves demonstrated better biocompatibility compared to natural rubber and nitrile rubber gloves. According to different application scenarios, various types of itaconate latexes can be selected to produce gloves, showing their potential applications in disposable and industrial protective gloves.

In the silica-filled system, PDXIBA matrices with different side chain structures and XNBR, ESBR showed significant differences in filler dispersion and interfacial compatibility. Among them, the tensile strength of silica/PDXIBA nanocomposites ranged from 24.9 MPa (silica/PDBIBA) to 29.5 MPa (silica/PDMIBA), with the latter already exceeding that of the medium-acrylonitrile XNBR composite (silica/Nipol LX550L, 27.1 MPa).While maintaining high mechanical properties, silica/PDMIBA nanocomposites also exhibited better oil resistance and thermal-oxidative aging performance than commercial medium/high acrylonitrile content XNBR nanocomposites. This was attributed to the good barrier effect provided by the highly polar side chains structure and the formation of effective interfacial adhesion with silica, which enhanced the stability of the composites in oil media and high-temperature aging environments. This indicates that carboxylated itaconate elastomers are not only suitable as a base rubber material, but also has the potential to construct high-performance silica-reinforced composites.

5.6 References

[1] WHITE W C. Butadiene Production Process Overview [J]. Chem Biol Interact, 2007, 166(1): 10-14.

[2] TAALMAN R D F M. Isoprene: Background and Issues [J]. Toxicology, 1996, 113(1): 242-246.

[3] ANDERSON E V, BROWN R, BELTON C E. Styrene—Crude Oil to Polymer [J]. Industrial & Engineering Chemistry, 1960, 52(7): 550-556.

[4] QIAO H, XU W, CHAO M, et al. Preparation and Performance of Silica/epoxy Group-functionalized Biobased Elastomer Nanocomposite [J]. Industrial & Engineering Chemistry Research, 2017, 56(4): 881-889.

[5] JI H, YANG H, LI L, et al. Development of Sustainable Tire Tread Using Novel Biobased Itaconate Elastomers [J]. ACS Sustainable Chemistry & Engineering, 2023, 11(44): 15826-15840.

[6] ZHOU X, JI H, HU G-H, et al. A Solvent-less Green Synthetic Route toward A Sustainable

Bio-based Elastomer: Design, Synthesis, and Characterization of Poly(dibutyl itaconate-co-butadiene) [J]. Polymer Chemistry, 2019, 10(45): 6131-6144.

[7] WANG R, MA J, ZHOU X, et al. Design and Preparation of a Novel Cross-Linkable, High Molecular Weight, and Bio-based Elastomer by Emulsion Polymerization [J]. Macromolecules, 2012, 45(17): 6830-6839.

[8] LEI W, ZHOU X, RUSSELL T P, et al. High Performance Bio-based Elastomers: Energy Efficient and Sustainable Materials for Tires [J]. Journal of Materials Chemistry A, 2016, 4(34): 13058-13062.

[9] GAWCHIK S M. Latex Allergy [J]. Mount Sinai Journal of Medicine: A Journal of Translational and Personalized Medicine, 2011, 78(5): 759-772.

[10] LI B S, ESTLANDER T, JOLANKI R, et al. Advantages and Disadvantages of Gloves [M]//JOHN S M, JOHANSEN J D, RUSTEMEYER T, et al. Kanerva's Occupational Dermatology. Cham; Springer International Publishing. 2020: 2547-2561.

[11] SATO T, INUI S, TANAKA H, et al. Kinetic and ESR Studies on the Radical Polymerization of Di-n-butyl Itaconate in Benzene [J]. Journal of Polymer Science Part A: Polymer Chemistry, 1987, 25(2): 637-652.

[12] SATO T, MASAKI K, KONDO K, et al. Solvent Effects on the Radical Polymerization of N-dodecylmaleimide [J]. Polymer Bulletin, 1995, 35(3): 345-350.

[13] CHEREMISINOFF N P, CHEREMISINOFF P N. Elastomer Technology Handbook [M]. CRC press, 2020.

[14] BOGUSKI J, PRZYBYTNIAK G, ŁYCZKO K. New Monitoring by Thermogravimetry for Radiation Degradation of EVA [J]. Radiation Physics and Chemistry, 2014, 100: 49-53.

[15] LI Y-M, DENG C, WANG Y-Z. A Novel High-temperature-resistant Polymeric Material for Cables and Insulated Wires via the Ceramization of Mica-based Ceramifiable EVA Composites [J]. Composites Science and Technology, 2016, 132: 116-122.

[16] CHEN G-Q, JIANG X-R. Next Generation Industrial Biotechnology Based on Extremophilic Bacteria [J]. Current Opinion in Biotechnology, 2018, 50: 94-100.

[17] GUI Y, ZHENG J, YE X, et al. Preparation And Performance of Silica/SBR Masterbatches with High Silica Loading by Latex Compounding Method [J]. Composites Part B: Engineering, 2016, 85: 130-139.

[18] YATSUYANAGI F, SUZUKI N, ITO M, et al. Effects of Secondary Structure of Fillers on The Mechanical Properties of Silica Filled Rubber Systems [J]. Polymer, 2001, 42(23): 9523-9529.

[19] LI S, NIE J, SHI Y, et al. Contributions of Different Functional Groups to Contact Electrification of Polymers [J]. Advanced Materials, 2020, 32(25): 2001307.

[20] MENGISTU T, PAZUR R J. The Thermal Oxidation of Hydrogenated Acrylonitrile-co-Butadiene Rubber from Ambient to 150 °C [J]. Polymer Degradation and Stability, 2021, 188: 109574.

[21] YANG H, JI H, LI L, et al. Acrylic Nanocomposites Modified by Biobased Itaconates: Mechanical Properties, Oil Resistance, and Heat Resistance [J]. Industrial & Engineering Chemistry Research, 2022, 61(35): 13168-13176.

Chapter 6 General Conclusions and Perspectives

6.1 General conclusions

This thesis addresses the key challenge of developing sustainable elastomeric materials that simultaneously exhibit bio-based origin, tunable structure, and high mechanical performance. To tackle this challenge, a systematic material design strategy was proposed, combining carboxyl functionalization of itaconate elastomers, ZnO-induced ionic cross-linking, and side-chain structure regulation. Based on this strategy, the synthesis methods, microstructural regulation, structure–property relationships, and application potential of bio-based carboxylated itaconate elastomers were comprehensively investigated. The effectiveness of this approach was further validated through their performance in silica-filled composites and disposable glove materials. The main research findings can be summarized in the following four aspects:

Firstly, carboxylated dibutyl itaconate elastomers (PDBIBAs) were synthesized via emulsion polymerization using dibutyl itaconate (DBI), butadiene (BD), and methacrylic acid (MAA), achieving functionalized modification. Experimental results showed that with increasing methacrylic acid content, the number-average molecular weight (M_n) of PDBIBAs ranged from 173 to 310 kg/mol, and the glass transition temperature (T_g) increased from -57 °C to -32 °C. Moreover, the mechanical properties were significantly enhanced through cross-linking between carboxyl groups and zinc oxide, with tensile strength increasing from 3.1 MPa to 14.1 MPa. Based on this, PDBIBAs were applied in the preparation of silica-filled nanocomposites. Benefiting from hydrogen bonding between carboxyl groups and hydroxyl groups on the silica surface, the interfacial interaction between elastomer and filler was significantly strengthened, effectively suppressing filler agglomeration and improving the dispersion uniformity of silica in the matrix. In addition, the introduction of carboxyl groups

significantly improved the abrasion resistance, oil resistance, and thermo-oxidative aging performance of the composites. Under oil media and high-temperature aging conditions, the materials maintained high strength and stability, demonstrating excellent comprehensive durability. In summary, carboxyl functionalization not only effectively improved the basic properties of elastomers, but also provided favorable conditions for interfacial construction with inorganic fillers, offering a new approach for the development of high-performance bio-based composites.

Secondly, by adjusting the ZnO content, a reversible ionic cross-linking network was introduced to construct PDBIBA ionomers with thermal responsiveness and thermoreversibility. FTIR confirmed the gradual formation of zinc carboxylate structures, and SAXS measurements revealed ion cluster radii ranging from 0.88 to 2.98 nm. Tensile testing showed that increasing the ZnO content from 2 phr to 15 phr led to a rise in tensile strength to 15.3 MPa, with an increase of 467%, attributed to the enhancement of the sacrificial bond mechanism. In terms of dynamic properties, with increasing ZnO content, the temperature of the α-relaxation associated with the glass transition increased from -35 °C to -30 °C, and the ionic transition temperature (T_i) rose from 45 °C to 71 °C, reflecting the relaxation behavior of polymer chains near the ionic clusters. Rubber process analysis and low-field NMR further confirmed the dynamic and reversible nature of ionic cross-linking points at different temperatures. This part of the study clearly demonstrated the dynamic network tunability of ZnO-crosslinked PDBIBA and its potential in recyclable and thermally responsive materials.

To optimize the comprehensive properties of the material and expand its application prospects in the field of protective materials, itaconate monomers with different side chain structures, namely dibutyl itaconate (DBI), diethyl itaconate (DEI), and dimethyl itaconate (DMI), were selected and copolymerized with butadiene (BD) and methacrylic acid (MAA) via emulsion polymerization to synthesize three structure-adjustable carboxylated itaconate elastomers (PDBIBA, PDEIBA, and PDMIBA). Experimental results showed that as the side chains shortened from butyl to ethyl and methyl, the synthesized PDXIBA latexes exhibited significant structural and performance differences: the number-average molecular weight (M_n)

decreased from 256 kg/mol to 99 kg/mol, while the glass transition temperature (T_g) increased from -46 °C to -16 °C. This structural evolution significantly affected the mechanical and processing properties of the materials. In terms of macroscopic performance, the tensile strength increased with the shortening of the side chain (from 25.5 MPa to 28.0 MPa), while the elongation at break decreased (from 553% to 311%). Compared with commercial carboxylated nitrile rubber (XNBR) latexes with medium/high acrylonitrile content (Nipol LX550L and SH-830), PDMIBA exhibited comparable or even superior oil and abrasion resistance, while PDEIBA demonstrated better biocompatibility in cytotoxicity and skin sensitization tests, indicating the application potential of PDXIBA latexes as environmentally friendly alternatives in disposable and medical protective gloves.

In the silica/PDXIBA nanocomposite system, the side chain structure had a significant impact on filler dispersion and interfacial bonding. Among them, PDMIBA prepared with highly polar short side chain monomers performed best, with its composite exhibiting a tensile strength of 29.5 MPa, exceeding that of the commercial medium acrylonitrile content carboxylated nitrile rubber Nipol LX550L (27.1 MPa), and showing better stability than the high acrylonitrile content carboxylated nitrile rubber SH-830 under oil media and high-temperature aging conditions. This was mainly attributed to the shielding effect and hydrogen bonding brought by the stronger polar side chains in the PDMIBA molecules, which enhanced interfacial interaction with silica and constructed a dense and stable filler network structure. The results indicate that PDXIBA elastomers are not only suitable for the field of protective gloves, but also have application potential in constructing high-performance silica-filled composites.

6.2 Perspectives

This study preliminarily established a carboxylated elastomer material system based on itaconate, and conducted systematic exploration from molecular structure regulation and ionic cross-linking construction to composite material application, verifying its feasibility as a green

high-performance elastomer. Based on the research foundation of this work, future research can be further expanded and deepened in the following aspects:

Expansion of functionalization strategies and construction of diversified cross-linking networks: the current study mainly used methacrylic acid to introduce carboxyl groups and ZnO-induced ionic cross-linking to improve material performance. In the future, other functional groups (such as hydroxyl, amino, sulfonic acid) can be introduced or multifunctional monomers can be designed to achieve multi-site reactions or the construction of synergistic cross-linking networks. At the same time, it is also worthwhile to explore the construction of composite ionic cross-linking structures by co-using metal ions (such as Ca^{2+}, Mg^{2+}, Al^{3+}).

To realize a 100% bio-based itaconate elastomer system, future research can proceed synergistically from two aspects: raw material selection and filler system optimization. On the one hand, in the construction of the elastomer backbone, domestically matured microbial fermentation technologies can be relied upon to utilize key monomers such as bio-based isoprene and butadiene, and natural terpenes can be explored to replace traditional petroleum-based diolefins, so as to realize a fully bio-based main chain structure.

On the other hand, in the construction of the filler system, attention can be focused on biomass fillers with wide sources and low cost, such as lignin, rice husk silica, and cellulose. Through interfacial modification or composite reinforcement strategies, the dispersion and interfacial compatibility of the fillers in the elastomer matrix can be improved, thereby constructing green, high-performance bio-based composite materials. In addition, dynamic dielectric spectroscopy could be employed to further investigate the interfacial dynamics and polarization behavior between the filler and the matrix, providing deeper insights into interfacial interactions. The above studies will play an important foundation for the development of a sustainable elastomer system with full lifecycle friendliness and tunable functionality.

Appendix

Additional materials for Chapter 3

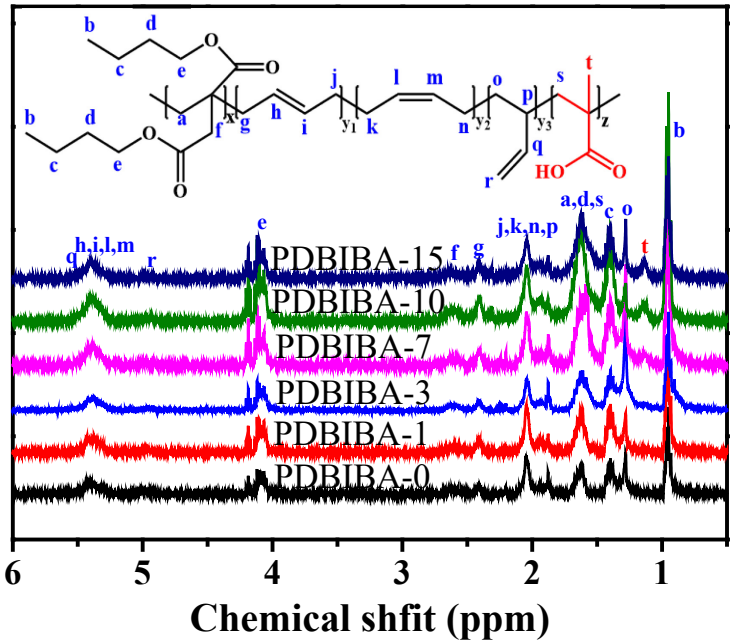

Figure S3.1. ^{1}H NMR spectra of neat PDBIBAs.

Table S3.1 Mechanical properties of unfilled cross-linked PDBIBAs with different MAA contents.

PDBIBAs	Tensile strength / MPa	Stress at 100% / MPa	Stress at 300% / MPa	Elongation at break / %
PDBIBA-0	3.1±0.2	1.1±0.2	-	283±15
PDBIBA-1	4.9±0.5	1.2±0.3	4.0±0.4	331±35
PDBIBA-3	6.5±0.3	1.4±0.1	5.5±0.2	334±50
PDBIBA-7	8.5±0.5	1.9±0.4	6.5±0.5	347±38
PDBIBA-10	10.4±0.8	2.2±0.3	9.1±0.6	318±28
PDBIBA-15	14.1±0.6	3.8±0.2	12.7±0.8	317±20

Table S3.2 Mechanical properties of silica/PDBIBA nanocomposites with different MAA contents.

Silica/PDBIBAs	Tensile strength / MPa	Stress at 100% / MPa	Stress at 300% / MPa	Elongation at break / %
Silica/PDBIBA-0	15.5±0.9	3.0±0.3	12.7±0.5	345±30
Silica/PDBIBA-1	18.0±0.7	3.3±0.2	13.1±0.9	374±52
Silica/PDBIBA-3	21.0±1.0	3.5±0.3	14.5±1.2	393±26
Silica/PDBIBA-7	23.5±0.5	3.5±0.5	17.3±0.7	377±44
Silica/PDBIBA-10	23.1±1.1	3.8±0.7	19.7±0.6	341±34
Silica/PDBIBA-15	24.4±0.6	13.3±0.9	-	200±39

Table S3.3 Retention ratios of tensile strength (R_σ) and elongation at break (R_ε) of silica/PDBIBA nanocomposites after thermo-oxidative aging at 100 °C for 72 h.

Silica/PDBIBAs	Retention ratios	
	R_σ / %	R_ε / %
Silica/PDBIBA-0	75	60
Silica/PDBIBA-1	77	73
Silica/PDBIBA-3	79	84
Silica/PDBIBA-7	87	79
Silica/PDBIBA-10	98	71
Silica/PDBIBA-15	144	41

Table S3.4 Retention ratios of tensile strength (R_σ) and elongation at break (R_ε), as well as the percentage of mass gain (Δm) and volume gain (ΔV) of silica/PDBIBA nanocomposites after oil resistance at 100 °C for 72 h.

Silica/PDBIBAs	Retention ratios		Percentage of mass and volume gain	
	R_σ / %	R_ε / %	Δm / %	ΔV / %
Silica/PDBIBA-0	5	29	104	127
Silica/PDBIBA-1	9	29	107	119
Silica/PDBIBA-3	10	36	90	117
Silica/PDBIBA-7	17	40	57	76
Silica/PDBIBA-10	24	46	47	65
Silica/PDBIBA-15	24	60	35	56

Additional materials for Chapter 4

Table S4.1. Mechanical properties of cross-linked PDBIBA/ZnO with varying amount of ZnO.

Cross-linked PDBIBA/ZnO	Tensile strength / MPa	Stress at 100% / MPa	Stress at 300% / MPa	Elongation at break / %
ZnO-2.0	2.7±0.3	0.5±0.2	0.9±0.7	727±30
ZnO-3.6	5.0±0.7	0.8±0.2	1.9±0.6	629±25
ZnO-5.0	7.2±0.8	1.2±0.5	2.9±0.6	577±19
ZnO-10	14.5±0.5	1.7±0.3	5.2±0.3	498±21
ZnO-15	15.3±0.3	2.0±0.6	6.0±0.4	487±27

Additional materials for Chapter 5

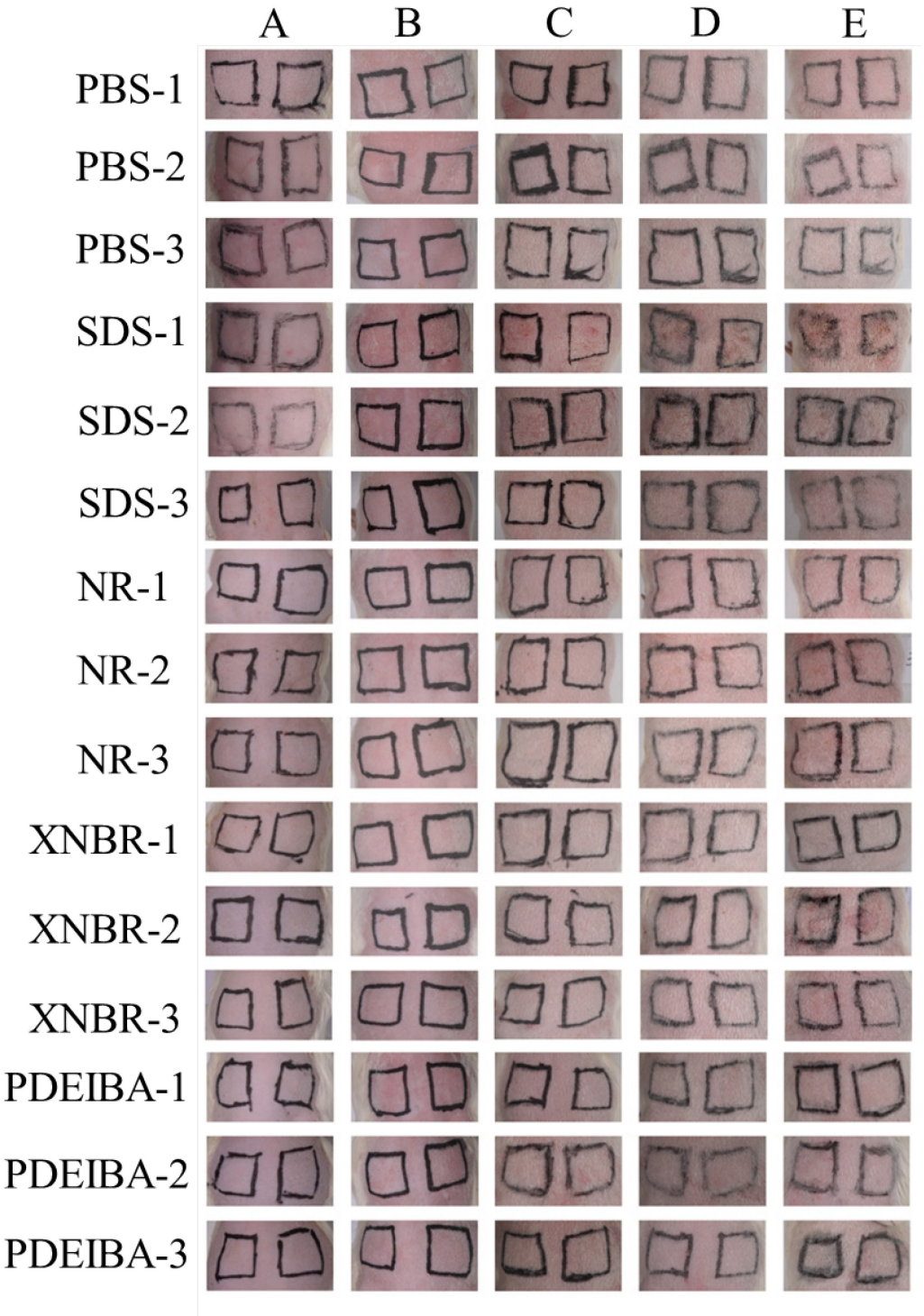

Figure S5.1 Skin responses in guinea pigs during the sensitization test. Rows represent different sample groups: PBS (negative control), SDS (positive control), NR (natural rubber), XNBR (nitrile rubber), and PDEIBA. Each group includes three individual samples. Columns A–E represent the observation time points. A: pre-administration, B: Day 7, C: Day 14 (before final administration), D: 24 h after final administration, and E: 48 h after final administration.

Table S5.1 Mechanical properties of cross-linked PDXIBA and XNBR films.

Cross-linked PDXIBA and XNBR films	Tensile strength / MPa	Stress at 100% / MPa	Stress at 300% / MPa	Elongation at break / %
PDBIBA	25.5±0.3	5.7±0.2	12.5±0.5	553±20
PDEIBA	27.1±0.5	7.7±0.4	18.3±0.6	420±16
PDMIBA	28.0±0.6	9.7±0.5	26.9±0.1	311±13
Nipol LX550L	28.4±0.7	2.8±0.2	6.8±0.5	656±23
SH-830	41.9±0.4	6.6±0.3	19.6±0.4	481±19

Table S5.2 Retention ratios of tensile strength (R_σ) and elongation at break (R_ε), as well as the percentage of mass gain (Δm) and volume gain (ΔV) of cross-linked PDXIBA and XNBR films after oil resistance at 100 °C for 24 h.

Cross-linked PDXIBA and XNBR films	Retention ratios		Percentage of mass and volume gain	
	R_σ / %	R_ε / %	Δm / %	ΔV / %
PDBIBA	14	193	133	153
PDEIBA	34	141	47	57
PDMIBA	58	129	21	23
Nipol LX550L	30	112	37	42
SH-830	37	104	28	22

Table S5.3 Erythema and edema scores of PBS, SDS, and glove materials (NR, XNBR, and PDEIBA) at 24 h and 48 h after the final administration.

Group	24 h after final administration				48 h after final administration			
	Erythema score		Edema score		Erythema score		Edema score	
PBS-1	0	0	0	0	0	0	0	0
PBS-2	0	0	0	0	0	0	0	0
PBS-3	0	0	0	0	0	0	0	0
SDS-1	2	3	2	2	2	2	2	2
SDS-2	2	2	2	2	1	2	1	2
SDS-3	1	1	1	1	1	1	1	1
NR-1	0	0	0	0	1	1	1	1
NR-2	0	0	0	0	1	1	1	1
NR-3	0	0	0	0	0	0	0	0
XNBR-1	0	0	0	0	0	0	0	0
XNBR-2	0	0	1	0	0	0	1	1
XNBR-3	0	0	0	0	0	0	1	0
PDEIBA-1	0	0	0	0	0	0	0	0
PDEIBA-2	0	0	0	0	1	0	0	0
PDEIBA-3	0	0	0	0	0	0	1	0

Table S5.4 Mechanical properties of silica/PDXIBA, silica/XNBR and silica/ESBR nanocomposites.

Silica/rubber nanocomposites	Tensile strength / MPa	Stress at 100% / MPa	Stress at 300% / MPa	Elongation at break / %
Silica/PDBIBA	24.9±0.5	4.0±0.2	21.8±0.3	334±23
Silica/PDEIBA	25.6±0.3	5.2±0.2	24.5±0.5	324±16
Silica/PDMIBA	29.5±0.6	9.6±0.4	-	272±18
Silica/Nipol LX550L	27.1±1.0	6.5±0.7	-	263±20
Silica/SH-830	34.1±1.3	5.3±0.6	29.9±0.7	336±16
Silica/ESBR	27.4±0.6	2.5±0.4	16.8±0.3	424±22

Table S5.5 Dynamic mechanical properties of silica/PDXIBA, silica/XNBR and silica/ESBR nanocomposites.

Silica/rubber nanocomposites	The temperature of the α-relaxation associated with the glass transition (°C)	Tan δ		
		0 °C	60 °C	Max
Silica/PDBIBA	-21.9	0.311	0.160	0.744
Silica/PDEIBA	-2.5	0.812	0.186	0.812
Silica/PDMIBA	21.5	0.055	0.234	0.892
Silica/Nipol LX550L	-9.1	0.400	0.163	0.576
Silica/SH-830	1.6	0.607	0.172	0.642
Silica/ESBR	-40.4	0.159	0.137	0.983

Table S5.6 Retention ratios of tensile strength (R_σ) and elongation at break (R_ε) of silica/PDXIBA, silica/XNBR, and silica/ESBR nanocomposites after thermo-oxidative aging at 100 °C for 168 h.

Silica/rubber nanocomposites	Retention ratios	
	R_σ / %	R_ε / %
Silica/PDBIBA	71	46
Silica/PDEIBA	71	58
Silica/PDMIBA	97	71
Silica/SH-830	91	60
Silica/Nipol LX550L	92	65
Silica/ESBR	43	31

Table S5.7 Retention ratios of tensile strength (R_σ) and elongation at break (R_ε), as well as the percentage of mass gain (Δm) and volume gain (ΔV) of silica/PDXIBA, silica/XNBR, and silica/ESBR nanocomposites after oil resistance at 100 °C for 72 h.

Silica/rubber nanocomposites	Retention ratios		Percentage of mass and volume gain	
	R_σ / %	R_ε / %	Δm / %	ΔV / %
Silica/PDBIBA	12	43	66	81
Silica/PDEIBA	38	60	24	34
Silica/PDMIBA	69	80	12	23
Silica/Nipol LX550L	49	66	21	32
Silica/SH-830	57	61	20	25
Silica/ESBR	0.4	12	226	296

Nomenclature

DBI	Dibutyl itaconate
DEI	Diethyl itaconate
DMI	Dimethyl itaconate
BD	Butadiene
MAA	Methacrylic acid
PDBIBA-n	Poly(dibutyl itaconate-co-butadiene-co-methacrylic acid), where n represents the weight percentage of MAA relative to the total mass of DBI and BD in the monomer feed.
PDBIBA	Poly(dibutyl itaconate-*co*-butadiene-*co*-methacrylic acid)
PDEIBA	Poly(diethyl itaconate-*co*-butadiene-*co*-methacrylic acid)
PDMIBA	Poly(dimethyl itaconate-*co*-butadiene-*co*-methacrylic acid)
PDXIBA	General abbreviation for poly(itaconate-*co*-butadiene-*co*-methacrylic acid) elastomers with different side chains (X = D for DBI, E for DEI, M for DMI)
Silica/PDBIBA	Silica-filled PDBIBA nanocomposite
Silica/PDEIBA	Silica-filled PDEIBA nanocomposite
Silica/PDMIBA	Silica-filled PDMIBA nanocomposite
Silica/PDXIBA	General term for silica-reinforced nanocomposites based on PDXIBA elastomers
M_n	Number-average molecular weight
M_w	Weight-average molecular weight
$Đ$	Molecular weight distribution, M_w/M_n
T_g	Glass transition temperature, °C
T_i	Ionic transition temperature, °C

$T_{5\%}$	Temperature at 5% weight loss, °C
T_{max}	Temperature at maximum decomposition rate, °C
σ	Tensile strength, MPa
ε	Elongation at break, %
R_σ	Retention ratios of tensile strength, %
R_ε	Retention ratios of elongation at break, %
Δm	Percentage of mass gain, %
ΔV	Percentage of volume gain,%
Tan δ	Loss factor
R_g	Radius of gyration

Scientific Production

[1] **LI L**, WANG R, ZHANG L, HU G et al. Dynamic evolution of ionic bonds and performance characteristics in bio-based dibutyl itaconate elastomers[J]. Polymer, 2025, 334: 128687.

[2] **LI L**, WANG R, ZHANG L, HU G et al. Role of carboxyl groups in the performance optimization of bio-based itaconate elastomers and nanocomposites [J]. European Polymer Journal, 2025, 239: 114280.

[3] ZHANG L, **LI L**, WANG R, et al. A bio-based carboxylated itaconate elastomer, rubber glove material and its preparation method: 202311348092.8 [P].

[4] SUN C, **LI L**, WANG R, ZHANG L, et al. The use of crude carbon dots as green, low-cost and multifunctional additives to improve the curing, mechanical, antioxidative and fluorescence properties of epoxy natural rubber/silica composites [J]. Composites Part A: Applied Science and Manufacturing, 2024, 182: 108177.

[5] **LI L**, WANG R, ZHANG L, HU G. Molecular design, synthesis and process development of bio-based functional itaconate elastomers. International Rubber Conference 2023, Nov. 7-9, 2023, Haikou, China.